UNIVERSITY OF SOUTHAMPTON
FACULTY OF ENGINEERING AND APPLIED SCIENCE

SOUND RADIATION PREDICTION BY SCALE MODELS

by

Roberto Pompoli

Thesis submitted for the Degree of
Doctor of Philosophy in the Institute
of Sound & Vibration Research

May 1983

UNIVERSITY OF SOUTHAMPTON

ABSTRACT

FACULTY OF ENGINEERING AND APPLIED SCIENCE
INSTITUTE OF SOUND AND VIBRATION RESEARCH

Doctor of Philosophy

SOUND RADIATION PREDICTION BY SCALE MODELS

by Roberto Pompoli

The majority of acoustic modelling has been concerned with sound quality inside rooms and auditoria. Little attempt has been made to model the structural stiffness of the walls. These "rigid" walled models have given good results for auditoria but cannot be used for vehicles etc. On the other hand the structural dynamics work has been concerned almost exclusively with the vibration of structures in vacuo. The coupling of the wall vibration with the enclosed space has not been investigated thoroughly. Analytical solutions are available for a few special cases and the finite element method is being developed for use in such coupled problems.

It is considered that there is a need for a technique which is able to take account of the details of the construction of a real structure. Dynamic models could play an important part in the advance checking of the details of new designs and may have important practical application in developing structural modifications to produce the desired acoustical environment.

The aim of this thesis is to verify the possibility of predicting, by scale models, the sound pressure levels inside enclosed structures which are mechanically excited.

The thesis is divided into two main parts: in the first part theoretical considerations have been developed with the aim of deriving similarity conditions between the prototype and the model. For this purpose the wave equation in an acoustic medium and the equations of motion of simple structures have been non-dimensionalized.

The second part is concerned with experimental work on two models: a 1/5 scale plastic model of a safety cab of a tractor and a simple apparatus which consists of a rigid cylindrical cavity that is closed at one end by a flexible panel.

The first model is intended to verify the possibility of having a prediction of the dynamic and acoustic behaviour of the real structure comparable to that obtainable by measurements performed directly on it.

The second apparatus has the aim of verifying the actual possibility of using an acoustic medium different from air but compatible with the plastic models.

ACKNOWLEDGEMENTS

I should like to express my sincere gratitude to Professor B.L. Clarkson for his helpful supervision and his patient assistance during the preparation of the thesis.

I am particularly grateful to Franca, my wife, for her continuous encouragement even when the work interfered with our family life.

Acknowledgements are also given to the staff of the acoustic Laboratory of Italiana Keller where most of the experiments were carried out.

The C.N.R. is thanked for financial support of this work (Contract n. 81.00881.07, 82.01554.07).

CONTENTS

LIST OF SYMBOLS

Capital letters

A	Cross-sectional area	m^2
C	Dimensional constant	-
D	Bending stiffness	$N \cdot m$
	Diameter of the cylinder	m
E	Young's modulus	$\frac{N}{m^2}$
F	Force	N
G	Green function	$\frac{N}{m^2} \cdot \frac{s}{m^3}$
	Coordinate of the centre of gravity	m
H	Frequency response function between sound pressure level and force	$\frac{N}{m^2} \cdot \frac{1}{N}$
	Frequency response function between acceleration and force	$\frac{m}{s^2} \cdot \frac{1}{N}$
I	Moment of inertia	m^4
I_n	Hyperbolic Bessel function	-
J_n	Bessel function	-
K	Membrane stiffness	$\frac{N}{m}$
L	Typical length dimension	m
M	Moment of force	$N \cdot m$
N	Membrane force resultant	$\frac{N}{m}$
	Axial force	N
P	Strength of the sound source	$\frac{m^3}{s}$
Q	Shear resultant	$\frac{N}{m}$

R	Radius	m
	Radius of curvature	m
$\bar{R}$	Position vector	m
S	Surface	m^2

Small letters

b	Width of the plate	m
c_o	Sound velocity of acoustic medium	
c	Wave velocity	$\frac{m}{s}$
$\bar{d}$	Vector displacement	m
e	Neper's number	-
f	Frequency	Hz
h	Thickness	m
i	Imaginary unit	-
k	Wave number	m^{-1}
l	length of the test cylinder	m
m	Moment of force per unit length	$\frac{N \cdot m}{m}$
$\bar{n}$	Normal vector	-
p	Sound pressure	$\frac{N}{m^2}$
q	Force per unit area	$\frac{N}{m^2}$
q'	Force per unit length	$\frac{N}{m}$
r	Radius of gyration	m
s	Curvilinear element length	m
t	Time	s
u	η - component of $\bar{d}$	m
v	ζ - component of $\bar{d}$	m
w	ξ - component of $\bar{d}$	m

x		
y	Absolute rectangular coordinates	m
z		

Greek letters

α	Angle	rad
	Curvilinear coordinate	m
α_n	n^{th} radial eigenvalue	-
β	Angle	rad
γ	Ratio of specific heats	-
$\bar{\zeta}$	Direction of component v of the vector displacement $\bar{d}$	-
η	Loss factor	
	Principal axis of inertia	-
$\bar{\eta}$	Direction of component u of the vector displacement $\bar{d}$	-
θ	Angle of cylindrical coordinates	degree
ν	Poisson's ratio	-
ξ	Direction of component u of the vector displacement $\bar{d}$	-
	Principle axis of inertia	-
π	Dimensionless factors	-
ρ_o	Volume density of acoustic medium	$\frac{kg}{m^3}$
ρ	Volume density of structural material	$\frac{kg}{m^3}$
τ	Shear force per unit length	N/m
ϕ	Phase factor	degree

ψ	Acoustic potential function	$\frac{m^2}{s}$
ω	Circular frequency	s^{-1}
Γ	Mechanical mobility function	$\frac{m}{N \cdot s}$

Subscripts

a	aluminium
b	bars
g	glass
j	drive-point location of the forces on the structure
k	points on the structure
m	model
n	axis of rotation of the real cross-section of the prototype normal direction
o	position of acoustic source
p	prototype
px	perspex
s	steel
t	tangential direction
x	axis of inertia
y	axis of inertia
ξ	principle axis of inertia
η	principle axis of inertia
G	centre of gravity

LIST OF FIGURES

CHAPTER 5

CHAPTER 1

Introdution

In recent years, one of the aspects which has gained increasing engineering importance in the design of transport vehicles such as cars, ships, aircraft, trains etc.,has been the requirement to guarantee acceptable acoustic levels. In the present state of the art it is difficult, if not impossible, to predict during the design stage the acoustic consequences of some technical choices. If the design is unsatisfactory modifications must be made at a late stage in the production process. Sometimes this may even be after the first series of the production line.

It is easy to realize that in this situation the actual possibilities to perform a correct "acoustic design" are certainly restricted and that eventual modifications of the general design, necessary from an acoustical point of view, become difficult if not impossible. With the term "acoustic design" it is intented to summarize a succession of procedures which, starting from a diagnostic analysis of all the noise sources, proceed with the identification of all the noise transmission paths, and conclude with suggestions of practical actions to reduce the noise not only inside but also outside the vehicle.

The diagnostic analysis of the noise sources as well as the identification of the noise transmission paths start usually from experimental measurements which can be performed on prototypes in the field. Alternatively measurements can be made inside well-equipped acoustical laboratories where

it is necessary to acquire a lot of data in a relatively short time.

In fact the sizes of these vehicles are usually so big that, in order to get significant information on the acoustical response of the structure, it is necessary to check a lot of measurement points. This requires long analysis times if the laboratory has not on-line acquisition facilities.

In this respect it has been considered of some interest to investigate the possibility of carrying out this "acoustic design" from the beginning of the general design of the structure by using scale models. The advantages are evident: if the model is built in such a way that the similarity conditions between the prototype and the model itself are respected, it will be possible to obtain useful information on the future acoustical behaviour of the real structure directly from the model. This means that if structural modifications are required, it will be easy to do them and then to check their efficacy. The measurements necessary on the model are usually simpler than they would be on the prototype: they can be carried out in the laboratory and repeated tests can usually be made at the convenience of the experimenter.

In this way the model becomes a versatile design tool which is able to give a lot of useful information. For example, if it is considered that the acoustic field inside an enclosed cavity is produced by the dynamic interaction between the acoustic medium and the elastic vibrations of the boundary walls, it is easy to identify as the model can give information on the dynamic behaviour of structure also.

In other application, models have been used for many

years in design. They are particularly useful when a complex configuration or interaction within a system make analytical solutions difficult.

Originally, geometrical similarity between the system and the model was probably the only criterion considered in model design. Eventually the importance of applied and induced forces was recognized and empirical rules for the scaling of forces were introduced. The writings of Galileo [1] contain observations on models, scaling, and similarity. Froude [2] established procedures for the design of models of ships, and Reynolds [3] investigated the similarity of flow in pipes. Summaries of their contributions have been published by Eisner [4] .

Fluid flow problems, including those concerned with river hydraulics and aerodynamics, as well as structural stability problems occupied the attention of investigators for several years. More recently the techniques of scaling and modelling have been extended to such fields as shock and vibration.

Published research dealing with the design of experimental models in the field of vibration can be classified as follows: acoustics, fluid dynamics, structural impact and vibrations. Inevitably, these four categories overlap because a specific system may be subjected to more than one driving force or develop more than one type of response.

Acoustic Models

Although acoustic models have been used to a limited extent for many years, particularly in auditorium and loud speaker design, they are now being used extensively in noise abatement design. Because acoustic phenomena are associated

with pressure waves in a fluid, usually air, the properties that control pressure transmissions are critical. The sound absorbing characteristics of the materials in the system, as well as their acoustical capacitance and the inertance of the sound transmitting fluid are significant. The designer must give particular attention to energy dissipation [5] and to the surrounding geometry because of its influence upon acoustical capacitance and the accompanying echoes and beats. Physical models of acoustic systems have been developed using analogues, particularly electrical ones [6].

Scale model tests used in noise research have involved externally blown flaps with engines over or under the wing [7-12] and STOL aircraft [13]. Surface blowing nozzle flap concepts have been investigated using small scale models [14].

The aerodynamic and acoustic characteristics of a fully reversible pitch fan has been studied with a scale model over a range of conditions [15] . Results with a model of a low tip-speed fan correlated well with full-scale fan data [16] . Noise levels and performance of a thrust reverser have been determined using a scale model with a length scale of three [17].

Aerodynamic and acoustic scaling techniques have been described [18] ; the results of tests on a one-seventh scale model of a gas turbine exhaust are included. Lighthill's acoustic analogy has been used to develop scaling laws for combustion generated noise in open turbulent flames [19]. Scaling laws for both power and frequency were verified.

An important factor in assessing the reliability of acoustic models is the environment in which the tests are

conducted. Recognition of this fact has led to the development of experimental test facilities. The design of one such facility was aided by the design, construction, and testing of a one-twelfth scale model of the proposed anechoic measurment area [20]. In another instance, tests of one-fifteenth scale models were conducted in an acoustic facility to verify its suitability for model tests [21].

Fluid dynamic models

Generally fluid dynamic models are used to evaluate the forces developed at the interface of a solid and a fluid when one is in motion relative to the other. The relative rigidity of the solid is such that it is assumed to undergo no distortion, but it can be displaced or vibrate as a rigid body. In contrast, the fluid particles exhibit relative motion at both the fluid boundaries and within the body of the fluid.

In this context, models of rivers have been used for many years to predict alterations in stream configuration, trasportation of sediment and influence of river structures on flow phenomena. Models of boats and ships have been tested in towing tanks for nearly a century to evaluate performance characteristics. Recent model research as the interaction between ships and other structures with water and waves include resonance of jetties [22] and vibration induced by the slamming of a ship bottom in regular waves [23].

Models in wave tanks have contributed to a better understanding of dynamic effects induced by waves [24].

Structural Impact Models

Structural impact models are designed to predict the behaviour of a structural element or a structural system when subjected to an impulsive or an impact load.

The basic design of the model involves the geometry, the material, and the loading. The parameters usually create no major difficulties in the basic design. However, the complex geometrical details sometimes make the construction of a model that faithfully reproduces to scale every detail of every structural element prohibitively intricate and costly. The result is a compromise in which the model reproduces major features at an acceptable cost.

During a comprehensive study of the effect of diaphramgs in prestressed concrete girder and slab bridges [25], for example, four models were tested under static, cyclic, and impact loads. The experimental data were used to develop correlations with theory. The feasibility of using small scale Lexan plastic models to predict the response of a cylindrical element to impulsive loading [26] demonstrated the simultaneous use of strain gauges,accelerometers, and photoelasticity. The use of scale models to investigate the collapse of corrugated tubular sections has been reported [27].

Powerful explosives have been used to excite scale models of the primary coolant containment shell of an LMFBR to predict the structural dynamic response to a hypothetical accident [28]. The effects of waves on rectangular tank-like submerged objects have been studied using models [29]. One result of the study was the development of a format for use on model studies of submerged structures.

Vibration models

Vibration models differ from fluid dynamic models in that the influence of the deformation of the solid component of the system becomes significant. Non uniform fluid forces cause relative displacements in the solid that in turn cause variations in the fluid forces. These variations can become periodic and initiate large-scale effects that culminate in rupture of the solid eg. cavitation, fracture of a turbine blade, helicopter rotor, or aircraft wing. In such situations the model must account for the significant characteristics of the solid component of the system. These characteristics include the modulus of elasticity and damping: two characteristics of primary significance.

Their inclusion of course imposes additional requirements on the design of the model.

Scaling relationships used in designing models of systems in which vibrations in structural elements are induced by fluid flow have been discussed [30]. Special attention is given to flow-induced vibration of banks of cylinders in single phase, turbulent, cross flow. In a nuclear reactor, for example, the coolant is circulated through the core and the heat exchangers by means of large pumps.

Some of the energy generated in these circulating pumps appears as acoustic pressure waves in the coolant, which in turn can excite the reactor components into vibration. This acoustically induced vibration is a potential source of fatigue or wear.

An extensive model study of the coupled vibration and sound levels in an advanced gas-cooled nuclear reactor has been made by Fahy and Rivenaes [31]. This used a similar metal (steel) for the structure but used Freon to model the hot, compressed carbon dioxide heat exchanging gas. More recently an

acoustic vibration model of a sodium-cooled fast reactor has been made by Firth et al. [32]. In the paper the theoretical principles are described in some detail and an outline of the construction of a model is given, together with some preliminary results.

All these applications show that in vibration and shock investigation, scale modelling may provide a convenient method for determining the behaviour of complex mechanical systems. In this context plastic models have been particularly suitable for the analysis and design improvement of complicated or irregularly shaped structures, or of machinery structures on distributed foundations.

An extensive review of the use of scaled plastic models has been made by Bannister [33]. In this paper the Author illustrates how small scale plastic models have been used to study the behaviour of large structures. Scaling, plastic properties, model design and fabrication techniques have been reviewed in order to give the designer an insight into the employment of plastic models in studying structural systems.

If a plastic model is an exact scaled duplicate of a prototype structure, the resonance frequencies and average response levels of the model correspond closely with those of the prototype. Because of somewhat different damping in the model and prototype structures, peak levels of vibration do not correspond so well. This is usually of secondary importance however because the resonance frequencies, average response levels and mode shapes are of main interest.

The design of a dynamic model can be complex or fairly simple, depending upon the desired results from the labora-

tory test. For example, Bannister describes a 1/8 scale plastic model of a turbine-generator set installed on a bedplate in which the model does not include the flexibility of the turbine rotor. This can be ignored since the resonant magnification of the rotor is low due to the high damping in the oil-film bearings. The turbine rotor and turbine casing, therefore, were simulated by a central solid cylinder with a thin wall drum added to one end. The turbine weights, flexplates and casing flexibilities at the point of attachment to the bedplate are scaled, however. The generator was also simplified somewhat by making the stator from one block of plastic, but the mass and mass moment of inertia of the major components were scaled.

A simple model of a prototype generator is also described. Using a trifilar suspension system [34], the measured inertia of the simplified and more complex generator models about three axes were within one percent of each other. Further verification that the simple generator model was representative of the actual generator model was obtained from the dynamic vibration response of a complete model. The resonance frequencies of the first five major flexing modes of the turbine-generator, set on a bedplate with the simplified generator, were within one percent of the frequencies measured when a more exact model of the generator was used.

Plastic models have also been used successfully to determine the deflections and stresses of large complex structures under known static loads [35, 36]. These loads include torques and distributed gravity or inertia loads. Concentrated loads are usually applied to the model by means of small weights, flexible cords, and ball bearing pulleys.

The deflection can be measured with a linear variable differential transformer, and strain gauges are used to measure the stress.

An example of a static test is given by a 1/32 scale model of a yoke which is a major structural part of the 200-in Mt. Palomar telescope that was built in 1940. The yoke, which supported the major optical elements, was designed to rotate along the polar axis of the stars. This plastic model, built more than forty years ago, was used to minimize the distortion of the yoke which was caused by the weight of the optical equipment it supported. An optimum structural arrangement was determined from the static deflection test.

Another example of a static test is given by a 1/25 scale plastic model of ship hull and propulsion gear case. In this study the gear case distortion and misalignment caused by various ship hull loadings was investigated, since excessive distortion of the actual gear case had caused gear teeth failures. This model study showed the structural modidification needed to decrease gear case distortion substantially.

A 1/8 scale plastic model of two turbine - generator sets mounted on common bedplate was analyzed in the laboratory and the results were checked against a prototype in the shop [37]. The machinery configuration consisted of six components-two turbines, two generators and two symmetrical halves of a bedplate. The prototype's bedplate rested upon resilient mounts during testing to provide an impedance mismatch with the shop floor, while the model bedplate was suspended with shock cord during laboratory testing.

A detailed mode-shape comparison was made for the first nine major flexing modes of the prototype and its

scale model. The biggest discrepancy occurred at the fundamental flexing mode. The error of fourteen percent was probably caused by the difference in suspension system. Except for the first mode, the small discrepancies between model and prototype frequencies may be attributable to the construction of the model. Design simplifications may have slightly altered local flexibilities, and assembly methods may have affected the response, even though the masses and mass moments of inertia of the machinery were carefully scaled.

A comparison between the dynamic responses of scaled plastic models and full-sized steel prototypes have shown that agreement may not exist at resonance. Usually, the main purpose of a dynamic plastic model study is to learn how to design or modify a structure so that it will not resonate when driven by the operating forces of the machinery. The ability to predict the exact magnitude of the response is of secondary importance.

The amplitude of vibration transmitted from resiliently mounted machinery, through resilient mounts and foundations to a terminating structure, such as a floor of a building or the hull of a ship, has also been investigated using scale models [38]. It has been determined that to reduce the airborne or waterborne sound output of a particular resiliently mounted machine by modifying the foundation, it is necessary to control the natural frequencies of the foundation and to utilize the damping components of the termination [39].

These experimental results show that scale plastic models can be used to determine i) resonant frequencies, ii)

mode shapes, iii) average response levels. The investigations proved the feasibility of using scale models to study the vibration behaviour of many machines at low frequency.

In all these applications the models do not duplicate exactly the prototype which often is a complicated structure. In this case in fact the model cannot comply with all the modelling conditions, and therefore a "distorted model" has to be accepted: however these distortions may be introduced in such a way that little or no inaccuracy is involved, in relation to the practical problem is to be studied.

None of these dynamic models had as an objective the study of the acoustic field radiated by the vibrations of the structure.

The considerations developed to arrive at the construction of these dynamic plastic models, even though necessary, are not sufficient, when it is intended to extend their application to the prediction of the acoustic field produced by the motion of the structure. In this case, it is necessary to consider the sound propagation inside the cavity, the vibrations of the walls which enclose the cavity itself, as well as the vibrations of all those parts of the structure which affect the motion of the boundary surfaces.

From these observations it follows that first of all these models, which can be named acoustic-dynamic models, have to satisfy for the whole structure, the dynamic similarity conditions at least in the acoustic frequency range. Then they must comply with the acoustic similarity conditions as well.

The main aim of this thesis is to develop and check procedures to build correctly acoustic-dynamic models, which are able to predict the sound field produced inside enclosed shell-like structures excited mechanically or acoustically.

The problem of the coupling interaction between the vibrations of the structure and the acoustic field produced has been investigated initially. Then the wave equation in an acoustic medium and the equations of motion of simple structures such as bars, plates and shells, have been taken into consideration. The aim is to derive a transformation of all the quantities in these equations into a set of dimensionless parameters which leads to a system equation which is independent of size and thus applies directly to both prototype and model.

On the basis of these dimensionless parameters (the similarity conditions) a 1/5-scale plastic model of a tractor safety cab has been built. The comparison between experimental results performed on the prototype as well as on the model showed a satisfactory agreement and thus verified the use of this acoustic-dynamic model as a design tool.

The possibility of substituting the acoustic medium by Freon gases has been also examined. In this way, it is possible to increase the number of free parameters which can be chosen for the model design. If Freon is used in the model the frequency range of the model tests is not increased as much as would be required by the inverse of the linear scale factor. To demonstrate this, a simple apparatus has been built. It consists of a rigid cylindrical cavity that is closed at one end by a flexible panel. A filling and control system for the Freon allows one to change the acoustic medium and to keep it at the required thermodynamic conditions. With this apparatus it has been possible to verify that Freon 11 is a convenient gas for use with plastic models.

CHAPTER 2

Theoretical formulation of the acoustic and structural vibration problem

This chapter of the thesis deals with the formulation of the coupled equations that govern the dynamic response of a structure vibrating in a fluid. The excitations, can either be in the form of driving forces or sound waves incident upon the structure. The purpose of this derivation at this early stage is to clarify the nature of the uncoupled acoustic and elastic solutions that are combined to formulate the interaction problem. Although solutions to the coupled equations cannot be obtained in many practical situations, useful information concerning model scale factors often can be derived from them and the important variables identified. If in addition to the variables involved, the specific equations of motion describing the prototype are known, (in the form of differential or integral equations), additional modeling parameters often may be found which reduce the complexity of the model.

2.1 - Statement of the problem

The acoustic field produced inside closed structures, excited acoustically or by mechanical forces, is due to the elastic vibrations of the structure itself. The structure in its turn, responds to the effect of the acoustic field. The fluctuating pressure on the surface of the structure constitutes a small radiation and inertia loading.

To obtain the resultant load, this distributed load-

ing is combined with the applied forces that are the prime sources of the structural vibrations. Because of the low density of air compared to structural materials radiation loading exerted by the atmosphere is generally small enough to have a negligible effect on the structural vibrations.

Thus, in most situations, the dynamic response of a structure in the atmosphere, excited by prescribed driving forces, can be determined as though the structure were vibrating in a vacum. Subsequently the uncoupled acoustical problem of evaluating the pressure field generated by a velocity distribution prescribed over the boundary of the acoustic medium can be solved independently.

Radiation loading modifies the motion of a structure vibrating in the atmosphere only under unusal circumstances.

Examples of this are found when a volume of air in contact with the structure is confined in a small enclosure or when the structure is exceptionally light. In these situations a structure experiences radiation loading comparable to the inertial and elastic forces. The radiation loading thus modifies the forces acting on the structure and, since these acoustic pressures depend on the velocity, a "feed back coupling" between the acoustic medium and the structure takes place. Fig. 2.1 shows this dynamic interaction between an elastic structure and an acoustic medium.

2.2 - Formulation of the structural response

Consider an elastic structure characterized by one dimension that is small compared to its other dimensions, specifically, a plate or shell. This structure is excited in vacuo by a time-dependent driving force applied in a

direction normal to the surface: the time dependence of this force is harmonic, the exciting force varying periodically with a constant circular frequency.

The drive-point location where the force is applied is identified by a position vector $\bar{R}_j$, which is a function of the drive-point coordinates (figure 2.2). The explicit expression for the driving force, in terms of its point of application and time dependence, is

$$F\ (\bar{R}_j,\ t) = R_e\ |F\ (\bar{R}_j)\ e^{-i\omega t}| \qquad (2.1)$$

In subsequent work the symbol R_e is omitted for simplicity.

The solution of the equation of motion of the structure vibrating in vacuo gives the vector displacement of the structure at a field point $\bar{R}_k$:

$$\bar{d}\ (\bar{R}_k,\ t) = |v(\bar{R}_k)\ \bar{\zeta} + w(\bar{R}_k)\bar{\zeta} + u(\bar{R}_k)\bar{\eta}|\ e^{-i\omega t} \qquad (2.2)$$

We shall here restrict our attention to the displacement component $w(\bar{R}_k)$ normal to the surface of the structure. This is done because the tangential and longitudinal displacements make little contribution to the sound radiation.

The formal solution of the elastic problem can be espressed in terms of a "mechanical mobility" function $\Gamma(\bar{R}_k/\bar{R}_j)$, which relates the normal velocity at a field point $\bar{R}_k$ to a force applied normally to the structure at the drive point $\bar{R}_j$:

$$\dot{w}(\bar{R}_k) = \Gamma(\bar{R}_k/\bar{R}_j) \cdot F(\bar{R}_j) \qquad (2.3)$$

When the field and drive points coincide ($\bar{R}_k = \bar{R}_j$) Γ is referred to as the "drive-point mobility". When the field and drive points do not coincide ($\bar{R}_k \neq \bar{R}_j$), Γ is the "transfer mobility".

The structural response to simultaneous normally applied exciting forces at N different points of the structure is obtained by superposition of the responses to the individual forces:

$$\dot{w}(\bar{R}_k) = \sum_{j=1}^{N} F(\bar{R}_j) \cdot \Gamma(\bar{R}_k/\bar{R}_j) \tag{2.4}$$

If the excitation is in the form of a distributed load, such as the sound pressure, the formal solution becomes a surface integral over the structure.

An area element of the structure is identified by a position vector, as $dS(\bar{R}_j)$. When the distributed force is the radiation loading, the surface of integration coincides with the structure-fluid interface.

Taking the force resulting from the pressure as positive in a direction opposite to the response $\dot{w}$, the formal solution of the structure now becomes

$$\dot{w}(\bar{R}_k) = -\int_S p(\bar{R}_j) \cdot \Gamma(\bar{R}_k/\bar{R}_j) dS(\bar{R}_j) +$$

$$+ \sum_{j=1}^{N} F(\bar{R}_j) \cdot \Gamma(\bar{R}_k/\bar{R}_j) \tag{2.5}$$

This equation represents the solution of the in vacuo structural problem, uncoupled from the acoustical problem. It is written in terms of the normal velocity components, and restricted to exciting forces applied normally to the structure.

2.3 - Formulation of the acoustic pressure field

The solution of the uncoupled acoustical problem consists of finding the pressure p at a field point $\bar{R}_j$ in response to an acoustic source at a point $\bar{R}_o$.

For our present purpose the source locations can be restricted to be on a rigid boundary coinciding with the interface of the structure with the acoustic medium. A rigid surface is defined here as having vanishing mechanical mobility.

Restricting ourselves to harmonic time variation, a point source is characterized by its strength which can be defined as its volume velocity:

$$P(\bar{R}_o,\ t) = \dot{w}(\bar{R}_o)\ dS(\bar{R}_o)\ e^{-i\omega t} \qquad (2.6)$$

The formal solution can be expressed conveniently in terms of an acoustical Green's function $G(\omega,\bar{R}_j/\bar{R}_o)$. The solution is obtained by multiplying the strength of the source by the Green's function as shown:

$$p(\bar{R}_j,t) = G(\bar{R}_j/\bar{R}_o)\ \dot{w}(\bar{R}_o)\ dS(\bar{R}_o)\ e^{-i\omega t} \qquad (2.7)$$

The resultant pressure produced by N sources can be expressed as a sum, in the form of equation (2.4). The limit of a continuous distribution of infinitesimal sources is equivalent to a prescribed velocity distribution over the boundary.

Suppressing the harmonic time dependence, the formal solution becomes a surface integral over the boundary

$$p(\bar{R}_j) = \int_S \dot{w}(\bar{R}_o) \cdot G(\bar{R}_j/\bar{R}_o) \cdot dS(\bar{R}_o) \qquad (2.8)$$

2.4 - The integral equation of the structure-fluid interaction

Having stated the formal solutions of the uncoupled structural and acoustical problems, the solution of the interaction problem can now be formulated.

Consider an elastic structure excited by N forces F_j, immersed in an acoustic fluid and hence exposed to radiation loading in the form of equation (2.8) with the field points $\bar{R}_j$ located on the structure-fluid interface. The acoustic surface pressure now contributes to the oscillatory forces applied to the structure and must therefore be included when computing the dynamic response of the strcture. When this acoustic surface pressure is substituted for $p(\bar{R}_j)$ in equation (2.5), the dynamic response of the submerged structure becomes

$$\dot{w}(\bar{R}_k) = -\int_S \Gamma(\bar{R}_k/\bar{R}_j) \cdot \left[\int_S \dot{w}(\bar{R}_o)\ G(\bar{R}_j/\bar{R}_o)\ dS(\bar{R}_o)\right] dS(\bar{R}_j)$$

$$+ \sum_{j=1}^{N} F(\bar{R}_j) \cdot \Gamma(\bar{R}_k/\bar{R}_j) \qquad (2.9)$$

Since $\dot{w}(\bar{R}_o)$ is unknown, the response $\dot{w}(\bar{R}_k)$ of the structure is the solution of an integral equation.

The discussion up to now has dealt with an elastic structure excited by prescribed concentrated forces.
Another situation of interest is a structure exposed to an incident sound wave. The dynamic response of such a structure is the solution of an integral equation of the form of equation (2.9), whose inhomogeneous term embodies the pressure $p(\bar{R}_j)$ on the surface of a rigid target. The configuration coincides with the outer surface of the actual,elastic target. From equations (2.8) and (2.9) one obtains:

$$\dot{w}(\bar{R}_k) = - \int_S \Gamma(\bar{R}_k/\bar{R}_j) \cdot \left[\int_S \dot{w}(\bar{R}_o)\ G(\bar{R}_j/\bar{R}_o)\ dS(\bar{R}_o) \right] dS(\bar{R}_j) + \int_S p(\bar{R}_j)\ \Gamma(\bar{R}_k/\bar{R}_j)\ dS(\bar{R}_j) \qquad (2.10)$$

2.5 - Considerations of the solution of the integral equation

Some approaches to the solution of equation (2.9) and (2.10) are described in the leterature [40]. Rather than applying these powerful, general techniques, many authors have evolved simpler specialized techniques for specific structural configurations, thus circumventing the need for solving the integral equation. This is the case of the study of the acoustic field and the normal modes of fluid-filled spherical shells developped by Junger and Feit [41].For the study of a rectangular panel backed by a closed rectangular cavity, A.J. Pretlove [42] gives an exact solution for the acoustic velocity potential; the panel was flexible while the other walls of the cavity were assumed to be rigid.

A simplified approach to coupled panel-cavity vibrations was also presented by Pretlove and Craggs [43]. Pagliarini and Pompoli [44] investigated a different geometrical configuration studying the sound pressure field within a cylindrical chamber with a flexible end wall.

The finite element method has been used in recent years to obtain approximate solutions for irregular shaped enclosures which have no analytical solution. Early contributions to the development of this technique were made by Craggs [45-47], Le Salver and Jennequin [48] and Shuku and Ishihava [49]. These were aimed at the provision of a practical method for analysing the acoustics of the automobile

passenger compartment. More recently, a general purpose finite element computer program, NASTRAN (NASa STructural ANalysis) [50, 51] was adapted by Wolf and Nepske [52] for the study of automobile interior noise, and its application in structural- acoustic analysis of the passenger compartment has been described [53, 54]. These developments of the finite element method for acoustic analysis have also been accompanied by experimental verification of the techniques. By using scale models of automobile compartments,the finite element predictions were verified experimentally by Shuku and Ishihara [49], Petyt et al. [55] and Richards and Jha [56].

Although an exhaustive description of this finite element technique is beyond the scope of this work, it has been considered of some interest to give a brief review of this general and powerful technique. This approach is likely to be used more widely for studying the acoustics of many kinds of vehicles. The finite element technique will be applied in section (4.7.3), to compute the acoustic resonance frequencies of the cab and to make comparison with the model results.

2.5.1 - Structural-acoustic finite element analysis

One of the main applications in acoustics of the finite element technique is the analysis of the acoustic modes and interior noise levels of a closed cavity. Two types of boundary conditions may be assumed: rigid walls or flexible walls.

The knowledge of these acoustic modes is particularly valuable in preliminary vehicle design. Major resonance fre

quencies of the panels enclosing the cavity which might occur at or near acoustic resonances, can be anticipated and then designed out.

More explicit structural design information can often be obtained from a forced vibration analysis in which the interior sound pressure field risulting from forced motion of the wall panels is computed. In this case the structural characteristics and the exciting forces must be known from tests or theoretical analysis.

More difficult is the case when the acoustic field may modify significantly the dynamic response of the structure. In this case it is also possible to predict resonance frequencies of the cavity as well as sound pressure distribution produced by external forces.

2.5.1.1 - Governing equations and finite element formulation

For an enclosed cavity, V, the governing equation for the sound pressure p is the well-known acoustic wave equation:

$$\nabla^2 p(\bar{R}_j) - \frac{1}{c_o^2} \frac{\partial^2 p(\bar{R}_j,t)}{\partial t^2} = 0 \qquad (2.11)$$

On the surfaces of the enclosed cavity the pressure field must satisfy the following conditions:

$$\left.\frac{\partial p(\bar{R}_j)}{\partial \bar{n}}\right|_S = - \rho_o \frac{\partial^2 w(\bar{R}_o)}{\partial t^2} \qquad (2.12)$$

For a hard surface (i.e. rigid) $\partial p/\partial n = 0$.

If one discretizes the cavity volume and represents it with finite elements, then the wave equation (2.11) can be reduced to a set of matrix equations of the form [57]:

$$|B| \{\ddot{p}\} + |C| \{p\} = - (\rho_o c_o) |A|^T \{\ddot{w}\} \qquad (2.13)$$

where the column matrix {p} gives the pressure at the grid points of the finite element mesh, |C| and |B| represent acoustic mass and siffness matrices, $\{\ddot{w}\}$ is the structural acceleration vector, and $|A|^T$ is the transposed matrix of the boundary surface areas of the acoustic cavity model. Equation (2.13) is the basic finite element equation which must be solved for acoustic analysis.

In the case of structural-acoustic interaction, the wall panels react to the cavity pressure and the structural motion couples with the acoustic field through the pressure loadings on the panels. In this case the structural finite element equations can be written as:

$$|M|\{\ddot{w}\} + |D| \{\dot{w}\} + |K| \{w\} = |A| \{p\}+\{F\} \qquad (2.14)$$

where {w} designates the structural desplacement vector |M|, |D| and |K| represent structural mass, damping, and stiffness matrices, {F} is the vector of external forces applied to the structure, and |A| is the structural-acoustic coupling matrix of the boundary surface area.

If rigid walls are assumed in the finite element model for the boundary panels($\{\ddot{w}\} = 0$ in equation (2.13)), then the only data necessary to compute the resonances of the cavity are its geometric data. In this hypothesis equation (2.13) may assume this form:

$$|G|\{p\} = 0 \tag{2.15}$$

If flexible walls are considered, then equation (2.13) may be written:

$$|G|\{p\} = -i\omega \ |A|\{\dot{w}\} \tag{2.16}$$

In order to find the solutions, it is necessary to find the matrix of coefficient $|G|$. The algorithm to compute this matrix is complicated and it depends on the element type (geometry, number of nodes) and on the form of the approximating function (linear, non-linear) within each element [58]. In general each element of $|G|$ contains ω as a parameter. In the case of the rigid wall, the second term of equation (2.15) beeing zero, it is necessary that the determinant of matrix $|G|$ be zero. This means that only some values of this condition will be satisfied (i.e. $|G(\omega)| = 0$). The n eigenvalues of this matrix will give the n acoustic modes of the cavity. In this case, however, only the resonance frequency of the cavity will be obtained. Information on the acoustic field produced by external forces can not be obtained.

In the case of flexible walls, the circular frequency ω is known and in general it will not reduce the determinant of matrix $|G|$ to zero. Therefore it will be possible to get the acoustic pressure at each element by the following relation:

$$\{p\} = -i\omega \ |G|^{-1} \ |A|\{\dot{w}\} \tag{2.17}$$

which has been obtained from the hypothesis that the inverse of the matrix $|G|$ exists.

It is easy to note the similarity between the equations (2.17) and (2.8): the elements of $|G|^{-1}$ represent the values of the Green function between the volume elements and those of the flexible walls.

Assuming that the flexible walls are not mechanically excited by external forces, and that from equation(2.14) it is possible to derive the velocity $\{\dot{w}\}$ as a function of the sound pressures $\{p\}$, the solution will be of the form:

$$\{\dot{w}\} = |\Gamma|^{-1} |A|\{p\} \tag{2.18}$$

Substituting this value into equation (2.16) one obtains:

$$|G|\{p\} + i\omega|A||\Gamma|^{-1}|A|\{p\} = 0 \tag{2.19}$$

which can also be written as:

$$|Q|\{p\} = 0 \tag{2.20}$$

The matrix $|Q|$ can be obtained from matrices $|G|$, $|A|$ and $|\Gamma|$ by the usual rules of the matrix calculus.

In order for equation (2.20) to be satisfied, the determinant of the matrix $|Q|$ must be zero: this happens only for "n" values of ω (the eigenvalues).

The resonat frequencies of the cavity with flexible walls may be computed in a similar way. These values are usually different from those of rigid walled cavities. However, if the system is characterized by an acoustic stiffness which is considerably less than the panel stiffness, this difference becomes negligible.

In the case of an enclosed cavity with flexible walls

mechanically excited by a force {F}, equation (2.18) becomes:

$$\{\dot{w}\} = |\Gamma|^{-1} \left(|A|\{p\} + \{F\}\right) \tag{2.21}$$

Substituting this equation into equation (2.16) one obtains

$$\left(|G| + i\omega|A||\Gamma|^{-1}|A|\right)\{p\} = -i\omega|A||\Gamma|^{-1}\{F\} \tag{2.22}$$

Writing now:

$$|U| = |G| + i\omega|A||\Gamma|^{-1}|A| \tag{2.23}$$

from equation (2.22) it follows:

$$\{p\} = -i\omega|U|^{-1}|A||\Gamma|^{-1}\{F\} \tag{2.24}$$

As will be explained in section (4.6.2), the term:

$$|H|^{-1} = -i\omega|U|^{-1}|A||\Gamma|^{-1} \tag{2.25}$$

which on substituting in equation (2.24) gives:

$$\{p\} = |H|^{-1}\{F\} \tag{2.26}$$

may be considered to be the frequency response function between force and sound pressure.

A general solution of the structural-acoustic problem may be found in the NASTRAN computer program [50, 51], which was first adapted for automobile structural acoustic analysis in 1975 [52].

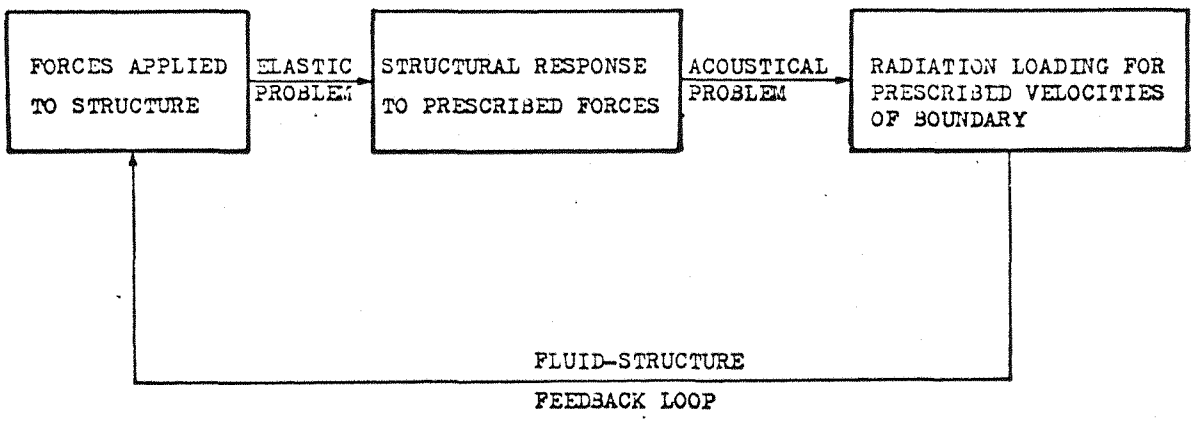

Figure 2.1 Diagram illustrating the dynamic interaction of an elastic structure and an acoustic medium.

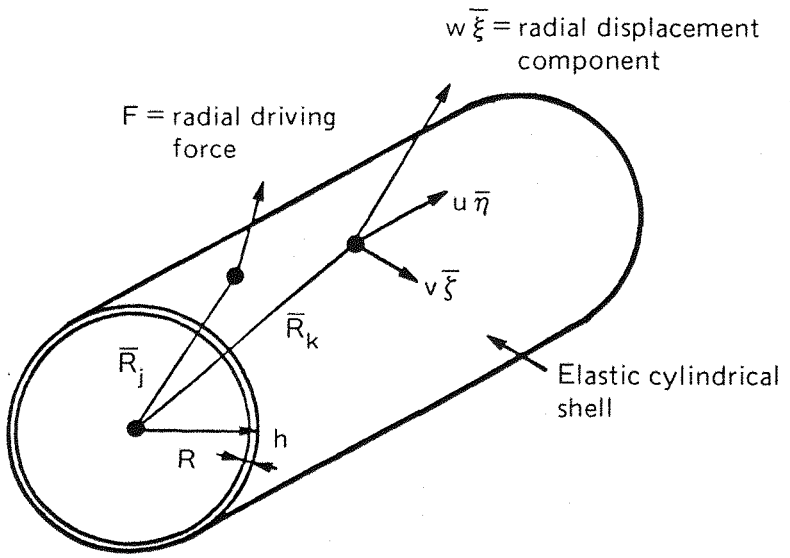

Figure 2.2 Location of drive and field points illustrated for a cylindrical shell.

CHAPTER 3

Similarity condition for acoustic-dynamic models

The formulation of the acoustic and structural interaction so far developped presents the advantage to point out the mutual influence between acoustic field and elastic structural vibrations, but the solution of equations(2 9) and (2 10) is generally so difficult that practically it becomes useless. Real structures are usually in fact so complicated that these equations are without solution.

To study the acoustic and dynamic behaviour of such a structure, experimental measurements are required in order to investigate the velocity of the structure, the impedance of the structure, and the sound pressure levels of the acoustic field. It has been already observed that in many situations these experimental measurements on the prototype are expensive in time and effort, and do not make it possible to test rapidly the effects of structural modifications.

In such a case scale modelling may provide a convenient method for determining the behaviour of complex mechanical systems at least in comparison with the direct investigation of the real structure. In fact, where prototypes of a large physical size are involved, small scale models often are comparatively inexpensive to build and test.

Moreover models may often be designed in such a way that the necessary measurements are simpler than they would be on the prototype. The fact that the model measurements can be made in the laboratory, and that repeated tests can

usually be made at the convenience of the experimenter, may also be an important advantage. The models may often be designed in a simpler form than the prototype, and hence the problem of the control and the variation of the parameters during test may be simplified.

The use of scale models may show some disadvantages such as the impossibility of reproducing all the important features of the prototype. In these cases the investigator must be sure that the elements of the system which are not correctly modelled do not influence the test significantly. Care must be taken to ensure that such approximations do not reduce the accuracy of the results to an unsatisfactory level. The precision required for measurements on small models may be difficult to attain. For example, the use of a small scale structural model may involve such small deflection that a very precise measuring device is required.

In general, the more that is known about the behaviour of the prototype, and of the laws which describe it, the easier it is to design the model, but the less necessary the model is. The optimum situation for model application is that in which the general features of prototype behaviour may be known, but in which such details as complex geometry may make it difficult to obtain quantitative information by analytical means.

The conditions for designing and testing a model can be obtained by one of several methods which can be derived from the basic principles of dimensional analysis [59, 60].

3.1 - Dimensional analysis

A consideration of the dimensions of the quantities appearing in a physical problem may lead to useful information about the nature of the solution. The equations embodying the fundamental laws of mechanics are independent of the size of the fundamental units, and hence any equation derived from these fundamental laws also have this same independence. Such equations are called physical equations.

Suppose that in a particular system involving N fundamental units there are n variables (v_1, v_2, ...,v_n) which are of importance. The behaviour of the system is described by a physical equation

$$f\ (v_1,\ v_2,\ .....,\ v_n) = 0 \qquad (3.1)$$

If it is required that the function f (v_1, v_2...,v_n) be unchanged under a change in size of the fundamental units entering into the v's, it can be shown that it is always possible to write the equation in the form [61]:

$$F(\pi_1,\pi_2,.....,\pi_{n-N}) = 0 \qquad (3.2)$$

where the π terms are dimensionless factors. The factors themselves are composed of products of powers of the variables v and involve not more than (N + 1) variables in any one factor. Since the v's themselves are formed of products of powers of the fundamental units, the dimensionless π factors also must be products of powers of the fundamental units.

The above considerations can be summarized in the form of the Buckingham theorem [62].

A physical equation having n variables in N fundamental units can be written as

$$F\ (\pi_1,\pi_2,....,\pi_{n-N}) = 0 \qquad (3.3)$$

where the π factors are independent dimensionless terms having the form of products of powers of the variables.The number of such terms will be not less than $(n - N)$.".

3.2 - The theory of models

The basic theory of models can be developed directly from the preceding discussion of dimensional analysis. Suppose the variables which are important for the particular problem are known. The theorem, equation (3.3), indicates that the variables can be arranged in dimensionless groups so that the equation describing the system is

$$F\ (\pi_1, \pi_2, ...) = 0 \tag{3.4}$$

Since these terms are independent, each will involve one variable which does not appear in the other terms. Solving this equation for the factor which contains the variable of primary importance in the particular problem yields:

$$\pi_1 = F'(\pi_2, \pi_3, ...). \tag{3.5}$$

Since this is a general relationship, it will apply to both prototype and model:

$$\begin{aligned} \pi_{1p} &= F'(\pi_{2p},\ \pi_{3p}\ ....), \\ \pi_{1m} &= F'(\pi_{2m},\ \pi_{3m}\ ....). \end{aligned} \tag{3.6}$$

If the model is designed and tested so that

$$\pi_{2m} = \pi_{2p},\quad \pi_{3m} = \pi_{3p},\ .... \tag{3.7}$$

then the functions are equal:

$$F'\ (\pi_{2p}, \pi_{3p}, ...) = F'(\pi_{2m},\ \pi_{3m}, ...) \tag{3.8}$$

Thus

$$\pi_{1p} = \pi_{1m} \qquad (3.9)$$

Equations (3.7) are the conditions which specify the design and method of testing of the model, and from equation (3.9) the prototype behaviour can be determined in terms of the model behaviour. Equations (3.7) are called the "design equations", (or "similarity conditions") and equation (3.9) is called the "prediction equation".

3.3 - Model analysis based on the equations of motion

There are three basic methods of establishing model equations and test conditions all based on the dimensional analysis principles.

i. If all that is known about the prototype is that the basic mechanical quantities of force, mass, length and time are sufficient to describe its behaviour, the model laws can be based on a general principle of dynamic similarity. The model conditions in such a case are comparatively restrictive, and model studies of complex systems may become difficult.

ii. If more information is available about the problem, to the extent that the specific variables which are important and those that can be neglected are known, modelling conditions based on dimensional analysis become less restrictive, and model techniques may be much simplified.

iii. If in addition to the variables involved, the specific equations of motion describing the prototype are known, in the form of differential or integral equations, additional modelling parameters often may be found which further reduce the complexity of the model.

Considering that the structures of vehicles very often can be regarded as made up of bars, plates and shells (whose equation of motion are well known), this third (iii) method of establishing model equations may be the most suitable.

In fact, when the specific equations of motion describing the system of parts of it are known, the modelling conditions may be derived by transformation of all the quantities in the equation into a set of dimensionless parameters.This leads to a system equation which is independent of size,and thus applies directly to both protype and model.

In the following paragraphs this method will be employed. At first the wave equation in an acoustic medium will be considered, this will be followed by the equation of motion of structures excited acoustically or/and mechanically. As has been mentioned already, three kind of simple structural elements will be treated: bars, plates and shells. The problem of the acoustic and structural interaction will be finally taken into consideration: in this way the feed-back loop of figure (2.1) will be closed.

3.3.1 - Assumptions

Both the fluid and the structure are assumed to obey linear constitutive equations. For the structure this means that each component of stress is a linear function of the strain components and, for the fluid, that pressure deviations from the hydrostatic pressure are a linear function of the fractional density change (the condensation) and of the corresponding fractional volume change (the dilatation).

The equations of motion of these media are thus restricted to small quantities. The solid and fluid media are assumed to be homogeneous and initially at rest. The acous-

tic fluid is inviscid, and thus can exert only normal loads on the structure.

3.3.2 - Acoustic equation

With these hypotheses, it is possible to show that the acoustic pressure in an acoustic medium is described by the three-dimensional wave equation:

$$\nabla^2 p(\bar{R}_j) - \left(\frac{1}{c_o^2}\right) \frac{\partial^2 p(\bar{R}_j,t)}{\partial t^2} = 0 \qquad (3.10)$$

Considering a harmonic solution of the form:

$$p(\bar{R}_j,t) = p(\bar{R}_j)\, e^{-i\omega t} \qquad (3.11)$$

the wave equation becomes:

$$(\nabla^2 + k^2)\, p(\bar{R}_j) = 0 \qquad (3.12)$$

This is the three-dimensional Helmoltz equation for steady-conditions. The pressure field on the radiating surface must satisfy the following condition:

$$\left.\frac{\partial p(\bar{R}_j)}{\partial \bar{n}}\right|_s = -\rho_o \frac{\partial^2 w(\bar{R}_o)}{\partial t^2} = \rho_o \omega^2\, w(\bar{R}_o) \qquad (3.13)$$

The variables in these equations can now be transformed to the following dimensionless variables:

$$\begin{aligned} \nabla^{*2} &= L^2\nabla^2, & p^* &= p/\bar{p}, \\ t^* &= \omega t, & w^* &= w/L, \\ n^* &= n/L, \end{aligned} \qquad (3.14)$$

where L is a characteristic length of the radiating surface; ∇^*, p^*, w^*, n^*, are dimensionless variables and $\bar{p}$ a constant reference-value.

In these new variables, equations (3.10) and (3.13) become:

$$\bar{p}\left[\nabla^{*2} p^* - \left(\frac{1}{c_o^2}\right) \omega^2 L^2 \frac{\partial^2 p^*}{\partial t^{*2}}\right] = 0 \qquad (3.15)$$

$$\frac{\partial p^*}{\partial n^*} = \frac{\rho_o \omega^2 L^2}{\bar{p}} \cdot w^*. \qquad (3.16)$$

The modelling conditions thus become:

$$\frac{\omega L}{c_o} = \text{const}, \qquad (3.17)$$

$$\frac{\rho_o \omega^2 L^2}{\bar{p}} = \text{const}. \qquad (3.18)$$

Condition (3.17) states that if the acoustic medium is unchanged, frequencies increase as the length decreases.

Condition (3.18) states that, if the acoustic medium is always unchanged, and condition (3.17) holds, the acoustic pressure is the same. Both these conditions must be maintained when an acoustic model is to be built.

3.3.3 - Longitudinal vibrations of an elastic bar

Elastic structures characterized by a dimension that is small compared to its other dimensions have been considered in Chapter 2; in the following paragraphs longitudinal and flexural vibrations of bars will be examined.

The longitudinal vibrations of bars are not usually themselves an important source of sound radiation, but they can excite flexural waves in plates and shells that might be attached to them and these flexural waves can be efficient sound radiators.

The end constraints on the bars are replaced by forces and moments. The axial force applied at the end of the bar is not a forcing term but a boundary condition of the structure. However any plates that are connected to the bar transmit forcing actions to the bar itself. This forcing action is indicated in the following equations as q' | N/m | .

Consider a long thin elastic bar, of uniform cross-sectional area A, with its centre line in the x-axis. If during the motion of the structure, the cross-section remains plane and the stress over it is uniform, the equation of motion can be obtained by using a force balance between the elastic and inertial forces acting on a small portion of the bar. The equation of motion for longitudinal vibrations is then:

$$\frac{\partial^2 u(x,t)}{\partial x^2} = \frac{\rho}{E} \frac{\partial^2 u(x,t)}{\partial t^2} + \frac{q'_t(x,t)\cdot L}{EA} \quad . \tag{3.19}$$

The boundary conditions are as follows:
fixed edges:

$$u(x=0,t) = 0 \tag{3.20}$$

free-excited-edges:

$$N(x=0,t) = EA \frac{\partial u(x=0,t)}{\partial x} = F(t) \tag{3.21}$$

The variables of these equations are now transformed into the following dimensionless variables:

$$t^* = t\cdot\omega \ , \qquad u^* = u/L, \qquad x^* = x/L. \tag{3.22}$$

With these new variables equations (3.19), (3.20) and (3.21) become:

$$\frac{\partial^2 u^*}{\partial x^{*2}} = \frac{\rho}{E} \omega^2 L^2 \frac{\partial^2 u^*}{\partial t^*} + \frac{q'_t L}{EA}, \tag{3.23}$$

$$u^*(x^* = 0,\ t^*) = 0, \tag{3.24}$$

$$\frac{\partial u^*}{\partial x^*} = \frac{F}{EA}. \tag{3.25}$$

The modelling conditions are thus as follows:

$$\frac{\rho\ \omega^2 L^2}{E} = \text{const.} \tag{3.26}$$

$$\frac{q'_t \cdot L}{EA} = \text{const,} \tag{3.27}$$

$$\frac{F}{EA} = \text{const.} \tag{3.28}$$

The first condition relates the frequency to the sound velocity ($c = \sqrt{E/\rho}$). If condition (3.17) is to satisfied also, it follows that the sound velocity in the structure must remain constant.

3.3.4 - Flexural vibrations of an elastic bar

An elastic beam, in addition to its longitudinal motion, can also vibrate in a transverse direction normal to the longitudinal axis.

Consider a long, slender beam of uniform cross-section whose center line lies on the x-axis. The forces causing the motion of the beam act in transverse plane of symmetry and vary periodically with a constant circular frequency.

In the elementary theory of bending, cross - sections initially perpendicular to the neutral surface are assumed to remain so after deformation. Using these hypotheses the equation of motion becomes:

$$\frac{\partial^4 w}{\partial x^4} + \frac{\rho A}{EI}\frac{\partial^2 w}{\partial t^2} = \frac{q'_n(x,t)}{EI}\ , \tag{3.29}$$

subjects to the boundary conditions:

$$\text{free edges:} \quad \frac{\partial^3 w}{\partial x^3} = -\frac{F}{EI}, \quad \frac{\partial^2 w}{\partial x^2} = -\frac{M}{EI}, \tag{3.30}$$

$$\text{fixed edges:} \quad w = 0, \quad \frac{\partial w}{\partial x} = 0, \tag{3.31}$$

$$\text{hinged edges:} \quad w = 0, \quad \frac{\partial^2 w}{\partial x^2} = -\frac{M}{EI}, \tag{3.32}$$

where F and M are concentrated loads applied at the end of the beam.

As usual, the following dimensionless parameters are substituted into the previous equations.

$$t^* = t\omega, \quad w^* = w/L, \quad x^* = x/L. \tag{3.33}$$

It follows:

$$\frac{\partial^4 w^*}{\partial x^{*4}} + \frac{\rho A}{EI}\omega^2 L^4 \frac{\partial^2 w^*}{\partial t^{*2}} = -\frac{L^3 q'_n}{EI}, \tag{3.34}$$

$$\frac{\partial^3 w^*}{\partial x^{*3}} = -\frac{FL^2}{EI}, \quad \frac{\partial^2 w^*}{\partial x^{*2}} = -\frac{M}{EI}, \tag{3.35}$$

$$w^* = 0, \quad \frac{\partial w^*}{\partial x^*} = 0, \tag{3.36}$$

$$w^* = 0, \quad \frac{\partial^2 w^*}{\partial x^{*2}} = -\frac{ML}{EI}, \tag{3.37}$$

The modelling conditions are thus:

$$\frac{\rho A\ \omega^2 L^4}{EI} = \text{const} \tag{3.38}$$

$$\frac{q'_n L^3}{EI} = \text{const} \tag{3.39}$$

$$\frac{FL^2}{EI} = \text{const} \tag{3.40}$$

$$\frac{ML}{EI} = \text{const} . \qquad (3.41)$$

The first condition links the frequency scale with the properties of materials (E/ρ) and with the parameter $I/A=r^2$ (where r is the radius of gyration). This must always satisfied. If conditions (3.17) and (3.26) are satisfied, it follows from condition (3.38) that:

$$\frac{r}{L} = \text{const.} \qquad (3.42)$$

The equations relating to the boundary conditions (3.39) to (3.41) are equivalent, but for true similarity the condition (3.42) must also be satisfied.

3.3.5 - Longitudinal vibrations of thin elastic plates

The wave equation of longitudinal vibration of thin elastic plates is substantially the same as the equation (3.19) for bars. In this case however, the lateral contraction of the volume element of the plate is restrained, and therefore Young's modulus E must be devided by the Poisson's Ratio factor $(1-\nu^2)$.

Equation (3.19) now becomes:

$$\frac{\partial^2 u}{\partial x^2} = \frac{\rho(1-\nu^2)}{E}\frac{\partial^2 u}{\partial t^2} + \frac{q_t \cdot b(1-\nu^2)}{E\, h \cdot b} \qquad (3.43)$$

where h is the thickness of the plate and b its width.

In the same way equation (3.21) becomes:

$$\left.\frac{\partial u}{\partial x}\right|_{x=0} = \frac{q'_t(1-\nu^2)}{E\, h} . \qquad (3.44)$$

It is important to note that q_t is a tangential load

$|N/m^2|$ applied on the plate surface, while q'_t is a linear load $|N/m|$ applied at the free edge of the plate. Using the same dimensionless variables of equation (3.22),one obtains:

$$\frac{\omega^2 L^2 \rho(1-\nu^2)}{E} = \text{const}, \tag{3.45}$$

$$\frac{q_t L(1-\nu^2)}{E\,h} = \text{const}, \tag{3.46}$$

$$\frac{q'_t(1-\nu^2)}{E\,h} = \text{const}. \tag{3.47}$$

3.3.6 - Flexural vibrations of thin elastic plates

If h is the uniform thickness of an elastic plate, oriented so that its underformed middle surface contains the x and y axes of a rectangular coordinate system, the equation of motion governing the displacement $w(\bar{R}_k)$ which is perpendicular to the middle surface of the plate is [63]:

$$\nabla^4 w + \frac{\rho 12(1-\nu^2)}{E\,h^2} \cdot \frac{\partial^2 w}{\partial t^2} = -\frac{q_n 12(1-\nu^2)}{E\,h^3}. \tag{3.48}$$

The boundary conditions are:

fixed edge:

$$w\Big|_l = 0\,, \quad \frac{\partial w}{\partial y}\Big|_l = 0 \tag{3.49}$$

hinged edge:

$$w\Big|_l = 0\,, \quad \frac{\partial^2 w}{\partial y^2}\Big|_l = -\,m\,\frac{12(1-\nu^2)}{E\,h^3}, \tag{3.50}$$

free edge:

$$\frac{\partial^3 w}{\partial y^3} + (2-\nu)\,\frac{\partial^3 w}{\partial x^2 \partial y}\Big|_l = \frac{12(1-\nu^2)}{E\,h^3}\,(\tau + \frac{\partial m}{\partial y}), \tag{3.51}$$

$$\left.\frac{\partial^2 w}{\partial y^2} + \nu \frac{\partial^2 w}{\partial x^2}\right|_1 = \begin{cases} 0 \\ -m \dfrac{12(1-\nu^2)}{E\,h^3}, \end{cases} \tag{3.52}$$

m is the moment per unit length and τ is the shear force per unit length.

With the usual dimensionless variables,

$$t^* = t\omega \qquad x^* = x/L \qquad y^* = y/L \tag{3.53}$$
$$w^* = w/L \qquad \nabla^{*4} = \nabla^4 L^4$$

Equations (3.48) to (3.52) become:

$$\nabla^{*4} w^* + \frac{\omega^2 L^4 \rho(1-\nu^2)}{E\,h^2} \cdot 12 \frac{\partial^2 w^*}{\partial t^{*2}} = -12 \frac{q_n L^3 (1-\nu^2)}{E\,h^3}, \tag{3.54}$$

fixed edge:

$$w^* = 0\,, \quad \frac{\partial w^*}{\partial y^*} = 0, \tag{3.55}$$

hinged edge:

$$w^* = 0\,, \quad \frac{\partial^2 w^*}{\partial^2 y^{*2}} = -12 \frac{mL(1-\nu^2)}{E\,h^3}, \tag{3.56}$$

free edge:

$$\frac{\partial^3 w^*}{\partial y^{*3}} + (2-\nu) \frac{\partial^3 w^*}{\partial x^{*2} \partial y^*} = 12 \frac{L^2(1-\nu^2)}{E\,h^3} \left(\tau + \frac{\partial m}{\partial y}\right),$$

$$\frac{\partial^2 w^*}{\partial y^{*2}} + \nu \frac{\partial^2 w^*}{\partial x^{*2}} = -12 \frac{mL(1-\nu^2)}{E\,h^3}. \tag{3.57)(3.58}$$

The modelling conditions are thus:

$$\frac{\omega^2 L^4 \rho(1-\nu^2)}{E\,h^2} = \text{const}, \tag{3.59}$$

$$\frac{q_n L^3 (1-\nu^2)}{E\,h^3} = \text{const}. \tag{3.60}$$

$$\frac{mL(1-\nu^2)}{E\,h^3} = \text{const}, \tag{3.61}$$

$$\left(\tau + \frac{\partial m}{\partial y}\right)\frac{L^2(1-\nu^2)}{E\,h^3} = \text{const}, \tag{3.62}$$

$$\nu = \text{const}. \tag{3.63}$$

The first equation, shows that for bending vibrations the thickness h must be included in the non-dimensional parameter. Equation (3.60) and (3.61) give the conditions for scaling the external loads. Finally, equations (3.62) and (3.63), give more restrictions for the case of plate with free edges. Condition (3.63) is particularly strict, as it is difficult to find modelling material with the same Poisson's ratio as in the prototype.

3.3.7 - Shell vibrations

In this section the vibrations of structural elements that in their underformed state have an appreciable amount of curvature are considered. The vibration behaviour of shell-like structures has gained increasing engineering importance in aeronautics and astronautics.

Analytical solutions of this problem exist only in the case of simple geometric shapes, such as cones, cylinders, spheres etc. and with more or less complex boundary conditions.Knowledge of such eigen solutions enables the engineer to predict the forced responses of these shells. Moving on to less easily definable geometries, numerical techniques such as the finite-difference method or the finite-element method take over.

However, it becomes apparent that in such cases the extraction of information is sometimes expensive in time and effort.

3.3.8 - True similarity conditions for vibrating thin shells

In the literature the equations of motion of thin shells are derived from several assumptions. Generally they deal with a linear theory of shell deformation so that displacements are assumed to be small in comparison to the thickness of the shell. Furthermore, the thickness of the shells considered should be small compared with the smallest radius of curvature of the shell. In addition to the above assumption it will be assume the Kirckhoff hypothesis, namely i) the fibers of the shells initially perpendicular to the shell middle surface remain so after deformation and are themselves not subject to elongation, ii) the normal stress acting on planes parallel to the shell middle surface is negligible in comparison with other stresses.

The following symbols are adopted (see figure 3.1):

α_1, α_2 curvilinear coordinates

R_1, R_2 radius of curvature

u_1, u_2 deflections in α_1, α_2 directions

w displacement component normal to surface

Q_1, Q_1 shear resultants

q_{t1}, q_{t2} forcing function per unit area in α_1, α_2 directions

N_1, N_2 membrane force resultants

N_{12}, N_{21} internal shear stresses

q_n normal forcing load per unit area.

The length of the shell surface element is given by the form:

$$ds^2 = A_1^2 (d\alpha_1)^2 + A_2^2 (d\alpha_2)^2$$

where A_1 and A_2 are coefficients used to describe the shape of the surface.

These coefficients A_1, A_2 are, generally, functions of the position of the volume element, and may be expressed in terms of the radii of curvature.

With these assumptions the Reissner version [64] of Love's equations [65], describes adequately for most applications the small oscillation behaviour of thin shells. The equations of motion are:

$$\frac{\partial(N_1A_2)}{\partial\alpha_1} + \frac{\partial(N_2\,A_1)}{\partial\alpha_2} + N_{12}\frac{\partial A_1}{\partial\alpha_2} - N_2\frac{\partial A_2}{\partial\alpha_1} + \tag{3.65}$$

$$+ A_1A_2\left(\frac{Q_1}{R_1} + q_{t1}\right) = A_1A_2\rho h\frac{\partial^2 u_1}{\partial t^2}$$

$$\frac{\partial(N_2A_1)}{\partial\alpha_2} + \frac{\partial(N_{12}\,A_2)}{\partial\alpha_1} + N_{21}\frac{\partial A_2}{\partial\alpha_1} - N_1\frac{\partial A_1}{\partial\alpha_2} + \tag{3.66}$$

$$+ A_2A_1\left(\frac{Q_2}{R_2} + q_{t2}\right) = A_2A_1\rho h\frac{\partial^2 u_2}{\partial t^2},$$

$$\frac{\partial(Q_1A_2)}{\partial\alpha_1} + \frac{\partial(Q_2A_1)}{\partial\alpha_2} - A_1A_2\left(\frac{N_1}{R_1} + \frac{N_2}{R_2}\right) - \tag{3.67}$$

$$- A_1A_2q_n = A_1A_2\rho h\frac{\partial^2 w}{\partial t^2}.$$

It is observed that equation (3.66) is obtained after permutation of indices 1 and 2 from equation (3.65) whereas equation (3.67) is unchanged by interchanging the indices.

In these equations the internal forces N and Q, are given by very complicated relations as a function of the displacement component u, v, w, of the radii of curvature R_1 and R_2 and of the bending and membrane stiffness given by:

$$D = \frac{E\,h^3}{12(1-\nu^2)}, \qquad \text{bending stiffness} \tag{3.68}$$

$$K = \frac{E\,h}{(1-\nu^2)}, \qquad \text{membrane stiffness} \tag{3.69}$$

For example, it is possible to write:

$$N_1 = K\left[\frac{1}{A_1}\cdot\frac{\partial u_1}{\partial \alpha_1} + \frac{u_2}{A_1A_2}\cdot\frac{\partial A_1}{\partial \alpha_2} + \frac{w}{R_1} + \nu\left(\frac{1}{A_2}\frac{\partial u_2}{\partial \alpha_2} + \frac{1}{A_1A_2}\cdot\frac{\partial A_2}{\partial \alpha_1} + \frac{w}{R_2}\right)\right] \tag{3.70}$$

Similar relations, much more complicated, can be written for the other internal forces.

The following dimensionless variables can now be introduced:

$$\begin{aligned} u_1^* &= u_1/L \qquad u_2^* = u_2/L \qquad w^* = w/L \\ \alpha_1^* &= \alpha_1/L \qquad \alpha_2^* = \alpha_2/L \\ R_1^* &= R_1/L \qquad R_2^* = R_2/L \qquad t^* = t\cdot\omega \end{aligned} \tag{3.71}$$

Substituting these variables into equation (3.70), one obtains:

$$N_1 = K\left[\frac{1}{A_1}\frac{\partial u_1^*}{\partial \alpha_1^*} + \frac{u_2^*}{A_1A_2}\frac{\partial A_1}{\partial \alpha_2^*} + \frac{w^*}{R_1^*} + \nu\left(\frac{1}{A_2}\frac{\partial u_2^*}{\partial \alpha_2^*} + \frac{1}{A_1A_2}\cdot\frac{\partial A_2}{\partial \alpha_1^*} + \frac{w^*}{R_2^*}\right)\right] \tag{3.72}$$

In this equation the terms in square brackets are dimensionless; thus it is possible to write:

$$N_1^* = N_1/K \tag{3.73}$$

The general form will be:

$$\begin{aligned} N_i^* &= N_i/K \\ Q_i^* &= Q_iL^2/D \end{aligned} \tag{3.74}$$

Substituing equations (3.71) and (3.74) into the Love's equations, and using equations (3.68) and (3.69), one obtains:

$$\frac{\partial N_1^* A_2}{\partial \alpha_1^*} + \frac{\partial N_{12}^* A_1}{\partial \alpha_2^*} + N_{12}^* \frac{\partial A_1}{\partial \alpha_2^*} - N_2^* \frac{\partial A_2}{\partial \alpha_1^*} + \frac{A_1 A_2}{12} \frac{Q_1^*}{R_1^*} \left(\frac{h}{L}\right)^2 +$$

$$+ A_1 A_2 q_{11} \frac{L(1-\nu^2)}{E\,h} = \rho \frac{\omega^2 L^2 (1-\nu^2)}{E} A_1 A_2 \frac{\partial^2 u_1^*}{\partial t^{*2}}, \qquad (3.75)$$

$$\frac{\partial N_2^* A_1}{\partial \alpha_2^*} + \frac{\partial N_{21}^* A_2}{\partial \alpha_1^*} + N_{21}^* \frac{\partial A_2}{\partial \alpha_1^*} - N_1^* \frac{\partial A_1}{\partial \alpha_2^*} + \frac{A_2 A_1}{12} \frac{Q_2^*}{R_2^*} \left(\frac{h}{L}\right)^2 +$$

$$+ A_2 A_1 q_{12} \frac{L(1-\nu^2)}{E\,h} = \frac{\rho \omega^2 L^2 (1-\nu^2)}{E} A_2 A_1 \frac{\partial^2 u_2^*}{\partial t^{*2}}, \qquad (3.76)$$

$$\left(\frac{\partial Q_1^* A_2}{\partial \alpha_1^*} + \frac{\partial Q_2^* A_1}{\partial \alpha_2^*}\right) \frac{1}{12} \left(\frac{h}{L}\right)^2 - \left(\frac{N_1^*}{R_1^*} + \frac{N_2^*}{R_2^*}\right) A_1 A_2 -$$

$$- A_1 A_2 q_n \frac{L(1-\nu^2)}{E\,h} = \frac{\rho}{E} \omega^2 L^2 (1-\nu^2) A_1 A_2 \frac{\partial^2 w^*}{\partial t^{*2}}. \qquad (3.77)$$

The modelling conditions are therefore:

$$h/L = \text{const} \qquad (3.78)$$

$$\frac{q_i (1-\nu^2)}{E} = \text{const.} \qquad i = t_1, t_2, n. \qquad (3.79)$$

$$\frac{\rho \omega^2 L^2 (1-\nu^2)}{E} = \text{const} \qquad (3.80)$$

As it has been already observed these true similarity conditions are very restrictive. The most difficult is the requirement to scale the thickness of the shell in proportion to the typical surface dimensions. The problem of scaling can be simplified considerably if we assume that the predominant effect is either membrane or bending. These two cases will now be derived.

3.3.9 - Approximate scaling conditions for thin shells: membrane effect

The membrane effect is usually most important at low order mode and might extend to the first few modes of vibration of the shell. Taking equations (3.75), (3.76) and (3.77), and making the bending terms zero one obtains:

$$\frac{\partial N_1^* A_2}{\partial \alpha_1^*} + \frac{\partial N_{12}^* A_1}{\partial \alpha_2^*} + N_{12}^* \frac{\partial A_1}{\partial \alpha_2^*} - N_2^* \frac{\partial A_2}{\partial \alpha_1^*} + \frac{A_1 A_2 q_{t_1} L(1-\nu^2)}{12\, E\, h} =$$

$$= \frac{\rho}{E} \omega^2 L^2 (1-\nu^2)\, A_1 A_2 \frac{\partial^2 u_1^*}{\partial t^{*2}} \qquad (3.81)$$

Again, equation (3.82) is obtained by permutation of indices:

$$\frac{\partial N_2^* A_1}{\partial \alpha_2^*} + \frac{\partial N_{21}^* A_2}{\partial \alpha_1^*} + N_{21}^* \frac{\partial A_2}{\partial \alpha_1^*} - N_1^* \frac{\partial A_1}{\partial \alpha_2^*} + \frac{A_2 A_1 q_{t_2} L(1-\nu^2)}{12\, E\, h} =$$

$$= \frac{\rho}{E} \omega^2 L^2 (1-\nu^2)\, A_2 A_1 \frac{\partial^2 u_2^*}{\partial t^{*2}}, \qquad (3.82)$$

$$- \left(\frac{N_1^*}{R_1^*} + \frac{N_2^*}{R_2^*}\right) A_1 A_2 - \frac{q_n L(1-\nu^2)}{12\, E h} A_1 A_2 =$$

$$= \frac{\rho}{E} \omega^2 L^2 (1-\nu^2)\, A_1 A_2 \frac{\partial^2 w^*}{\partial t^{*2}}. \qquad (3.83)$$

In this case the similarity conditions become:

$$\frac{\rho \omega^2 L^2 (1-\nu^2)}{E} = \text{const}, \qquad (3.84)$$

$$\frac{q_i L(1-\nu^2)}{E\, h} = \text{const}, \qquad i = t_1,\ t_2,\ n. \qquad (3.85)$$

These two conditions coincide with equations (3.45) and (3.46) which are the result for the longitudinal vibrations of thin elastic plates.

3.3.10 - Approximate scaling conditions for thin shells: bending effect

With increasing mode number, bending influences will start to dominate. In this situation it is possible to neglect membrane forces (resultant N) in comparison to shear forces (resultant Q). Equations (3.75), (3.76), and (3.77) now become:

$$\frac{1}{12}\frac{Q_1^*}{R_1^*} + \frac{q_{t_1}L^3(1-\nu^2)}{E\,h^3} = \frac{\rho}{E}\,\omega^2\frac{L^4}{h^2}\,(1-\nu^2)\,\frac{\partial^2 u_1^*}{\partial t^{*2}}, \tag{3.86}$$

$$\frac{1}{12}\frac{Q_2^*}{R_2^*} + \frac{q_{t_2}L^3(1-\nu^2)}{E\,h^3} = \frac{\rho\omega^2L^4(1-\nu^2)}{E\,h^2}\cdot\frac{\partial^2 u_2^*}{\partial t^{*2}}, \tag{3.87}$$

$$\frac{1}{12}\frac{\partial Q_1^* A_2}{\partial\alpha_1^*} + \frac{\partial Q_2^* A_1}{\partial\alpha_2^*} - A_1A_2\,\frac{q_n L^3(1-\nu^2)}{E\,h^3} =$$

$$= \frac{\rho\omega^2L^4\,(1-\nu^2)}{E\,h^2}\,A_1A_2\,\frac{\partial^2 w^*}{\partial t^{*2}}. \tag{3.88}$$

The scaling conditions are thus:

$$\frac{\rho\omega^2L^4(1-\nu^2)}{E\,h^2} = \text{const}, \tag{3.89}$$

$$\frac{q_i L^3(1-\nu^2)}{E\,h^3} = \text{const}, \quad i = t_1,\ t_2,\ n. \tag{3.90}$$

Equations (3.89), (3.90) coincide with conditions (3.59), (3.60) respectively obtained for the case of flexural vibrations of thin elastic plates.

Changes in thickness will not affect the natural frequencies of the membrane-effect dominated shell (equation (3.84)),but will cause proportional natural frequency changes in a bending-effect dominated shell(equation (3.89)).

However there is the practical difficulty to decide,

for a given shell, whether dominance of membrane effects should be assumed for the mode range of interest,or whether dominance of bending effects should be the overriding consideration. Only by experimental exploration or by investiga tion of an approximate theoretical solution can this question be resolved.

Care has to be taken that both the original shell and the scaled shell are be governed by the same dominant effect.

3.3.11 - The problem of the boundary conditions

The boundary conditions for shells can be formally expressed by relations similar to equation (3.44) for longitudinal vibrations and to equations (3.49) to (3.51), and (3.52) for flexural vibrations. Therefore the same similarity conditions are yet valid: i.e, equation (3.47) in the case of forces applied on anedge and tangent to shell; and equations (3.61), (3.62) in the case of the other types of loads. It is showed also that, as in the case of plates, for free edges the further condition

$$\nu = \text{const}, \tag{3.91}$$

must be satisfied.

3.3.12 - Structure - fluid interaction

The similarity conditions given by this interaction, can be obtained by considering that the acoustic field generated by the vibrating structure exerts a pressure upon the surface of the structure itself. This load can be regarded as an external force per unit area $p = q_n$. Since the acoustic pressure in the acoustic medium has to satisfy conditions (3.17) and (3.18), it follows that:

$$p \propto \rho_o c_o^2 \tag{3.92}$$

and then the similarity conditions for structure-fluid interaction are easily obtained by substituting $\rho_o c_o^2$ for q_n in the previous similarity conditions.

3.3.13 - Damping of structural materials

In the previous sections the equations of motion of bars, plates and shells have dealt exclusively with undamped material.

However, in the case of sinusoidally varying excitation, the internal damping of structural material can be taken into account by expressing the Young's elastic modulus as a complex quantity, i.e:

$$E^* = E + i\, E_i = E\,(1 + i\eta) \tag{3.93}$$

where η indicates the "loss factor" of the structure and is related to an internal frictional force per volume unit which is proportional to the inverse of the velocity of each point $\left| \frac{N}{m^3} \cdot \frac{1}{m/s} \right|$.

With this substitution the later similarity condition which has to be taken into account to consider real damped material will be:

$$\eta = \text{const.} \tag{3.94}$$

3.4 - Design of models

The dimensionless parameters derived in the previous paragraphs can now be summarized as in table (3.1). For a true model test all these parameters must be the same on the scale model as they are on the prototype. This table shows

that in making models, there are different possibilities for choosing scale factors materials, and acoustic media. In practice models are usually made in one of the four following ways:

i) models built of the same materials and acoustic media
ii) models built of different materials and the same acoustic medium
iii) models built of the same materials and different acoustic media
iv) models built of different materials and different acoustic media.

Every one of these models is correct if it matches the similarity conditions given in table (3.1). The choice will depend on the particular problem that is to be solved.

Sometimes it is not possible to satisfy completely these scaling requirements and then we must accept a "distorted model". However these distortions may be introduced in such a way that little or no inaccuracy is involved. In any case if the main purpose of the model is to study the enclosed acoustic field produced by vibrating structures, the conditions (3.17) and (3.18) are the most important.

In the present study the structure is to be modelled by an assemblage of bars and plates. The scaling laws for such elements will be derived from the table. It has been shown already that the non-dimensional parameters for shells are the same as plates except for coupled transverse and longitudinal vibrations. Similar design consideration will therefore apply.

3.4.1 - Models built of the same materials and acoustic media as in the prototype

The construction of such models satisfies the Newton's scaling law discussed previously. In this case the model uses scale ratios as a function only of the length scale ratio.

Let us consider table (3.I) for bars and plates: if the materials and acoustic medium are the same, i.e ρ, E, ν, ρ_o, c_o = const, from table (3.I) it is possible to derive tables (3.II) and (3.III) for bars and plates respectively. In the case of plates only flexural vibrations have been taken into account because they are the main source of sound radiation.

For bars table (3.II) shows that relations (II.1) and (II.3) lead to the same similarity condition: i.e. the frequency scale ratio is the inverse of the length scale ratio. Relation (II.2) requires that the scale ratio of the radii of gyration is the same as the length scale ratio. Relations (II.4) and (II.5) show that forces have to be scaled like $1/L^2$, and finally relation (II.6) shows that sound pressure level is kept unchanged.

Table (3.III) shows that plates require the same scale ratio for the frequency scale ratio and for forces and pressure as for bars. Relations (III.1) and (III.3) show that in addition the thickness scale ratio has to be like the length scale ratio.

Considering for example $L_m/L_p = 1/5$ the scale ratios will be as follows:

$$\begin{aligned} h_m/h_p &= 1/5 & \omega_m/\omega_p &= 5 \\ w_m/w_p &= 1/5 & \dot{w}_m/\dot{w}_p &= 1 \\ p_m/p_p &= 1 & \rho_m/\rho_p &= 1/125 \end{aligned} \qquad (3.95)$$

$$\ddot{w}_m/\ddot{w}_p = 5, \qquad F_m/F_p = 1/25,$$
$$\Gamma_m/\Gamma_p = 25, \qquad r_m/r_p = 25, \tag{3.95}$$

The major feature of these models is that the sound pressure levels remain the same on the prototype as on the model. The acceleration on the model is increased and thus the smaller transducers in the model will not require such a high sensivity.

Newton's scaling law however, sometimes proves to be too restrictive, since it is not always convenient to scale the thickness of the structure in direct proportion to the typical surface dimensions.

With such models the minimum thickness of the material will limit the length scale which can be used. This problem can be overcome by a change in the material of the model as discussed in the next section.

3.4.2 - Models built of different materials and the same acoustic medium

If we now relax the condition thath h/L remains constant, we can adjust the other quantities in such a way as to keep the main non-dimensional quantities constant. The simplest way to do this is to keep the acoustic medium constant and to change the material of the model.

Consider again the general table (3.I) and assume the use of different material but the same acoustic medium (ρ_o, c_o = const); tables 3.IV and 3.V have been derived in this case for bars and plates respectively.

For bars, table (3.IV) shows once again that the fre-

quency scale ratio is inverse of the length scale ratio. Relation (IV.2) gives the same scale ratio of the radii of giration, whereas relation (IV.1) imposes a new condition for bars. The material choosen for the model must have the same longitudinal sound velocity as for the prototype. Finally relations (IV.4) and (IV.5) show that the force scale ratio depends on the elastic properties of materials and relation (IV.6) shows that the sound pressure level remains the same.

In reference to flexural vibrations of plates, table (3.V) shows the same frequency scale ratio as for bars. However relations (V.1) and (V.3) link the structural properties of the material to the ratio h/L. If these two relations have to be satisfied simultaneously, it is necessary to change the ratio h/L according to the relation $h/L \propto 1/\rho$: The choice of the model material is now considerably constrained. This can be shown by eliminating the ratio h/L from relations (V.1) and (V.3). This new dimensional relation is then obtained as follows:

$$C_1 = \frac{\rho^3 (1-\nu^2)}{E} = \text{const.} \qquad (3.96)$$

For bars it is necessary to keep ρ/E constant.Thus as shown in equation (3.96) it is not possible to use the same material for the model plate as for the model bar. Tables (3.VI) and (3.VII) summarize the values of $\sqrt{\rho/E}$ and C_1 for a group of representative materials. Looking at the first row of table (3.VI) which shows the values of C_1, it is clear that it is almost impossible to find a model material which has the same value as the prototype material such steel or aluminium. This means that practical models will introduce distorsions in relation to the coupling interaction.

However in some problems it is possible to match the most important conditions and disregard the others. In studying the acoustic field produced by mechanical excitations of the structure, it will be much more important to comply with structural conditions (such as equation (3.59)), than with "coupling" conditions. At least in this case the acoustic field is considered not able to modify significantly the dynamic behaviour of the structure. This is likely to be a good approximations for many practical structures such as vehicle compartments.

However, also in the case of acoustic excitation it is necessary to comply with the structural condition (3.59). In fact, the coupling condition can be easly matched by changing the value of the sound pressure level which excites the structure. One should not forget that this coupling condition is a particular case of the boundary condition where q_n is the sound pressure of the acoustic field.

From condition (V.1) of table (2.V), it follows that using model materials with $c_m < c_p$ (plastic, for example), the thickness scale ratio $h_m/h_p = (L_m/L_p) \cdot (c_p/c_m)$ will be greater than the length scale ratio: this fact may be particularly useful in the case of thin structures such as plates and shells.

In order to verify the feasiblity of such models, a steel and glass prototype has been compared with its 1/5 plexiglass and aluminum model. These experimental measurements will be described in Chapter 4.

3.4.3 - Models built of the same materials and different acoustic media

In some cases the acoustic condition (3.17) ($\omega L/c_o$ = = const) does not allow the construction of a model with a small scale length. In fact, as has been observed in the previous sections, if the same acoustic medium is used, the frequency scale factor increases as the length scale factor decreases. Therefore, small values of L_m/L_p raise the frequencies in model experimentation and this could cause difficulties for transducers and analysis instrumentation. In these cases, it seems useful to reduce the frequency range by using for the model an acoustic medium which has a sound velocity smaller than in the prototype. If, for example, we design a model with a length scale of 1/5 and an acoustic medium with a sound velocity of 1/5 in respect to the prototype, it will be possible to make measurements on the model over the same frequency range as on the prototype.

Considering again table (3.I) and assuming we change only the acoustic medium, the following two tables have been obtained (Tab. 3.VIII and Tab. 3.IX). In the case of bars, table (3.VIII) shows that relation (VIII.1) imposes the usual condition on the frequency scale ratio, and therefore the acoustic condition states that the sound velocity must be the same (relation VIII.3). It is therefore impossible to model bars with a change of acoustic medium.

In the case of plates under flexural vibrations, table (3.IX) shows that in order to satisfy simultaneously the relations (IX.1) and (IX.3) it is necessary to change the value of the thickness ratio, according to this relation $h/L \propto \rho_o$. In the same time one has to match the dimensional relationship:

$$C_2 = \frac{\rho_o^2}{c_o^2} = \text{const}, \tag{3.97}$$

obtained by elimination of the ratio h/L from relations (IX.1) and (IX.3).

This new dimensional parameter C_2, depends on the physical properties of the acoustic medium and therefore it has to be kept the same in the model as in the prototype. If the acoustic medium is a gas, it is possible to write:

$$c_o = \sqrt{\gamma \frac{p_o}{\rho_o}} \tag{3.98}$$

where p_o is the equilibrium room pressure and γ the ratio of the specific heat of the gas at constant pressure to the specific heat at constant volume.
In this case, from equation (3.98) it follows:

$$C_2 = \frac{\rho_o^3}{\gamma p_o} = \text{const} \tag{3.99}$$

Since it is most desiderable that pressure and temperature in the acoustic medium of the model and prototype are the same, this last condition (3.99) cannot easily be fulfilled.

If these restrictions on pressure and temperature are not required, the pressure p_o becomes a free parameter for the design of the model and therefore condition (3.99) can be satisfied.

Tables (3.VI) and (3.VII) show the values of c_o and C_2 for a group of reppresentative acoustic medium at the ambient pressure p_o = 1 bar.

However it is important to oberve that condition (3.97) and the other one on the thickness scale radio $h/L \propto \rho_o$ have to be satisfied only in condition where the coupling action

of the inner sound pressure is determining for the dynamic behaviour of the structure.

If this is not the case, only the structural condition (IX.1) is to be matched. In this case however, as the sound velocity $(c_o)_m$ should be smaller than in the prototype, the thickness scale ratio $h_m/h_p = (L_m/L_p) \cdot (c_o)_m/(c_o)_p$ becomes smaller than the length scale ratio, and this can be a very restrictive condition for modelling thin surfaces or shells.

3.4.4 - Models built of different materials and different acoustic media

This is the most general case where it is possible to change all the parameters to satisfy the similarity conditions. From table (3.I) it is possible to derive tables (3.X) and (3.XI) for bars and plates respectively.

In the first case, table (3.X) shows the same relations obtained as in the previous sections. The relation(3XI) introduces a new condition that the ratio between the sound velocity in the medium and in the structure must r e m a i n constant. Table (3.VII) gives the values of these ratios for different materials and acoustic media. This table can be useful design chart to guide the choice of a proper material and acoustic medium to model bars.

For flexural vibrations in plates, table (3.XI) shows once again that the requirement to verify simultaneously conditions (XI.1) and (XI.3) imposes the change of the thickness ratio according to this relation: $h/L \propto \rho/\rho_o$. It is also necessary to satisfy the condition:

$$\frac{\rho^2}{c^2} \cdot \frac{c_o^2}{\rho_o^2} (1 - \nu^2) = \text{const.} \qquad (3.100)$$

It is easy to observe that this parameter is given also by the ratio C_1/C_2.

Table (3.VI) gives the values of these ratios for different materials and acoustic media at the ambient pressure p_o = 1 bar.

Also in this case it is important to point out that condition (3.100) and $h/L \propto \rho/\rho_o$ are to be satisfied only if the coupling interaction is an important part of the dynamic behaviour of the structure. If this is not the case only the structural condition (XI.1) must be matched. Now the thickness scale ratio h_m/h_p depends not only on the ratio $(c_o)_m/(c_o)_p$, but also on the ratio $(c)_p/(c)_m$ (usually > 1) which tends to raise its value.

3.4.5 - Final remarks

Four different possibilities for building models have been examined. The first type of model, the Newtonian, is perhaps the more exact because it can satisfy all the similarity conditions. However it requires a precise modelling of all the geometrical dimensions, and for all but the simplest prototype this can be difficult and expensive to make.

The second type of model (different materials, same medium) gives good results in the case of structures which are mechanically and/or acoustically excited. The structural condition imposes a thickness scale ratio which is particularly favourable.

When coupling conditions are important it seems quite impossible to find materials able to satisfy both the structural and the coupling requirements. Moreover bars and plates

made of the same materials in the prototype have to be modelled with different materials.

The third type of model (same material different acoustic media) allows the reduction of the frequency scale ratio if the acoustic medium has a sound velocity $(c_o)_m < (c_o)_p$. In practice these models do not allow bars to be reproduced correctly and do not model the coupling interaction of plates. In this case the structural condition imposes a thickness scale ratio which is unfavourable, being smaller than the length scale ratio.

Within these limits, such kind of models may be used for structures excited both mechanically and acoustically.

The fourth type of models (different materials and acoustic media) permits the reduction of the frequency scale ratio if the acoustic medium has a sound velocity $(c_o)_m < (c_o)_p$. Moreover these models offer some possibilities to choose proper material and acoustic medium to comply simultaneously with the structural and the coupling conditions. In the case that this coincidence is not required, the structural condition imposes a thickness scale ratio more favourable than in the third type of model. Therefore these models seem to be the most useful to study structures excited both mechanically and acoustically at high frequency.

Both these last types of models need to use different acoustic media. In some circustances this requirement may introduce difficulties for the model experiment such as temperature and pressure control, toxicity and chemical compatibility with the structural material. In order to verify the actual possibility of using such models, the use of Freon 11 in presence of plastic material has been investigated (see chapter 5).

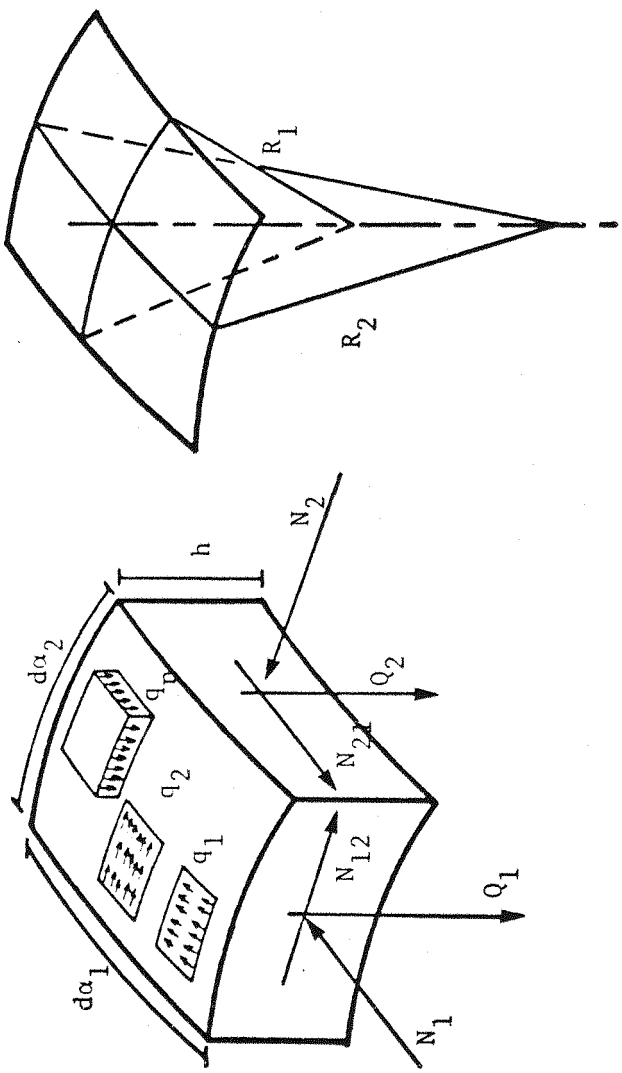

Figure 3.1 Element of doubly curved shell.

Tab. 3.I - Dimensionless parameters for investigating natural and forced vibrations of submerged structures.

STRUCTURAL ELEMENT		BARS	PLATES	SHELLS	ACOUSTIC MEDIUM
LONGITUDINAL VIBRATIONS	STRUCTURAL CONDITION	$\frac{\rho\omega^2L^2}{E}$ (3.26)	$\frac{\rho\omega^2L^2(1-\nu^2)}{E}$ (3.45)	(*) $\frac{\rho\omega^2L^2(1-\nu^2)}{E}$ (3.84)	$\frac{\omega L}{c_0}$ (3.17)
	COUPLING CONDITION			(*) $\frac{\rho_0 c_0^2 L(1-\nu^2)}{Eh}$ (3.92)	
	BOUNDARY CONDITION	$\frac{q_t' L}{EA}$ (3.27) $\frac{F}{EA}$ (3.28)	$\frac{q_t L(1-\nu^2)}{Eh}$ (3.46) $\frac{q_t'(1-\nu^2)}{Eh}$ (3.47)	(*) $\frac{q_i L(1-\nu^2)}{Eh}$ (3.85)	$\frac{\rho_0\omega^2L^2}{p}$ (3.18)
TRANSVERSE VIBRATIONS	STRUCTURAL CONDITION	$\frac{\rho A\omega^2L^4}{EI}$ (3.38)	$\frac{\rho\omega^2L^4(1-\nu^2)}{Eh^2}$ (3.59)	(*) $\frac{\rho\omega^2L^4(1-\nu^2)}{Eh^2}$ (3.89)	
	COUPLING CONDITION		$\frac{\rho_0 c_0^2 L^3(1-\nu^2)}{Eh^3}$ (3.92)	(*) $\frac{\rho_0 c_0^2 L^3(1-\nu^2)}{Eh^3}$ (3.92)	
	BOUNDARY CONDITION	$\frac{q_n' L^3}{EI}$ (3.39) $\frac{FL^2}{EI}$ (3.40) $\frac{ML}{EI}$ (3.41)	$\frac{q_n L^3(1-\nu^2)}{Eh^3}$ (3.60) (**) ν (3.63)	(*) $\frac{q_i L^3(1-\nu^2)}{Eh^3}$ (3.90) (**) ν (3.91)	
TRANSVERSE AND LONGITUDINAL VIBRATIONS	STRUCTURAL CONDITION			$\frac{h}{L}$ (3.78) $\frac{\rho\omega^2L^2(1-\nu^2)}{E}$ (3.80)	
	COUPLING CONDITION			$\frac{\rho_0 c_0^2(1-\nu^2)}{E}$ (3.92)	
	BOUNDARY CONDITION			$\frac{q_i(1-\nu^2)}{E}$ (3.79) (**) ν (3.91)	

(*) Approximate similitude condition (**) Free edge boundary condition.

Tab. 3.II - Dimensionless parameters for modelling bars: models built of the same materials and acoustic media.

BARS	LONGITUDINAL VIBRATIONS	TRANSVERSE VIBRATIONS	ACOUSTIC FIELD
STRUCTURAL CONDITION	$\left(\frac{\rho}{E}\right)\omega^2 L^2$ (II.1)	$\left(\frac{\rho}{E}\omega^2 L^2\right)\frac{L^2 A}{I} \equiv \frac{L}{r}$ (II.2)	$\left(\frac{1}{c_0}\right)\omega L$ (II.3)
BOUNDARY CONDITION	$\left(\frac{1}{E}\right)\cdot\frac{F}{A}$ (II.4)	$\left(\frac{1}{E}\right)\cdot\frac{FL^2}{I}$ (II.5)	$(\rho_0\omega^2 L^2)\frac{1}{\bar{P}}$ (II.6)

Tab. 3.III - Dimensionless parameters for modelling plates: models built of the same materials and acoustic media.

PLATES	TRANSVERSE VIBRATIONS	ACOUSTIC FIELD
STRUCTURAL CONDITION	$\left(\frac{\rho}{E}\omega^2 L^2\right)\cdot\frac{L^2}{h^2}$ (III.1)	$\left(\frac{1}{c_0}\right)\cdot\omega L$ (III.2)
COUPLING CONDITION	$\left(\frac{\rho_0 c_0^2}{E}\right)\cdot\frac{L^3}{h^3}$ (III.3)	
BOUNDARY CONDITION	$\left(\frac{1}{E}\right)\cdot q_n\frac{L^3}{h^3}$ (III.4)	$(\rho_0\omega^2 L^2)\cdot\frac{1}{\bar{p}}$ (III.5)

Tab. 3.IV - Dimensionless parameters for modelling bars: models built of different materials and same acoustic medium.

BARS	LONGITUDINAL VIBRATIONS	TRANSVERSE VIBRATIONS	ACOUSTIC FIELD
STRUCTURAL CONDITION	$(\omega^2 L^2)\,\frac{\rho}{E}$ (IV.1)	$\left(\omega^2 L^2\,\frac{\rho}{E}\right)\frac{AL^2}{I} = \frac{L}{r}$ (IV. 2)	$\left(\frac{1}{c_0}\right)\omega L$ (IV.3)
BOUNDARY CONDITION	$\frac{F}{EA}$ (IV.4)	$\frac{FL^2}{EI}$ (IV.5)	$(\rho_0 \omega^2 L^2)\,\frac{1}{\bar{P}}$ (IV. 6)

Tab. 3.V - Dimensionless parameters for modelling plates: model built of different materials and same acoustic medium.

PLATES	TRANSVERSE VIBRATIONS	ACOUSTIC FIELD
STRUCTURAL CONDITION	$(\omega^2 L^2)\,\frac{\rho L^2}{Eh^2}$ (V.1)	$\left(\frac{1}{c_0}\right)\cdot \omega L$ (V.2)
COUPLING CONDITION	$(\rho_0 c_0^2)\,\frac{1}{E}\cdot\frac{L^3}{h^3}$ (V.3)	
BOUNDARY CONDITION	$\frac{q_n L^3}{Eh^3}$ (V.4)	$(\rho_0 \omega^2 L^2)\cdot\frac{1}{\bar{p}}$ (V.5)

Tab. 3.VI - Values of the ratio C_1/C_2 (eq. (3.100)) for different structural materials and acoustic media.

ACOUSTIC MEDIA \ STRUCTURAL MATERIALS		GLASS	WOOD	MAGNE-SIUM	ALUMIN-IUM	POLY-PROPYLE NE	ACRYLIC	POLY-STYRENE	PLEXI-GLAS	DELRIN	ACETAL	POLY-VINYL CHLOR.	CELLULO-SE ACETATE	TENITE II	STEEL	CUPPER	LEAD
	C_1	$2.2\ 10^{-2}$	$3.7\ 10^{-2}$	$1.2\ 10^{-1}$	$2.5\ 10^{-1}$	$2.6\ 10^{-1}$	$2.7\ 10^{-1}$	$2.8\ 10^{-1}$	$2.9\ 10^{-1}$	$4.4\ 10^{-1}$	$6.1\ 10^{-1}$	$6.2\ 10^{-1}$	$8.3\ 10^{-1}$	$9.0\ 10^{-1}$	2.23	5.34	86.1
	C_2 (*)																
HYDROGEN	$3.6\ 10^{-9}$	$0.6\ 10^{7}$	$1.0\ 10^{7}$	$3.2\ 10^{7}$	$6.7\ 10^{7}$	$7.2\ 10^{7}$	$7.6\ 10^{7}$	$7.9\ 10^{7}$	$7.9\ 10^{7}$	$1.2\ 10^{8}$	$1.7\ 10^{8}$	$1.7\ 10^{8}$	$2.3\ 10^{8}$	$2.5\ 10^{8}$	$6.2\ 10^{8}$	$1.5\ 10^{9}$	$2.4\ 10^{10}$
HELIUM	$2.8\ 10^{-8}$	$0.8\ 10^{6}$	$1.3\ 10^{6}$	$4.2\ 10^{6}$	$8.7\ 10^{6}$	$9.3\ 10^{6}$	$9.8\ 10^{6}$	$1.0\ 10^{7}$	$1.0\ 10^{7}$	$1.6\ 10^{7}$	$2.2\ 10^{7}$	$2.2\ 10^{7}$	$3.0\ 10^{7}$	$3.3\ 10^{7}$	$8.0\ 10^{7}$	$1.9\ 10^{8}$	$3.1\ 10^{9}$
STEAM	$2.1\ 10^{-6}$	$1.0\ 10^{4}$	$1.7\ 10^{4}$	$5.4\ 10^{4}$	$1.1\ 10^{5}$	$1.2\ 10^{5}$	$1.3\ 10^{5}$	$1.3\ 10^{5}$	$1.3\ 10^{5}$	$2.0\ 10^{5}$	$2.8\ 10^{5}$	$2.9\ 10^{5}$	$3.8\ 10^{5}$	$4.2\ 10^{5}$	$1.0\ 10^{6}$	$2.5\ 10^{6}$	$4.0\ 10^{7}$
METHANE	$2.5\ 10^{-6}$	$8.9\ 10^{3}$	$1.5\ 10^{4}$	$4.7\ 10^{4}$	$9.8\ 10^{4}$	$1.0\ 10^{5}$	$1.1\ 10^{5}$	$1.1\ 10^{5}$	$1.1\ 10^{5}$	$1.8\ 10^{5}$	$2.5\ 10^{5}$	$2.5\ 10^{5}$	$3.3\ 10^{5}$	$3.7\ 10^{5}$	$9.0\ 10^{5}$	$2.2\ 10^{6}$	$3.5\ 10^{6}$
NH_3	$3.0\ 10^{-6}$	$7.4\ 10^{3}$	$1.3\ 10^{4}$	$3.9\ 10^{4}$	$8.1\ 10^{4}$	$8.7\ 10^{4}$	$9.2\ 10^{4}$	$9.5\ 10^{4}$	$9.6\ 10^{4}$	$1.5\ 10^{5}$	$2.0\ 10^{5}$	$2.1\ 10^{5}$	$2.8\ 10^{5}$	$3.0\ 10^{5}$	$7.5\ 10^{5}$	$1.8\ 10^{6}$	$2.9\ 10^{6}$
NEON	$3.6\ 10^{-6}$	$6.1\ 10^{3}$	$1.0\ 10^{4}$	$3.3\ 10^{4}$	$6.7\ 10^{4}$	$7.2\ 10^{4}$	$7.6\ 10^{4}$	$7.9\ 10^{4}$	$8.0\ 10^{4}$	$1.2\ 10^{5}$	$1.7\ 10^{5}$	$1.7\ 10^{5}$	$2.3\ 10^{5}$	$2.5\ 10^{5}$	$6.2\ 10^{5}$	$1.5\ 10^{6}$	$2.4\ 10^{6}$
AIR	$1.2\ 10^{-5}$	$1.9\ 10^{3}$	$3.2\ 10^{3}$	$1.0\ 10^{3}$	$2.1\ 10^{4}$	$2.2\ 10^{4}$	$2.4\ 10^{4}$	$2.4\ 10^{4}$	$2.5\ 10^{4}$	$3.8\ 10^{4}$	$5.3\ 10^{4}$	$5.4\ 10^{4}$	$7.1\ 10^{4}$	$7.8\ 10^{4}$	$1.9\ 10^{5}$	$4.6\ 10^{5}$	$7.4\ 10^{6}$
CO_2	$5.3\ 10^{-5}$	$4.1\ 10^{2}$	$7.0\ 10^{2}$	$2.2\ 10^{3}$	$4.5\ 10^{3}$	$4.8\ 10^{3}$	$5.1\ 10^{3}$	$5.3\ 10^{3}$	$5.3\ 10^{3}$	$8.2\ 10^{3}$	$1.1\ 10^{4}$	$1.1\ 10^{4}$	$1.5\ 10^{4}$	$1.7\ 10^{4}$	$4.2\ 10^{4}$	$1.0\ 10^{4}$	$1.6\ 10^{6}$
PROPANE	$5.5\ 10^{-5}$	$4.0\ 10^{2}$	$6.8\ 10^{2}$	$2.1\ 10^{2}$	$4.4\ 10^{3}$	$4.7\ 10^{3}$	$5.0\ 10^{5}$	$5.2\ 10^{3}$	$5.2\ 10^{3}$	$8.1\ 10^{3}$	$1.1\ 10^{4}$	$1.1\ 10^{4}$	$1.5\ 10^{4}$	$1.6\ 10^{4}$	$4.0\ 10^{4}$	$9.7\ 10^{4}$	$1.6\ 10^{6}$
BUTANE	$1.3\ 10^{-4}$	$1.7\ 10^{2}$	$2.9\ 10^{2}$	$9.1\ 10^{2}$	$1.9\ 10^{3}$	$2.0\ 10^{3}$	$2.1\ 10^{3}$	$2.2\ 10^{3}$	$2.2\ 10^{3}$	$3.5\ 10^{3}$	$4.8\ 10^{3}$	$4.9\ 10^{3}$	$6.5\ 10^{3}$	$7.1\ 10^{3}$	$1.7\ 10^{4}$	$4.2\ 10^{4}$	$6.7\ 10^{5}$
FREON 12	$1.2\ 10^{-3}$	$1.9\ 10^{1}$	$3.2\ 10^{1}$	$1.0\ 10^{2}$	$2.1\ 10^{2}$	$2.2\ 10^{2}$	$2.3\ 10^{2}$	$2.4\ 10^{2}$	$2.4\ 10^{2}$	$3.8\ 10^{2}$	$5.1\ 10^{2}$	$5.3\ 10^{2}$	$7.1\ 10^{2}$	$7.7\ 10^{2}$	$1.9\ 10^{3}$	$4.6\ 10^{3}$	$7.3\ 10^{4}$
FREON 11	$1.2\ 10^{-3}$	$1.9\ 10^{1}$	$3.2\ 10^{1}$	$1,0\ 10^{2}$	$2.1\ 10^{2}$	$2.2\ 10^{2}$	$2.3\ 10^{2}$	$2.4\ 10^{2}$	$2.4\ 10^{2}$	$3.8\ 10^{2}$	$5.2\ 10^{2}$	$5.3\ 10^{2}$	$7.1\ 10^{2}$	$7.7\ 10^{2}$	$1.9\ 10^{3}$	$4.6\ 10^{3}$	$7.3\ 10^{4}$
WATER	$4.7\ 10^{-1}$	$5.0\ 10^{-2}$	$8.0\ 10^{-2}$	$2.5\ 10^{-1}$	$5.2\ 10^{-1}$	$5.5\ 10^{-1}$	$5.8\ 10^{-1}$	$6.0\ 10^{-1}$	$6.0\ 10^{-1}$	$9.5\ 10^{-1}$	$1.3\ 10^{0}$	$1.3\ 10^{0}$	$1.8\ 10^{0}$	$1.9\ 10^{0}$	$4.7\ 10^{0}$	$1.1\ 10^{1}$	$1.8\ 10^{2}$

(*) The values of C_2 are refered to a pressure $p_0 = 1$ bar : for different pressures the values of the ratio C_1/C_2 must be multiplied by $(p_0/p)^2$.

Tab. 3.VII - Values of the ratio c/c_0 for different structural materials and acoustic media.

STRUCTURAL MATERIALS / ACOUSTIC MEDIA	c[m/s] / c_0[m/s]	TENITE II	LEAD	CELLULOSE ACETATE	POLY-VINYL CHLOR.	POLY-PROPYLENE	ACETAL	DELRIN	POLY-STYRENE	PLEXI-GLASS	ACRYLIC	CUPPER	WOOD	MAG-NESIUM	STEEL	ALUM-INIUM	GLASS
	1130	1157	1193	1620	1656	1687	1689	1854	2030	2080	3620	3706	4909	5050	5150	5200	
FREON 11	140	8.07	8.26	8.52	11.57	11.82	12.05	12.06	13.24	14.50	14.85	25.85	26.47	35.06	36.07	36.78	37.14
FREON 12	149	7.58	7.76	8.00	10.87	11.11	11.32	11.33	12.44	13.62	13.95	24.29	24.87	32.9	33.89	34.56	34.89
BUTANE	215	5.25	5.38	5.54	7.53	7.70	7.84	7.85	8.62	9.44	9.67	16.84	17.24	22.83	23.49	23.95	24.19
CO_2	246	4.59	4.70	4.85	6.59	6.73	6.86	6.87	7.54	8.25	8.46	14.72	15.07	19.96	20.53	20.93	21.14
PROPANE	248	4.56	4.67	4.81	6.53	6.68	6.80	6.81	7.48	8.19	8.39	14.60	14.94	19.79	20.36	20.77	20.97
AIR	346	3.27	3.34	3.45	4.68	4.79	4.88	4.88	5.36	5.87	6.01	10.46	10.71	14.19	14.60	14.88	15.03
STEAM (*)	405	2.79	2.86	2.95	4.00	4.09	4.17	4.17	4.58	5.01	5.14	8.94	9.15	12.12	12.47	12.72	12.84
NH_3	407	2.78	2.84	2.93	3.98	4.07	4.14	4.15	4.56	4.99	5.11	8.89	9.11	12.06	12.41	12.65	12.78
METHANE	417	2.71	2.77	2.86	3.88	3.97	4.05	4.05	4.45	4.87	4.99	8.68	8.89	11.77	12.11	12.35	12.47
NEON	433	2.61	2.67	2.76	3.74	3.82	3.90	3.90	4.28	4.69	4.80	8.36	8.56	11.34	11.66	11.89	12.01
HELIUM	973	1.16	1.19	1.23	1.66	1.70	1.73	1.74	1.91	2.09	2.14	3.72	3.81	5.05	5.19	5.29	5.34
HYDROGEN	1211	0.93	0.96	0.99	1.34	1.37	1.39	1.39	1.53	1.68	1.72	2.99	3.06	4.05	4.17	4.25	4.29
WATER	1460	0.77	0.79	0.82	1.11	1.13	1.16	1.16	1.27	1.39	1.42	2.48	2.54	3.36	3.46	3.53	3.56

(*) t = 100 °C

Tab. 3.VIII - Dimensionless parameters for modelling bars: models built of the same material and different acoustic media.

BARS	LONGITUDINAL VIBRATIONS	TRANSVERSE VIBRATIONS	ACOUSTIC FIELD
STRUCTURAL CONDITION	$\left(\frac{\rho}{E}\right)\omega^2 L^2$ (VIII.1)	$\left(\frac{\rho}{E}\omega^2 L^2\right)\frac{AL^2}{I} = \frac{L}{r}$ (VIII.2)	$(\omega L)/c_0$ (VIII.3)
BOUNDARY CONDITION	$\left(\frac{1}{E}\right)\frac{F}{A}$ (VIII.4)	$\left(\frac{1}{E}\right)\frac{FL^2}{I}$ (VIII.5)	$\frac{\rho_0 c_0^2}{\bar{p}}$ (VIII.6)

Tab. 3.IX - Dimensionless parameters for modelling plates: models built of the same material and different acoustic media.

PLATES	TRANSVERSE VIBRATIONS	ACOUSTIC FIELD
STRUCTURAL CONDITION	$\left(\frac{\rho}{E}\right)c_0^2\frac{L^2}{h^2}$ (IX.1)	$(\omega L)/c_0$ (IX.2)
COUPLING CONDITION	$\left(\frac{1}{E}\right)\rho_0 c_0^2\frac{L^3}{h^3}$ (IX.3)	
BOUNDARY CONDITION	$\left(\frac{1}{E}\right)q_n \cdot \frac{L^3}{h^3}$ (IX.4)	$\frac{\rho_0 c_0^2}{\bar{p}}$ (IX.5)

Tab. 3.X - Dimensionless parameters for modelling bars: models built of different materials and different acoustic media.

BARS	LONGITUDINAL VIBRATIONS	TRANSVERSE VIBRATIONS	ACOUSTIC FIELD
STRUCTURAL CONDITION	$\frac{\rho}{E} c_0^2$ (X.1)	$\frac{\rho}{E} c_0^2 \frac{AL^2}{I} \equiv \frac{L}{r}$ (X.2)	$\frac{\omega L}{c_0}$ (X.3)
BOUNDARY CONDITION	$\frac{F}{EA}$ (X.4)	$\frac{F \cdot L^2}{EI}$ (X.5)	$\frac{\rho_0 c_0^2}{\bar{p}}$ (X.6)

Tab. 3.XI - Dimensionless parameters for modelling plates: models built of different materials and different acoustic media.

PLATES	TRANSVERSE VIBRATIONS	ACOUSTIC FIELD
STRUCTURAL CONDITION	$\frac{\rho}{E} c_0^2 \frac{L^2}{h^2}$ (XI.1)	$\frac{\omega L}{c_0}$ (XI.2)
COUPLING CONDITION	$\frac{\rho_0 c_0^2}{E} \frac{L^3}{h^3}$ (XI.3)	
BOUNDARY CONDITION	$\frac{q_n}{E} \frac{L^3}{h^3}$ (XI.4)	$\frac{\rho_0 c_0^2}{\bar{p}}$ (XI.5)

CHAPTER 4

Experimental work: the first model

Previous experimental work has shown that plastic model can play an important part in the understanding of the dynamic behaviour of structures [36-38]. The experimental work reported in this thesis examined the possibility of extending this technique to predict sound radiation from structures excited by point forces or distributed pressures. For this purpore a 1/5 scale plastic model of a safety cab of a tractor was built. The model was tested in air (the same medium as for the prototype).

This part of the thesis is concerned with the description of the test prototype and its model as well as with the description of the measurement procedures. The experimental results and their comparison between prototype and model conclude the chapter.

4.1 - Description of the prototype

The prototype which was used is a safety cab of a FIAT tractor. In order to have a good understanding of the construction procedures of this cab its technical drawings have been supplied by FIAT. At the same time the production line was visited and pictures of components of the cab were taken (see pictures 4.1 to 4.4). In this way it was possible to get a good idea of the relative importance of the major sub assemblies. In particular 5 major parts have been identified (fig. 4.5):

a) bottom platform

b) left side panel

c) right side panel

d) rear panel

e) cover.

The components (a), (b), and (c) are obtained by cutting and stamping a steel plate of 2 mm thickness.Attachment plates, stiffeners, etc. are then spot welded to the pressing. The most complicated structural form is the bottom platform as shown in figure (4.3). Under the platform there are two attachments for the connection of the front of the cab to the tractor through two vibration isolation blocks.These attachments are made of pressed steel plates of 3 mm thickness which are welded to the platform itself (see picture 4.3). The two rear supports are fixed to the base of the box structure attached to the side panels (see picture 4.6). These two supports also connect the cab to the tractor through vibration isolation blocks.

The four components (a), (b) (c) and (d) are connected together by bolts and thus make a monolithic structure.

The fifth part of the cab, the cover (e) is attached by bolts through an elastic neoprene sheet to the side panels and base. The steel frame of this structure must provide adeguate stiffness to prevent damage if the tractor over turns. The driver's enclosure is completed by glass surfaces of 6 mm thickness. The steel frame is made of pressed steel plates of 2 mm thickness connected by spot welds to form the required closed cross-sections (see § 4.4.1, and figures (4.7) to (4.12)). All the glass-surfaces are joined to this steel structure by a rubber seal with two apposite grooves. The roof shows two openings: one for an upper window and one for the temperature control compartment. (see picture 4.4).

This cab has to assure the safety and comfort of the driver. Basically the safety is provided by the frame of the cab which is made by steel members with high stiffness.When the windows are closed the whole cab is air tight and air changes are made by a fan which draws in external air through filters placed on the roof of the cab. In order to assure thermal comfort an air-conditioning unit can be set up on the roof together with the air-filtering system.The cab must also provide suitable sound insulation not only against the airborne noise, but also against the structure-borne noise transmitted through the resilient supports connecting the cab to the tractor.

4.2 - Choice of the type of model and its length scale factor

The length scale factor chosen for the model is 1/5. This value allows the reproduction of the main components with sufficient accuracy. The major details of the components which might affect the sound radiation of the structure can be included in the model. The size of the model is sufficiently small to be handled conveniently. At the same time it is large enough to accomodate the transducers without distortion of the response. It was decided to use plastic materials to model the prototype. These kind of models have given good results for investigating dynamic behaviour of large and complicated machinery structures. In particular acrylic materials seem to be the most suitable as they permit models to be built with bigger thicknesses as structural connections can be made using shavings of acrylic materials dissolved in solvent. In this way it is possible to maintain the material continuity of the structure. Acrylic materials have the advantages of being easily workable. In fact they can be cut with a hand saw, can be folded by heat,

can be finished by a file, and can be drilled with ease. In addition they are transparent, which makes it possible to see imperfectly cemented joints.

For the present model, Perspex has been used. Table (4.I) shows some of the physical properties of this material, as well as those of the prototype materials. In this table are also indicated the properties of aluminium; in fact this material has been used to model the frame of the upper cover as will be discussed later.

In order to choose the acoustic medium, the frequency range of investigation must be considered. In these kind of structures, low frequency noise is of primary interest (20 - 400 Hz). The maximum frequency value of the model investigations will be 2000 Hz (5x400) if air is used as the acoustic medium. This is an acceptable value for every kind of vibration and acoustic instrumentation and therefore it is possible to work in air. This condition reduces considerably the complexity of experimental measurements as well as the construction of model, and allows direct reading of the sound pressure level on the model. On the basis of these choices the model which has been built is of the type described in section (3.4.2).

4.3 - Experimental measurements to be performed on the model and the prototype

The experimental measurements performed on model and prototype will be discussed later. However the knowledge of the type of experimental measurement which has to be made on the prototype is an important condition in the construction of a proper model. In fact, it is possible to built the model in such a way to make these measurements more easily and suitable.

Generally the measurements which are performed on structures of this kind, tend to investigate noise sources and propagation paths contributing to the noise inside the cab. Basically two types of measurement are made to determine the "frequency response function" H(f). This function relates the exciting forces on the cab to a) the accelerations of significant points of the structure, or b) the internal sound pressure level produced by the structural vibrations of the flexible walls of the cab.

From the measurements of type (a) it is possible to obtain an indication of the dynamic behaviour of the structure. This is necessary to identify those structural components which cause high sound radiation and are therefore potential sources of noise. From these data it is also possible to determine mode shapes of the whole structure.

Measurements of type (b) give a complete indication of the acoustic behaviour of the cab in relation to the motion of the flexible walls of the cab. Together with the previous measurements they permit the singling out of components which radiate noise with high efficiency and permit the acoustical modal characteristics of the cavity to be known. From these data it is possible also to investigate the nature of the coupling interaction between structure and cavity. The principal aim is to give useful information to the designer, who, modifying the structure, can now reduce the noise transmitted inside the cab.

4.4 - Design of the model

As it has been shown in figure (4.5) the prototype is composed of 5 parts. The model has also been built of 5 parts which have been assembled using the same procedure as the

prototype. Welds have been modelled by the structural cementing system which assures the continuity of mechanical properties of the model material. Moreover as in the prototype, the upper cover (e) is joined to the others parts through screws with the interposition of a thin layer of rubber. The glass windows have been connected to the frames by means of a silicon seal to model the rubber seal. In the model each of these five parts is obtained by joining simple structures such as plane surfaces and bars. Proper materials, thickness and cross-sections of these elements have been deduced from the similarity conditions given in table (3.I).

4.4.1 - Bars

The frame of the cover (e) in the prototype is not constructed from uniform solid bars, but is made up from a box structure which has a varying cross-section. However in the model this composite structure has been modelled by solid bars. In order to choose material and size, the following similarity conditions have been examined:

$$\frac{\omega L}{c_o} = \text{const}, \qquad \text{(acoustic condition)} \tag{4.1}$$

$$\frac{\omega^2 L^2 \rho}{E} = \text{const}, \qquad \text{(longitudinal vibration)} \tag{4.2}$$

$$\frac{q'_t L}{EA} = \text{const}, \qquad \text{(longitudinal forcing action)} \tag{4.3}$$

$$\frac{\omega^2 L^4 \rho}{E\, r^2} = \text{const}, \qquad \text{(flexural vibration)} \tag{4.4}$$

$$\frac{q'_n L^3}{EI} = \text{const}. \qquad \text{(normal forcing action)} \tag{4.5}$$

For simplicity, but without loss of generality for the results obtained, all the bars have been considered fixed at the end.

From condition (4.1), being the same acoustic medium, one gets:

$$(\omega L)_m = (\omega L)_p . \tag{4.6}$$

As the length scale ratio L_m/L_p is 1/5, from equation (4.6) it follows that the frequency scale ratio ω_m/ω_p is 5.

From conditions (4.2) and (4.6) one obtaines:

$$\left(\frac{\rho}{E}\right)_m = \left(\frac{\rho}{E}\right)_p , \tag{4.7}$$

that is to say:

$$(c)_m = (c)_p . \tag{4.8}$$

Therefore the longitudinal sound velocity of the model and prototype material must be the same.

This is a very restrictive condition, but it must be matched. The longitudinal vibrations of these bars, even if they are not of themselves an important source of sound radiation, can excite flexural waves in the glass surfaces that are attached to them, and these flexural waves can be efficient sound radiators.

The material chosen to build these bars is aluminium. This satisfies condition (4.8), it is light, and it is a suitable material for modelling.
Table (4.I) shows some of its physical properties.

Considering now condition (4.4) and remembering conditions (4.6) and (4.7), one obtains:

$$\left(\frac{L}{r}\right)_m = \left(\frac{L}{r}\right)_p \qquad (4.9)$$

Radii of gyration have to show the same scale factor as lengths.

From condition (4.9), it follows that conditions (4.3) and (4.5) for the forcing actions are equivalent.

4.4.1.1 - Choice of the cross-section of the bars

In the previous paragraph it has been concluded that the radii of gyration of bars must have the same scale factor as lengths. First of all it is necessary to choose the reference axes about which to evaluate the radii of gyration. Since these bars form a frame on which the windows will be set up, it was decided to choose cross-sections with sides parallel to the window surfaces. For this reason the chosen reference axes y and z are parallel and orthogonal to these window surfaces. At the same time it can be seen that these are the directions in which the external loads from the glass surfaces exert their action on the bars.

It is evident that these axes will not coincide with the principle axes of inertia of the cross-sections of the prototype, but they will coincide for the bars of the model. This means that the product moments of inertia of the cross sections of the prototype have been disregarded in respect with its moments of inertia (I_y, I_z). This approximation is acceptable only if the two principle moments of inertia are comparable or the angle α between axes y, z, and those central of inertia ξ, η is small (*).

(*) In fact it is possible to write:

$$I_{yz} = \frac{I_\xi - I_\eta}{2} \sin 2\alpha$$

In this respect one can observe that disregarding the product moments of inertia gives an orthogonal flexion instead of the actual non orthogonal bending. The real cross sections of the prototype will rotate around an axis "n" which generally does not coincide with the axis y. This approximation will produce an incorrect evaluation of the displacements due to the external forces. The error will depend on the ratio I_n/I_y.

4.4.1.2 - Computation of the geometric properties of the main cross-sections of the prototype

Figure (4.7) shows the position of the main cross-sections of the cover (e) of the prototype.

The calculation of the properties of these main cross-sections has been performed by a computer program, named "AREE". This is a general program which gives:

- area of the section: A
- static moments S_y, S_z about the chosen reference axes "y" and "z"
- coordinates of the centre of gravity about the same reference axes: Y_G, Z_G
- moments of inertia I_y, I_z and product moment of inertia I_{yz},
- principle moments of inertia I_ζ, I_η
- angle α between axes y, z and those central of inertial ζ, η.
- moments of inertia I_n
- angle β between axes y and n.

As the cross-sections of the prototype are rather complicated, it has been necessary to replace them with straight segments as it is shown in figures (4.8) to (4.12).

The same figures give the value of all the structural parameters, as well as they represent the axis ζ, η, y, z and n.

Finally, table (4.II) summarizes the values of I_n, I_y and shows the values of the ratio I_n/I_y giving an idea of the approximation introduced by considering an orthogonal flexion around the axis y instead of the real deflection around the axis n.

4.4.1.3 - Computation and choice of the geometric properties of the main cross-sections of the model

A range of extruded aluminium bars is available commercially. The catalogues show the main sizes and thicknesses of various types of cross-section:

- solid square (P)
- hollow square (Q)
- T section (T)
- L section with equal sides (L)
- solid rectangle (B)
- channel section (U).

The letters refer to the sections shown in table (4.III).

These commercial lists do not give the properties of the cross-sections. A new Pascal program, named PROFIL, was written to compute the area inertia moments and radii of gyration of all these sections. Computation were made for 300 commercially available cross-sections. The previous program AREE could have been used but it would have been much longer because of the extra information which it computes.

From the comparison of the data obtained from the AREE program for the full scale sections and the data obtained by the PROFIL program for the model sections it was easy to

choose the most suitable cross-section of the commercial bars which satisfied the similarity condition (4.9). In the case of different cross-sections having equal values of radii of gyration, it was decided to choose that which gave less difficulties in assembling the model and which looked like the original in the prototype. Table (4.III) shows the properties of the chosen commercial cross-sections, and figures (4.8) to (4.12) compare these sections of the model with the main cross-sections of the prototype.

4.4.1.4 - Force scale ratios

After having decided the materials, the length scale factors and the type of cross-sections it is possible to obtain the force scale ratios. From equation (4.3) one obtains the scale ratio of the longitudinal forces, that is:

$$\left(\frac{q'_t L}{EA}\right)_m = \left(\frac{q'_t L}{EA}\right)_p \quad . \tag{4.10}$$

From the definition of q'_t it is possible to write:

$$F_{tm} = q'_{tm} \cdot L_m \quad \text{and} \quad F_{tp} = q'_{tp} \cdot L_p \quad .$$

Substituting these relations into equation (4.10) one gets:

$$\frac{F_{tm}}{F_{tp}} = \frac{E_m A_m}{E_p A_p} \cdot \frac{L_p}{L_m} \quad . \tag{4.11}$$

As the length scale ratio is known, as well as the Young's modulus of aluminium and steel, it is possible to write:

$$\frac{F_{tm}}{F_{tp}} = 0.36 \, \frac{A_m}{A_p} \quad . \tag{4.12}$$

From equation (4.5) one obtains the scale ratio of the normal forces:

$$\left(\frac{q'_n L^3}{EI}\right)_m = \left(\frac{q'_n \cdot L^3}{EI}\right)_p \quad . \tag{4.13}$$

With the same previous substitution of $q'_n = F_n/L$, one gets:

$$\frac{F_{nm}}{F_{np}} = \frac{E_m I_m}{E_p I_p} \cdot \frac{L_p^2}{L_m^2} \quad . \tag{4.14}$$

Substituting the numerical values of E_m/E_p and L_p/L_m, one obatins:

$$\frac{F_{nm}}{F_{np}} = 8.575 \frac{I_m}{I_p} \quad . \tag{4.15}$$

If the condition (4.9) is satisfied for all the cross-sections, equations (4.15) and (4.12) lead to the same value of the force scale ratio. For the chosen sections this is not exactly the case; therefore two different series of force scale ratio have been obtained. Table (4.IV) compares all the properties of the cross-sections of model and prototype as well as the value of the force scale ratios. The values of r and I have been computed about a y axis parallel to the window surfaces. As has been already observed, this is the direction which mainly reacts to the transverse vibration of the window.

By looking at this table (4.IV) it is clear that the similarity conditions are not complitely satisfied for all the sections. An assessment of the effects that these "distortions" can produce on the final results will be made later (see § 4.4.3).

4.4.2 - Plane surfaces

In the prototype there are two types of plane surfaces

or pressed surfaces that can be considered plane. These are the metal surfaces which form the floor side and rear panels and the glass surfaces which form the cover.

For both these types of surfaces the similarity conditions that have to be satisfied are those shown in table (3.I). In our case, however, only the conditions related to flexural vibrations are of interest. Therefore the similarity conditions which must be considered for the design of these parts of the model are as follows:

$$\frac{\omega L}{c_o} = \text{const}, \tag{4.16}$$

$$\frac{\rho \omega^2 L^4 (1-\nu^2)}{Eh^2} = \text{const}, \tag{4.17}$$

$$\frac{\rho_o c_o^2 L^3 (1-\nu^2)}{Eh^3} = \text{const}, \tag{4.18}$$

$$\frac{q_n L^3 (1-\nu^2)}{Eh^3} = \text{const}. \tag{4.19}$$

As there are no free edges, the conditions ν = const is not required. From conditions (4.16) and (4.17) it follows:

$$\left| \frac{\rho L^2 (1-\nu^2)}{Eh^2} \right|_m = \left| \frac{\rho L^2 (1-\nu^2)}{Eh^2} \right|_p . \tag{4.20}$$

From the coupling interaction condition (4.18) one gets:

$$\left| \frac{L^3 (1-\nu^2)}{Eh^3} \right|_m = \left| \frac{L^3 (1-\nu^2)}{Eh^3} \right|_p . \tag{4.21}$$

Finally, from equations (4.19) it is possible to obtain the scale ratio of the forces:

$$\left|\frac{q_n L^3(1-\nu^2)}{Eh^3}\right|_m = \left|\frac{q_n L^3(1-\nu^2)}{Eh^3}\right|_p . \qquad (4.22)$$

Having already chosen the length scale factor and the material for the model (in our case, Perspex), both the equations (4.20) and (4.21) can be considered as design equations to obtain the value of the ratio h_m/h_p. These two equations provide the same value of h_m/h_p only if the condition

$$\left|\frac{\rho^3(1-\nu^2)}{E}\right|_m = \left|\frac{\rho^3(1-\nu^2)}{E}\right|_p \qquad (4.23)$$

is satisfied. If this is not the case one has to choose which of these two conditions one can satisfy. This problem was discussed in section (3.4.2).

4.4.2.1 - Modelling of the steel surfaces

From equation (4.20), and with the values of ρ, E and ν showed in table (4.I) for Perspex and steel, one obtains:

$$\frac{h_m}{h_p} = 0.48 . \qquad (4.24)$$

Since the steel surfaces have a thickness of 2 mm, it follows that the perspex plates would have 0,96 mm thickness: obviously this is not a commercial thickness, and therefore it has been decided to use perspex plates of 1 mm thickness.

From equation (4.21) and with the same values of ρ,E, and ν, one obtains:

$$\frac{h_m}{h_p} = 0.675 . \qquad (4.25)$$

This equation gives a different value of the thick-

ness, i.e. 1.35 mm.Again the final choice of the available commercial thickness would have been 1 mm.

In this way two different distortions have been introduced into the model: one as regards the structural condition (4.20), and another as regards the coupling condition (4.21). The probable effects of these distorsions on the model behaviour will be discussed later (see § 4.4.3).

Having established the commercial thickness of 1 mm that is $h_m/h_p = 0.5$, from equation (4.22) and with the usual values of ρ, E and ν one obtains the force scale ratio:

$$\left(\frac{F_{nm}}{F_{np}}\right)_{s}^{px} = \frac{(q_n L^2)_m}{(q_n L^2)_p} = \frac{1}{61.5} \cdot \qquad (4.26)$$

We now see that this value is different from the one obtained for the bars of the cover. This will be discussed later (see § 4.4.3).

4.4.2.2 - Modelling of the glass surfaces

With the values of ρ, E and ν of table (4.I) for Perspex and glass, one obtains from equation (4.20):

$$\frac{h_m}{h_p} = 0.485 \ , \qquad (4.27)$$

and from equation (4.21):

$$\frac{h_m}{h_p} = 0.465 \ . \qquad (4.28)$$

These two values of the thickness ratio are practically equal, and therefore both the structural and the coupling condition will be satisfied.

Since the thickness of the glass in the prototype is 6 mm, from conditions (4.27) and (4.28) one obtains 2,9 mm and 2,8 mm respectively.

The commercial thickness nearest to these values is 3 mm, which again produces a thickness ratio of 0,5.

With this thickness ratio of 0,5, and with the usual values of E, ρ, and ν for perspex and glass, from equation (4.22) it is possible to obtain the force scale ratio:

$$\left(\frac{F_m}{F_p}\right)_g^{px} = \frac{(q_n L^2)_m}{(q_n L^2)_p} = \frac{1}{20.2} \quad . \tag{4.29}$$

Now a further value of the force scale ratio has been obtained; its effect will be discussed in the next section.

4.4.3 - Discussion of the chosen scale ratios and of the effects produced by model distortions

In the previous paragraphs, materials, sizes and thicknesses of the model surfaces and bars, have been selected. The necessity of using commercially available thicknesses does not allow us to comply exactly with all the similarity conditions and therefore forced us to accept a distorted model. Table (4.V) shows the dimensionless parameters which have to be kept constant between prototype and model, and the values of their ratio for model and prototype respectively. It is clear that the condition of perfect similarity is obtained when this ratio is equal 1. Each of these parameter ratios is now discussed and the effect of the distortion is analyzed.

4.4.3.1 - Acoustic field.

(N_1): as the acoustic medium is unchanged and the length ratio is 1/5, having achieved the ratio $(N_1)_m/(N_1)_p$ equal 1, it follows that $\omega_m/\omega_p = 5$.

This value will be considered as the reference value of the frequency scale radio.

4.4.3.2 - Bars

(N_2): For the chosen materials, and length scale factor, the only effect of the distortion from unity of the ratio $(N_2)_m/(N_2)^s_p = (0,96)$ will be in modifying the frequency scale ratio. In this case one obtains:

$$\left(\frac{\omega_m}{\omega_p}\right)_{N_2} = 5.09 \qquad (4.30)$$

(N_4): In this dimensionless parameter, (related to the structural flexional vibration of the bar), the radius of gyration of the section appears: since various types of cross-section have been used there are various values of the ratio $(N_4)^{Al}_m/(N_4)^s_p$. From each one of these values there will be different values of the frequency scale ratio. Considering the theoretical value of $r_m/r_p = 1/5$, the ratio $(N_4)^{Al}_m/(N_4)^s_p$ is 0,96 and therefore the frequency scale ratio becomes:

$$\left(\frac{\omega_m}{\omega_p}\right)_{N_4} = 5.09 \qquad (4.31)$$

The effect produced by the distortions due to these dimensionless parameters N_2 and N_4 is a shift of about 2% in the resonance frequencies of those parts of the prototype modelled by bars.

(N_3) (N_5): From these dimensionless parameters it is possible to see the effects of the distortions of the force scale ratios. In the section (4.4.1.5) it has already been observed that since all the chosen cross-sections do not satisfy the condition (4.9), equations (4.12) and (4.15) lead to two different series of force scale ratio (see Table 4.IV).

The first one, coming from equation (4.12), gives the value of the ratios of tangential forces, the second one, obtained from equation (4.15) shows the values of the ratios of normal forces.

The difference between these values for corresponding cross-sections of the same kind are small. But there are big differences between the values of these ratios for the various cross-sections: they range from 1/61,7 to 1/8,2 for the first case and from 1/58,8 to 1/8,2 for the second. It is difficult to predict the effects introduced into the model by these distortions. They relate to the reactions which each bar exerts on its neighbors through the cementing system or on the plane surfaces connected through rubber seals. However in spite of these variations the average value of all the scale ratios of each series is about 1/25, the Newtonian value.

4.4.3.3 - Plane surfaces

(N_θ): The similarity condition used to design the plane surfaces has been that related to the flexural vibrations of the plate; the dimensionless parameter derived from this condition is N_θ. Having chosen commercial thickness the ratio of this dimensionless parameter between model and prototype is different from 1. Also in this case the effect of the distortion is to modify the frequency scale ratio. From the ratio of N_θ between model and prototype in the case

of modelling steel surfaces, one gets:

$$\left| \left(\frac{\omega_m}{\omega_p}\right)_s^{px} \right|_{N_8} = 5.21 \qquad (4.32)$$

and in the case of modelling glass surfaces one obtains:

$$\left| \left(\frac{\omega_m}{\omega_p}\right)_g^{px} \right|_{N_8} = 5.15 \qquad (4.33)$$

The expected effect will be an increase of the resonance frequencies of the plane surfaces of about 4% and 3%, for steel and glass surfaces respectively, in respect of the reference value of $\omega_m/\omega_p = 5$.

(N_9) (N_{10}): These two parameters are closely related. The first concerns the normal forces which excite the plane surfaces, the second concerns the coupling interaction between the vibrating structure and the acoustic field in the enclosed cavity.

Considering the case of Perspex surfaces modelling the steel surfaces of the prototype one obtains:

$$\left(\frac{p_m}{p_p}\right)_s^{px} = \left(\frac{F_{nm}}{Fnp}\right)_s^{px} \cdot \left(\frac{L_p}{L_m}\right)^2 = 0.406 \qquad (4.34)$$

Considering the case of Perspex surfaces modelling the glass surfaces of the prototype, from equation (4.29) one gets:

$$\left(\frac{p_m}{p_p}\right)_g^{px} = \left(\frac{F_{nm}}{F_{np}}\right)_g^{px} \cdot \left(\frac{L_p}{L_m}\right)^2 = 1.24 \qquad (4.35)$$

Two situations must now be considered. In the first (N_9) an acoustic field excites the structure and in the second (N_{10}) a structural vibration generates a sound field which in

turn exerts a radiation load on the structure itself.

In the first case to produce the same structural dynamic effect as in the prototype, the exciting sound pressure level in the model would be 7.8 dB lower for excitation of the steel plate. But in considering excitation of the glass plates the sound pressure level in the model must be 1.9 dB higher.

In the second case the sound pressure level generated by the vibrations of the structure produces a feed-back on the Perspex surfaces modelling the steel and glass surfaces which is 7.8 dB higher for the steel or 1.9 dB lower for the glass, than in the prototype. From this point of view these two different values of the pressure scale ratio can produce significant distortions only in the case where the acoustic feed-back gives an important contribution to the external loads and thus modifies the motion of the structure vibrating in the air. But this is not the case for our prototype.

(N_6): This dimensionless parameter is related to the longitudinal vibrations of the plate surfaces: the ratios $(N_6)_m/(N_6)_p$ both for steel and for glass show poor modelling of these structural vibrations. This is not a surprising result if it is considered that only the similarity conditions related to flexural vibrations have been used in designing the model. However, it is interesting to check the degree of discrepancy of these dimensionless parameters and then to asses the effects of the distortion so introduced.

Considering the use of Perspex and steel one finds $(N_6)_m/(N_6)_p = 5.74$. This value produces for the chosen materials length and thickness scale factors, a modified frequency scale ratio: that is to say:

$$\left| \left(\frac{\omega m}{\omega p} \right)^{px}_{s} \right|_{N_6} = 2.4 \qquad (4.36)$$

For Perspex and glass figure (4.20) gives $(N_6)_m/(N_6)_p$ = 5.90 and thus a modified frequency scale ratio of:

$$\left| \left(\frac{\omega_m}{\omega_p}\right)^{px}_{g} \right|_{N_6} = 2.4 \qquad (4.37)$$

Again, if the plate surfaces are considered fixed at the boundary, these modified frequency scale ratios have no influence on the results obtained from the model since we are interested only in the acoustic field which is produced by the flexural vibrations of the plate. This is not the case, if the boundary conditions of the plate surfaces are not fixed edges: in this case distortion will be introduced which will be discussed in section (4.4.3.4.).

(N_7): This dimensionless parameter concerns the external tangential forces acting on the plane surfaces. From the ratios $(N_7)_m/(N_7)_p$ for steel and glass surfaces, it is possible to deduce the tangential force scale ratio.Considering the case of Perspex and steel one finds:

$$\left| \left(\frac{F_{tm}}{F_{tp}}\right)^{s}_{px} \right|_{N_7} = \left(\frac{q_{tm}}{q_{tp}}\right) \left(\frac{L_m^2}{L_p^2}\right) = \frac{1}{384.5} \qquad (4.38)$$

and for Perspex and glass:

$$\left| \left(\frac{F_{tm}}{F_{tp}}\right)^{g}_{px} \right|_{N_7} = \left(\frac{q_{tm}}{q_{tp}}\right) \frac{L_m^2}{L_p^2} = \frac{1}{189} \qquad (4.39)$$

Only if the plate edges are not fully fixed will distortions be introduced by the effect of the transmission to neighboring structures.

4.4.3.4 - Effects of connections between bars and plates

When the boundary conditions are fully fixed each plate behaves independently of its neighbors. When different boundary conditions exist, the effect that each component exerts on the others has to be evaluated. That is forces and moments which are transmitted through the connection between each component must be considered. It is possible to obtain dimensionless parameters for these boundary effects.

These dimensionless parameters for the forces and moments at the junctions are exactly the same as the force scale ratios obtained for the fixed edges bars and plates.

In this case however the prediction of the effects introduced by distortions of the model becomes still more difficult. Only some general observations can be made, based on the average behaviour of the whole structure.

First of all consider the cover (e). This is made by bars of aluminium and plates of Plexiglas which model the glass surfaces.

The bars form the frame to which the plates are connected. These two components (bars and plates) transmit through the boundary edges longitudinal and normal forces per unit length q_t', q_n' as well as a moment per unit length m. In section (4.4.3.2) it has been observed that the values of these force scale ratios vary significantly with the type of cross-section chosen to model the prototype. However the average value of all these scale ratio is about 1/25, the newtonian value, and therefore it is reasonable to suppose that this kind of connection does not introduce significant distortions. The effect of the silicon strips in the joints is likely to be such as to reduce some of the distortions.

Consider now the steel components (a), (b), (c) and

(d) which form the lower part of the cab. The models of these components are connected by a structural cementing system modelling the welds of the prototype; each one of these components exchanges with its neighbors longitudinal and normal forces along the boundary edges. The scale ratios of these forces are the same as for the external forces: i.e. equations (4.26) and (4.38). The difference in the numerical values of the force scale ratios will certainly cause distortions of the model behaviour, but is not difficult to predict that they will be insignificant. In fact, these plates which form the lower part of the cab are orthogonally connected to each other and thus longitudinal force on one part becomes normal forces as the other and vice versa.

If now it is considered that the longidutinal stiffness of these thin plates is much greater than the bending stiffness it is clear that when these plates transmit loads longitudinally they act like as rigid structure and therefore significant errors are not introduced by the distortions due to the longitudinal vibrations. From this point of view the different value of the frequency scale ratio (4.36) does not introduce modelling errors, since the lowest resonance frequency of longitudinal vibrations is much higher than the frequency range of investigation of the present model. Therefore it is possible to conclude that, these distortions, introduced by different values of force scale ratio and frequency scale ratio of longitudinal vibrations, do not prejudice the final results obtained by the model.

Finally we will consider the connection between the cover (e) and the whole lower part of the cab obtained by assembling components (a), (b), (c) and (d).

As in the prototype this connection is made by screws put in the same positions and with an interface made of a

thin rubber strip. This careful simulation of the connection system, should avoid significant distortions in the model.

4.4.3.5 - Effects of damping

In section 3.3.13 it has been pointed out that for real damped structures the loss factor has to be kept constant (eq. 3.94). Table (4.I) shows the values of η for prototype and model structural materials: it is possible to observe a significant difference between the damping values. The internal damping of steel and glass are negligible, whereas the material damping of Perspex is relatively heigh.

As a consequence agreement between the dynamic response of model and prototype may not exist at resonance and therefore the peak heights will not correspond. Although joint damping may tend to dominate in a steel prototype, the material damping of Perspex will provide more attenuation of the response than desired. The net effect is that the total damping in true prototype is likely to be similar to that of the model.

However the main purpose of our model is to learn how to design or modify the structure so it will not resonate when driven by the operating forces of the engine: in this respect the ability to predict the exact magnitude of the response is of secondary importance. The resonance frequencies, average response levels and mode shapes are of main interest.

4.5 - Construction of the model

At this point of the work, having already chosen the main structural components it is necessary to decide on the

details of the attachments etc. In addition to plates of Perspex of 1 mm and 3 mm thickness, and aluminium bars, the following materials have been used:

- neoprene rubber of 1 mm thickness, to insert between the cover (e) and the assembled lower part;
- self-threading steel screws 12x2, to fix the cover (e) to the assembled lower part;
- acetic silicon to join modelled glass surfaces to the frames built by the aluminium bars;
- "Tensol Cement 12" for the structural connections between Perspex surfaces.

At the end of the construction the model was strong, light (2.4 kg) and handy, as shown in figures (4.13) and (4.14).

4.5.1 - The cardboard model

Before proceeding with the final construction of the model a cardboard model of 1/5 length scale was made. After having drawn and cut all the components, they were assembled by a transparent adhesive band. In this way it was possible to check the assembly of the complicated shapes and at the same time at the end of the construction it was easy to disconnet the cardboard pieces to get exact form of each component. These forms have been used as masks for cutting Perspex plates and aluminium bars.

4.5.2 - Cutting and assembling of the Perspex aluminium model

The cutting of the Perspex plates of 1 mm thickness has been made following the cardboard masks with a thin sharp knife.

All the components have been assembled by using "Tensol Cement 12". This is a structural cementing system

which practically reestablishes the material continuity of the structure. All the pressed shapes of the bottom plat form have been modelled by adding small pieces of Perspex plates. Both the front and rear supports have been modelled by Perspex plates assembled in such a way as to reproduce exactly the geometrical form of those in the prototype. (see figures (4.15) to (4.18)).

The other Perspex plates of 3 mm thickness have been cut by a thin milling tool, fixed on the chuck of a flexible cable of a drill. These parts, which model the glass surfaces of the prototype, have been connected to the frame by strips of acetic silicon.

Aluminium bars have been cut by a thin hand saw and finished with a grinding wheel.

The connection of these bars has been made by "Loctite" and by a two components paste using aluminium as base.

4.6 - Experimental measurements

In section (4.3) it has already been observed that the measurements which are generally made on structures of this kind, aim to investigate noise sources and their propagation paths. For this purpose two types of measurement are usually performed: a) determination of frequency response function between exciting forces and accelerations on significant points of the structure; b) determination of frequency response function between exciting forces and the internal sound pressure level produced by the structural vibrations of the walls of the enclosed cavity. These two types of measurements have been made both on this model and on its prototype. The measurements have been carried out at the

acoustic Laboratory of Italiana-Keller. (*) In this laboratory routine measurements on acoustic materials can be carried out. They include determination of loss factor, sound insulation and sound absorption. In addition studies are made of the noise generated inside vehicles in a large semi anechoic chamber with a roller-bank. It is in this division of the acoustic laboratory that the measurements on prototype and model have been carried out.

4.6.1 - General description of the data acquisition and processing system of the Italiana Keller Company

Any versatile acquisition system must include extensive signal conditioning equipement linked to the digital processor. It is for instance necessary to insure compatibility between the dynamic range of the signal to be acquired and that available in the digital system. This is often the major criterion for the analogue-digital convertion.

The analogue signal conditioning system is divided into two main parts. The first one is placed next to the test object and several units can be installed if many test stands are to be serviced by one central data processing system. The second part is placed next to the digital acquisition and processing system.

The signals coming from the transducers enter a first amplification stage in which the amplification can be changed for each test in order to adapt the sensitivity of each

---

(*) Italiana-Keller, Corso Nuovo Italia, 2 - Santhià (VC) - Italy.

channel to the transducer. The signal shape of the amplified signal is monitored on an oscilloscope.

This first module has two types of inputs for each channel. One is a charge amplifier to which piezo-electric accelerometers can be connected. The other is a voltage amplifier for signals coming from a microphone pre-amplifier or from other types of transducers. Each channel is further equipped with a phase inverter which can be switched in at will. This is in order to normalize the direction of the signal coming from differently mounted accelerometers. Information collected can thus be related to a given set of carthesian coordinates.

The signals enter the second signal conditioning module over a multiple pin connector which allows a rapid switching between different first input modeles which supply data coming from different test stands to the central processing equipment. The second module contains an amplifier of which the gain can be varied in steps of 10 dB. Also the following filters are included, A, B and CINOR weighting, highpass with a roll-off of 20 Hz, low pass with a roll-off of 8000 Hz and an inverse CINOR weighting filter. All these filters can be switched in under control of the operator and can be used independently of one another. The computer checks which filter has been switched in and reads the amplification set on the amplifier.

The signals coming from the various conditioning channels enter the digital system via 16 antialiasing filters which are controlled over the HP-IB interface and are set automatically at their optimum cut-off frequency depending on the selected digitisation frequency.

Between the output of the antialiasing filters and the digital system proper an analogue multiplexer is placed. This multiplexer is equipped with sample and hold amplifiers which are simultaneously triggered and which maintain the phase accurately between the signals in different channels.

Figure (4.18) shows the block diagram of the digital part of the system. The main part of the digital equipment is made up of two Hewlett-Packard 5451V Fourier analyzer systems. Each of these systems has a central computer of the type HP 21-13 MX-E with respectively 64 K and 128 K words of memory. In most situations the first system is used for data acquisition and the second prepares the outputs in graphical-numerical form. The sampling frequency of the signals is set by a HP 3325A frequency synthesizer which is controlled by the computer over HB-IB interface. In the operating conditions adopted as standard, this synthesizer generates a square-wave of 5 V, peak-peak amplitude and with a frequency of 2048 Hz. Because the usual blocklength used is 1024 points, one obtains a frequency resolution of 2 Hz. The output of graphical-numerical results on paper takes place essentially through the use of a Versatec 1640 printer plotter.

The system is equipped with a digital to analogue converter which makes it possible to generate any analogue signal starting from a given narrowband spectrum. This feature may be used to excite a structure with a series of frequencies having particular relationship both in frequency, amplitude and phase.

The system also has two oscilloscopes which are used for moving mode shape displays.

An extensive description of the data acquisition and processing system as well as the standard and custom software in given in |66|. Here, only the main types of possible investigations and the types of diagrams available after a standard measurements are shown (Tab. 4.VI).

Figure (4.19) shows an overall view of the data acquisition and processing system.

4.6.2 - Description of the measurements to be made

In section 4.3 a description of the experimental measurements which have to be made on the prototype and on the model has already been given.

The frequency response function is generally a complex number with real and imaginary part given by

$$\tilde{H}(f) = \mathcal{R}_e\, H(f) - i\mathcal{I}_m H(f) \tag{4.40}$$

or

$$H(f) = |H(f)|\, e^{-i\phi(f)} \tag{4.41}$$

where

$$|H(f)| = |\mathcal{R}_e^2 H(f) + \mathcal{I}_m^2 H(f)|^{\frac{1}{2}} \tag{4.42}$$

$$\phi(f) = \mathrm{Tan}^{-1} \left| \frac{\mathcal{I}_m H(f)}{\mathcal{R}_e H(f)} \right| \tag{4.43}$$

The magnitude $|H(f)|$ is commonly refered to as the system "gain factor" and the phase $\phi(f)$ is called the system "phase factor". The amplitude response $|H(f)|^2$ is given by the input/output autospectrum relation |67|:

$$G_{yy}(f) = |H(f)|^2\, G_{xx}(f), \tag{4.44}$$

where $G_{yy}(f)$ and $G_{xx}(f)$ are the power spectral density func-

tions of output and input signals respectively.

It is possible to show also that H(f) can be determined by the following relation:

$$G_{xy}(f) = H(f)\ G_{xx}(f), \tag{4.45}$$

this is called the input/output cross-spectrum relation.

These results apply only to ideal situations where no extraneous noise exists at input or output points, and the systems have no time-varying or nonlinear characteristics. Under this hypothesis it is easy to show that the "coherence function" between x(t) and y(t), given by:

$$\gamma^2_{xy}(f) = \frac{|G_{xy}(f)|^2}{G_{xx}(f) \cdot G_{yy}(f)} \tag{4.46}$$

is equal 1 at all frequencies: this is quickly verified by substituting equations (4.44) and (4.45) into equation (4.46).

To express this result physically, $\gamma^2_{xy}(f)$ is the percentage of the power-like quantity in the received signal y(t) due to the transmitted signal x(t).

Since the output signal y(t) results only from x(t), all of the power in the output depends on the input. If there is another signal source adding to the output y(t), such as a signal z(t) there the measured coherence will be less than 100%.

From the experimental point of view, the input signal x(t) was an impulse given by a force transducer fixed at the top of a small hammer hitting the structure. The output signals y(t) were given by accelerometer transducers or microphones.

The whole measuring system acquires and processes the

data and finally displays the modulus and phase values of H(f) as well as the coherence function between input and output signals.

4.6.3 - Measurements on the prototype

With the help of Italiana Keller technicians the measuring points were chosen: the positions were those which during a previous acoustic study proved to be the most significant for the understanding of the dynamic behaviour of the structure.

Figures (4.20) and (4.21) show the measuring points of acceleration (dots) and sound pressure levels (squares).

Microphones (2) and (3) were placed near the position of the head of the driver (fig. 4.22).

The whole cab was mounted on a movable frame through four resilient supports (fig. 4.23).

4.6.3.1 - Transducers

Eight B&K 4366 accelerometers (30 g weight) and two B&K 4169 microphones (1/2") have been used: the accelerometer transducers were screwed on small plates fixed on to the measuring points of the structure by a proper cementing system; the two microphones were fixed to a movable support (fig. 4.22). A B&K 8200 force transducer was fixed on the head of a small hammer used to excite the structure.

4.6.3.2 - Measurements procedures

a) *Preparation of the set-up.*

In the operation of the data acquisition system it is necessary to provide a control block of informations which

gives, for example, the number of channels and the digitation frequency and a series of identification data. This descriptive information has been used in the heading of all graphical outputs which have been derived from the data acquired.

b) *Calibration of the various channels.*

It was possible to read the output voltage after the first amplification stage while the calibration signal was applied to the transducer. For each type of physical unit, (force, acceleration or sound level) a normalized calibration factor was defined. For instance, for sound level it was defined that 100 millivolts R.M.S. corresponds to 94 dB sound pressure. This correspondence can be checked or corrected and adjusted without using the computer, simply by applying the pistonphone signal to the microphone and by reading the output signal with the digital voltmeter and adjusting the first gain stage.

c) *Instrument set-up.*

In this phase the computer sets the instruments which perform under its control. It implements the settings specified by the operator in the test set-up and it checks the position of the switches on the various filters.All switch-positions on the signal conditioning unit are checked against those specified in the system set-up.

d) *Acquisition.*

Before the actual acquisition is started, the program reads the gain setting on all signal conditioning channels and stores this information in order to be able to calculate the actual physical values measured. At this point it is sufficient to switch the "mode" corresponding to the acquisi

tion of transfer functions to start the process.

e) *Re-arranging of the data.*

At the end of the acquisition phase, the computer re-reads all the row data from the disc, di-multiplexes them and re-writes them in final form on disc after having performed the Fast-Fourier Transform (and calculated the transfer functions). During the re-reading and conversion of the data, the program also checks for overflow and underflow.

f) *Request of graphical output.*

Standard graphical outputs of any types can be requested by the operator in an interactive mode, or a larger number of diagrams can be requested via a so-called "plot-menu". A plot-menu is a list specifying a whole series of diagrams which are to be prepared one after the other. The output process can proceed without any further action on the part of the operator.

4.6.3.3. - Experimental results

During the previous acoustic study of the cab, the Italiana-Keller technicians observed that the low frequency noise (in approximately the 20-400 Hz frequency range) was of primary interest and particularly that this noise was generated by the structural vibration of the wall panels of the cab. Therefore it was decided to restrict the frequency field of investigation to 400 Hz.

Figures (4.24) to (4.28) show some of the results obtained. They present the values of "gain factor", and "phase factor" of the frequency response function between exciting force and accelerations and the coherence function between the two signals. The curves on each diagram repre-

sent the average value of 5 measurements performed by hitting each of the four supports of the cab and measuring the accelerations on the selected points of the structure. The point of excitation, and the point of measurement are also noted in the heading of each figure.

Figures (4.24) to (4.27) show "gain factor" and "phase factor" of the frequency response function between the exciting force and the inner sound pressure levels. Also in this case the curves of each diagram represent the average value of 5 measures.

The scale of the "gain factor" is expressed in logarithmic form, namely dB, and the positions of the point of excitation and the microphone are indicated in the heading of each figure.

4.6.4. - Measurements on the model

The points of measurements were exactly corresponding to those chosen for the prototype. The model was mounted on a table on a layer of resilient material (fig. 4.29).

4.6.4.1. - Transducers

The same B&K 8200 force transducer fixed on the head of the hammer was used. One B&K 4375 accelerometer (2 g weight) was screwed successively on small plates fixed by Loctite on the measuring points of the model (fig. 4.29). One microphone B&K 4169 (1/2") mounted on a flexible cable was introduced into the model through a small hole made in its front panel. In order to reduce the contact between the structure and this flexible cable, a thick ring of resilient material surrounded the cable.

4.6.4.2. - Measuring procedures

Set-up calibration, acquisition, re-arrangement of the data, and request of graphical output are carried out as for the prototype. On the assumption of linear behaviour it is considered permissible to apply the "reciprocity principle" and so simplify the measurement procedure. Since only one light accelerometer was available, it was easier to fix it in one position and excite the structure with the hammer at each of the previous measurement points.

4.6.4.3. - Experimental results

Since the reference value of the frequency scale ratio was 5 (§ 4.4.3), the frequency field of investigation was expanded to 2000 Hz.

Figures (4.24) to (4.28) show the experimental results correspondent to the same points of measurement previously examined. Figure (4.28) the frequency response functions between force and accelerations and figures (4.24) to (4.27) the frequency response functions between force and sound pressure levels.

4.6.5. - Comparison of the experimental results

In order to compare all the experimental results it was necessary to determine the vertical shift which was to made between the curves of the prototype and the model.This shift has been calculated according to the dimensionless parameters previously obtained.

a) *Frequency response function between force and acceleration*

If with the symbol | | is indicated dimension of the quantity, it is possible to write:

$$|H| = \frac{|a|}{|F|} = \frac{|F|}{|M|} \cdot \frac{1}{|F|} = \frac{1}{|M|} \cdot \tag{4.47}$$

The relation shows that the shift between the frequency response function of this kind for prototype and model is given by the ratio of the inverse of the mass of the structure; namely:

$$\frac{|H_m|}{|H_p|} = \frac{|M_p|}{|M_m|} = \frac{\rho_p \cdot h_p \cdot L_p^2}{\rho_m \cdot h_m \cdot L_m^2} = 335. \tag{4.48}$$

This value has been obtained considering $\rho_p/\rho_m = 6,7$ (Tab. 4.I), $h_m/h_p = 2$ and $L_p/L_m = 5$.

Using the scale of the diagrams this number corresponds to $10^{2,5}$. With this value of the shift figures (4.32) and (4.33) have been drawn.

b) *Frequency response function between force and sound pressure levels.*

With the above assumptions it is possible to write:

$$|H| = \frac{|p|}{|F|} \tag{4.49}$$

and then the shift will be given by:

$$\frac{|H_m|}{|H_p|} = \frac{|P_m|}{|P_p|} \cdot \frac{|F_p|}{|F_m|} \cdot \tag{4.50}$$

Since the sound pressure is the same in the prototype as in the model (Tab. 3.V) i.e. $p_m/p_p = 1$ it follows that this ratio H_m/H_p is equal to the inverse of the ratio of the forces: from relation (4.26) one gets:

$$\frac{|H_m|}{|H_p|} = \frac{1}{61.5} \cdot \tag{4.51}$$

Using the same scale of the diagrams this number cor-

responds to a shift of about 35 dB. Figures(4.30) and (4.31) show the comparison of these frequency response functions.

4.6.6. - General comments on the experimental results.

In this section only some general remarks on the results will be made; a deeper examination will be developed later.

From a general look of all the diagrams of figures (4.30) to (4.33), one can observe a satisfactory agreement between the model and the prototype. A better approximation has been obtained for the frequency response function between force and sound pressure level than for the acceleration response functions.

The acoustic frequency response function is perhaps the most important for studying the acoustic field inside the cavity but nevertheless the knowledge of H(f) between force and accelerations may give significant contributions to the understanding of noise generation mechanism.

Despite some local differences between the gain factors of H(f), the average values in the frequency range of investigation agree reasonably well. Also the resonance frequencies even if not yet well identified, seem to be well matched. A shift towards higher frequency values in the case of the model seems to agree with the predictions given by the relations (4.29) and (4.30). The phase factors show this effect clearly.

4.7. - Further measurements on the model

To investigate some of the features of the acoustic response further tests were made on the model in the Insti-

tute of Technical Physics - University of Bologna. The acoustic and vibration instrumentation of the Institute mainly consists of B&K traditional analogue equipment such as exciters, transducers, signal conditioners and read out devices. The first measurement which was made was to verify the linearity of the system; it was also possible to check with the Institute's instrumentation, some of the measurements made at Santhià. After that, acoustic resonance frequencies of the cavity were measured in order to separate clearly the contributions of the structural components. These last measurements were made both with the model in air and immersed in sand. The aim was to verify the influence of the flexible walls on the acoustic resonance frequencies of the cavity.

Also the influence of a driver inside the cab on these resonances has been checked by putting a little man inside. Finally, to have a better understanding of the results, the values of the resonances of the cavity were computed by a finite element technique.

4.7.1. - Verification of the "reciprocity principle"

This verification has been made exciting the model by a sinusoidal testing with sweeping frequency.

Figure (4.34) shows the arrangement for making automatic graphic recordings of the frequency response function between force and acceleration as function of frequency. As it is required to maintain a costant value of the input force (1 N) the output signal of a B&K 8200 force transducer mounted on the B&K 4810 mini-shaker, has been used in a servo loop to control the input level to the exciter. The signal from the B&K 4375 (miniature size) accelerometer, via a B&K 2635 preamplifier, enters a measuring amplifier and

finally is recorded on graphical form (B&K 2307).

The acceleration levels read from the level recorder give directly the value of the gain factor of the frequency response function. Figure (4.35) compares the results obtained exchanging the position between input force and acceleration. The curves show an excellent agreement.

Comparing now these results with those obtained in the acoustic laboratory of Italiana Keller, it is possible to observe some significant differences in the relative amplitudes between resonances but the general behaviour is respected. It should be remembered that not only the instrumentation was completely different, but also the testing methods. In Bologna a sinusoidal testing with sweeping frequency was used whilst in Santhià an impact testing was used.

4.7.2. - Acoustic resonance frequencies of the cavity

The arrangement for the investigation of modes inside the cavity is shown in figure (4.36).

A small loudspeaker was placed in one corner of the cavity in such a way that practically all the cavity modes were excited. The microphone, one B&K 4134, has been placed in two different positions: the usual one near the head of the driver (2) and one in the corner near the right foot of the driver (4). The loudspeaker was drived by a B&K 1023 sine generator which was controlled by a relatively slow frequency sweep rate. Because of its flat frequency response no compressor was used.

In order to reduce the influence of wall vibrations on the resonances of the cavity, the model was immersed in

sand. The likely size of such an effect exists has been discussed by |47| who found a shift of the values of the acoustic resonances.

Figure (4.37) shows the results obtained by this arrangement when the microphone was in position (2) and (4) respectively.

Because the geometry of the cavity is not very regular, it is difficult to associate each resonance peak with a specific mode of vibration. It is therefore difficult to predict which of these modes will be excited more readily by the structural components of the cab. A finite element analysis of the cavity was developed to increase on understanding of the spatial variations of the pressure field at each major resonance. It was then easier to point out structural component which have the greatest coupling effect.

In the next section the results obtained by this analysis are discussed.

4.7.3. - Finite element analysis of the cavity: acoustic modes of vibrations.

In section (2.6.1.1.) it has already been observed that if the walls of the cavity are assumed to be rigid, in the finite element model, then the only data necessary to compute the resonances of the cab are its geometric sizes. Although the cab is not exactly prismatic in shape, a reduction from the three-dimensional representation to a two-dimensional representation should give a good approximation for many of the lower modes. The compartment has then been represented by a two-dimensional finite element model using two different cross-sections: one through the central axis

of the cab and the other shifted towards the side of the cab (fig. 4.38). These two sections have been divided into triangular finite elements, with nodes at the vertices of triangles. The geometrical data was entered into a Fortran program, named "FEMAM", based on the finite element method proposed by |55| for irregularly shaped cavities. The output of the program provides a list of resonance frequencies, followed by a series of drawings showing, for each frequency, the behaviour of the sound pressure at each node.

Figures (4.39) to (4.46) show the distribution of sound pressure levels in the cab for the two sections considered and for each resonance frequency; nodal lines are also indicated. Microphone positions (2) and (4) are shown by black triangles.

To compute the resonance frequencies of the whole structure we must take into account the third dimension of the cab. This can be done by the relation:

$$f_{tot}^2 = f_t^2 + f_l^2 \qquad (4.52)$$

The value of the transverse resonance frequencies (f_t) can be easily obtained by the following equation:

$$f_t = \frac{nc_o}{2L} \qquad n = 1, 2, \ldots \qquad (4.53)$$

where L is the transverse size of the cab. With the value of L = 21 cm, one obtains:

$$\begin{aligned} f_{t1} &= 809.5 \qquad \text{for } n = 1 \\ f_{t2} &= 1619.0 \qquad \text{for } n = 2 \end{aligned} \qquad (4.54)$$

Table (4.VII) summarizes the values of two dimensional

results for the resonance frequencies both for the central section and the adjacent one, as well as their combination with the first transverse resonance frequency (809.5 Hz) according to equation (4.52).

Figure (4.47) compares the experimental results obtained for the model in the sand, with theoretical values of the resonance frequencies of table (4.VII). Immediately one can observe that not all the resonance correspond to peaks in the experimental curves. The reason of this is that the microphone positions (for some resonance frequencies of the cavity) are near nodal lines of the sound pressure. The dots in table (4.VII) indicate these values. After these eliminations it becomes clear that in figure (4.46) at MIC 2 the frequencies 653.3 Hz and 1136.1 Hz perfectly match the first and third peak of the curve. Also the first (1040 Hz) and the third (1394 Hz) resonance frequency of the whole cab correspond to the second and fourth peak of the curve. For frequencies higher than this fourth peak the experimental and theoretical results do not agree so well. However this frequency range is not very much important for our investigation.

Similar observations may be made from figure (4.47) at MIC 4, where the first (556.0 Hz), the third (1002.2 Hz) and fifth (1464.4 Hz) resonance frequency are quite well identified by pronounced peaks of the curve. Near this third value of the resonance frequency also the first (981.6 Hz) frequency of the whole cavity takes place.

An important peak around 1150 Hz may be assigned to the second resonance frequency of the whole cab. In this case it is not clear why one weak longitudinal mode has combined with a transverse mode to give a predominant peak. At frequencies higher than 1500 Hz it becomes difficult to

assign to each peak the corresponding mode shape. But, as it has been already observed, this frequency range is not so important fo r our purposes. Figure (4.48) shows a comparison between the same experimental curves and the theoretical resonance frequencies just identified.

4.7.4. - Acoustic resonance frequencies of the cavity with model in air.

In order to verify the influence of the motion of the flexible walls on the resonance frequencies of the cavity, some measurements have been carried out with the model in air. The measurement procedures were as described in the previous section, and the instrumentation set up is shown in figure (4.36). Figure (4.49) compares the results obtained with the model in sand and in air, when the microphone occupies position (4). Any significant difference is evident.

4.7.5. - Influence of the driver on the resonance frequencies of the cab.

In order to examine the influence that a driver may have on the values of the resonance frequencies, a 1/5 scale model of a driver was introduced into the model when this was immerged in the sand. The material used for the model was poljuretane. The measurements were made as in section 4.6.7.3. and the microphone was in position 4.

Figure (4.50) compares the results obtained with and without the driver. It is interesting to notice that the presence of the driver tends to lower the first few resonance frequencies of the cavity. This result was already observed by Nefske et al. [53] who compare both theoretical and experimental resonance frequencies of a car compartment with and without seats. The differences were in part explain

ed by an increase in the effective length of the cavity due to the presence of the seats. A similar effect may be ascribed to the presence of the driver.

4.8. - Final discussion of all the experimental results.

In the previous sections the following measurements have been described and their results shown:

a) frequency response function between force and sound pressure level for the prototype,
b) frequency response function between force and accelaration for the prototype,
c) as in a) but for the model,
d) as in b) but for the model,
e) acoustic resonance frequencies of the model.

From a comparison of these results it is possible to check the validity of the proposed model technique. In the sequence of discussion the design procedure will be adopted. That is: firstly it will be assumed that we have only the results obtained from the model. From these we will try to investigate the dynamic behaviour of the full scale structure in order to suggest to designers the noise characteristics. Finally the predictions from the model will be compared with the results from the full scale test to verify the modelling procedure.

4.8.1. - Discussion of the results obtained on the model.

The model results will now be analyzed to investigate

i) acoustic resonance frequencies of the cab,
ii) natural resonance frequencies of the structure
iii) those components which vibrating at resonance with the acoustic resonances may produce high sound pressure level in the cavity.

From a comparison of figure (4.48) and for example, figure (4.51) it is possible to begin to separate some structural resonance frequencies from the acoustic ones. Around 600 Hz, 1000 Hz and 1150 Hz there are a clear coincidences between the two curves, showing that these peaks of the H(f) are produced mainly because of the cavity resonances. Other peaks at about 200 Hz, 370 Hz, 710 Hz are also evident. They appear to be structural resonance frequencies as will now be described. In figure (4.52), which shows H(f) between acceleration of point MC 12, and the exciting force, two peaks, around 200 Hz and 350 Hz, are clearly evident. Also the phases of these two peaks are well matched to the pressure field which shows the same phases at these two frequencies. This means that the motion of the lateral member is in phase with the motion of the air in the cavity. Therefore these frequencies lie well below the first transverse resonance frequency of the cavity, and hence they are structural resonances uncoupled to the cavity. Similar conclusions can be made for the values of H(f) for other points on the lateral members.

From figure (4.53) showing the value of H(f) between acceleration of point MC 04 of the platform and the force one peak at about 200 is also clearly evident. The phase shows a small shift between acceleration and force and this suggests the presence of the first resonance frequency of the platform. Between the effects produced by these two components (lateral members and platform) the phase of H(f) between sound pressure and force, shows a greater importance of the lateral members which practically lead the inner sound field.

Let us consider the peak at 710 Hz. Figure (4.54) shows the value of H(f) between the acceleration of the point MC 02, on the platform, and the exciting force. Two

peaks are clearly evident: one at 720 Hz (the higher) and a second one at 960 Hz; the phases are about 180°. Looking again at figure (4.41) one sees that at 710 Hz the phase is 180° because the frequency is just above the first longitudinal resonance frequency of the cavity. The sound pressure is therefore produced by the motion of this component. At 960 Hz figure (4.51) shows a high peak which can be obtained by the superposition of the first resonance of the whole cavity (1040 Hz) with this structural resonance of the platform.

At this point one may conclude that, at least in the frequency range examined, the following peaks are probably produced by these components:

200 Hz: prevalent effect of the structural frame members with the superposition of the first resonance of the platform.

370 Hz: prevalent effect of the frame.

600 Hz: first longitudinal resonance frequency of the cab excited by the platform (fig. 4.53).

710 Hz: structural resonance of the platform.

950 Hz: first resonance frequency of the whole cab (1040 Hz) excited by the structural resonance of the platform at 960 Hz.

1130 Hz: Third longitudinal resonance frequency of the cab cavity. In this case there are not components which contribute specifically to this peak. However from figure (4.52) it is evident that the platform, also at this frequency, is submitted to high values of acceleration and therefore able to produce significant sound pressure in the cavity.

In figure (4.51) there are other important peaks, par

ticularly at about 1300 Hz and 1500 Hz, but to understand the mechanism which produces such peaks, it is necessary to measure the value of H(f) at many more points on the structure.

4.8.2. - Discussion of the results obtained on the prototype.

Figure (4.55) shows the value of H(f) between the sound pressure level and the force on the prototype for the same points as on the model. In this case a transparent sheet shows the main resonance frequencies of the cavity of the cab obtained by the finite element analysis on the model divided by 5 (ω_p/ω_m = 1/5). We can see that the two peaks at 120 Hz and 200 Hz match well with the resonances of the cavity. However there are other significant peaks around 40-50, 90 and 150 Hz.

Les us consider the peaks around 40-50 and 90 Hz. Figure (4.56) represents the values of H(f) between acceleration of point (PC14) on a frame member of the cab and the exciting force. This figure shows two significant peaks in the low frequency range up to 100 Hz. The phases at 40-50 Hz are at about 90° as in the case of figure (4.55). Thus we can conclude that the motion of the frame members drives the motion of the air in the cavity thus producing a uniform sound pressure in the inner environment. At 90 Hz there is a phase inversion (-180 to + 180) on figure (4.55) as well as in figure (4.54). The same effect may be observed in the values of H(f) for other points on the frame members of the cab. Looking through the values of H(f) for the points on the platform at the frequency of 50 Hz a significant peak is seen (for example fig. 4.57). This leads to conclude that the platform also contributes to the inner sound pressure.

From the same figure (4.57) a large peak is evident at about 150 Hz. Figure (4.58) shows that there is an additional peak at 120 Hz. While this last peak of the platform at 120 Hz matches well the first longitudinal frequency of the cavity, the peak at 150 Hz corresponds to the high peak of the frame members (see fig. (4.59)) which combine to produce high levels of the sound pressure in the cavity.

At the first tangential resonance of the cavity (200 Hz) there is a high peak of the curve of H(f) (fig. 4.55). However there are no components with evident resonances close to this frequency. Nevertheless for the platform there appear to be many important modes of vibration in the range just above 200 Hz as shown in the figure (4.58). Therefore it seems possible to conclude that the platform is mainly responsable for the peak in the cavity frequency response at 200 Hz. This argument is supported by the observation of the phase of H(f). From figure (4.55) at 200 Hz one finds a $\varphi \cong 0°$ exactly like from figure (4.58). It can also be observed that the cavity is easly excited in this frequency region as it has two near acoustic resonances: i.e. 200 Hz and 225 Hz.

We can therefore conclude:

40 - 50 Hz: prevalent effect of the frame members with
(200-250)(*) influence from the first resonance of the platform.

90 Hz: prevalent influence of the frame members
(450) alone.

(*) Model frequencies are shown in brackets.

120 (600) Hz: first longitudinal acoustic resonance of the cavity with the superposition of structural resonances of the platform and of the frame members.

150 (750) Hz: structural resonances of the platform and of the lateral members

200-225 (1000-1125) Hz: first tangential one and 225 Hz the third longitudinal one. In this region the platform is excited by important flexural vibrations which match well the acoustic field of the cavity.

4.8.3. - Comparison between the prototype and the model.

From the conclusions at the end of sections (4.8.1.) and (4.8.2.) a good agreement between model and prototype is seen to have been achieved. Almost all the components which contribute to the inner acoustic pressure have been correctly identified by the model. All the peak frequencies listed in the conclusion except that at 90 Hz full scale are in close agreement. The different frequency scale ratio between the 90 Hz of the prototype and the corresponding one of 370 Hz on the model ($\omega_m/\omega_p = 4$) should not be surprising if it is considered that the lateral members which excite these peaks have been modelled by aluminium bars with single cross sections. In fact the ratios between their radii of gyration and those of the real members of the prototype, show values different from the theoretical one of 1/5 (table 4.IV).

It can be emphasized that not only the frequency behaviour of H(f) has been well reproduced, but also its magnitude and phase.

The different values of the loss factors between model and prototype materials do not seem to have introduced si-

gnificant distorsions on the modelling of the cab. This is probably due to that the total damping of the cab and the model was very similar.

At this point of the work it is therefore possible to conclude that this modelling technique is a usefull tool for acoustic designers to predict acoustic and structural behaviour of shell structures.

Figure 4.1 - Picture of the major parts of the savety cab: right side of the cover.

Figure 4.2 - Picture of the major parts of the savety cab: inside view.

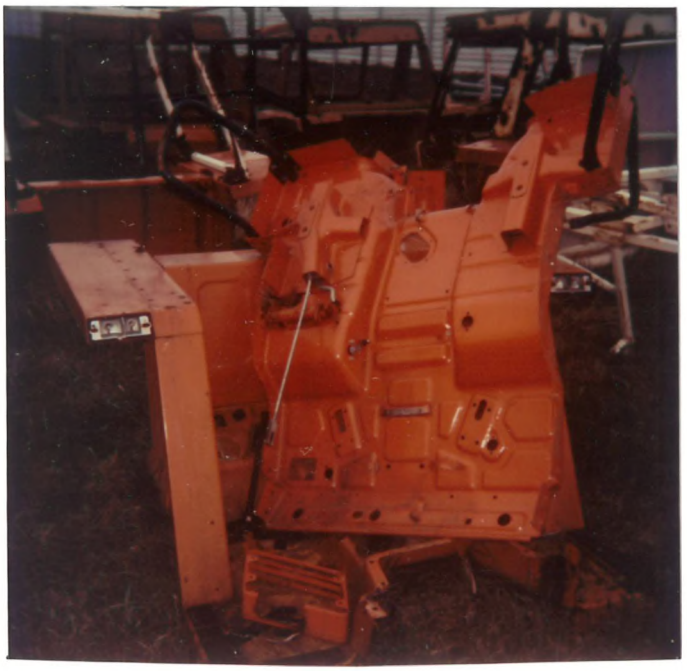

Figure 4.3 - Picture of the major parts of the savety cab: platform.

Figure 4.4 - Picture of the major parts of the savety cab: top of the cover.

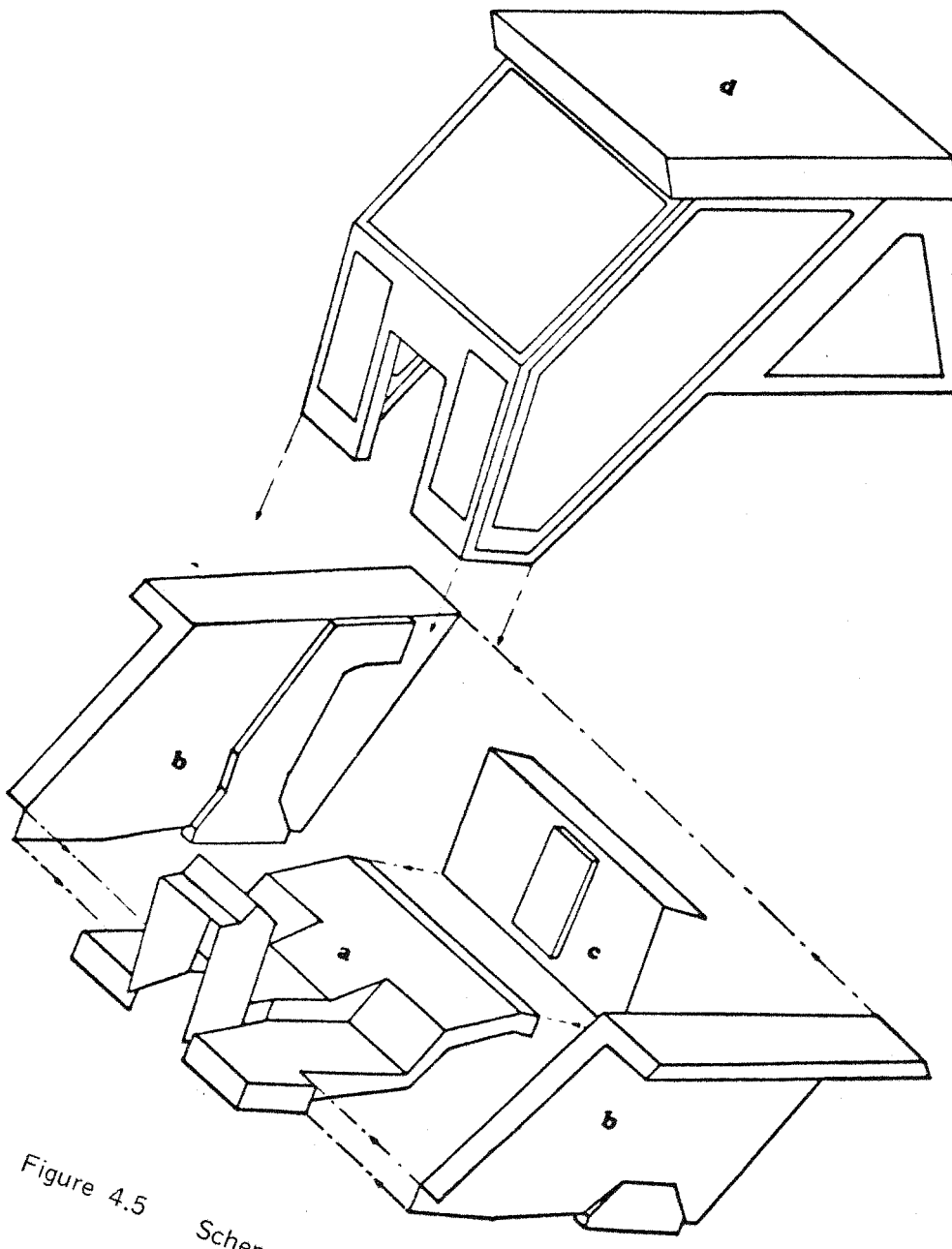

Figure 4.5 Scheme of the major parts of the savety cab.

Figure 4.6 Rear supports attached to the lateral side panels.

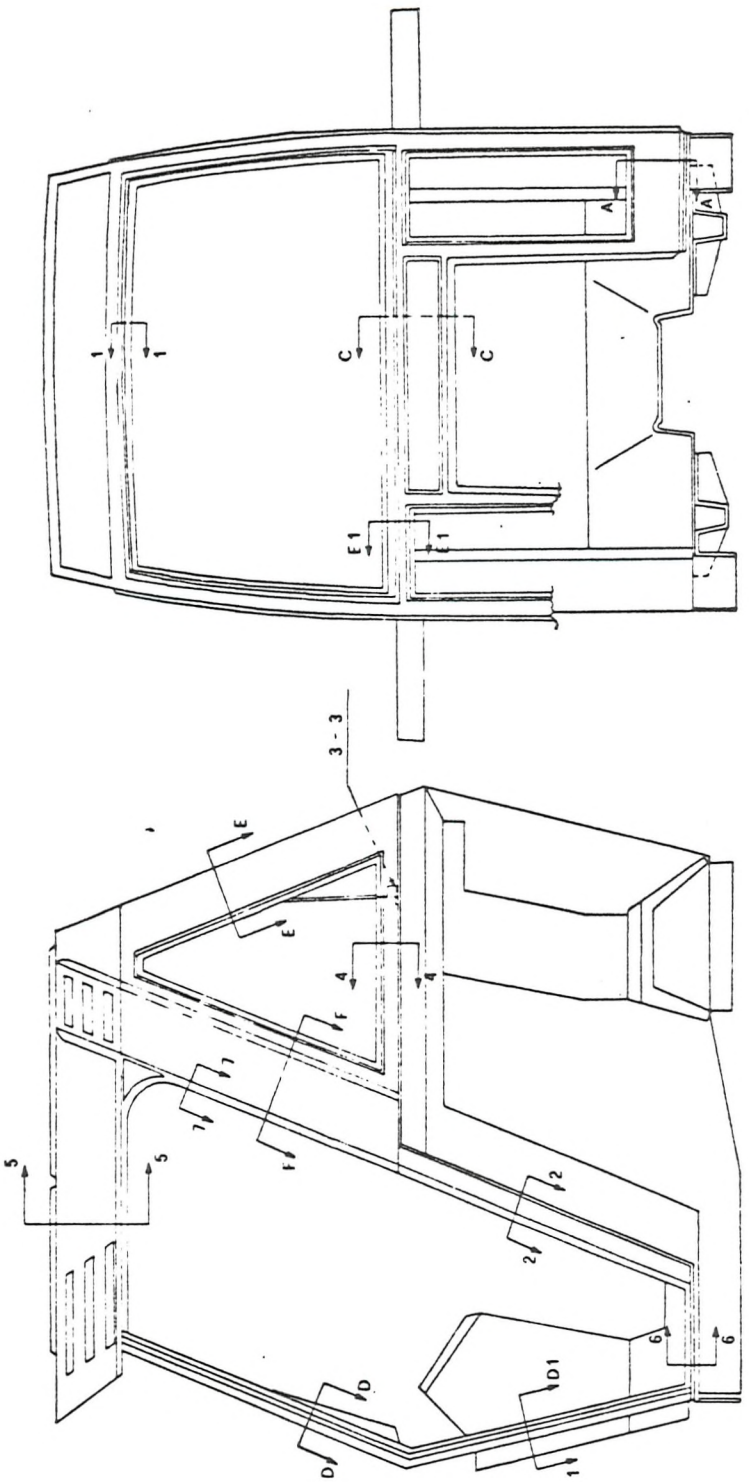

Figure 4.7 Position of the main cross-sections of the cover.

SECTION A-A SCALE 1:2

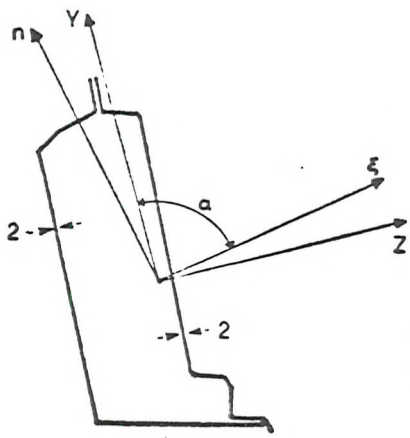

A = 793

I_y = 312 625

I_z = 1 811 937

G_y = 19,85

G_z = 47,8

I_{yz} = 273 200

I_n / I_y = 0.85

MODEL SCALE 1:2

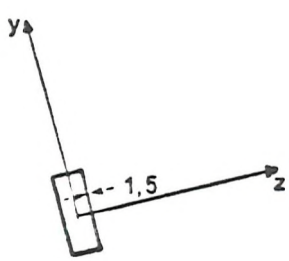

A = 111

I_y = 1624,8

I_z = 11 012,6

G_y = 3,83

G_z = 9,96

Figure 4.8 Geometric properties of section AA.

SECTION C-C SCALE 1:2

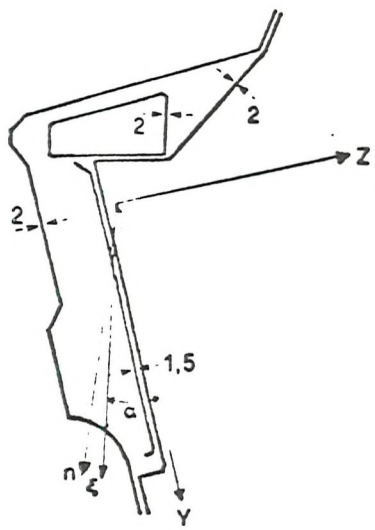

A = 1520

I_y = 1233 625

I_z = 4183062

G_y = 28.5

G_z = 52,45

I_{yz} = -851301

I_n / I_y = 0,83

MODEL SCALE 1:2

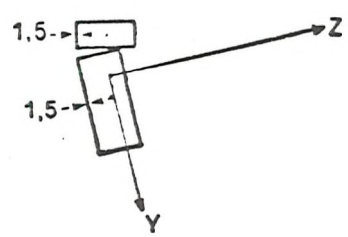

A = 222

I_y = 5866.1

I_z = 24612,4

G_y = 5,14

G_z = 10,52

Figure 4.9 Geometric properties of section CC.

SECTION D – D SCALE 1:2

A = 966

I_y = 416625

I_z = 451500

G_y = 20,75

G_z = 21,6

I_{yz} = 211932

I_n / I_y = 0,62

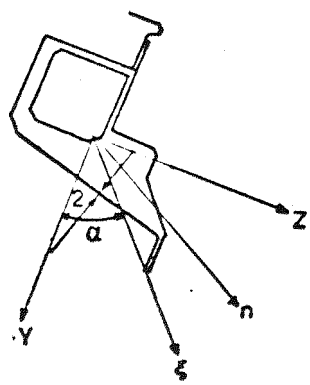

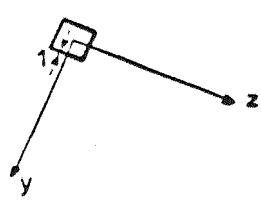

MODEL SCALE 1:2

A = 46

I_y = 892,7

I_z = 892,7

G_y = 4,41

G_z = 4,41

Figure 4.10 Geometric properties of section DD.

SECTION E-E SCALE 1:2

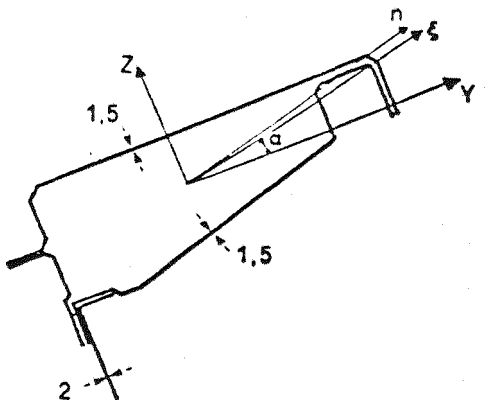

$A = 725$

$I_y = 304\,125$

$I_z = 1\,878\,625$

$G_y = 20,5$

$G_z = 50,9$

$I_{yz} = 382574$

$I_n/I_y = 0,71$

MODEL SCALE 1:2

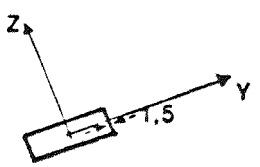

$A = 111$

$I_y = 1624,8$

$I_z = 11012,6$

$G_y = 3,83$

$G_z = 9,96$

Figure 4.11 Geometric properties of section EE.

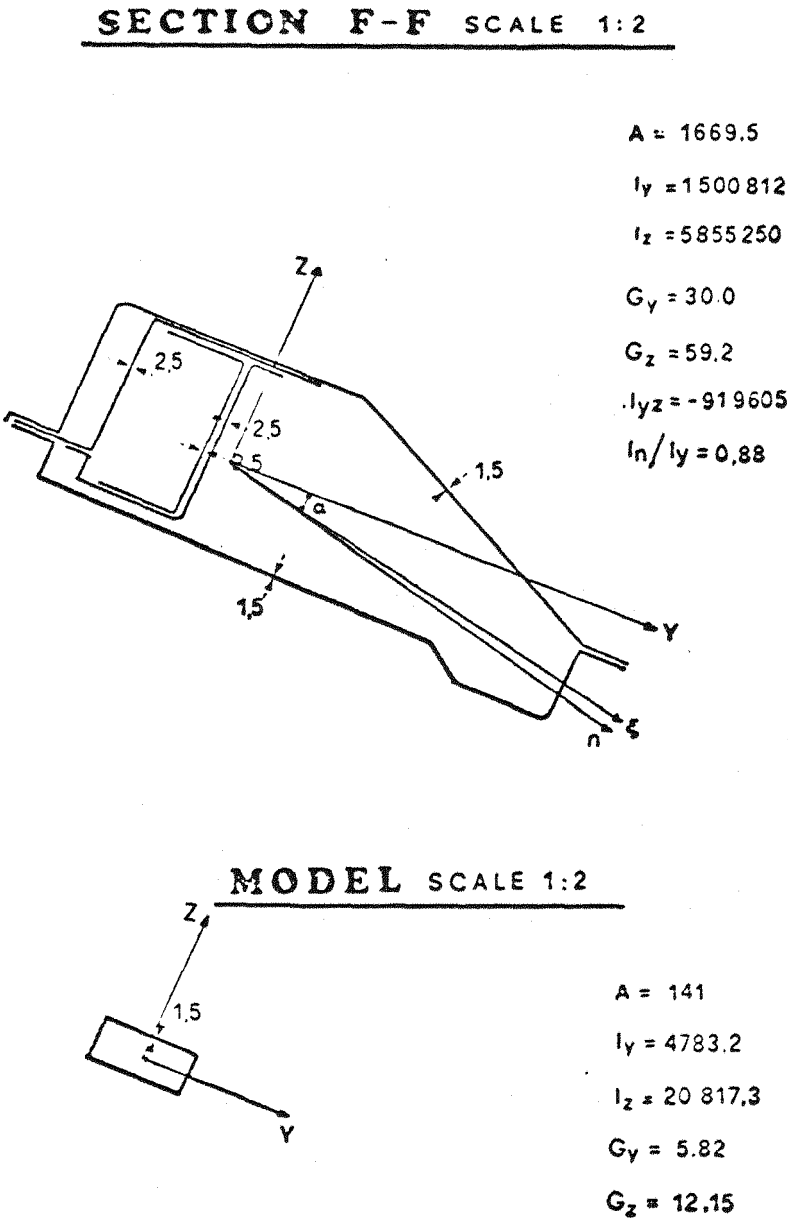

Figure 4.12 Geometric properties of section FF.

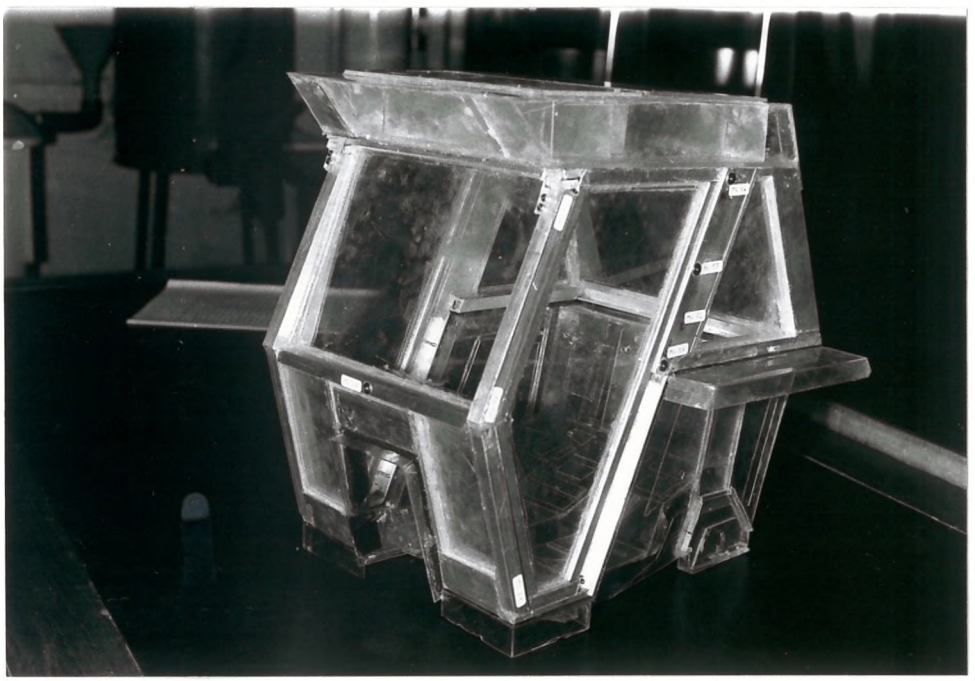

Figure 4.13 Picture of the Perspex model: lateral view.

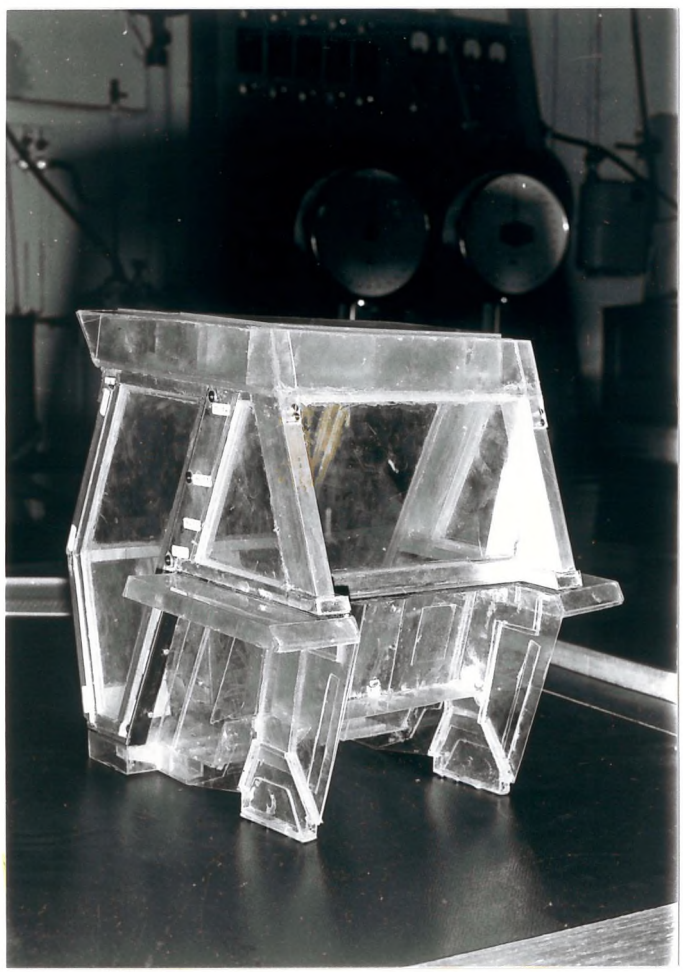

Figure 4.14 Picture of the Perspex model: rear view.

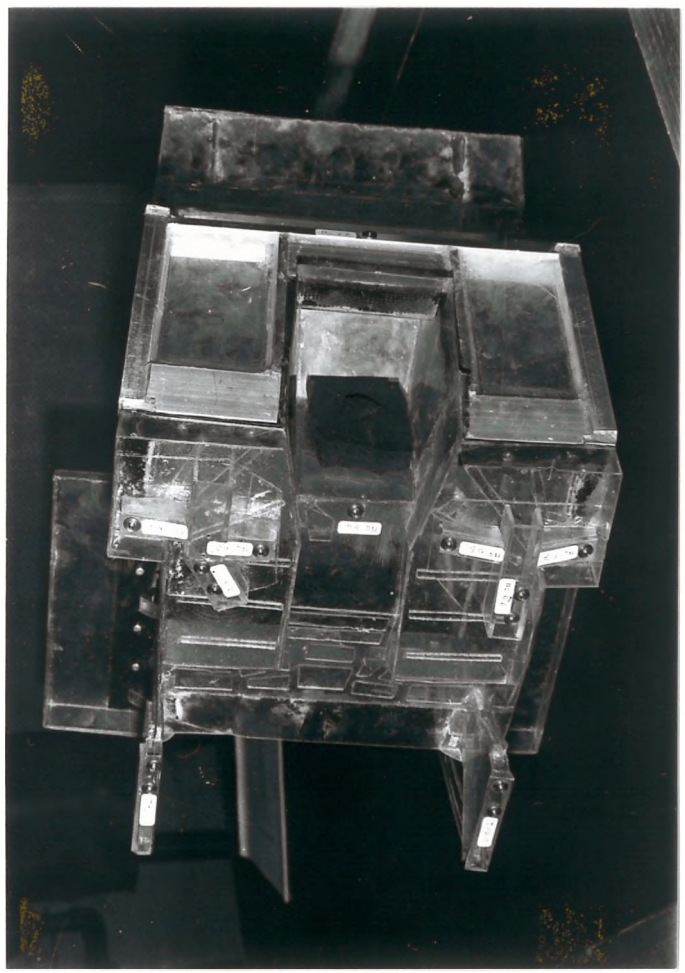

Figure 4.15 Picture of the Perspex model: bottom view.

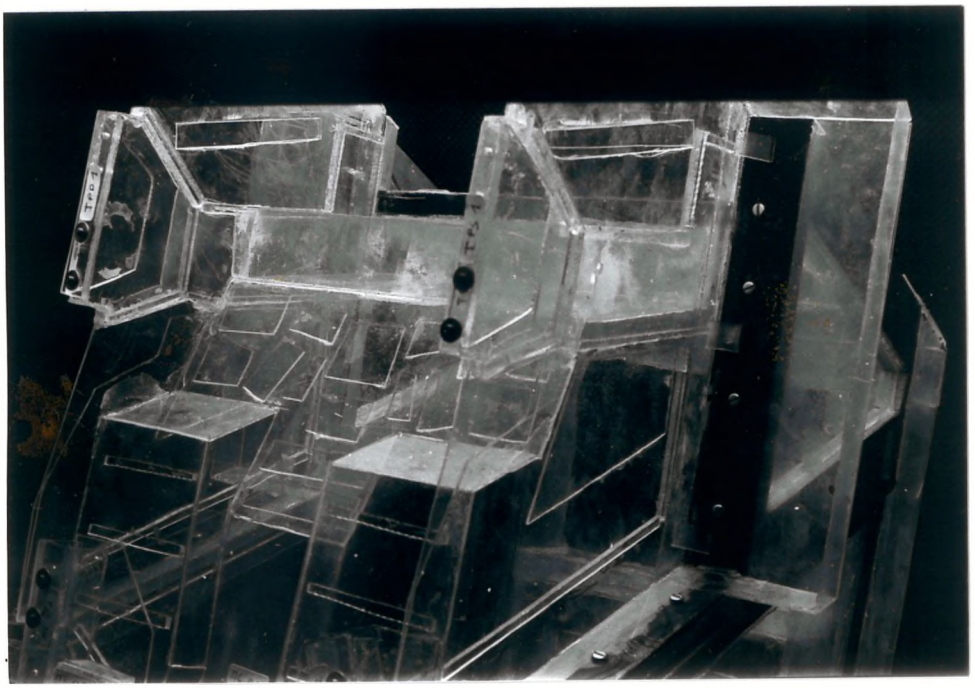

Figure 4.16 Picture of the Perspex model: rear supports.

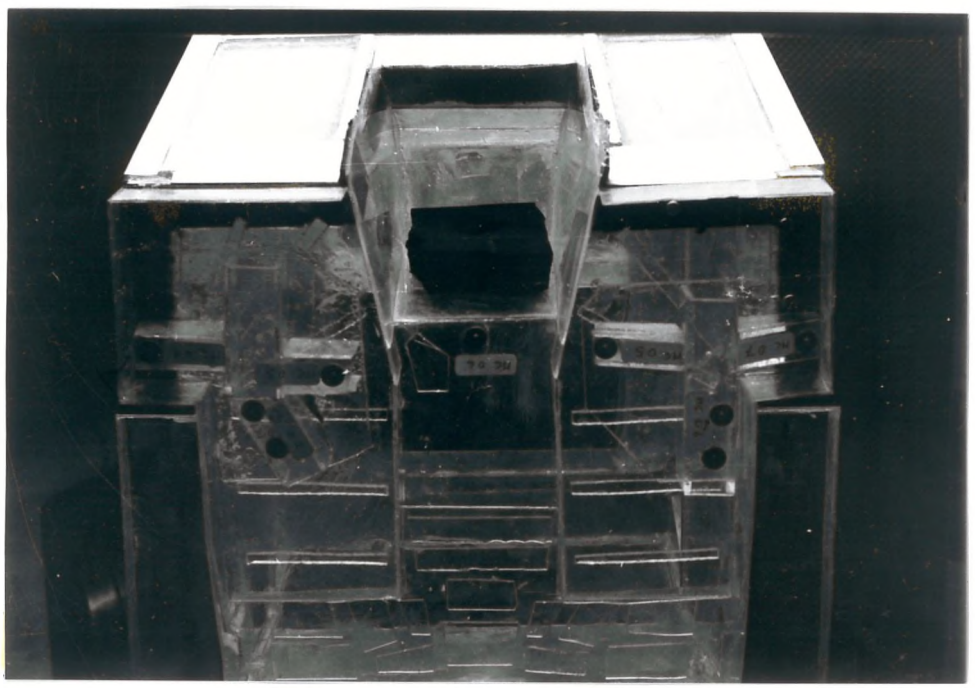

Figure 4.17 Picture of the Perspex model: front supports.

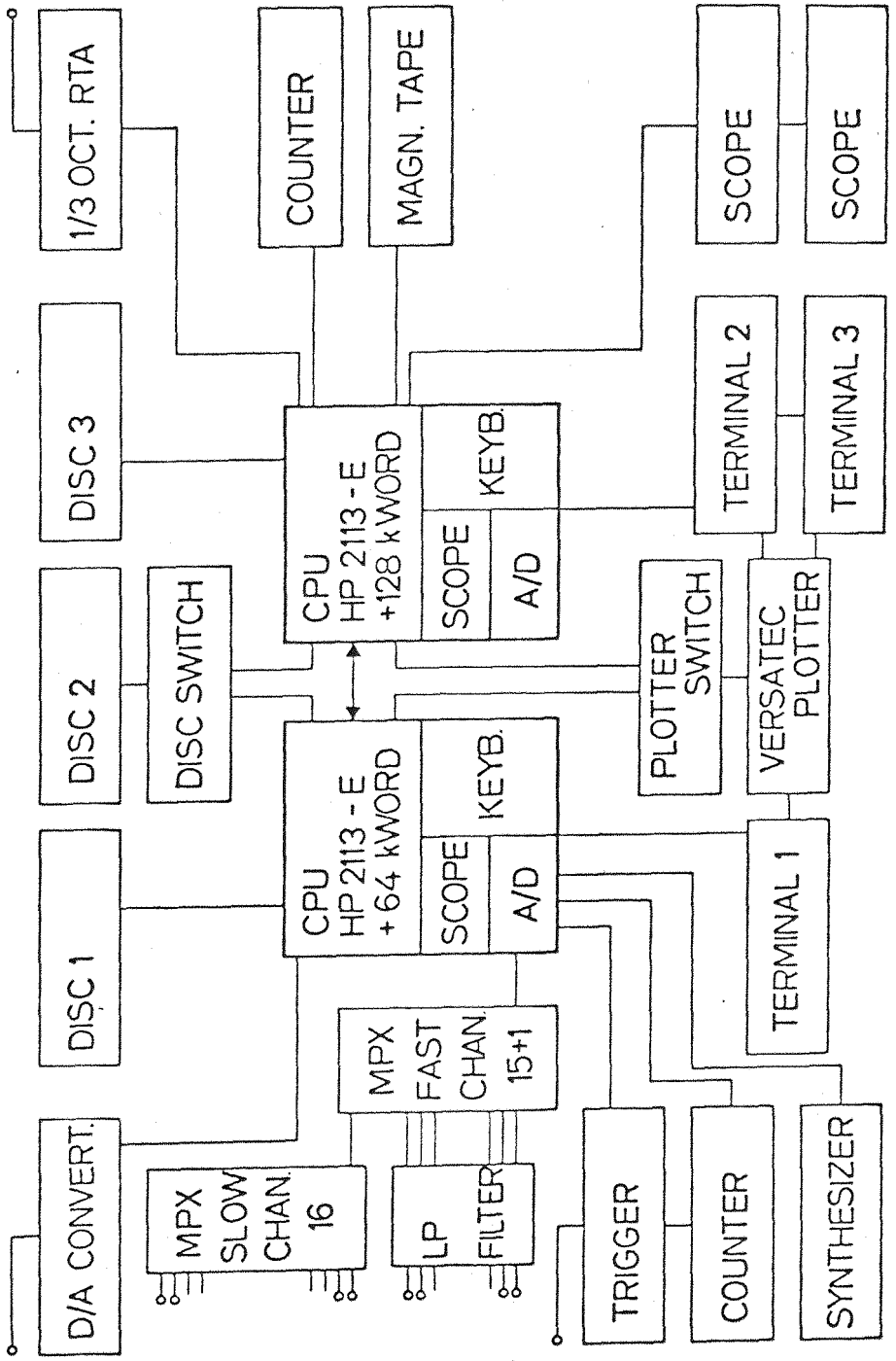

Figure 4.18 Scheme of the acquisition and processing system for acoustic and vibration signals (Italiana Keller, Santhià, Italy).

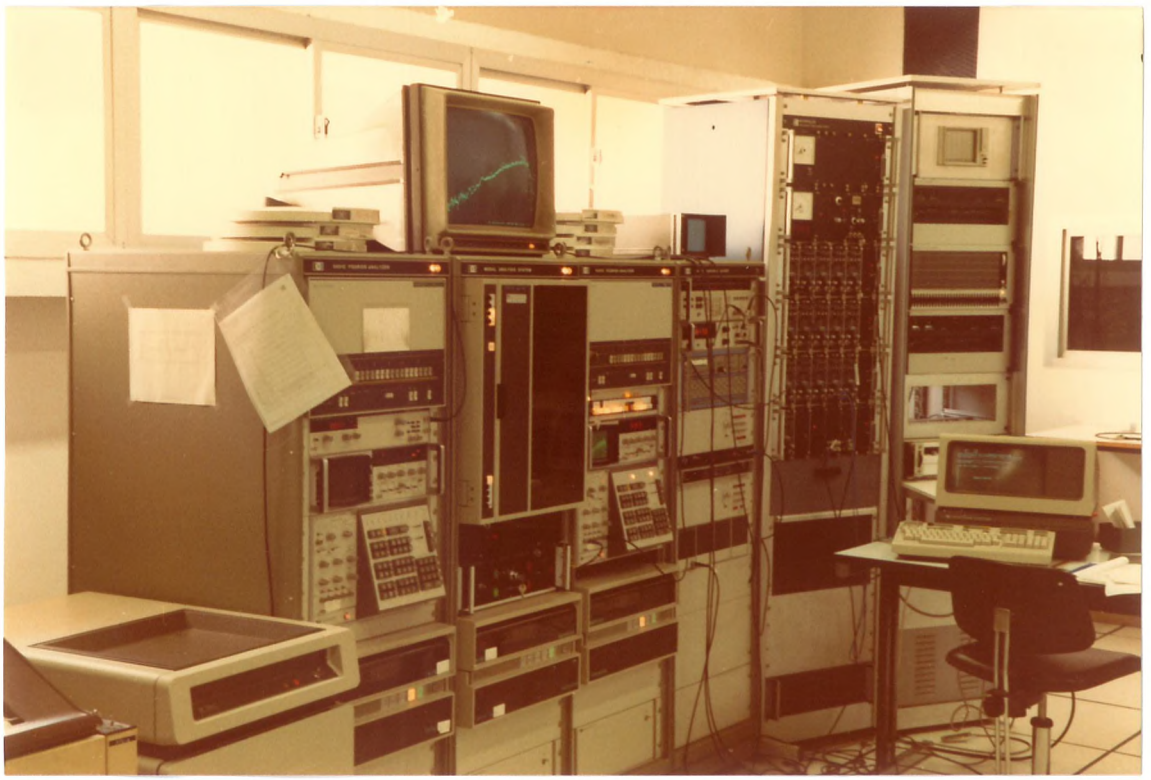

Figure 4.19 Picture of the acquisition and processing system for acoustic and vibration signals (Italiana Keller, Santhià, Italy).

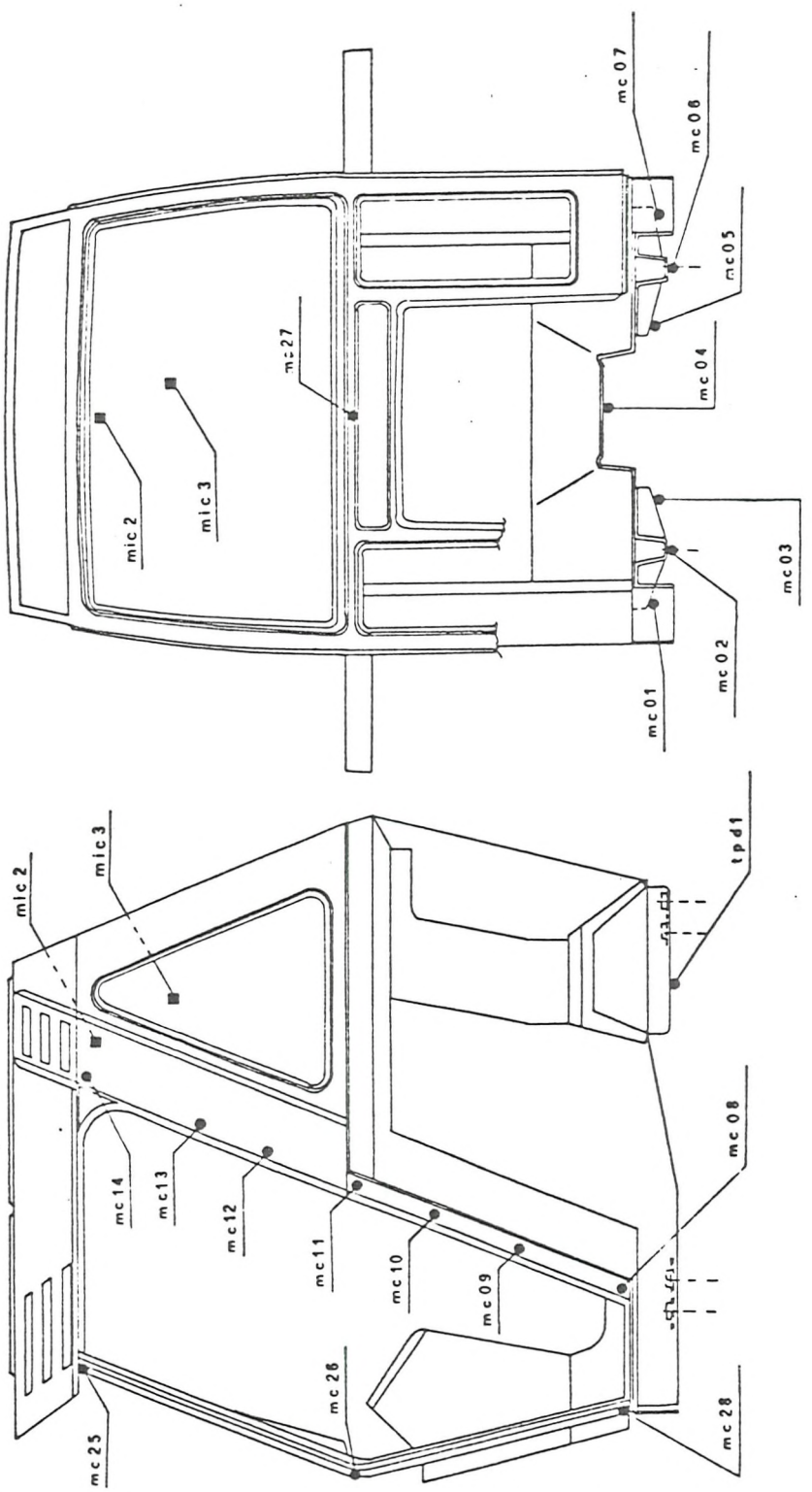

Figure 4.20 Position of the measurement points: left and front side.

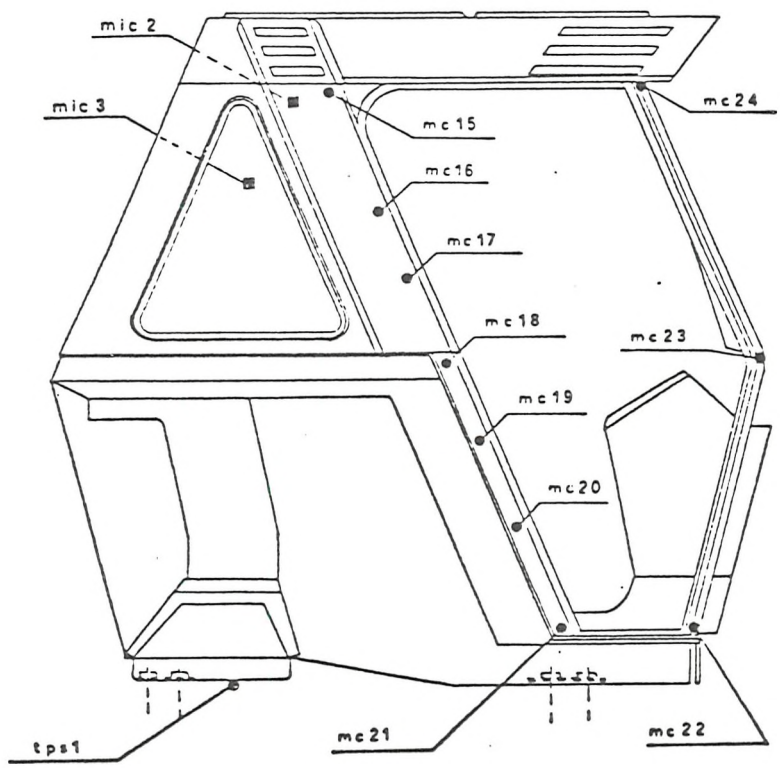

Figure 4.21 Position of the measurement points: right side.

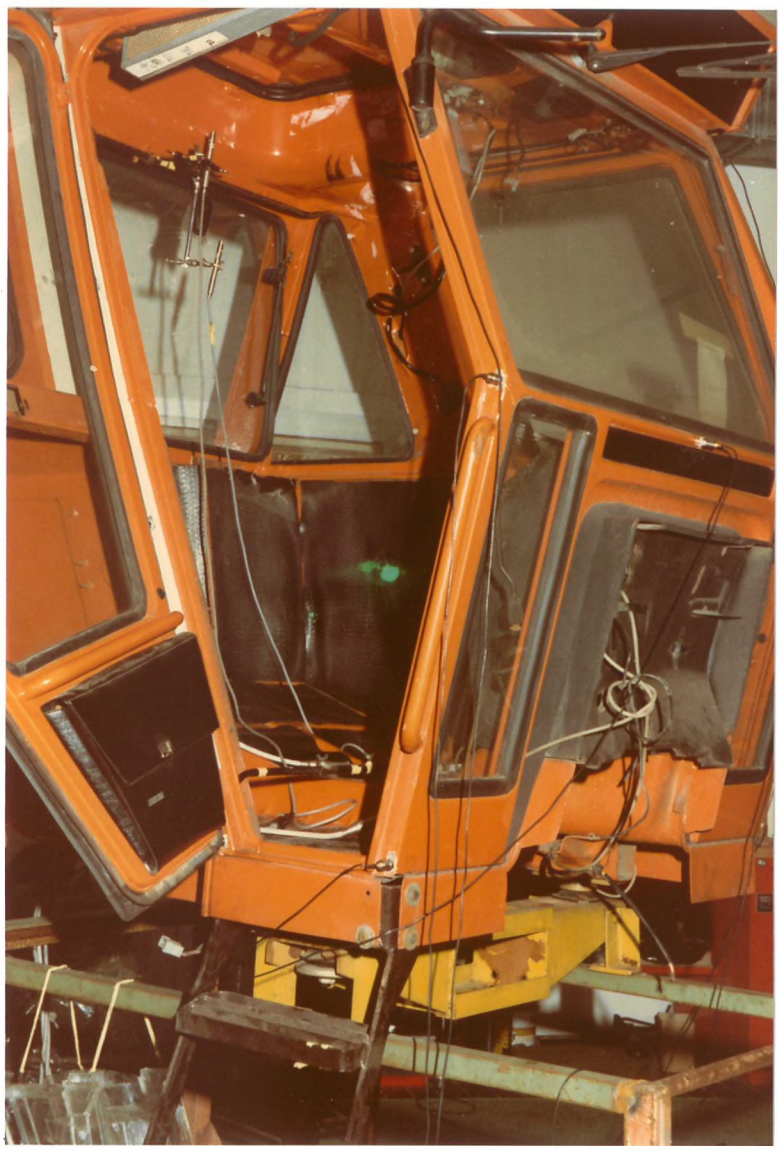

Figure 4.22 Picture of the microphones placed near the position of the head of the driver.

Figure 4.23 Picture of the whole cab mounted on a movable frame through four resilient supports.

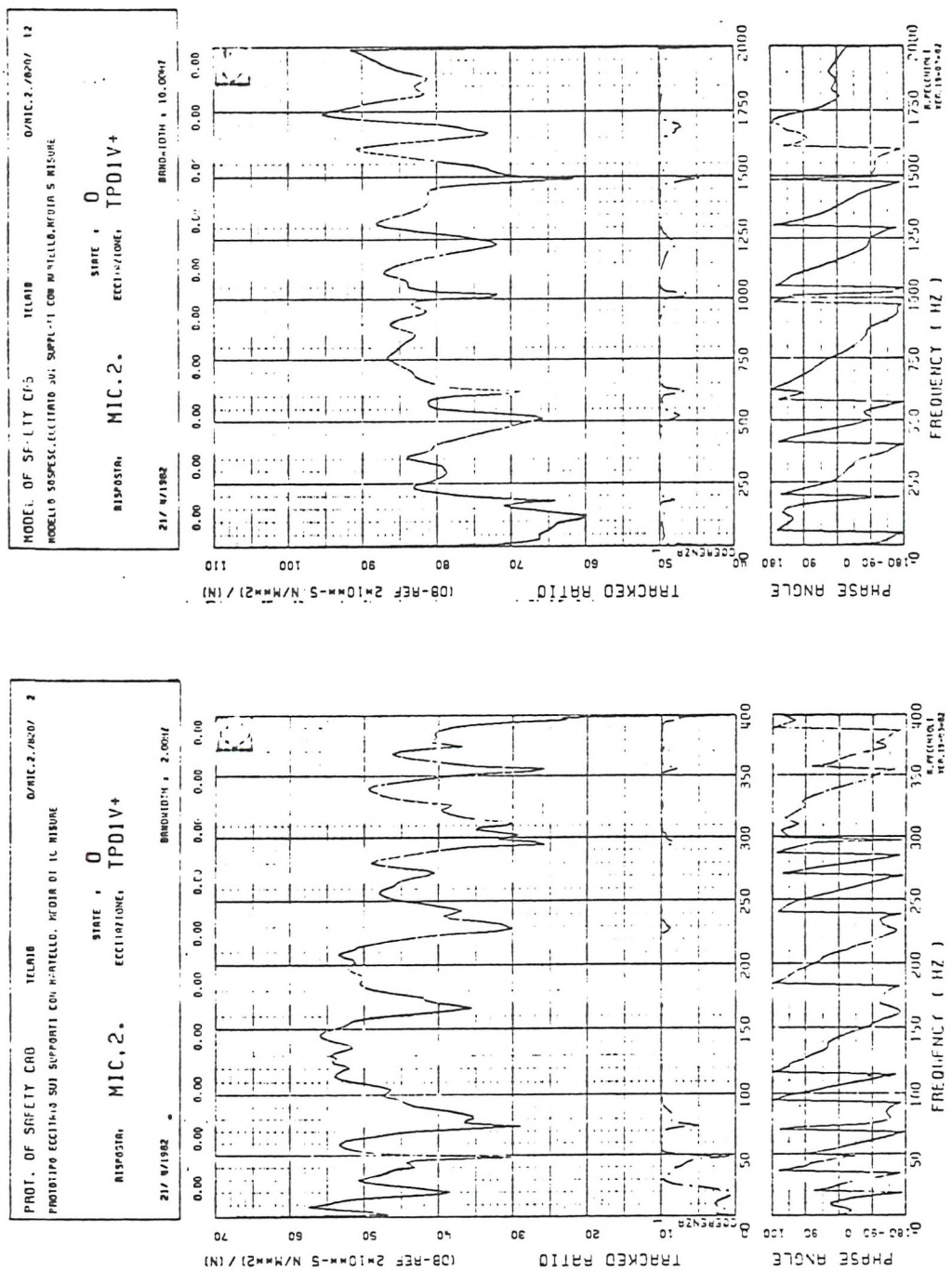

Figure 4.24 (a) Gain factors and phase factors of the frequency response function between the exciting force and the inner sound pressure levels. Measurements on the prototype: left side. Measurements on the model: right side.

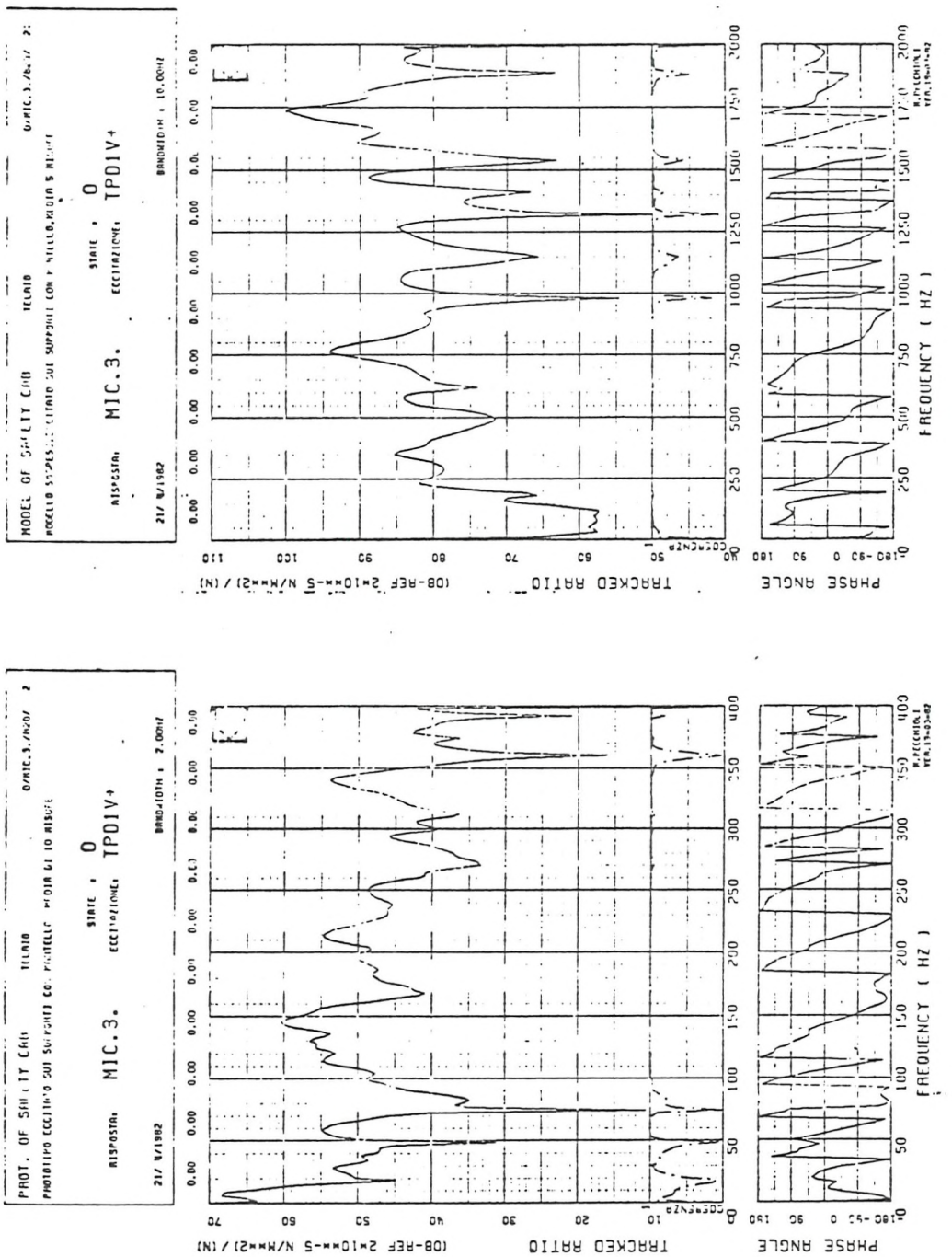

Figure 4.24 (b) Gain factors and phase factors of the frequency response function between the exciting force and the inner sound pressure levels. Measurements on the prototype: left side. Measurements on the model: right side.

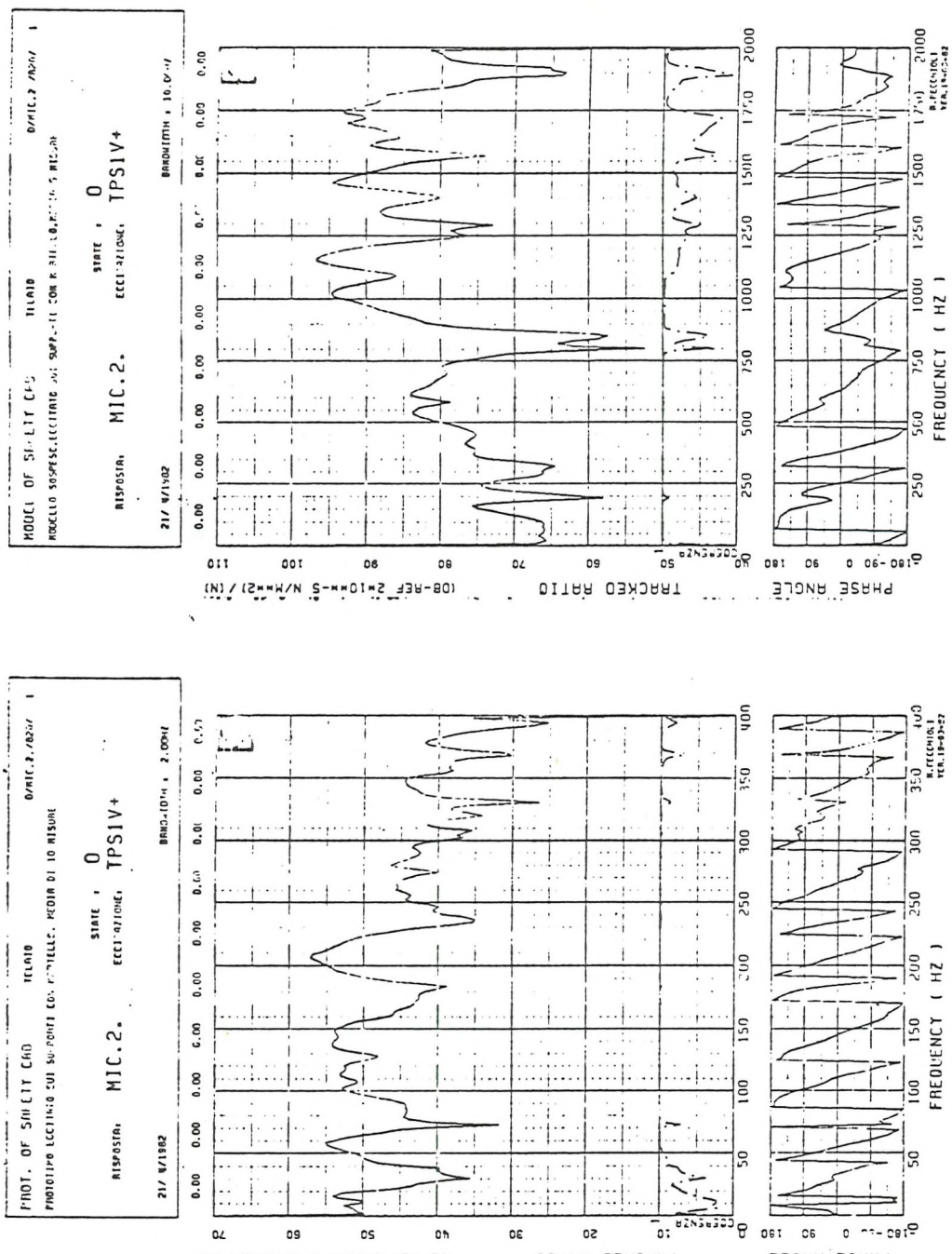

Figure 4.25 (a) Gain factors and phase factors of the frequency response function between the exciting force and the inner sound pressure levels. Measurements on the prototype: left side. Measurements on the model: right side.

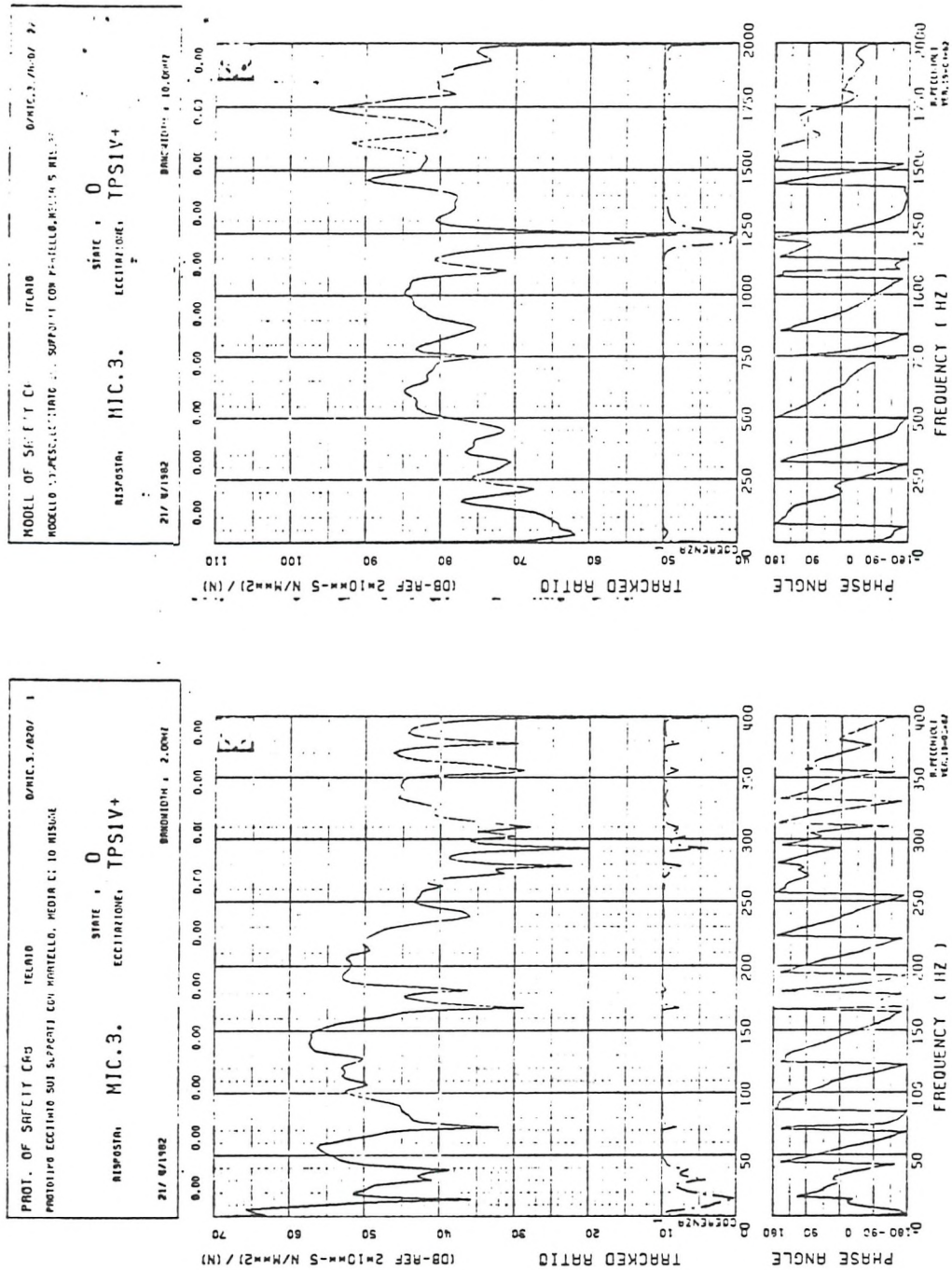

Figure 4.25 (b) Gain factors and phase factors of the freqeuncy response function between the exciting force and the inner sound pressure levels. Measurements on the prototype: left side. Measurements on the model: right side.

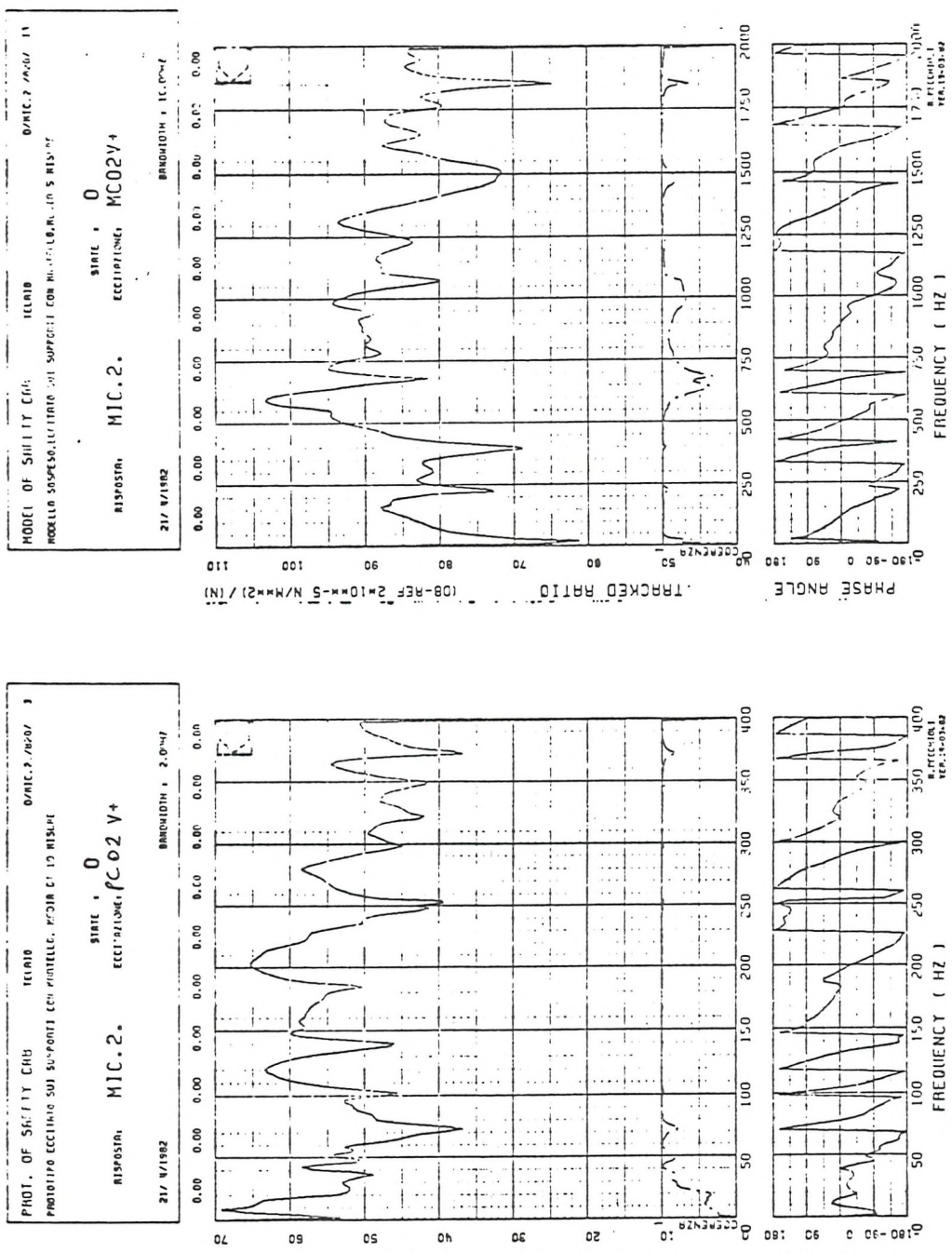

Figure 4.26 (a) Gain factors and phase factors of the frequency response function between the exciting force and the inner sound pressure levels. Measurements on the prototype: left side. Measurements on the model: right side.

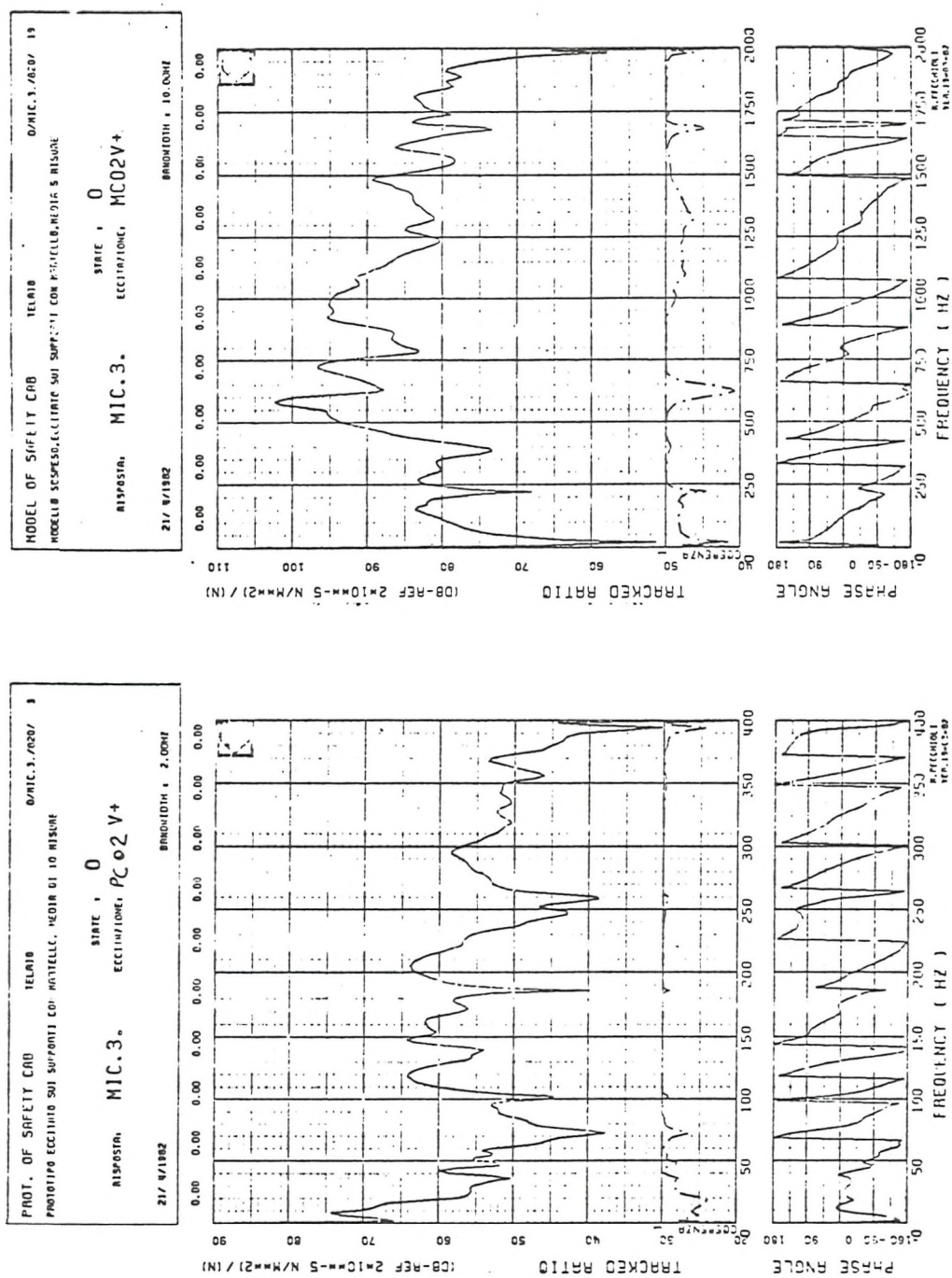

Figure 4.26 (b) Gain factors and phase factors of the frequency response function between the exciting force and the inner sound pressure levels. Measurements on the prototype: left side. Measurements on the model: right side.

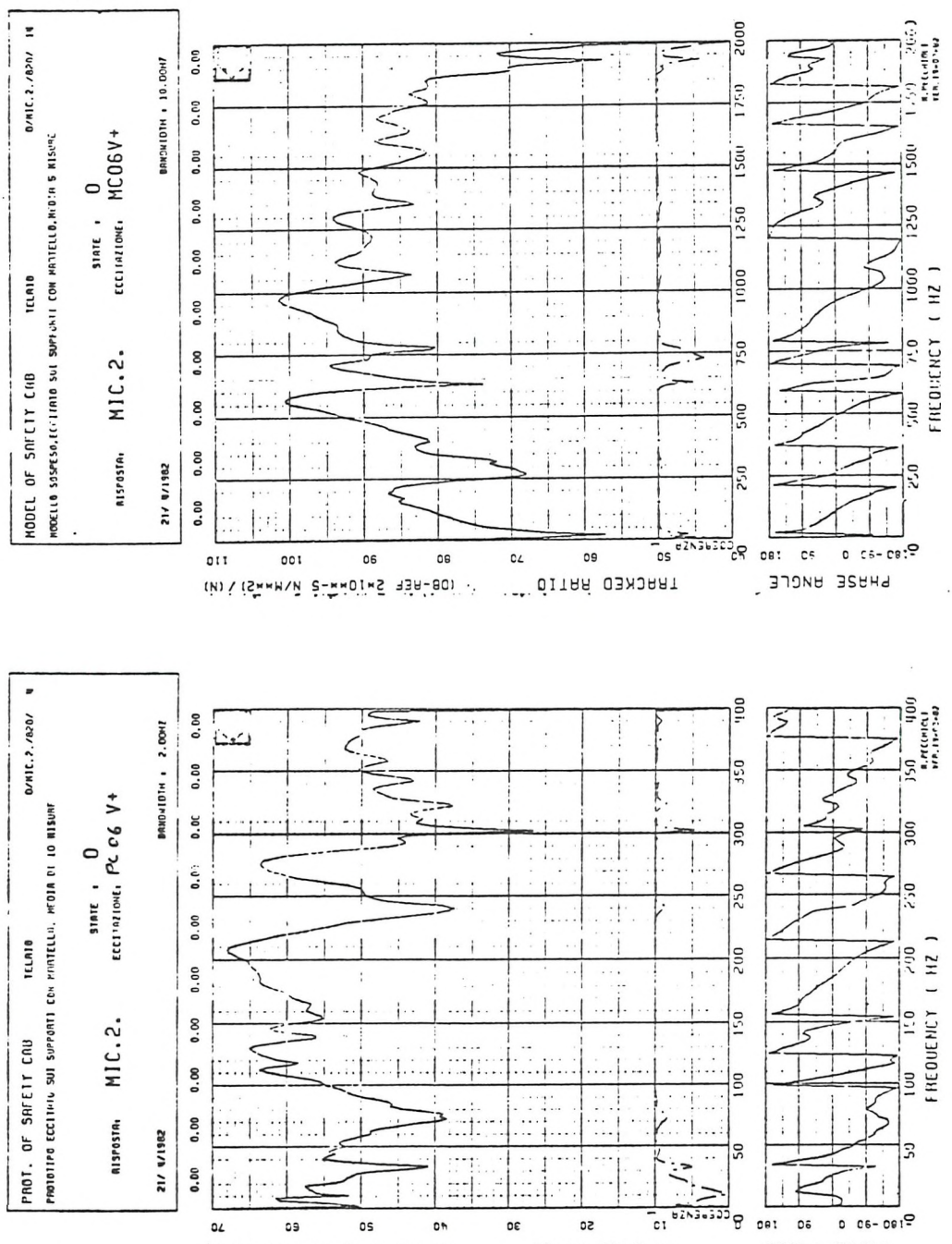

Figure 4.27 (a) Gain factors and phase factors of the frequency response function between the exciting force and the inner sound pressure levels. Measurements on the prototype: left side. Measurements on the model: right side.

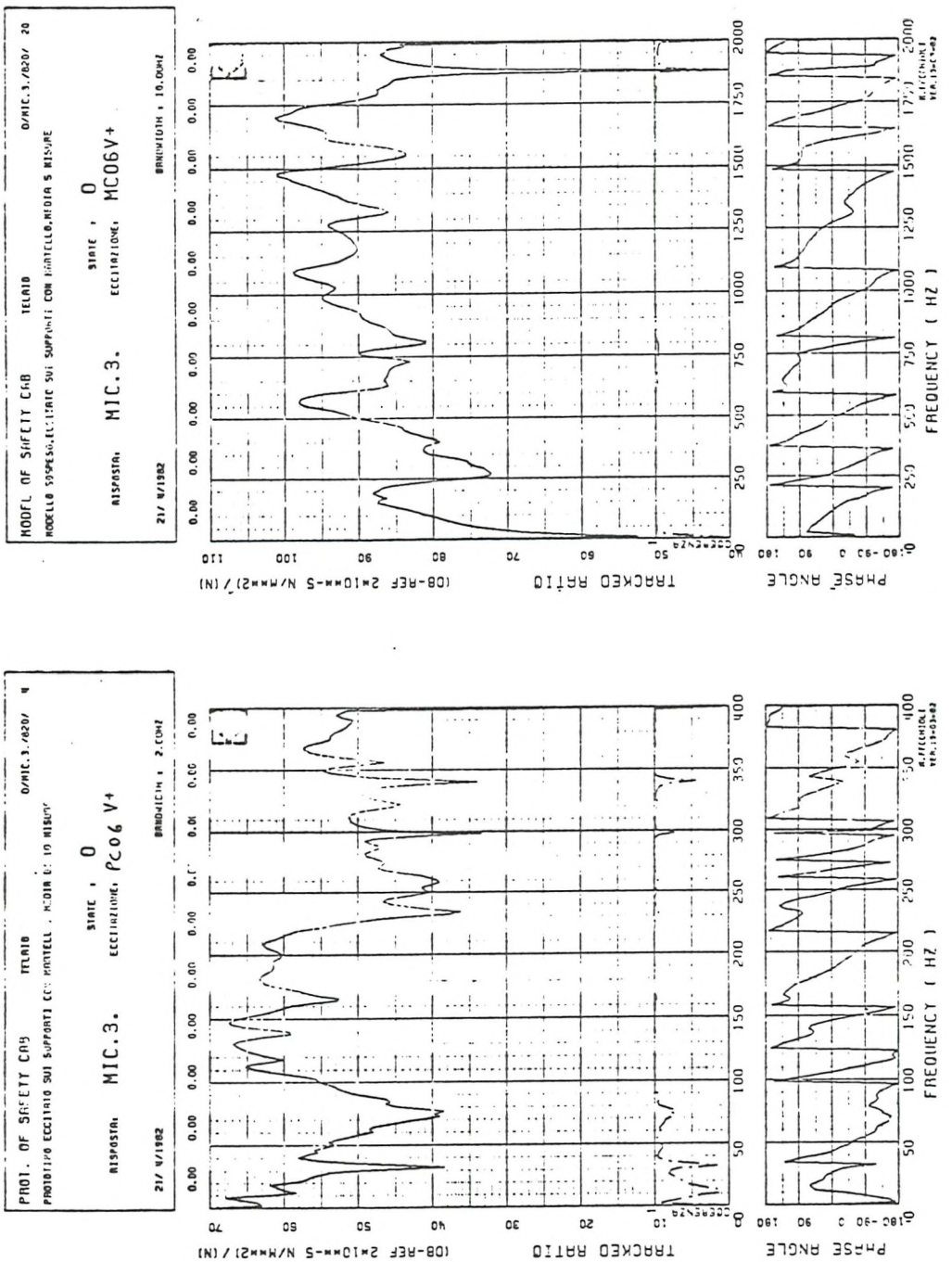

Figure 4.27 (b) Gain factors and phase factors of the frequency response function between the exciting force and the inner sound pressure levels. Measurements on the prototype: left side. Measurements on the model: right side.

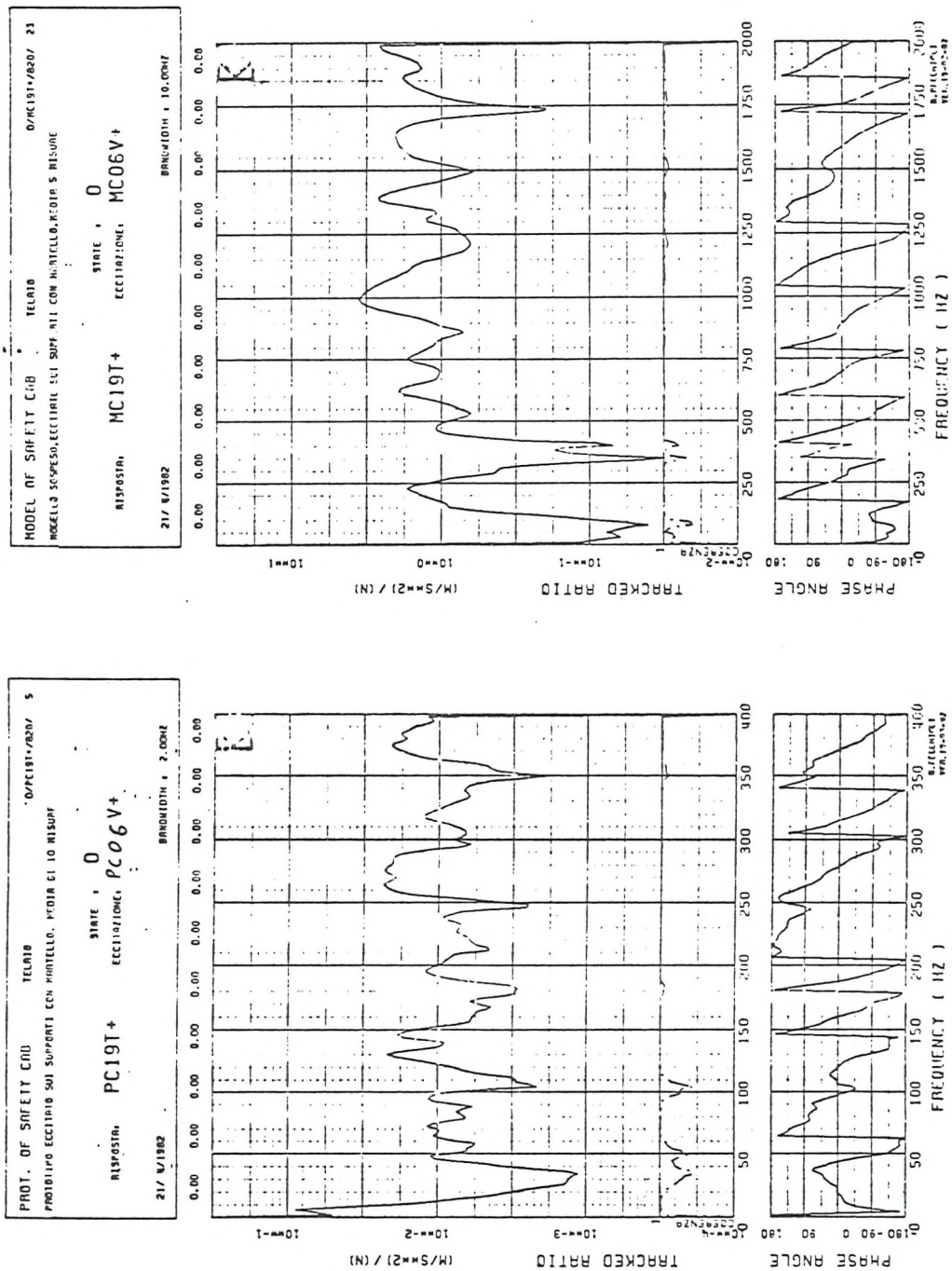

Figure 4.28 (a) Gain factors and phase factors of the frequency response function between the exciting force and the acceleration. Measurements on the prototype: left side. Measurements on the model: right side.

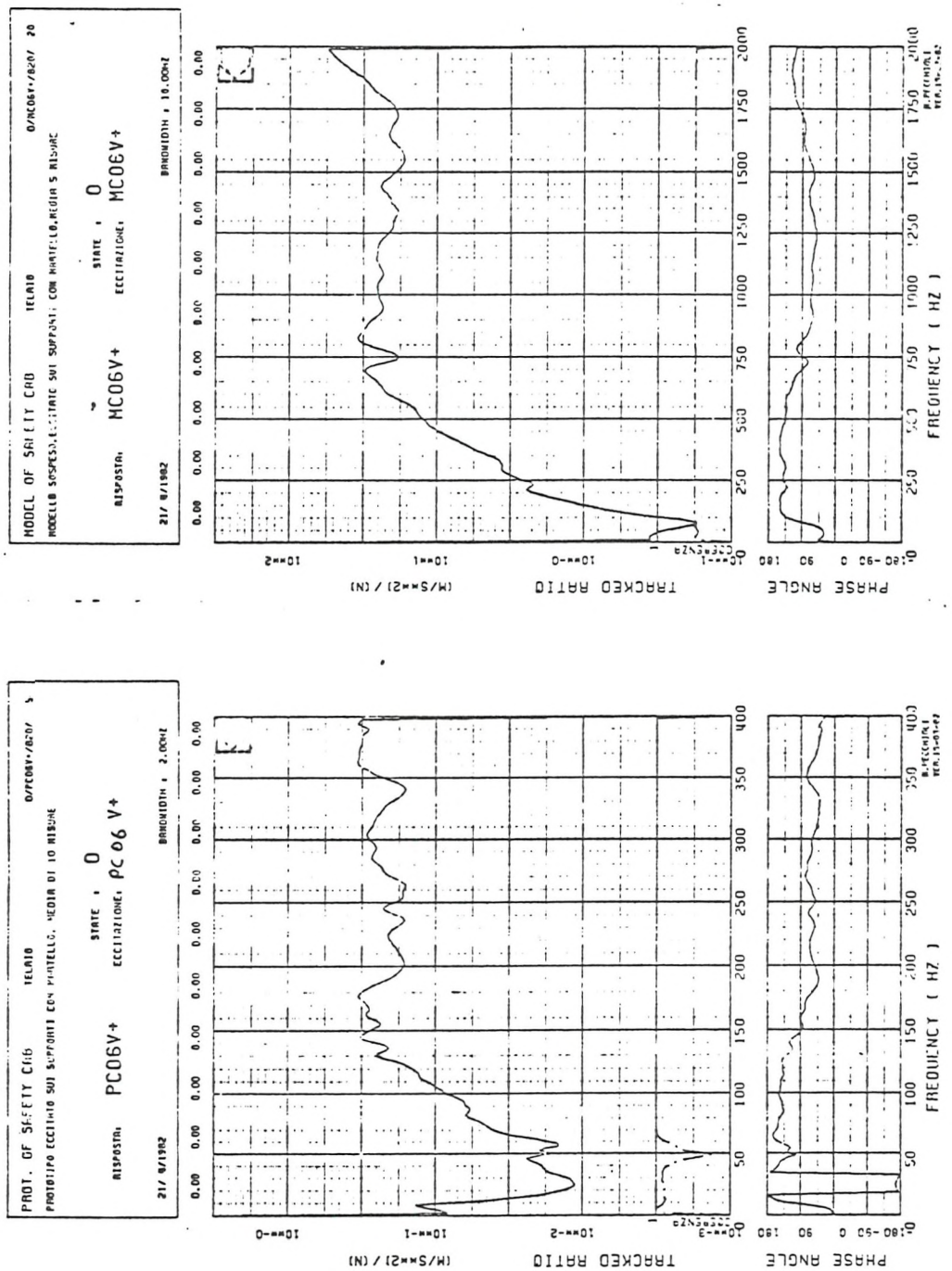

Figure 4.28 (b) Gain factors and phase factors of the frequency response function between the exciting force and the accelerations. Measurements on the prototype: left side. Measurements on the model: right side.

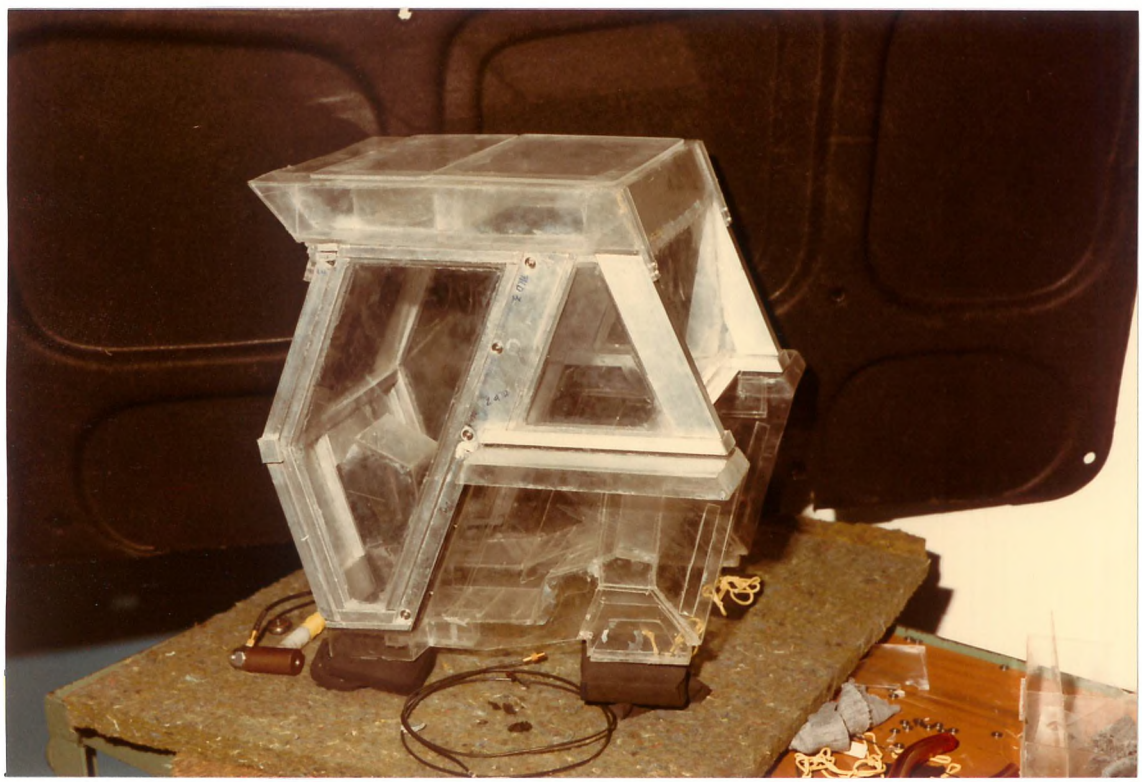

Figure 4.29 Picture of the model mounted on a layer of resilient material.

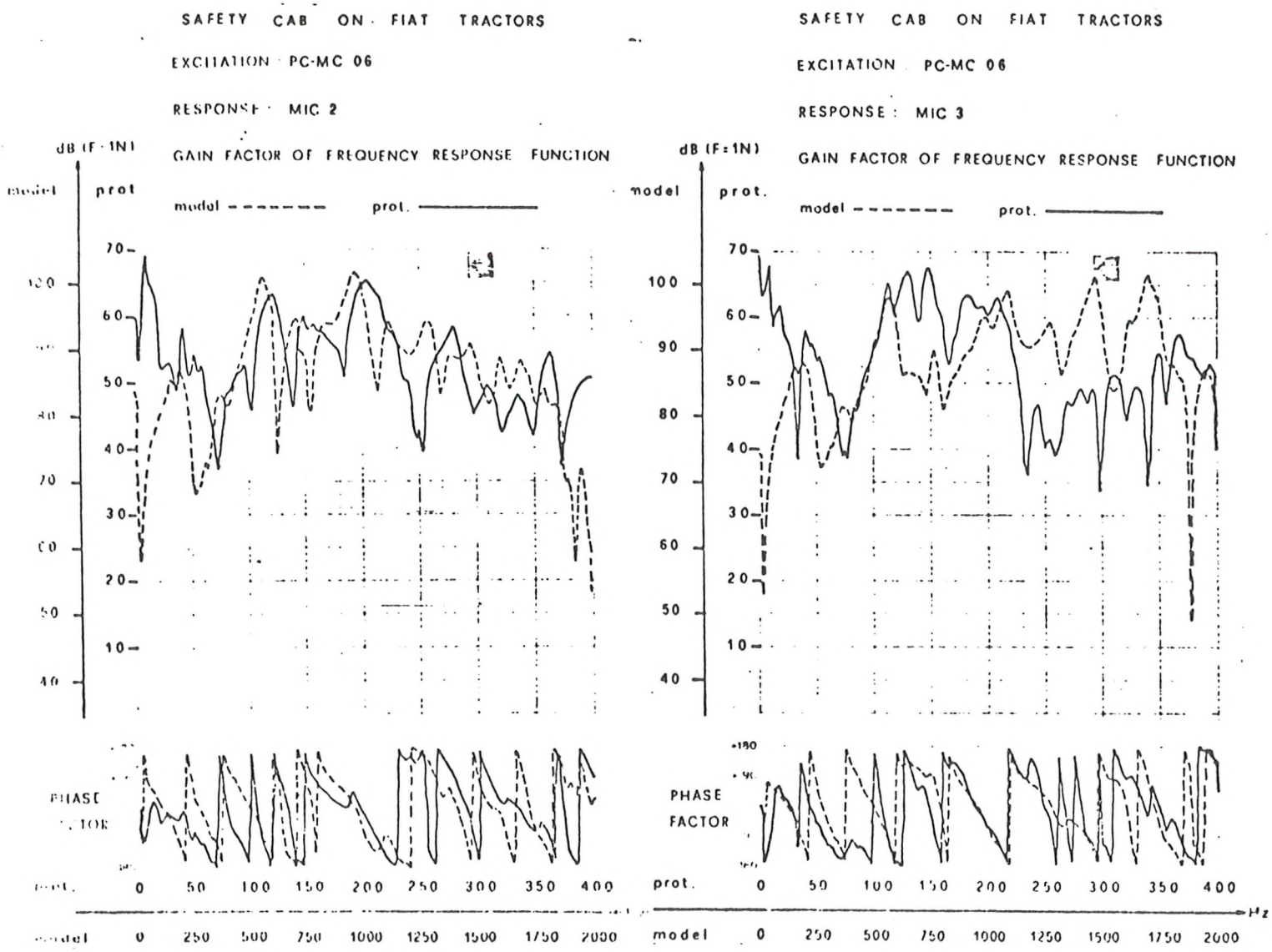

Figure 4.30 (a) Comparison of gain factors and phase factors of the frequency response function between the exciting force and the sound pressure levels: solid line: measurements on the prototype dashed line: measurements on the model.

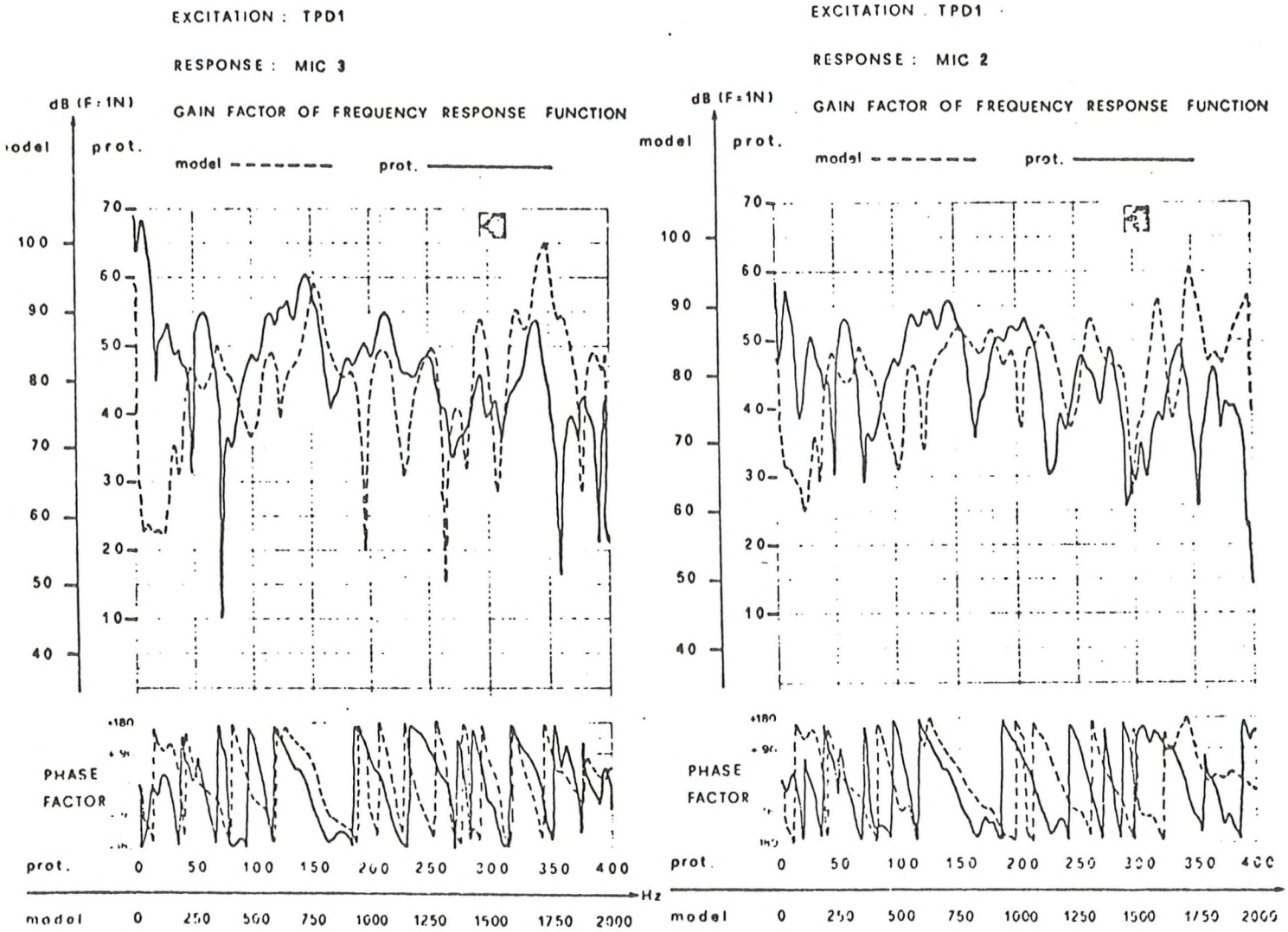

Figure 4.30 (b) Comparison of gain factors and phase factors of the frequency response function between the exciting force and the sound pressure levels: solid line: measurements on the prototype dashed line: measurements on the model.

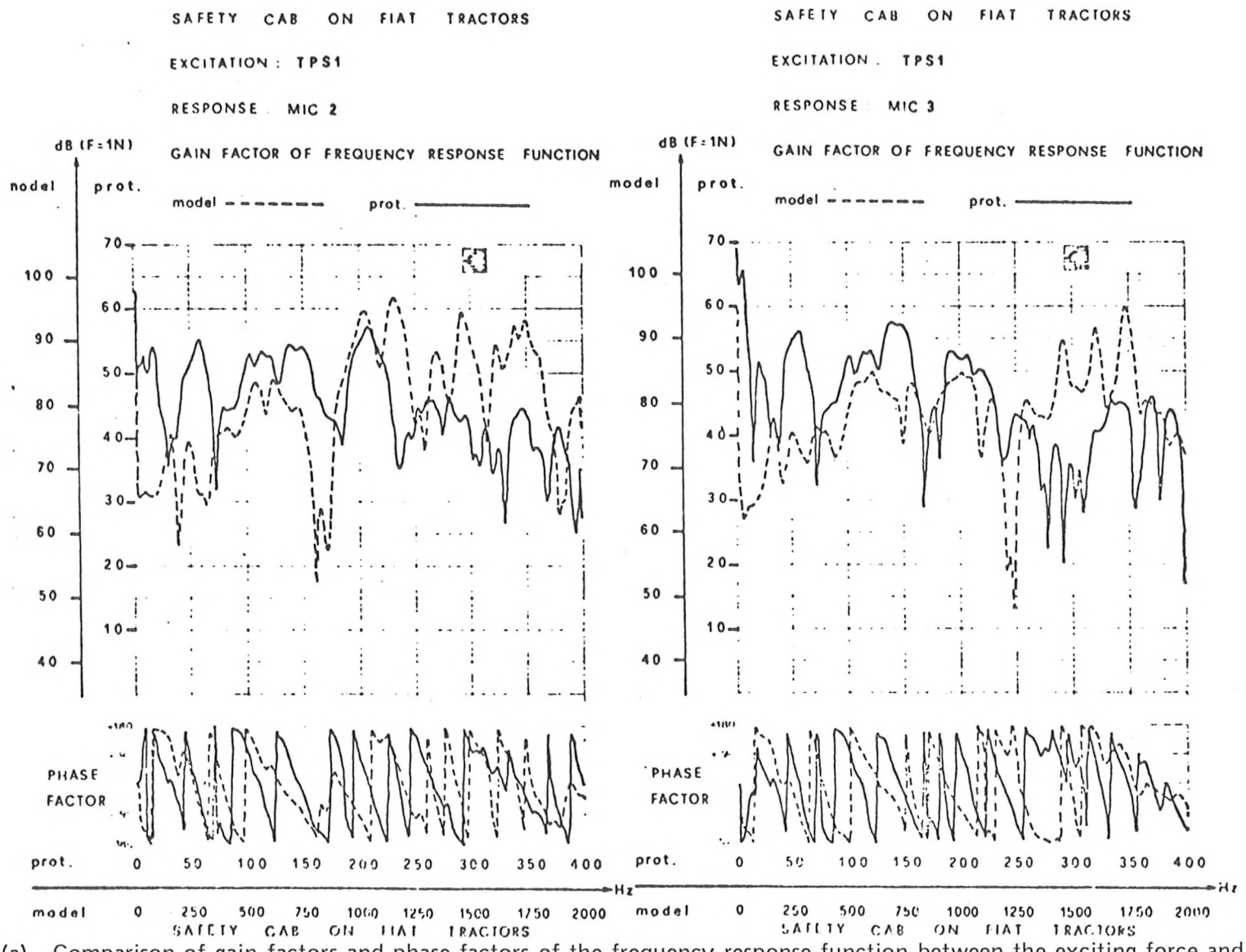

Figure 4.31 (a) Comparison of gain factors and phase factors of the frequency response function between the exciting force and the sound pressure levels: solid line: measurements on the prototype dashed line: measurements on the model.

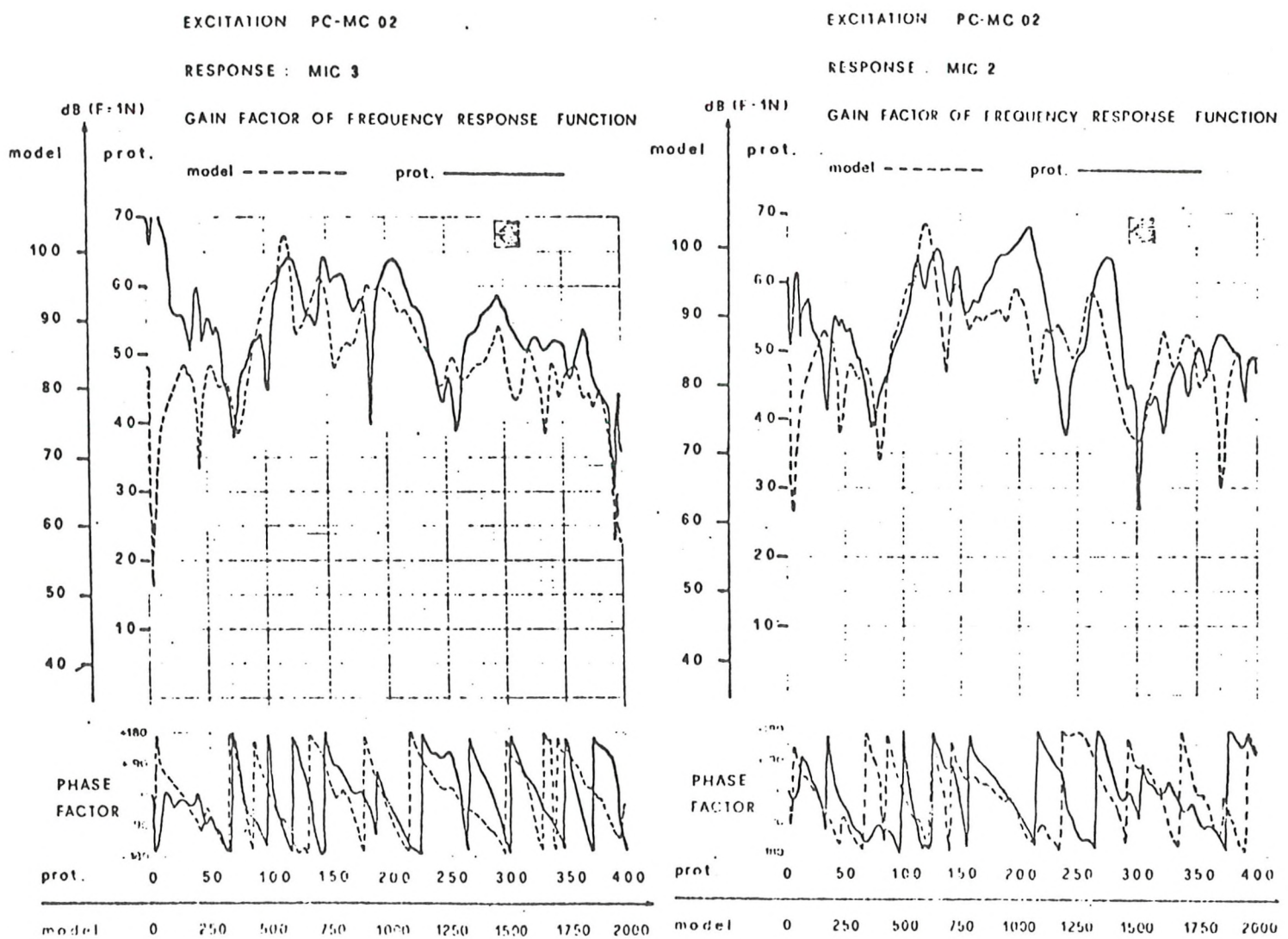

Figure 4.31 (b) Comparison of gain factors and phase factors of the frequency response function between the exciting force and the sound pressure levels: solid line: measurements on the prototype dashed line: measurements on the model.

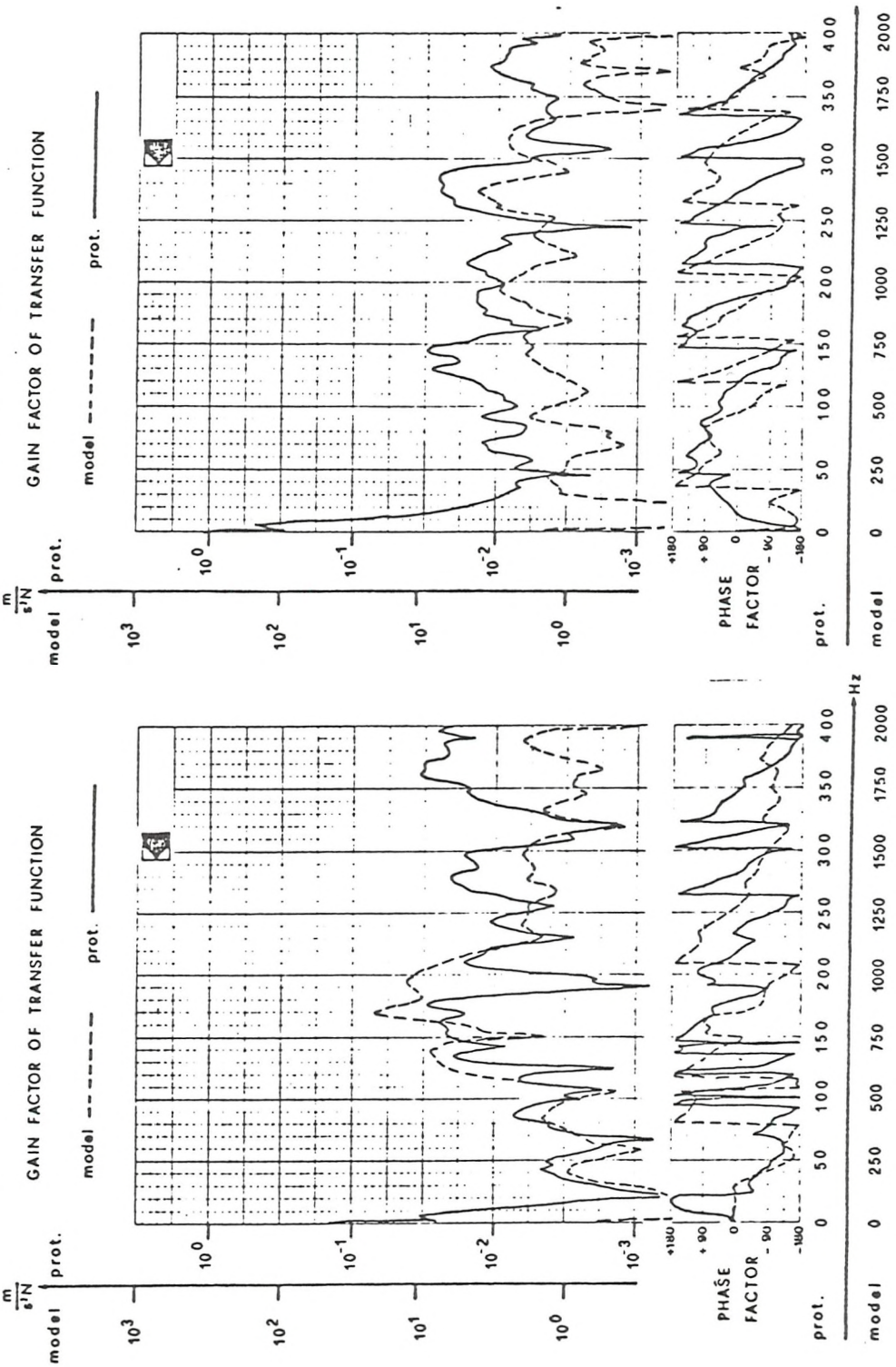

Figure 4.32 Comparison of gain factors and phase factors of the frequency response function between the exciting force and the acceleration: solid line: measurements on the prototype; dashed line: measurements on the model.

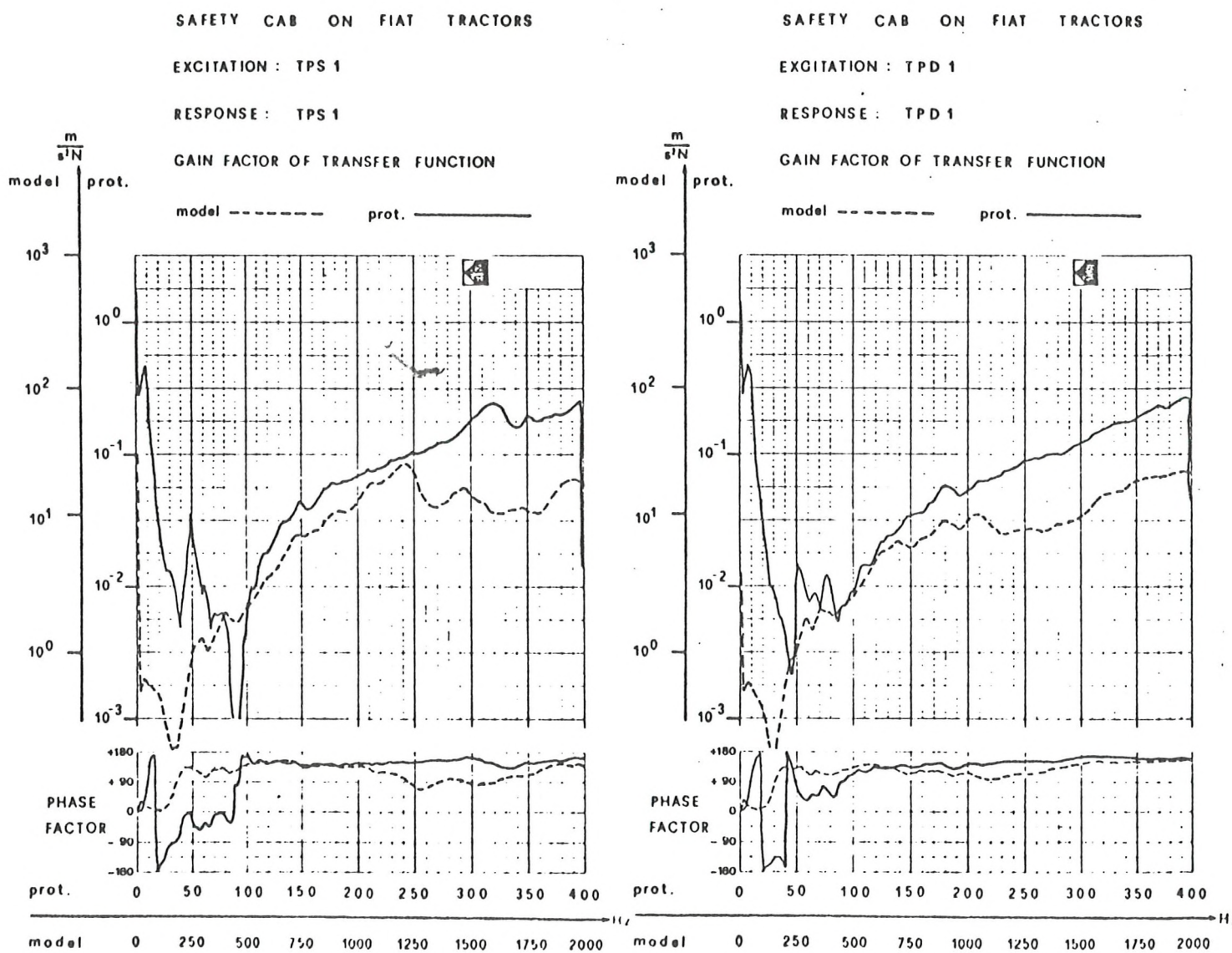

Figure 4.33 (a) Comparison of gain factors and phase factors of the frequency response function between the exciting force and the acceleration: solid line: measurements on the prototype; dashed line: measurements on the model.

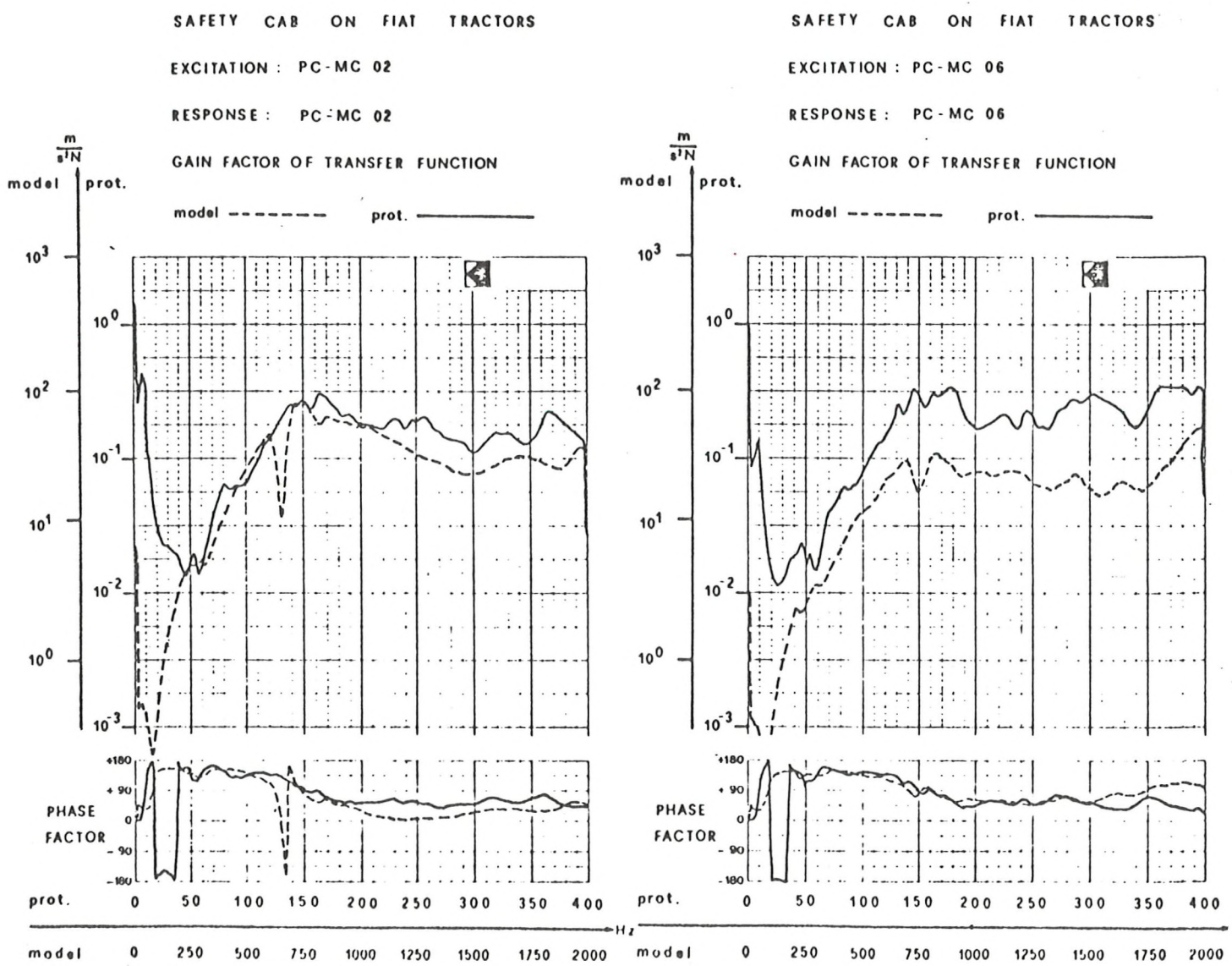

Figure 4.33 (b) Comparison of gain factors and phase factors of the frequency response function between the exciting force and the acceleration: solid line: measurements on the prototype; dashed line: measurements on the model.

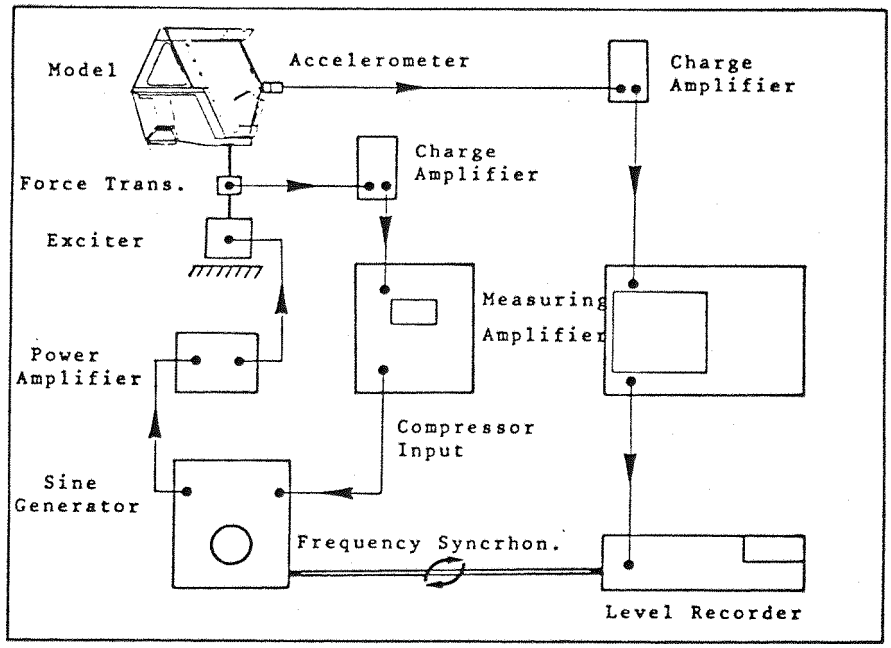

Figure 4.34 Arrangement for making automatic graphic recordings of the frequency response function between force and acceleration. Measurements on the model.

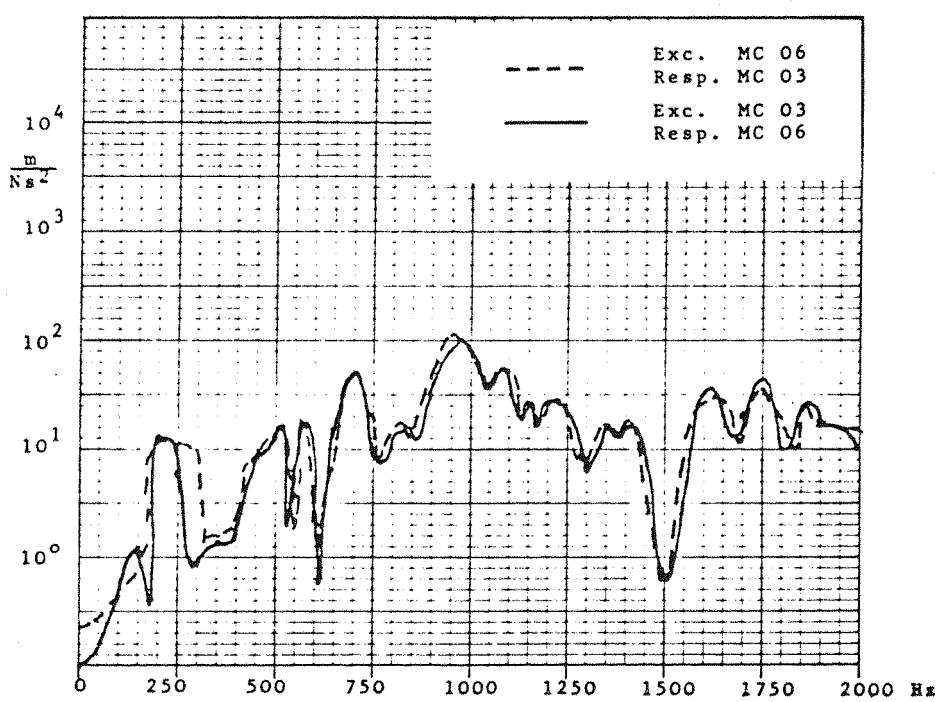

Figure 4.35 Comparison of the gain factor of the frequency response function between force and acceleration. Solid line and dashed line correspond to the results obtained exchanging the position between input force and acceleration.

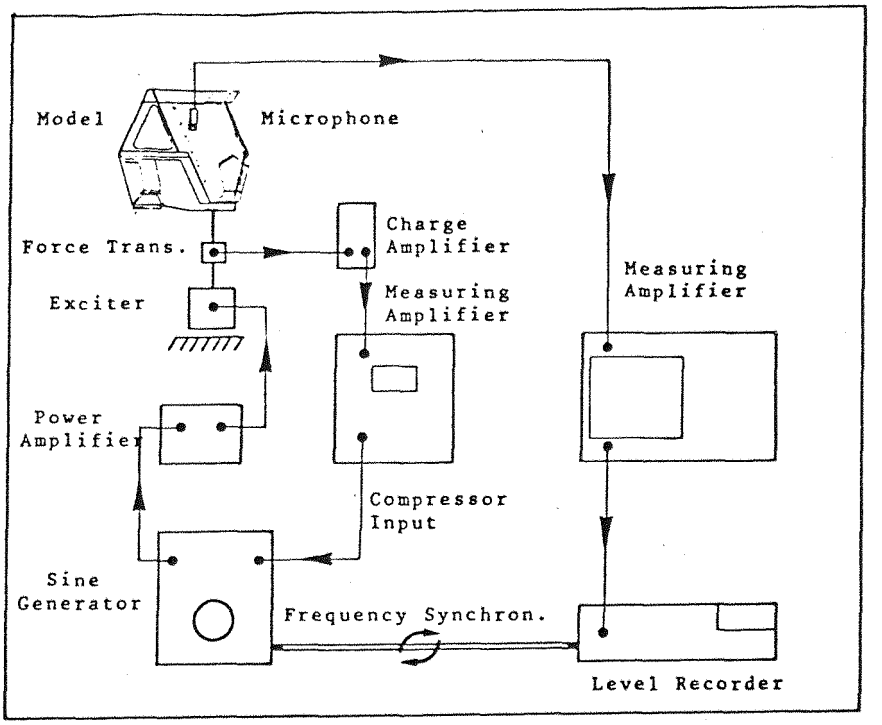

Figure 4.36 Arrangement for investigation of modes inside the cavity. Meaurements on the model.

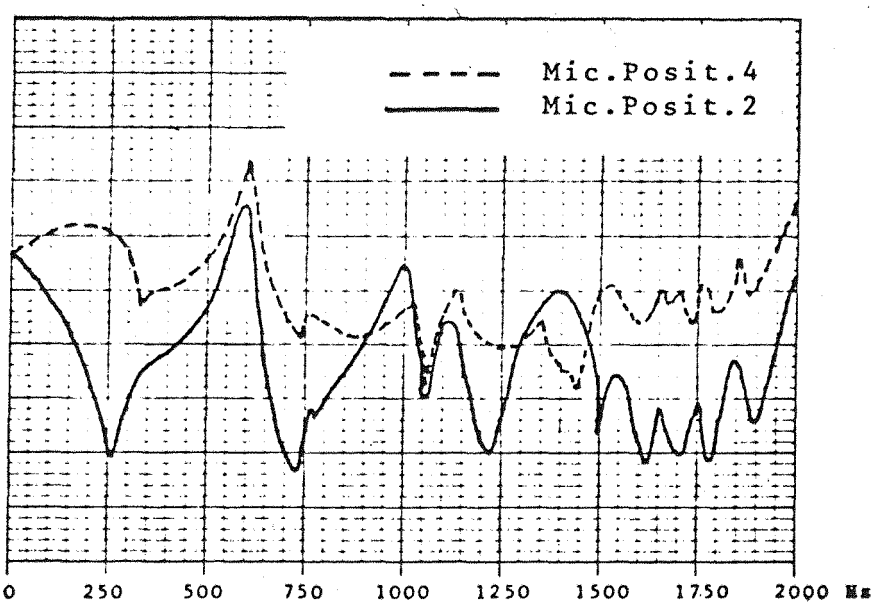

Figure 4.37 Resonance frequencies of the cavity when the model is immersed in sand;
solid line: microphone in position (2)
dashed line: microphone in position (4).

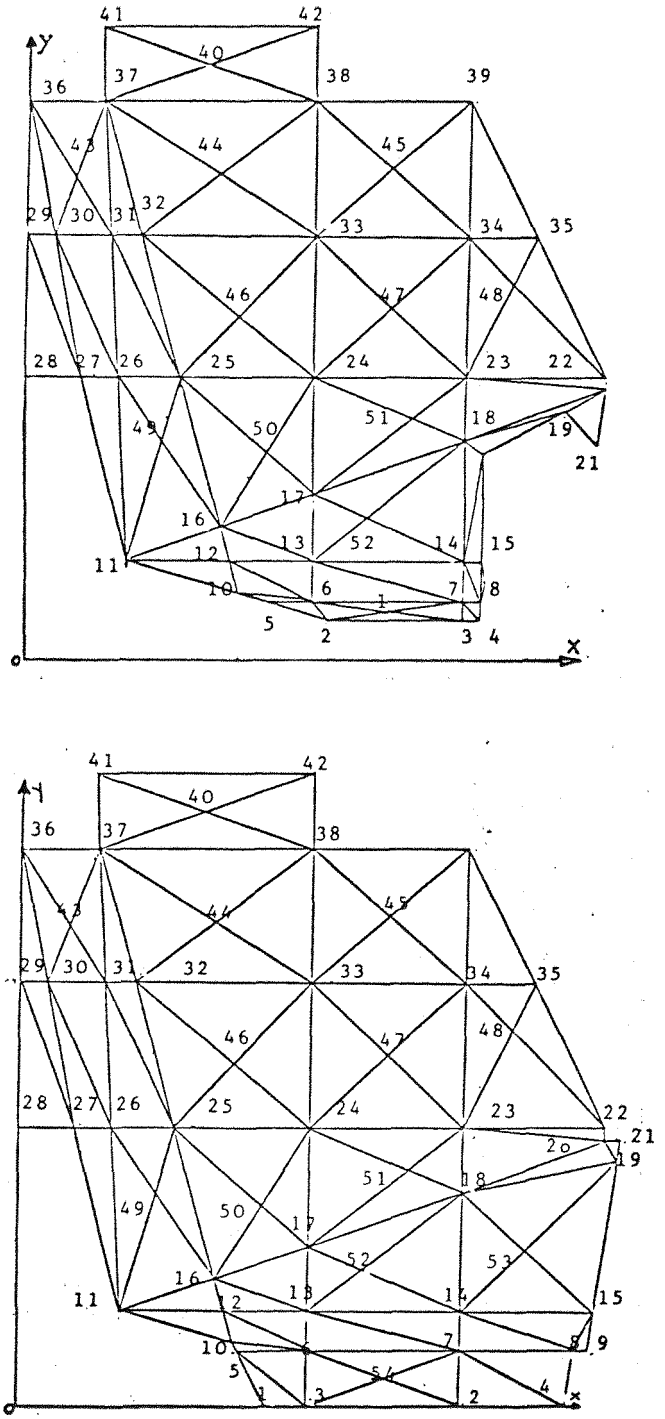

Figure 4.38 Two-dimensional finite element model of the cab. Up: section through the central axis. Low: section shifted towards the side of the cab.

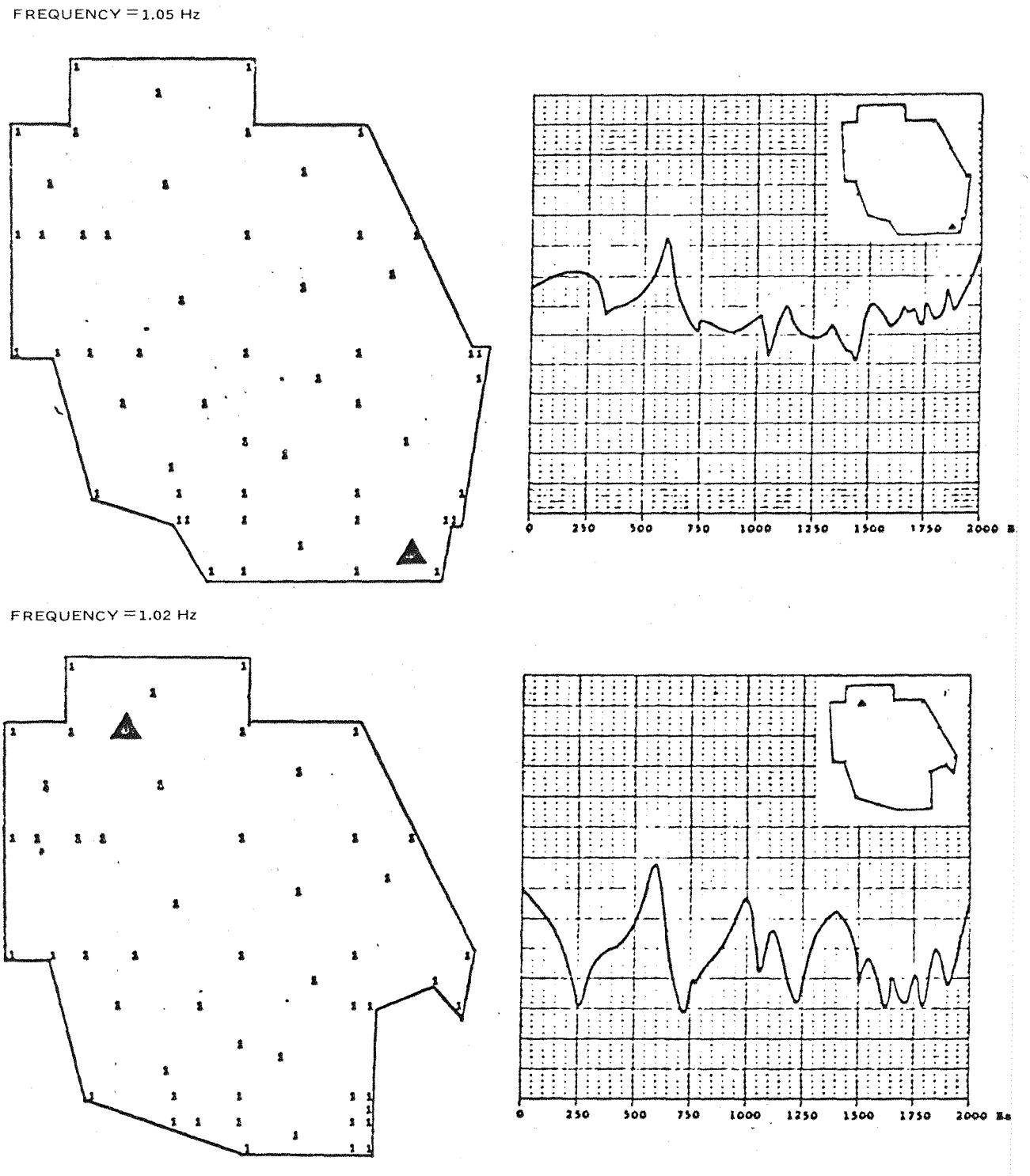

Figure 4.39 Distribution of sound pressure and nodal lines in the cavity cab at the resonance frequency.

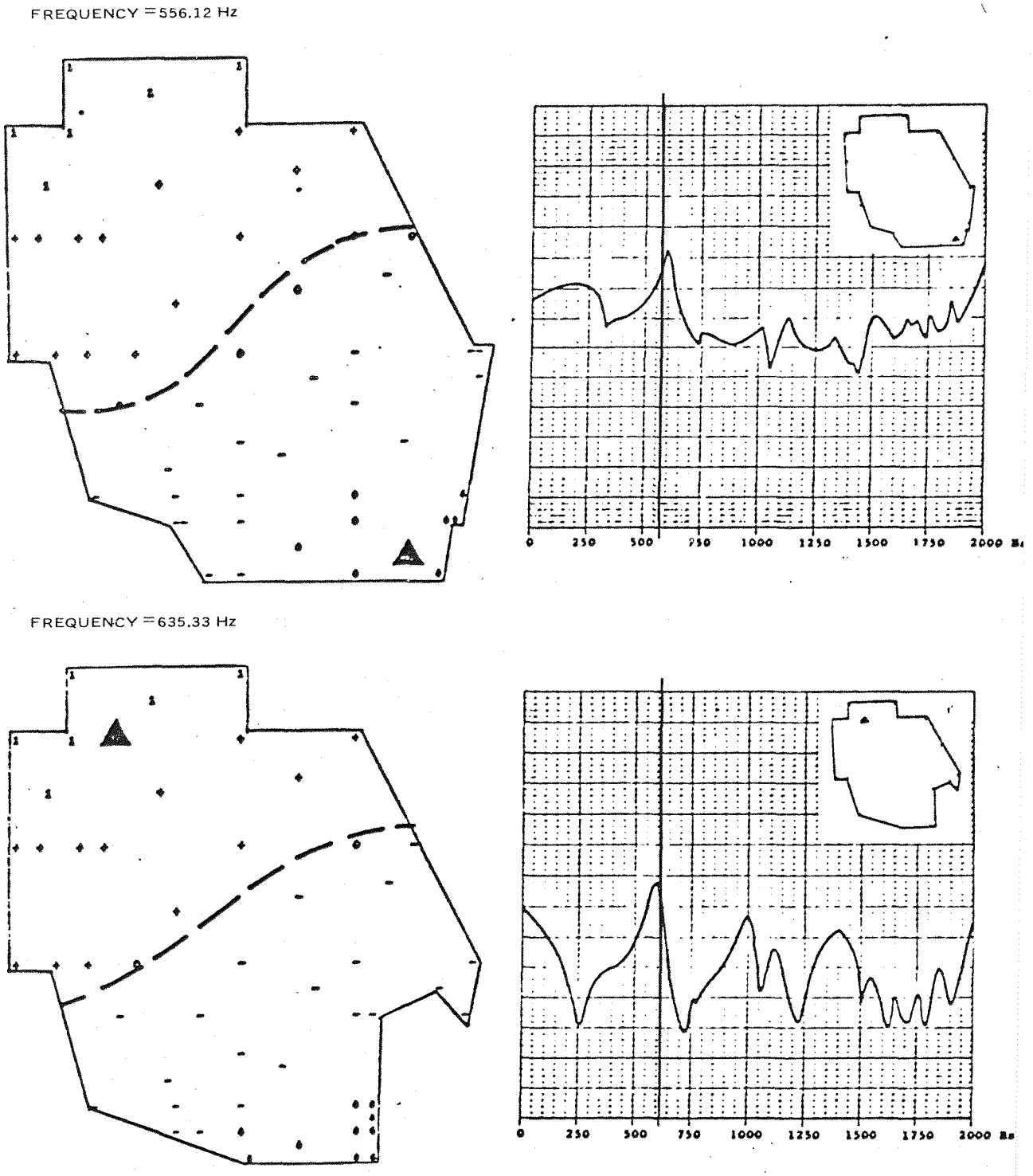

Figure 4.40 Distribution of sound pressure and nodal lines in the cavity cab at the resonance frequency.

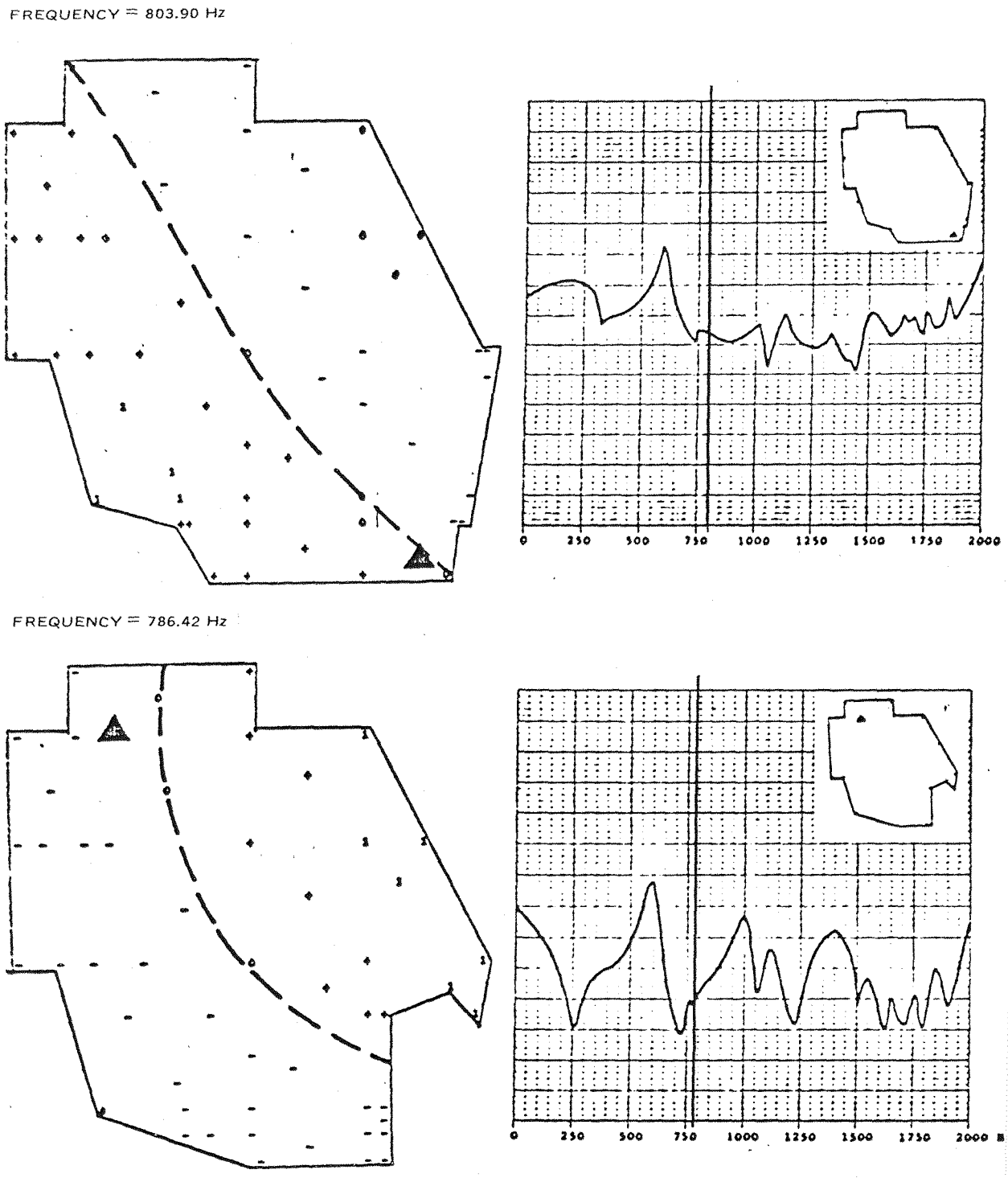

Figure 4.41 Distribution of sound pressure and nodal lines in the cavity cab at the resonance frequency.

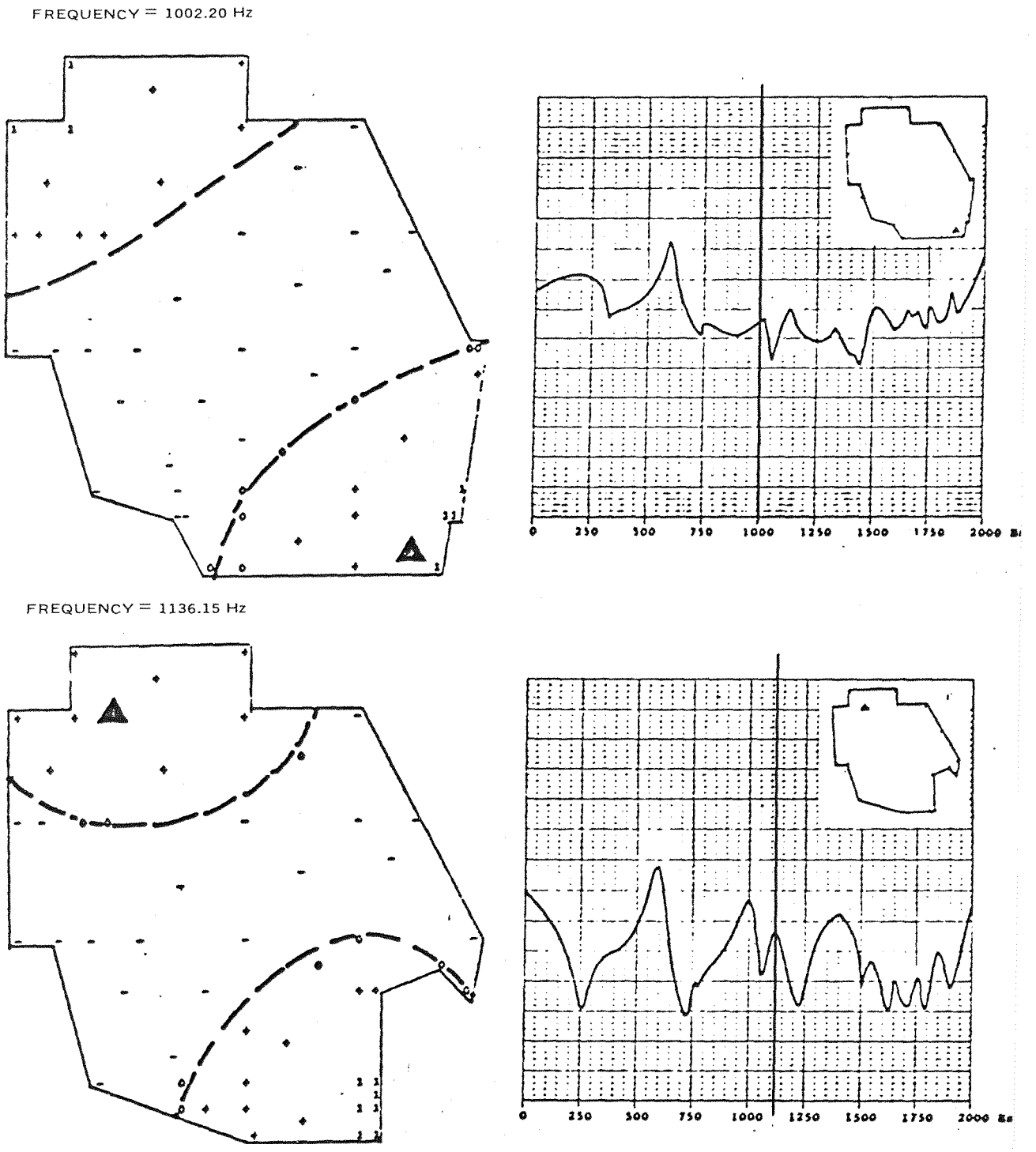

Figure 4.42 Distribution of sound pressure and nodal lines in the cavity cab at the resonance frequency.

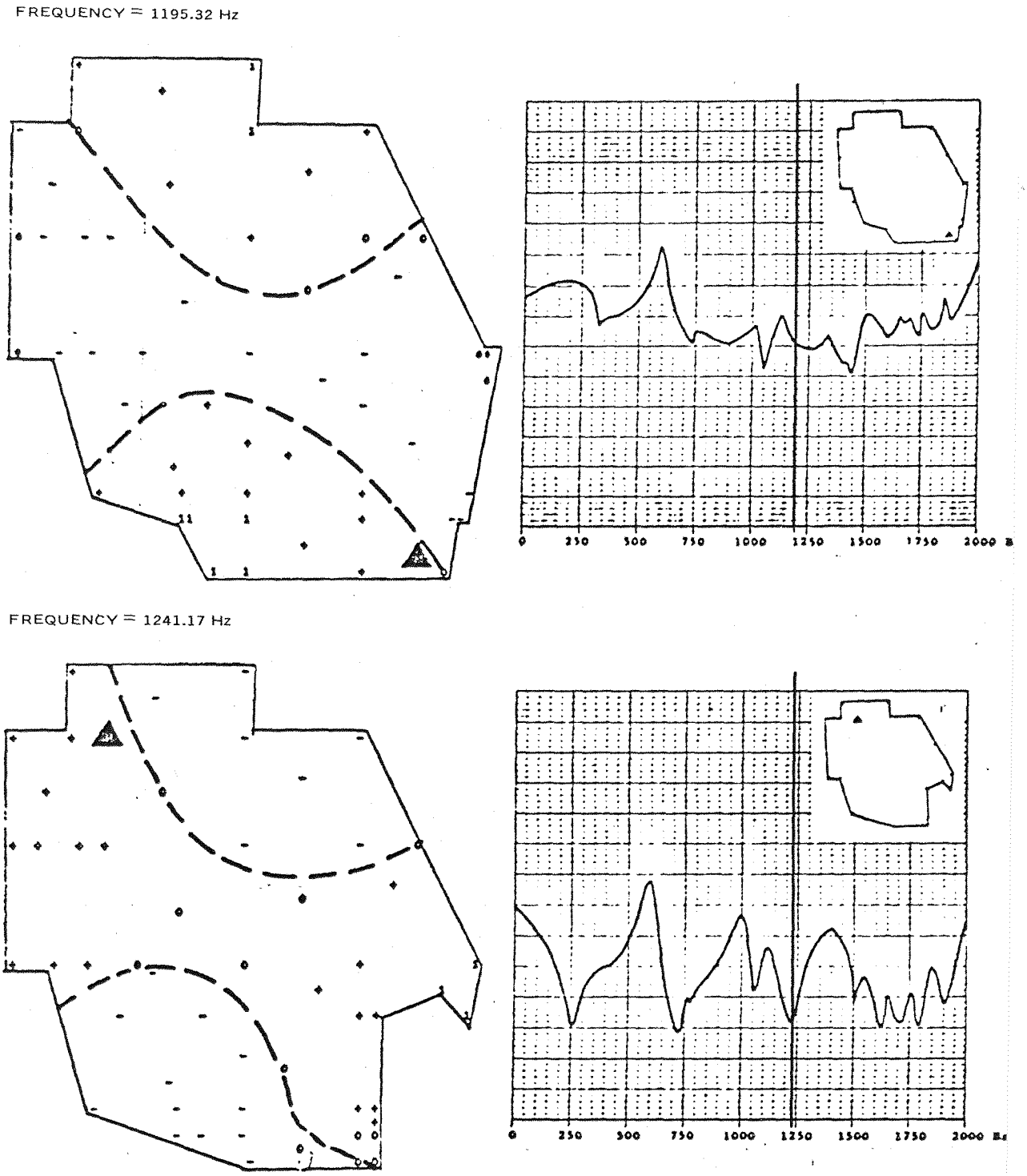

Figure 4.43 Distribution of sound pressure and nodal lines in the cavity cab at the resonance frequency.

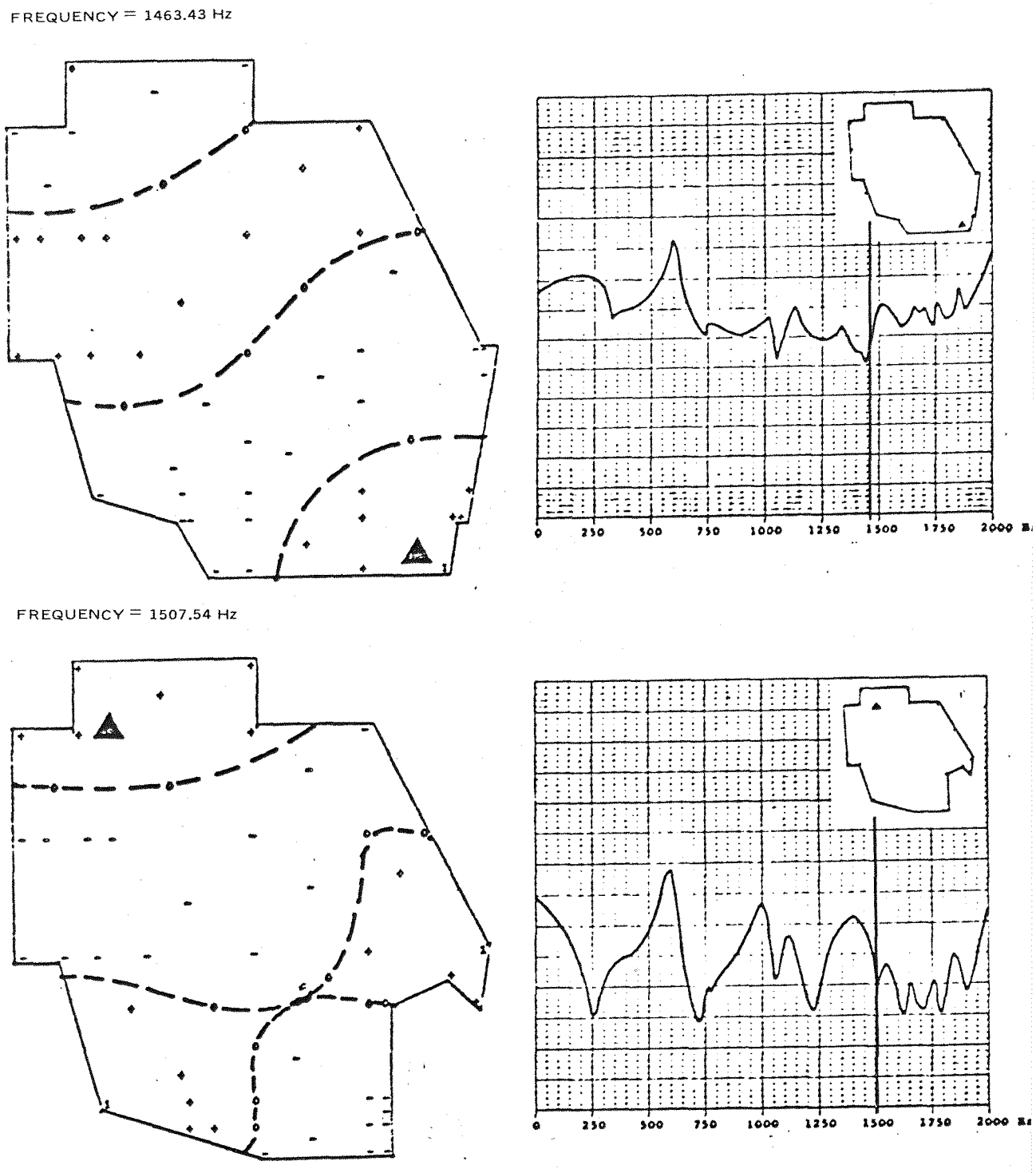

Figure 4.44 Distribution of sound pressure and nodal lines in the cavity cab at the resonance frequency.

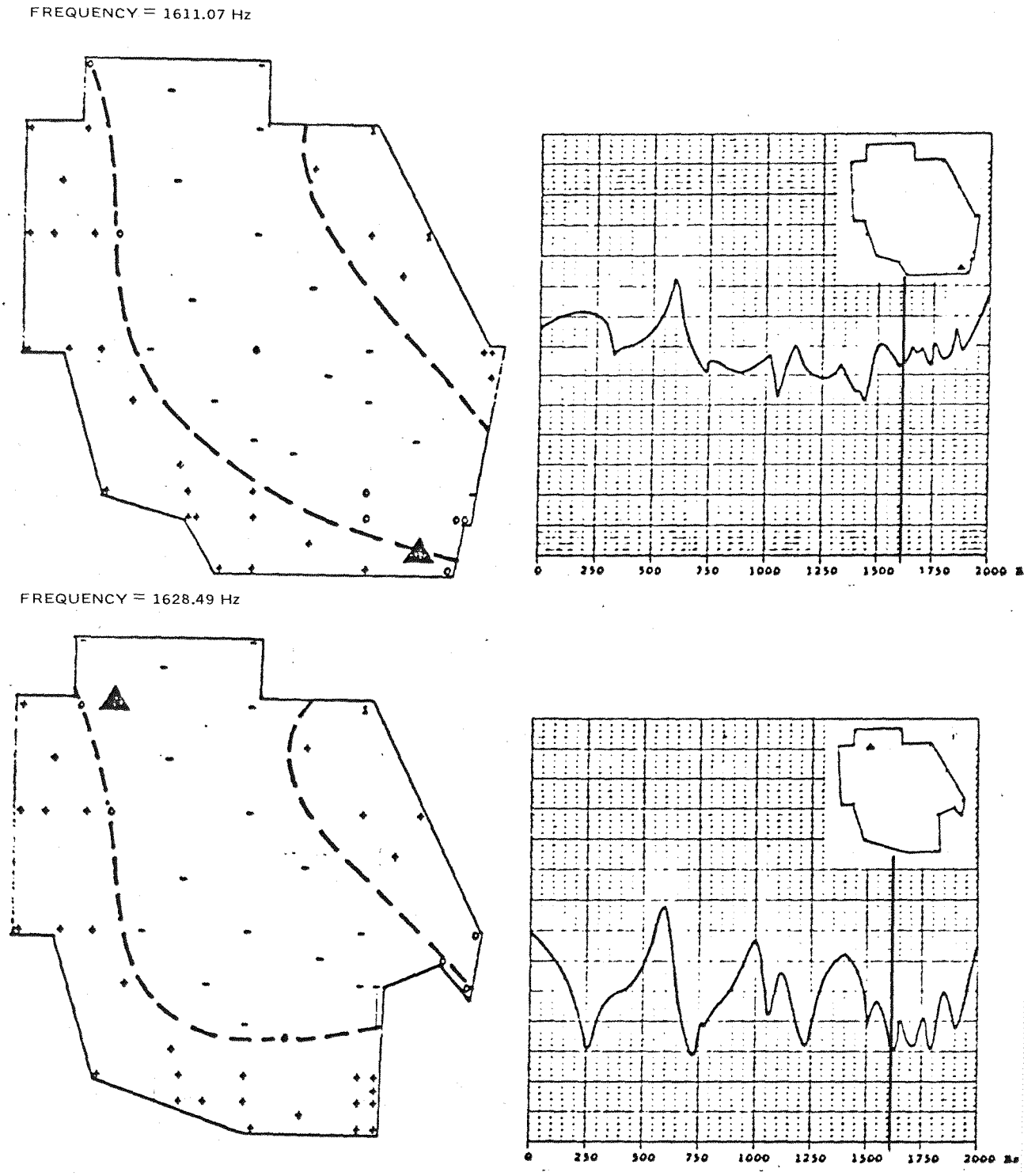

Figure 4.45 Distribution of sound pressure and nodal lines in the cavity cab at the resonance frequency.

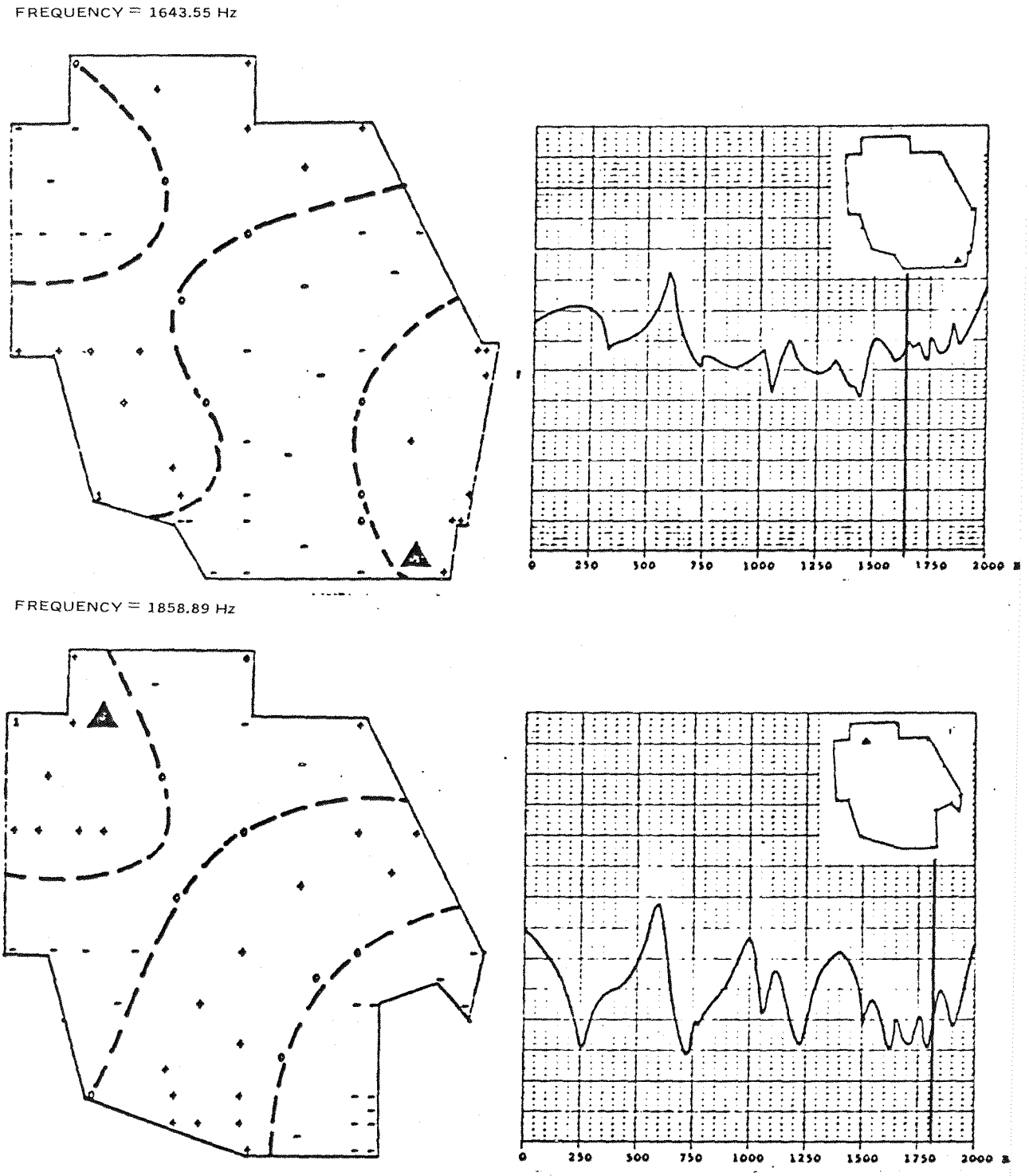

Figure 4.46 Distribution of sound pressure and nodal lines in the cavity cab at the resonance frequency.

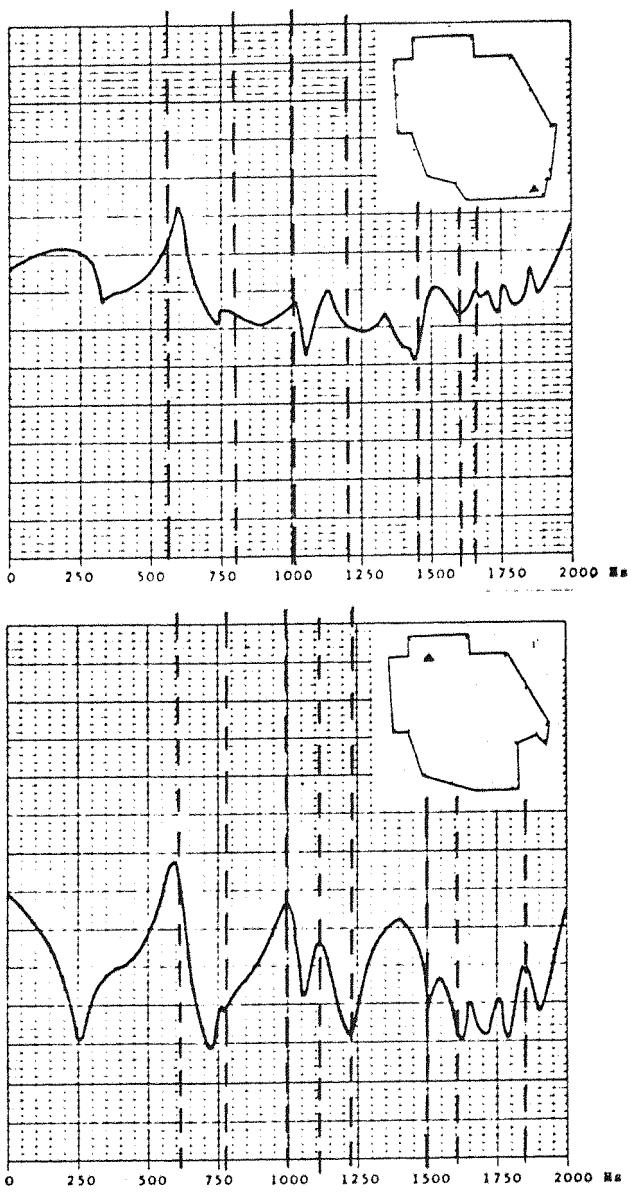

Figure 4.47 Comparison of the theoretical and experimental values of the resonance frequencies of the cab.

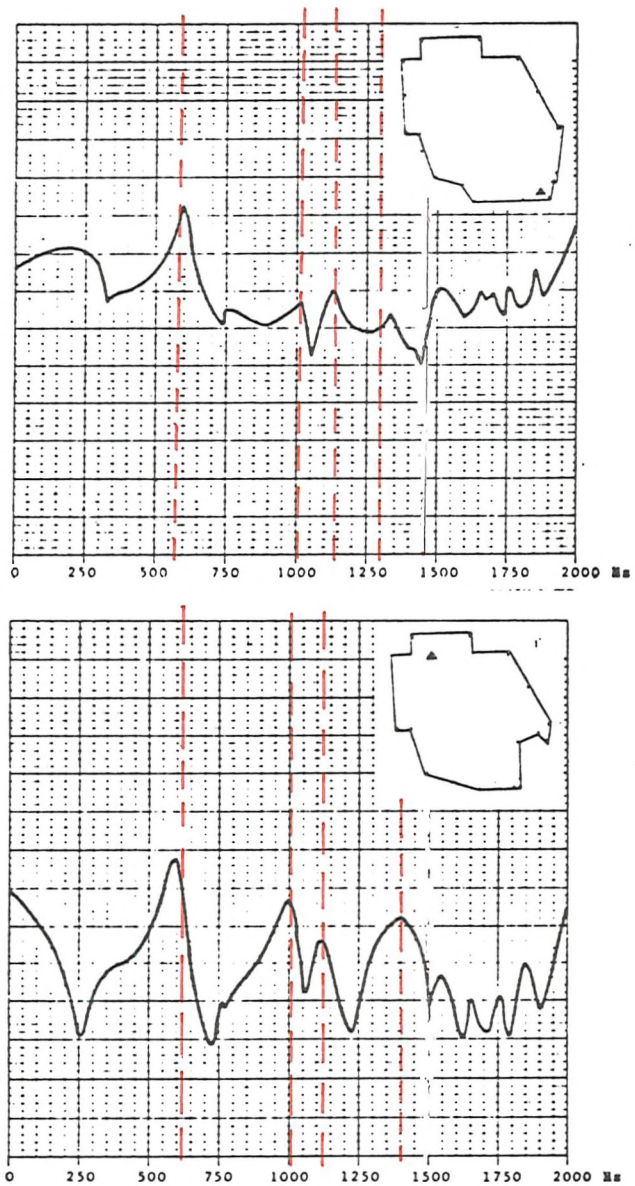

Figure 4.48 Comparison between the experimental and theoretical values of the resonance frequencies of the cab: only the frequencies marked by an asterisk in table (4.VII) are indicated.

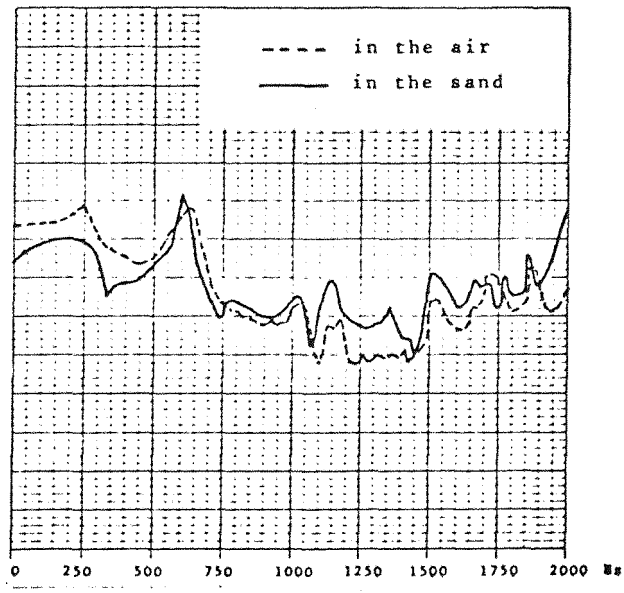

Figure 4.49 Comparison between the experimental results of the resonance frequencies of the cab obtained with the model in sand (solid line) and in air (dashed line).

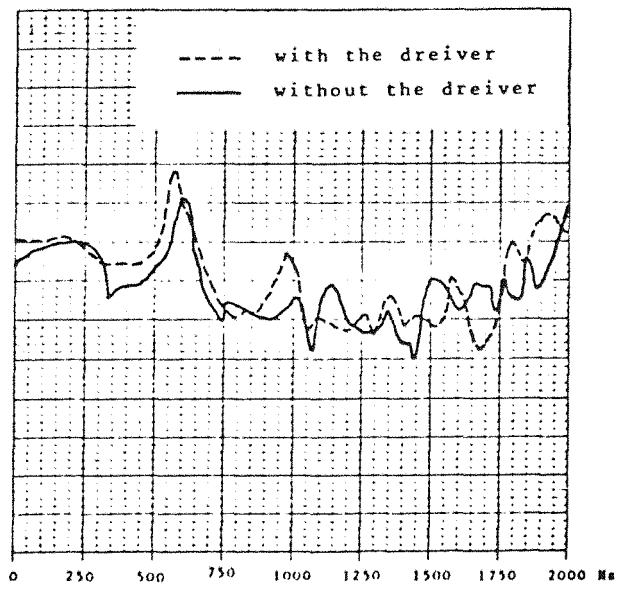

Figure 4.50 Comparison between the experimental results of the resonance frequencies of the cab obtained with the model in sand with driver (solid line) and without driver (dashed line).

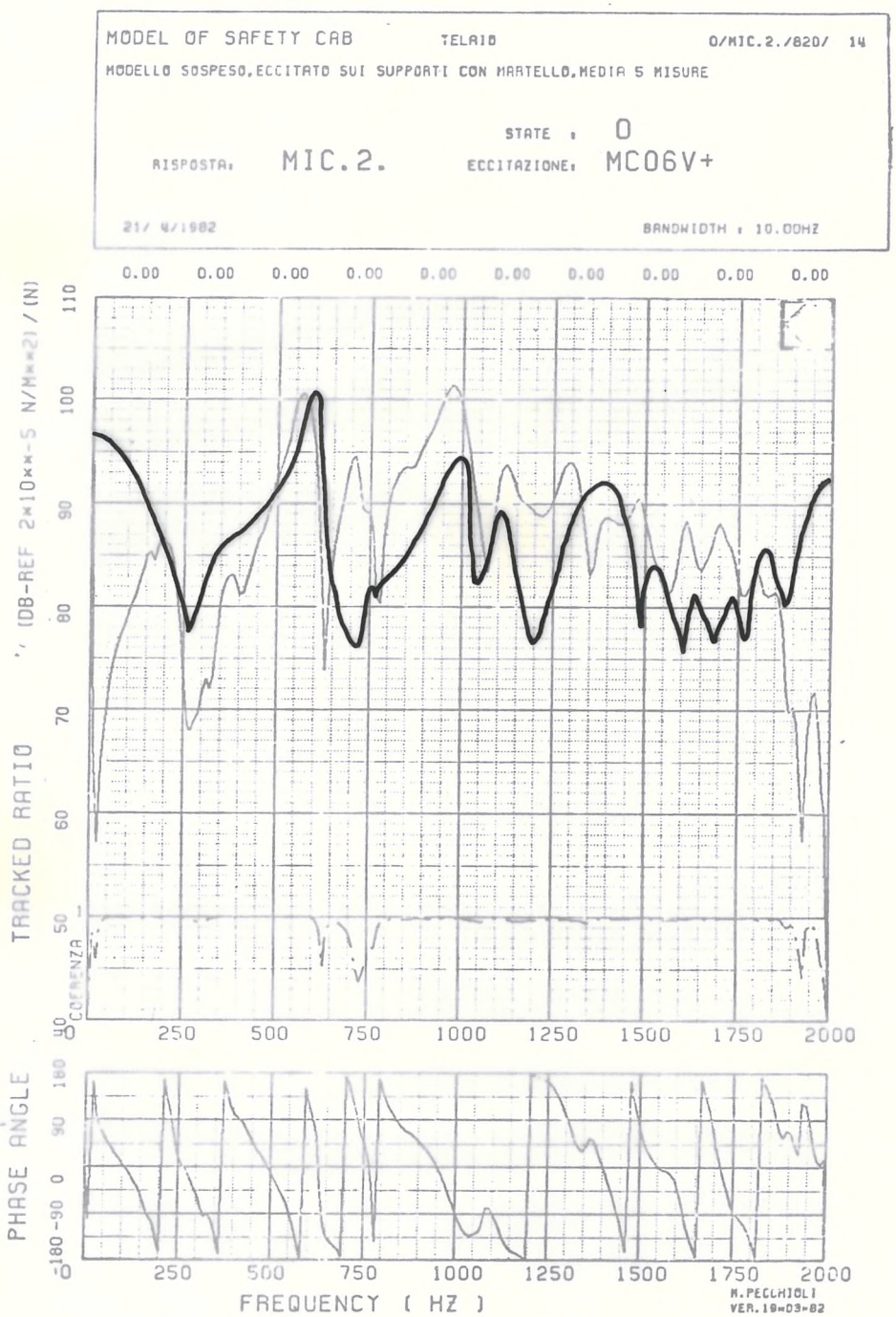

Figure 4.51 Comparison between the experimental results of the resonance frequencies of the cab obtained with the model in sand and the frequency response function between force (MC 06 +) and sound pressure level (MIC 2).

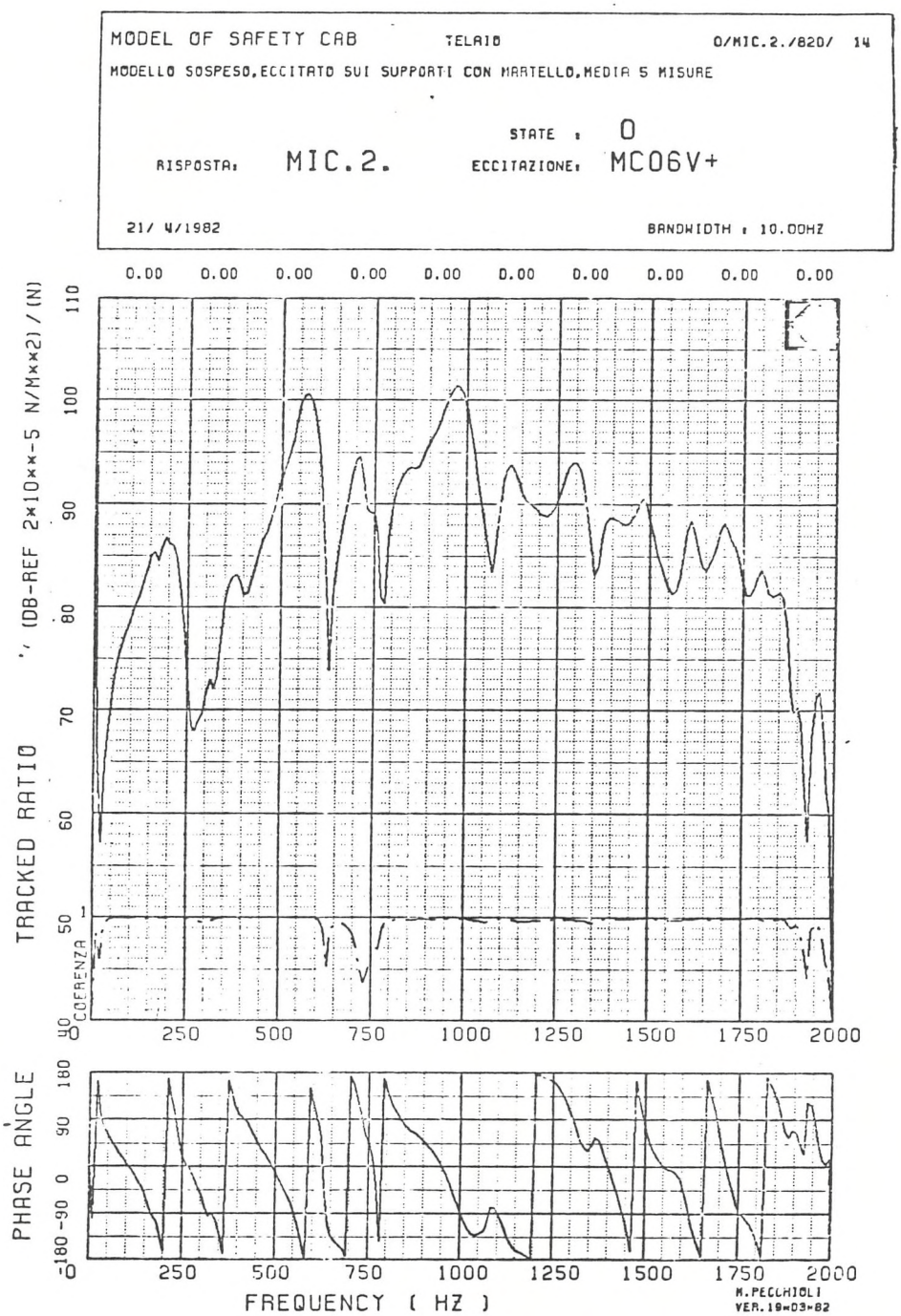

Figure 4.51 Comparison between the experimental results of the resonance frequencies of the cab obtained with the model in sand and the frequency response function between force (MC 06 +) and sound pressure level (MIC 2).

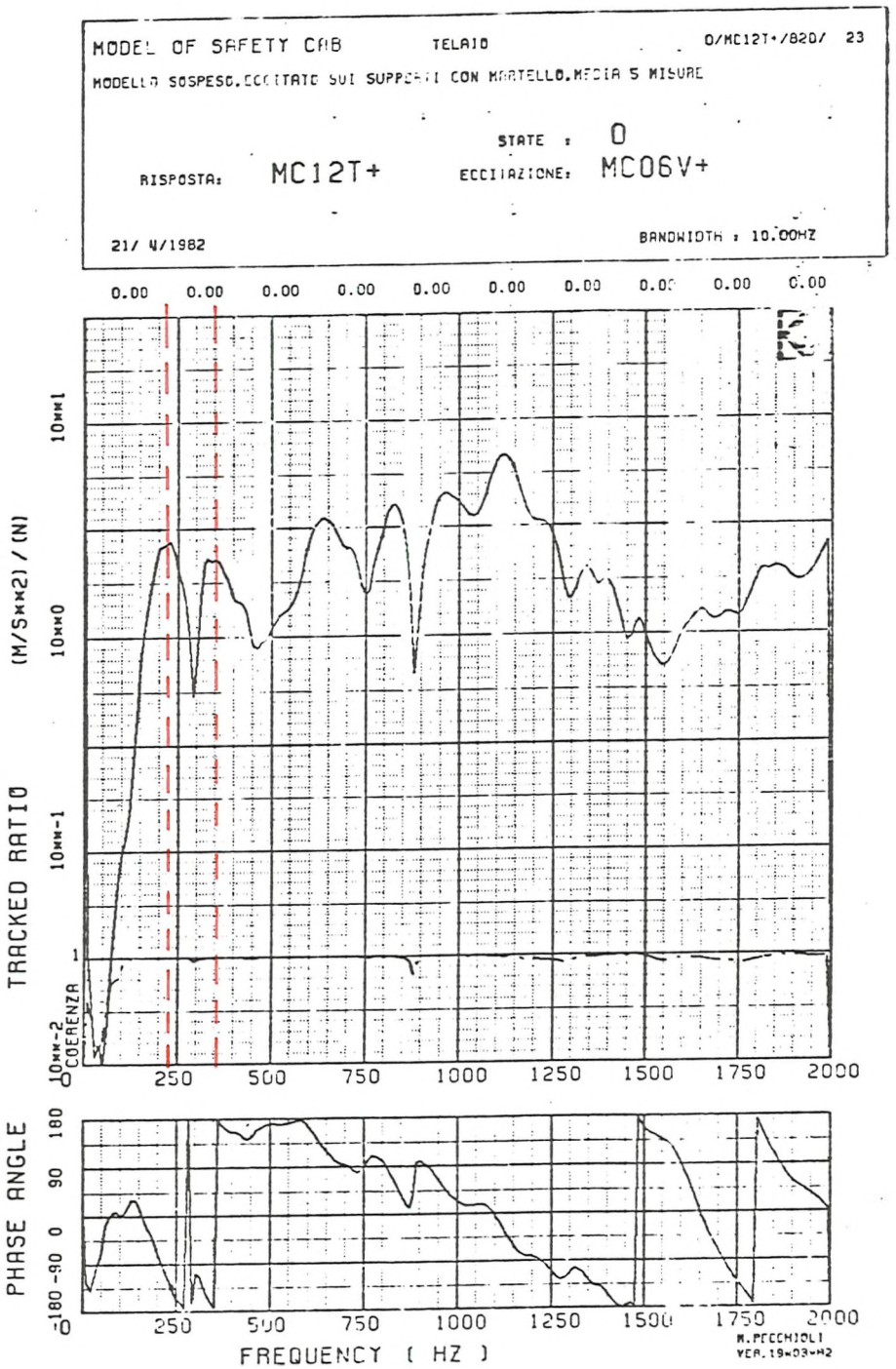

Figure 4.52 Frequency response function between force (MC 06 +) and acceleration (MC 12 T+). Measurement on the model.

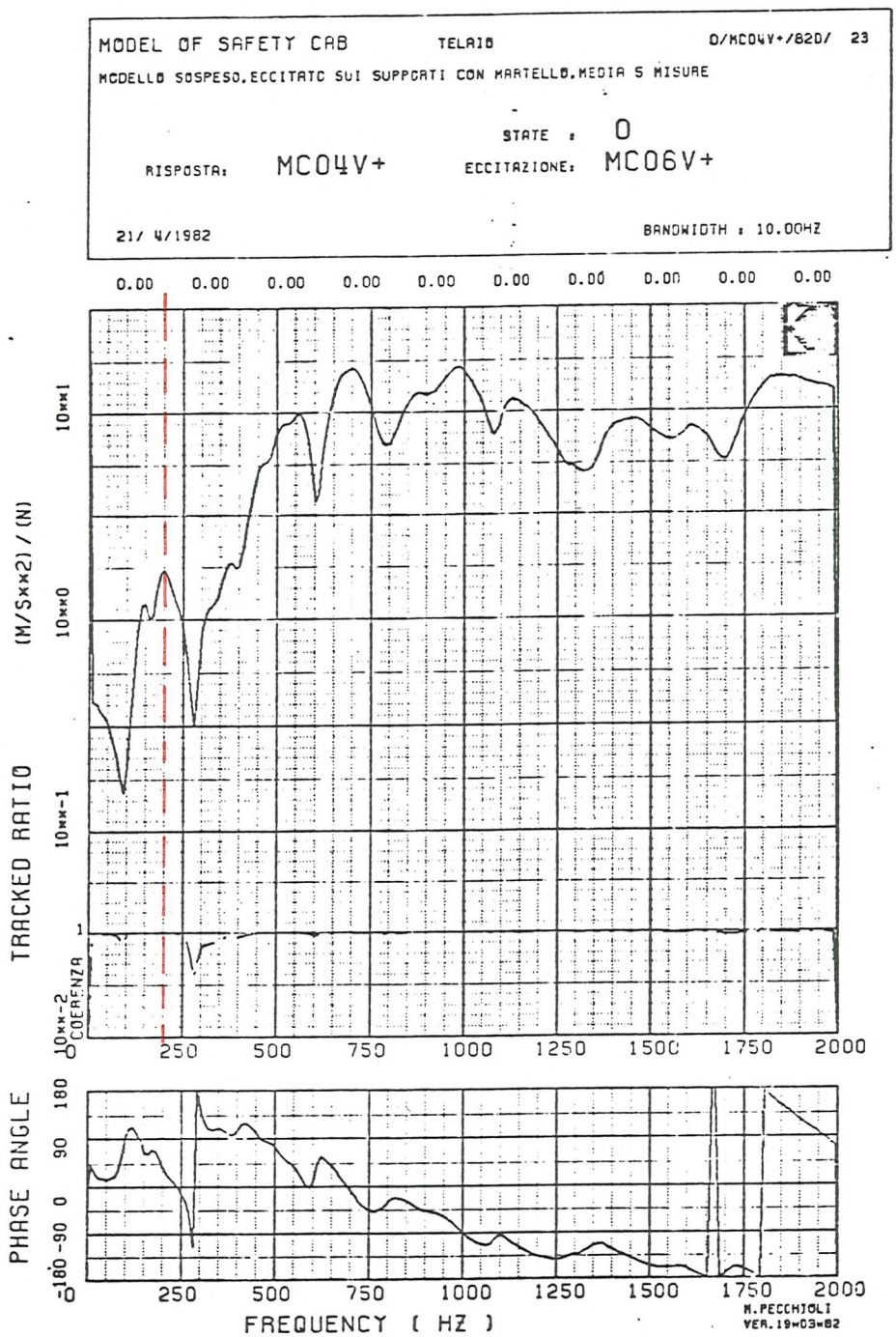

Figure 4.53 Frequency response function between force (MC 06+) and acceleration (MC 04 X). Measurement on the model.

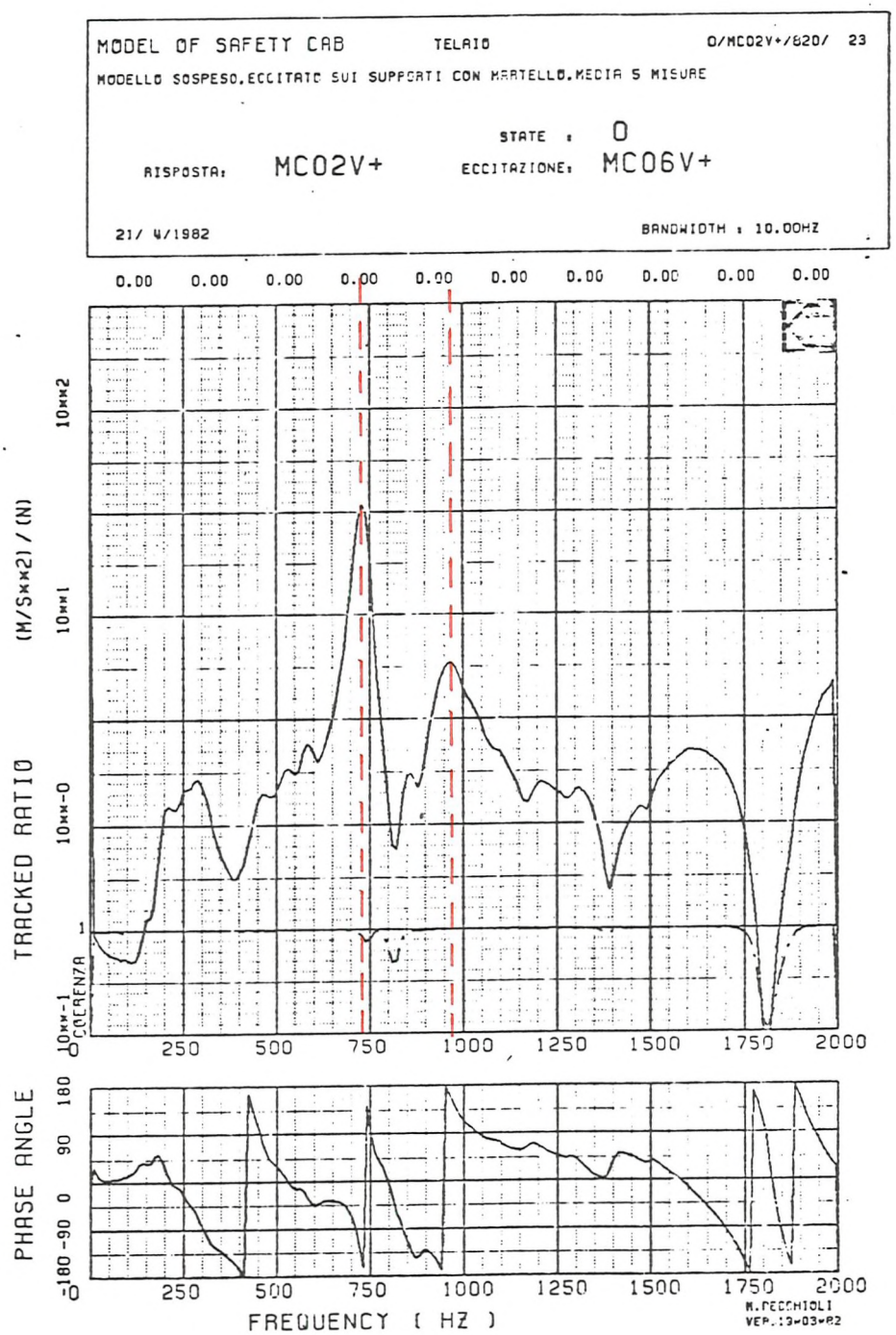

Figure 4.54 Frequency response function between force (MC 06 +) and acceleration (MC 02 +). Measurement on the model.

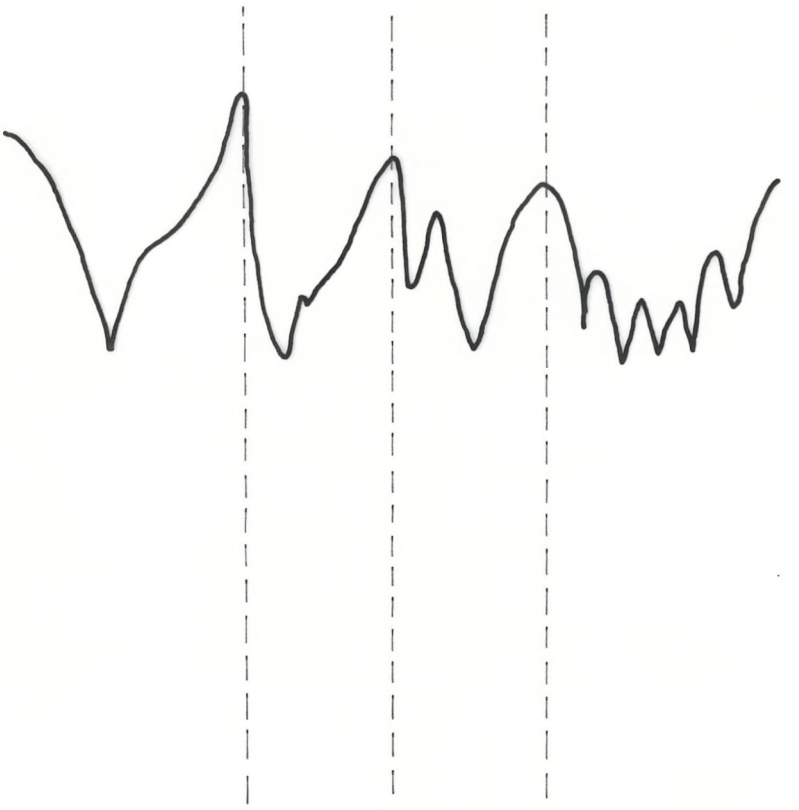

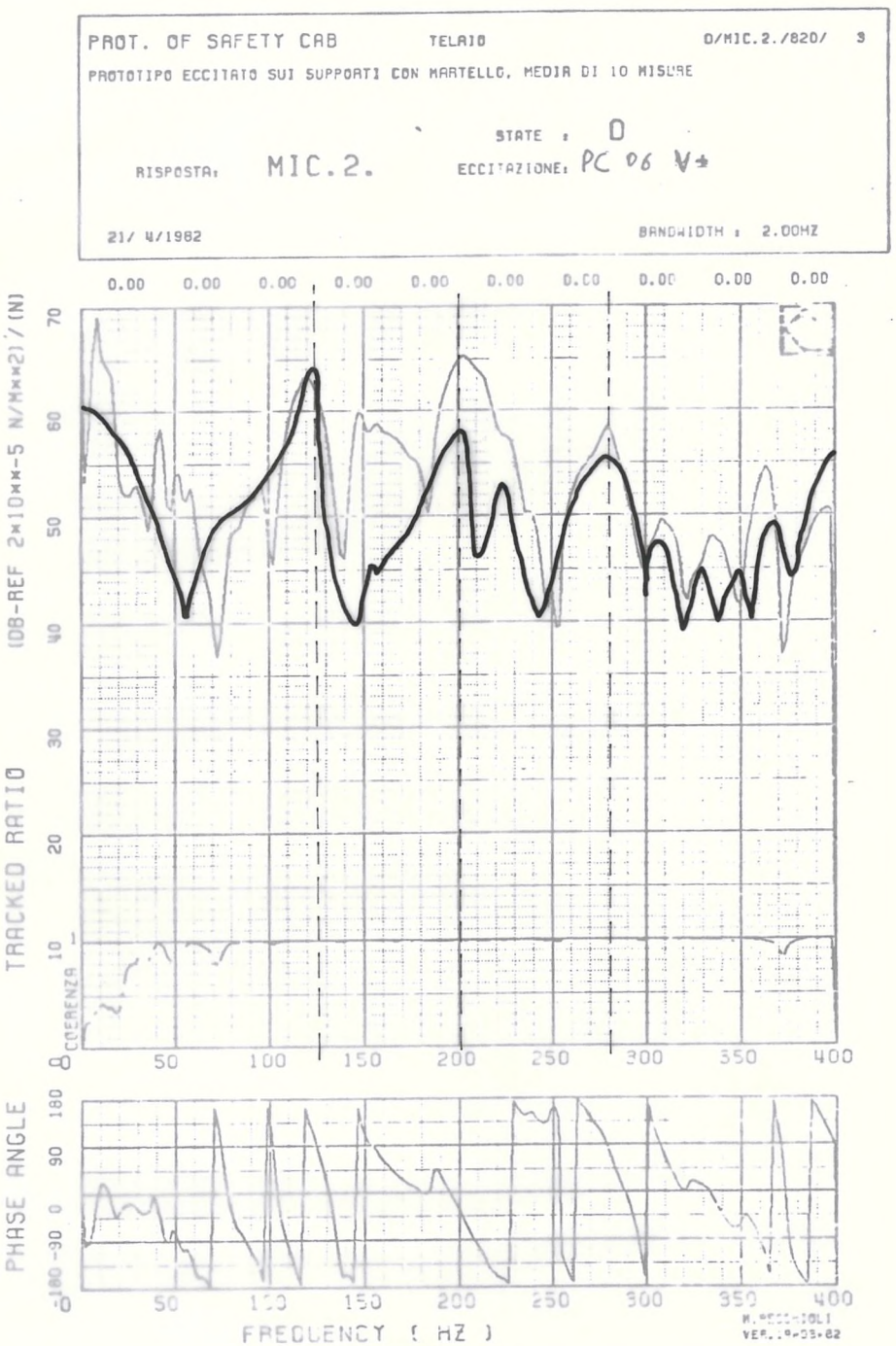

Figure 4.55 Comparison between the experimental results of the resonance frequencies of the cab and the frequency response function between force (PC 06 +) and sound pressure level (MIC. 2).

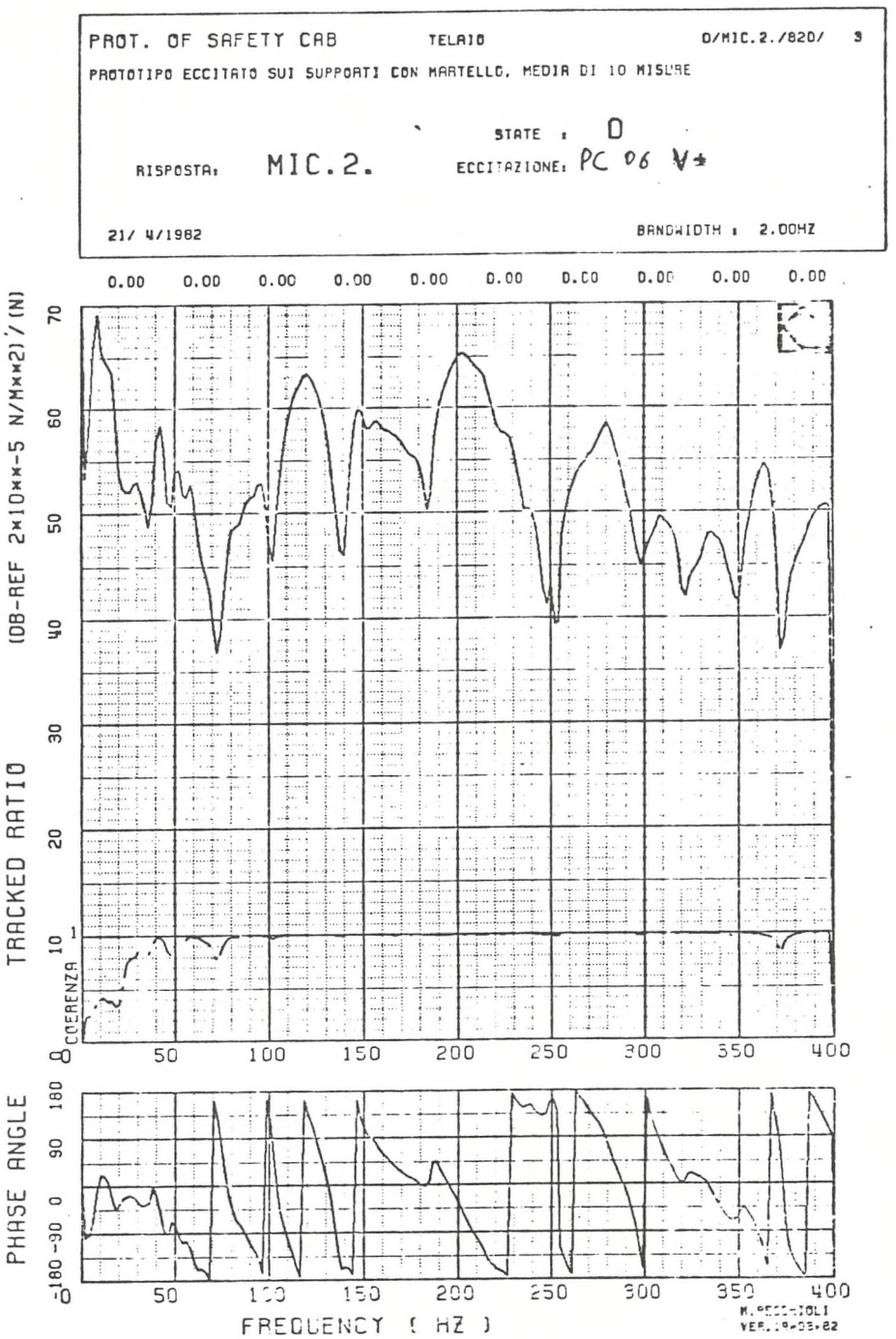

Figure 4.55 Comparison between the experimental results of the resonance frequencies of the cab and the frequency response function between force (PC 06 +) and sound pressure level (MIC. 2).

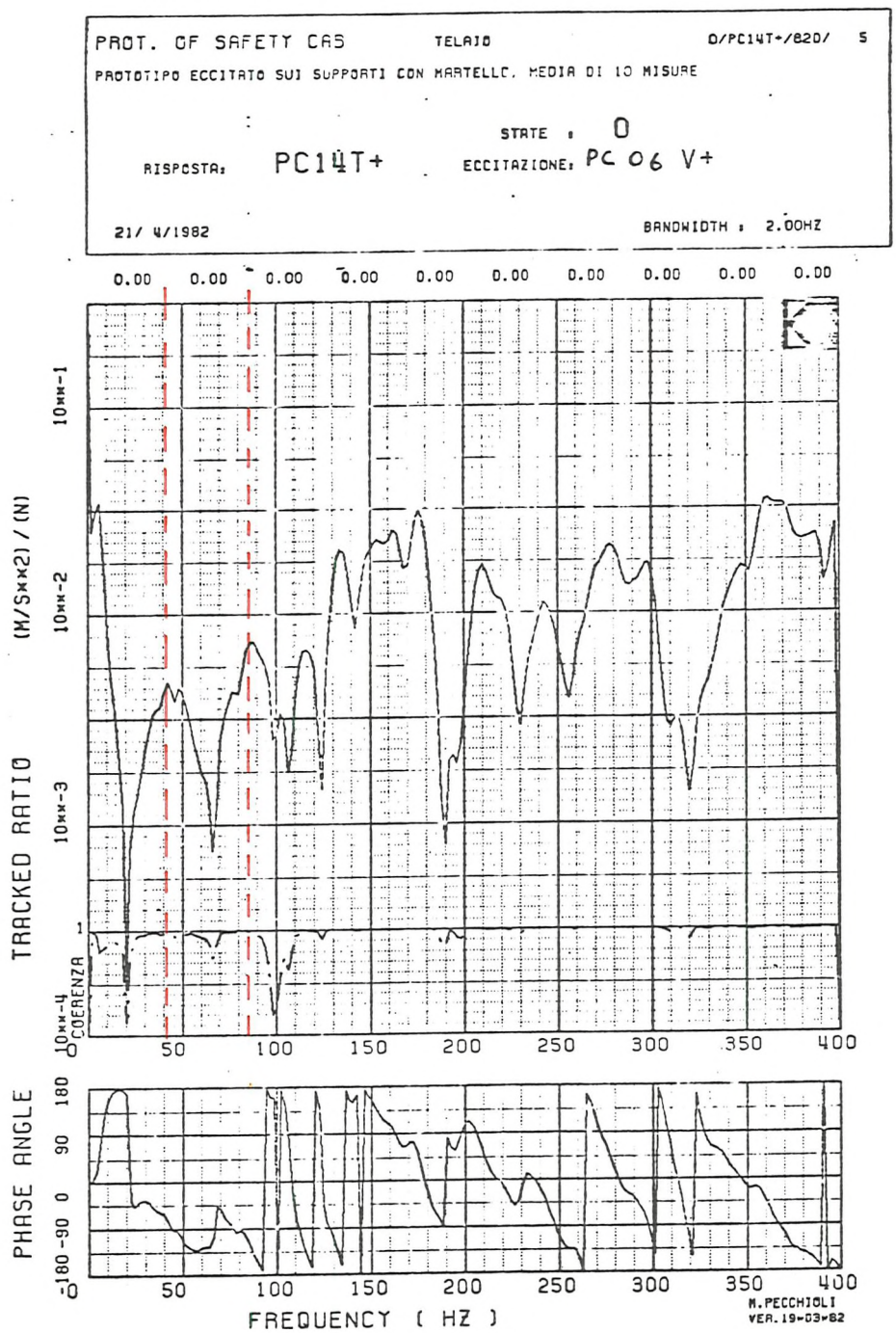

Figure 4.56 Frequency response function between force (PC 06 +) and acceleration (PC 14 T +). Measurement on the prototype.

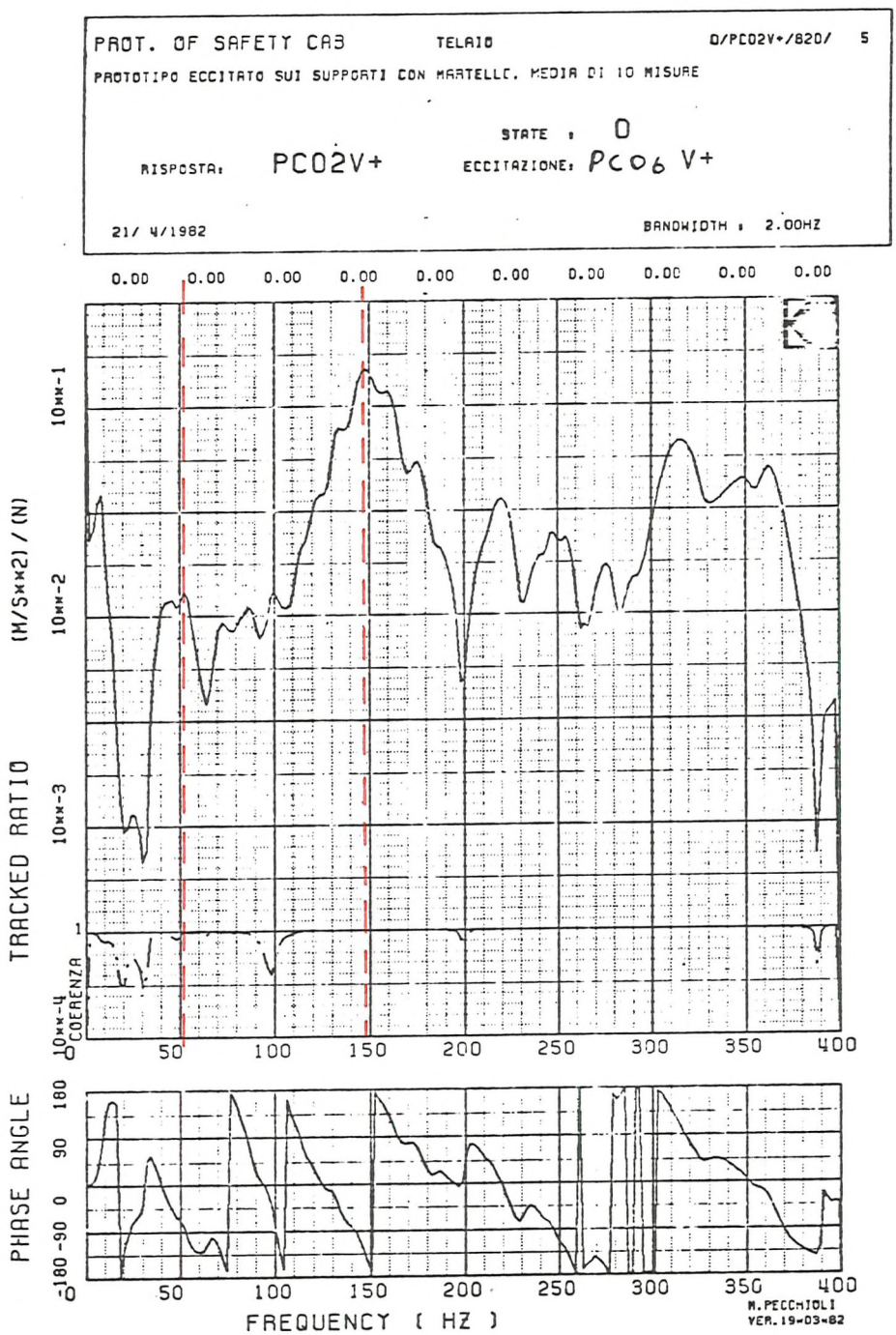

Figure_4.57 Frequency response function between force (PC 06 +) and acceleration (PC 02 V +). Measurement on the prototype.

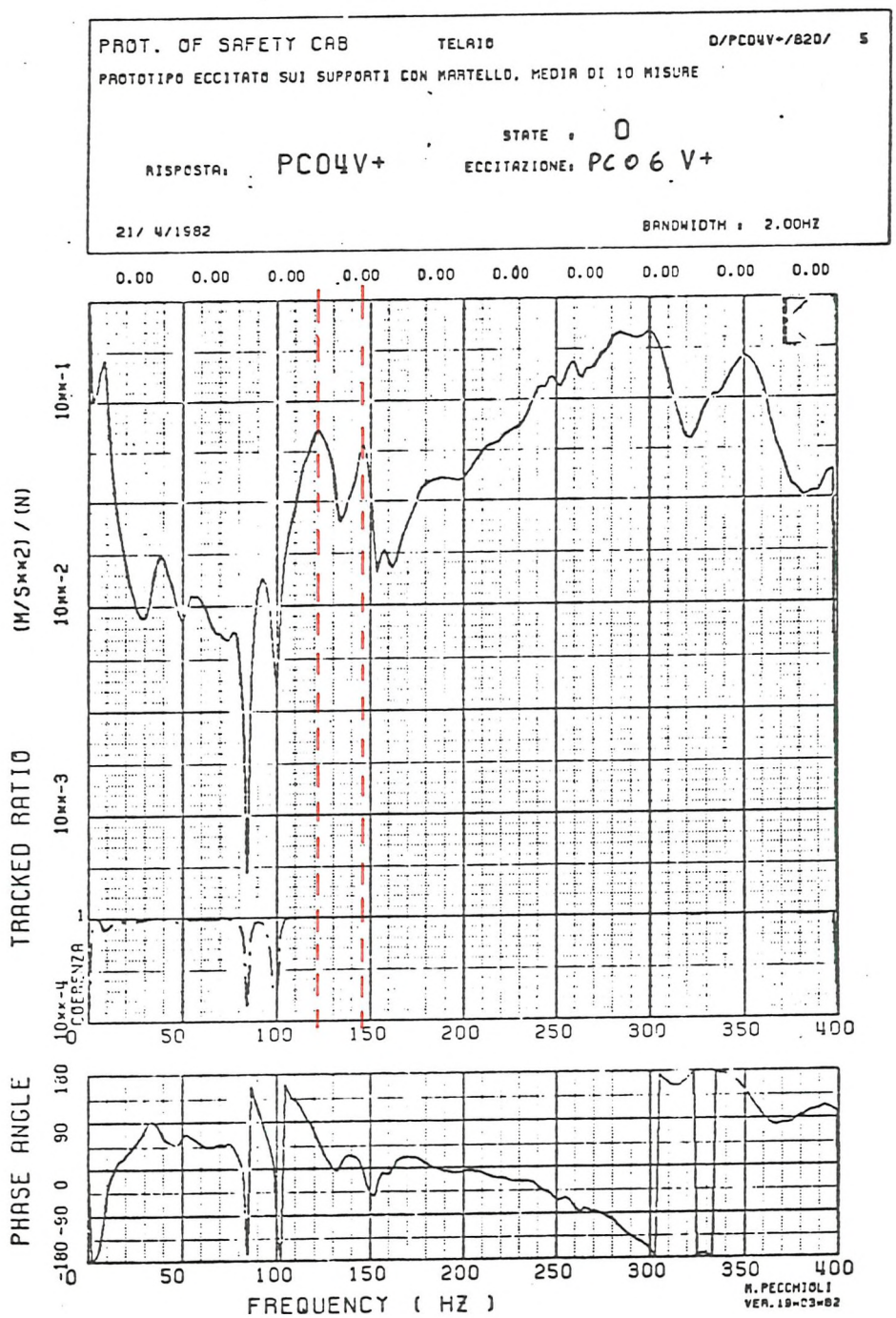

Figure 4.58 Frequency response function between force (PC 06+) and acceleration (PC 04 V +). Measurement on the prototype.

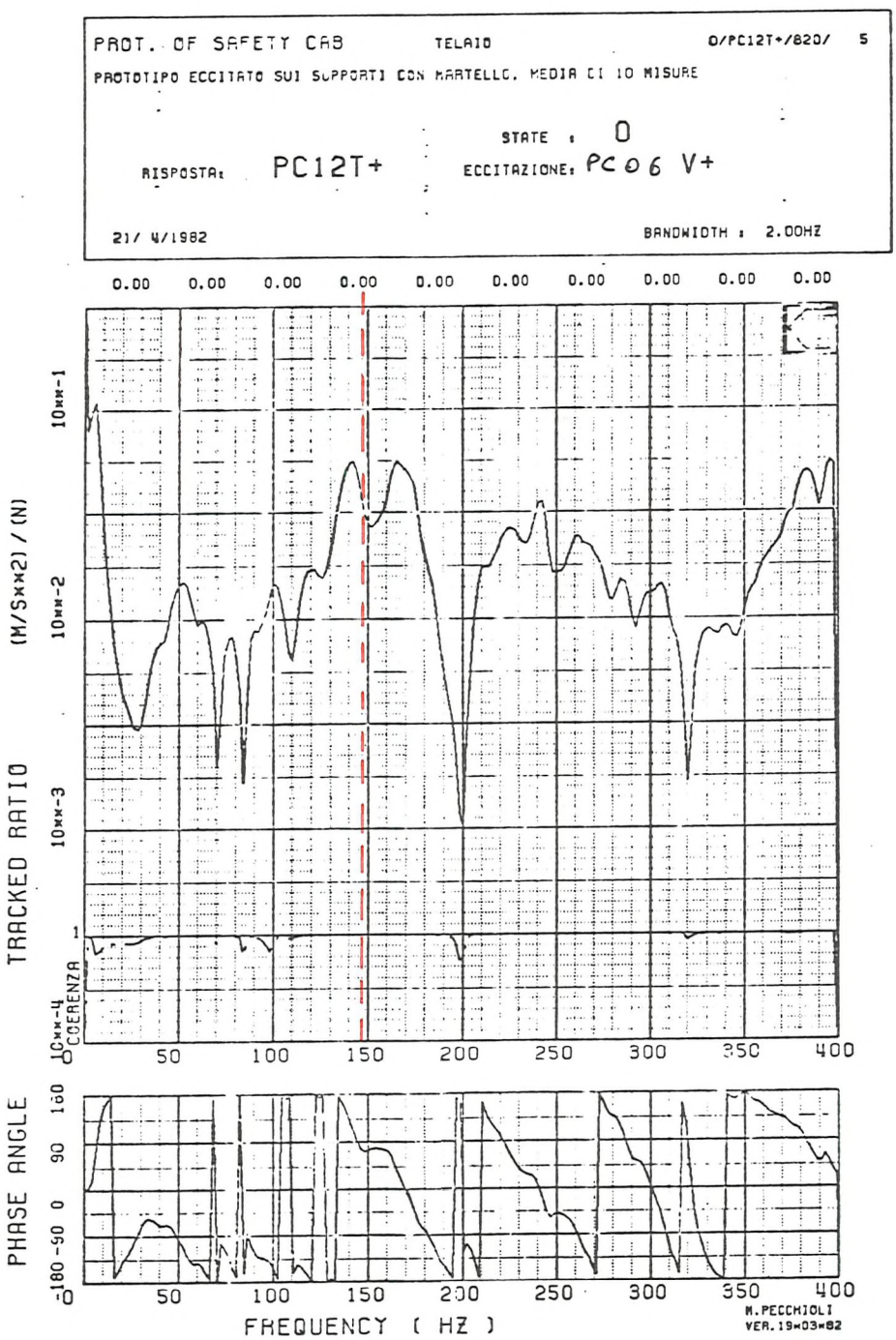

Figure 4.59 Frequency response function between force (PC 06 +) and acceleration (PC 12 T). Measurement on the prototype.

Tab. 4.I - Physical properties of prototype and model materials.

	MATERIAL		MASS DENSITY	MODULUS OF ELASTICITY	SPEDD OF LONG. WAVES	POISSON'S RATIO	DAMPING FACTOR AT 1000 Hz
			ρ [kg/m^3]	E [N/m^2]	c[m/s]	ν	η
PROTOTYPE	STEEL	[68]	7850	2.10^{11}	5050	0.28	$10^{-4} - 10^{-2}$
	GLASS	[68]	2500	$67.6.10^{9}$	5200	0.22	$10^{-3} - 10^{-2}$
MODEL	PERSPEX	[36]	1173	$4.83.10^{9}$	2030	0.38	$5 . 10^{-2}$
	ALUMINIUM	[68]	2700	$7.2 . 10^{10}$	5150	0.34	$10^{-4} - 10^{-2}$

Tab. 4.II - Moments of inertia of the main cross-sections of the bars of the prototype.

SECTION	I_ξ	I_η	α	I_ξ/I_η	I_n/I_y	I_{xz}
–	mm^4	mm^4	–	–	–	mm^4
1	106163	13265	0	8.00	1	0
2	276246	162942	61.5	1.69	0.92	47512
3	260106	87644	96.8	2.96	0.97	−20277
4	222433	1219323	105	0.182	0.47	249223
5	20287237	5858141	−45.2	3.46	0.53	−7214372
6	10402	94773	−6.49	0.109	0.91	9475
7	174396	58866	−43	2.96	0.60	−57624
A - A	1861041	263477	80.0	7.06	0.85	273200
E - E1	101778	691376	64.56	0.147	0.26	−228713
E - E	216158	1966604	−12.96	0.1099	0.71	382574
D - D	221430	646700	−42.67	0.342	0.62	211932
C - C	1005742	4410947	15	0.228	0.83	−851301
D - D1	158668	523495	−39	0.303	0.59	178427
F - F	1314763	6041304	11.45	0.217	0.88	−919605

Tab. 4.III - Geometric properties of the main coss-sections chosen for modelling prototype's members.

SECTIONS	TYPE	B	H	L	S	AREA	I_y	I_z	r_y	r_z
		mm	mm	mm	mm	mm^2	mm^4	mm^4	mm	mm
1	B			15	5	75	1406.3	156.3	4.33	1.44
2	T	15	15		1.5	42.75	425.7	911.3	3.16	4.62
3	T	15	15		1.5	42.75	425.7	911.3	3.16	4.62
4	R	25	10		1.5	96	6803.9	1353.8	8.42	3.76
5	Q			40	2	312	73312.0	73312.0	15.33	15.33
6	B			15	5	75	156.3	156.3	1.44	1.44
7	Q			10	1	38	490.3	490.3	3.59	3.59
A - A	R	30	10		1.5	111	1624.8	11012.6	3.83	9.96
E - E1	R	20	10		1.5	81	3795.1	1082.9	6.84	3.66
E - E	R	30	10		1.5	111	1624.8	11012.6	3.83	9.96
D - D	Q			12	1	46	892.7	892.7	4.41	4.41
C - C	R	35	15		1.5	141	4783.2	20817.3	5.82	12.15
D - D1	R	20	10		1.5	81	1082.9	3795.1	3.66	6.84
F - F	R	35	15		1.5	141	4783.2	20817.3	5.82	12.15

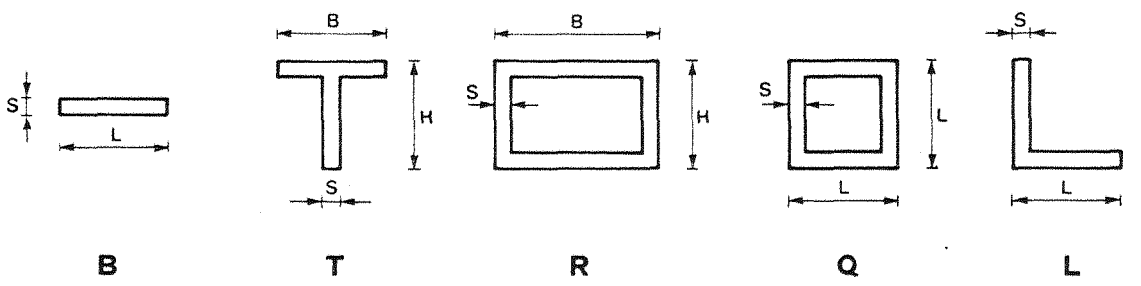

Tab. 4.IV - Comparison between the geometric properties of the main cross sections of the prototype (p) and the model (m).

SECTIONS	r_{yp}	r_{ym}	r_m/r_p	$(I_y)_p \cdot 10^4$	$(I_y)_m \cdot 10^2$	I_m/I_p	F_{nm}/F_{np} (eq. 4.15)	A_m	A_p	A_m/A_p	F_{tm}/F_{tp} (eq. 4.12)
	mm	mm	—	mm^4	mm^4	—	—	mm^2	mm^2	—	—
1	22.4	4.33	1/5.17	10.6	14.1	1/75	1/8.84	75	212	1/2.82	1/8.31
2	19.0	3.16	1/6.01	18.9	4.20	1/450	1/52.6	42.75	520	1/12.16	1/35.7
3	13.7	3.16	1/4.33	9.0	4.2	1/214	1/25	42.75	480	1/11.22	1/33
4	39.5	8.42	1/4.69	115.2	68.0	1/169	1/20	96	730	1/7.6	1/22.36
5	74.9	15.33	1/4.88	1300.8	733.1	1/177	1/20.8	312	2315	1/7.41	1/21.82
6	7.2	1.44	1/5	1.1	1.6	1/70.4	1/8.20	75	220	1/2.93	1/8.62
7	16.0	3.59	1/4.45	12.0	4.9	1/244	1/28.6	38	464	1/12.2	1/35.9
A - A	19.8	3.83	1/5.16	31.2	16.2	1/192	1/22.7	111	793	1/7.14	1/21
E - E1	26.8	6.84	1/3.91	58.2	37.9	1/153	1/18.2	81	809	1/9.98	1/29.37
E - E	20.5	3.83	1/5.35	30.4	16.2	1/187	1/22.2	111	725.25	1/6.53	1/19.21
D - D	20.7	4.41	1/4.69	41.7	8.9	1/468	1/58.8	46	966	1/21	1/61.7
C - C	28.5	5.14	1/5.54	123.4	58.6	1/210	1/30.3	141	1520.5	1/10.78	1/31.7
D - D1	16.2	3.66	1/4.42	15.8	10.8	1/146	1/17.2	81	606	1/7.48	1/22
F - F	30.0	5.82	1/5.15	150.1	47.8	1/314	1/37	141	1669.5	1/11.84	1/34.82

Tab. 4.V - Dimensionless parameters to be kept constant between prototype and model: values of their ratio.

	CHARACTERISTIC DIMENSIONLESS PARAMETERS	NUMERICAL VALUES OF THE RATIO $(N)_m/(N)_p$ EXACT SIMILITUDE CONDITION: $(N)_m/(N)_p = 1$	
ACOUSTIC FIELD	$N_1 = \frac{\omega L}{c_0}$	$(N_1)_m/(N_1)_p = 1$	
BARS — LONG. VIB.	$N_2 = \frac{\omega^2 L^2 \rho}{E}$	$(N_2)_m^{Al}/(N_2)_p^{s} = 0.96$	
	$N_3 = q_t' \frac{Lr^2}{EI}$	$(N_3)_m^{Al}/(N_3)_p^{s} = \frac{q'_{tm}}{q'_{tp}} \frac{I_p}{I_m} 2.22 \cdot 10^{-2}$	
BARS — TRANSV. VIB.	$N_4 = \frac{\omega^2 L^4 \rho}{Er^2}$	$(N_4)_m^{Al}/(N_4)_p^{s} = 0.96$	
	$N_5 = q_n' \frac{L^3}{EI}$	$(N_5)_m^{Al}/(N_5)_p^{s} = \frac{q'_{nm}}{q'_{np}} \frac{I_p}{I_m} 2.22 \cdot 10^{-2}$	
PLATES — LONG. VIB.	$N_6 = \frac{\omega^2 L^2 \rho (1-\nu^2)}{E}$	$(N_6)_m^{px}/(N_6)_p^{s} = 5.74$	$(N_6)_m^{px}/(N_6)_p^{g} = 5.90$
	$N_7 = q_n \frac{L(1-\nu^2)}{Eh}$	$(N_7)_m^{px}/(N_7)_p^{s} = \frac{q_{nm}}{q_{np}} 15.38$	$(N_7)_m^{px}/(N_7)_p^{g} = \frac{q_{nm}}{q_{np}} 7.55$
PLATES — TRANSV. VIB.	$N_8 = \frac{\omega^2 L^4 \rho (1-\nu^2)}{Eh^2}$	$(N_8)_m^{px}/(N_8)_p^{s} = 0.92$	$(N_8)_m^{px}/(N_8)_p^{g} = 0.94$
	$N_9 = q_n \frac{L^3(1-\nu^2)}{Eh^3}$	$(N_9)_m^{px}/(N_9)_p^{s} = \frac{q'_{nm}}{q'_{np}} 2.46$	$(N_9)_m^{px}/(N_9)_p^{g} = \frac{q_{nm}}{q_{np}} 0.81$
	$N_{10} = \frac{\rho_0 c_0^2 L^3 (1-\nu^2)}{Eh^3}$ (°)	$(N_{10})_m^{px}/(N_{10})_p^{s} = 2.46$	$(N_{10})_m^{px}/(N_{10})_p^{g} = 0.81$
	$N_{11} = \nu$ (∞)	$(N_{11})_m^{px}/(N_{11})_p^{s} = 1.36$	$(N_{11})_m^{px}/(N_{11})_p^{g} = 1.73$

(°) coupling interaction condition
(∞) free edge boundary condition

Al - Aluminium
px - Perspex
g - Glass
s - Steel
m - Model
p - Prototype

Tab. 4.VI - Types of investigations planned.

a)	Acoustic characterization of vehicles.
b)	Search for secondary sources of noise radiation.
c)	Acoustic holes.
d)	Development of experimental soundpackages.
e)	Optimization of soundpackages.
f)	Weight reduction studies.
g)	Motion and deformation of the power unit.
h)	Examination of force application points.
i)	Transmission path investigations (air-and solid borne).
j)	Dynamic deformation of the body.
k)	Acoustic modes in the passenger compartment.

Tab. 4.VII - Resonance frequencies of the cab obtained by a finite element method (Hz)

TRANSVERSE (f_t)		LONGITUDINAL (f_ℓ)			TOTAL $f^2_{tot} = f^2_t + f^2_\ell$		
		Central section (MIC 2)		Lateral section (MIC 4)	Central section (MIC 2)		Lateral section (MIC 4)
n = 0	0	653.3	*	556.0 *	1040.0	*	981.6 *
		786.4	(•)	803.9 (•)	1128.2		1140.5 *
n = 1	809.5	1136.1	*	1002.2 *	1394.7	*	1287.9 *
		1241.2	(•)	1195.3 (•)	1481.6		1443.3
		1507.5		1463.4	1710.8		1672.1
n = 2	1619.5	1628.5	(•)	1611.1 (•)	1818.4		1802.8
		1858.9	(•)	1643.5	2027.3		1831.8
				1981.0			

(•) Microphone position near a nodal line.

(*) Resonance frequencies identified in figure (4.48)

CHAPTER 5

Experimental work: second model

The aim of this experimental work is to verify the actual possibility of using a different acoustic medium in place of air, in the modelling technique. In sections(3.4.3) and(3.4.4),two types of models have been examined: with the same material, (models of the third type) and with different material (models of the fourth type). The main conclusions were that to avoid very small thickness scale ratios only the models of the fourth type could be used. In addition only this type of model gives some possibility of matching both the structural and the coupling condition.

Considering that plastic materials proved to be the must suitable for the modelling technique, the main aim of the second experiment has been to look for an acoustic medium that at room temperature and pressure could satisfy the modelling conditions and prove to be compatible with such plastic materials.

The experimental apparatus which has been designed and built is composed of a rigid cylindrical cavity that is closed at one end wall by a flexible panel which is driven by a sinusoidal force concentrated in the center of the panel itself. Part of this work has already been reported by the author |44| and therefore the results are not all repeated here. The paper is attached as an appendix(Appendix 1).

5.1. - Description of the prototype.

A detailed cross-section of the cavity is shown in fig. (5.1). The inside diameter of the cylinder is 0.38 m, the length is 0.61 m and the thickness of the rigid walls is $10 \cdot 10^{-3}$ m. The flexible end wall is an aluminium plate of 1 mm thickness which is clamped at its edges and driven by a normal force concentrated at the center of the panel. In the cavity there is air at room temperature and pressure.

The inner acoustic field produced by a sinusoidal exiting force has been theoretically studied. The solution, based upon Green's functions, represents an example of an analytical approach to the problem of the structure-fluid interaction. The determination of the sound pressure level within the cavity is obtained by the acoustic potential function $\psi(\bar{R}_j,t)$ which is related to the pressure $p(\bar{R}_j,t)$ by the following relationship:

$$p(\bar{R}_j,t) = - \rho_o \frac{\partial \psi(\bar{R}_j,t)}{\partial t} \tag{5.1}$$

If it is assumed that the driving force is oscillating with circular frequency ω, we can write:

$$p(\bar{R}_j) = - i\omega\rho_o\psi(\bar{R}_j) \tag{5.2}$$

The boundary conditions on $\psi(\bar{R}_j)$ at the various walls of the cavity (S) are:

$$\left.\frac{\partial \psi(\bar{R}_j)}{\partial \bar{n}}\right|_S = w(\bar{R}_k) \tag{5.3}$$

where $\bar{n}$ is the normal direction pointing outside the chamber,

$\bar{R}_k$ is the vector coordinate of the surface S,

$w(\bar{R}_k)$ is the normal component of the velocity of the surface S.

Introducing a system of cylindrical coordinates (r, θ, z) with origin at the centre of the panel and the z axis pointing into the cavity, and considering that only one end wall at z = 0 is flexible, from equation (5.3) one obtains:

$$\text{i)} \qquad \left.\frac{\partial\psi(r)}{\partial z}\right|_{z=0} = w(r) \tag{5.4}$$

$$\text{ii)} \qquad \left.\frac{\partial\psi(r)}{\partial r}\right|_{r=R} = \left.\frac{\partial\psi(r)}{\partial z}\right|_{z=l} = 0 \tag{5.5}$$

Having determined the velocity w(r) of the flexible panel through the equation of motion of a circular plate clamped at its edges driven by a sinusoidal force concentrated at the center of the plate itself, the following value of $\psi(r)$ has been obtained:

$$\psi(\bar{r}) = -i\omega \frac{F_o}{\rho h} \cdot \frac{1}{2\pi^2 R^4} \sum_{n,m} \frac{1 - J_o(\pi\beta_{om})/I_o(\pi\beta_{om})}{(\omega_{om}^2 - \omega^2) J_o^2(\pi\beta_{om})}$$
$$\cdot \frac{J_o(\pi/R\ \alpha_n \rho)}{\Delta\rho_n J_o^2(\pi\alpha_n)} \cdot Z(z) \cdot \int_{A'} J_o\left(\frac{\pi}{R}\alpha_n \rho'\right) y_{om}(\rho')\, dA', \tag{5.6}$$

where the function Z(z) is:

$$\frac{e^{\Delta\rho n z} + e^{\Delta\rho n (2l - z)}}{1 - e^{\Delta\rho n 2l}} \quad \text{for } \left|K^2 - \left(\frac{\pi}{R}\alpha_n\right)^2\right| \leq 0; \tag{5.7}$$

$$\frac{\cos|\Delta_{\rho n}(z - l)|}{\sin(\Delta_{\rho n} l)} \quad \text{for } \left|K^2 - \left(\frac{\pi}{R}\alpha_n\right)^2\right| \geq 0. \tag{5.8}$$

and $\Delta\rho_n = \left|\sqrt{k^2 - \left(\frac{\pi}{R}\alpha_n\right)^2}\right|$

The integral on the right-hand side of equation (5.6) is given by:

$$\int_{A'} J_o\left(\frac{\pi}{R}\,\alpha_n \rho'\right) y_{om}(\rho')\,dA' = 2R^2 \left\{ \frac{1}{\beta_{om}^2 - \alpha_n^2} \cdot \left[\beta_{om} J_o(\pi\alpha_n) \cdot \right.\right.$$

$$\left. J_1(\pi\beta_{om}) - \alpha_n J_o(\pi\beta_{om}) \cdot J_1(\pi\alpha_n) \right] - \frac{1}{\beta_{om}^2 + \alpha_n^2} \cdot \frac{J_o(\pi\beta_{om})}{I_o(\pi\beta_{om})}$$

$$\left. \cdot \left[\beta_{om} J_o(\pi\alpha_n) I_1(\pi\beta_{om}) + \alpha_n I_o(\pi\beta_{om}) \cdot J_1(\pi\alpha_n) \right] \right\} \qquad (5.9)$$

A comparison between the theoretical predictions given by equation (5.6), and the experimental values of the sound pressure levels shows a good agreement in respect of both amplitude and location of nodal-points at all the frequencies far from the acoustic and structural resonancies of the cavity and the plate. At these resonance frequencies the theoretical predictions were not valid, as we assumed zero loss factor for the structure and the acoustic medium.

5.2. - Description of the model (modelling the flexible end wall).

The model is formed by the same cylindrical cavity, but the flexible end wall was replaced by a model wall of Perspex sheet. As the diameter and the length of the cavity are as in the prototype, the scale ratio L_m/L_p is unit. Having already decided the structural material and length scale ratio, from table (3.XI) it follows that only two free parameters are left: i.e. sound velocity and the thichkness scale ratio.

If the structural and the coupling conditions are to be matched, the sound velocity and the thickness scale ratio must satisfy equation (3.100) and the relation:

$$\frac{h_m}{h_p} = \frac{L_m}{L_p} \quad \frac{\rho_m}{\rho_p} \cdot \frac{\rho_{op}}{\rho_{om}}, \qquad (5.10)$$

respectively.

From table (3.VI) one obtains that for aluminium and air (the prototype) equation (3.100) gives a value of the ratio C_1/C_2 which cannot be satisfied by any acoustic medium in presence of Perspex other than air. In order to use a different acoustic medium we now look at the structural condition (XI.1) of table (3.XI). There are two free parameters, c_o and h, but only one condition.
The problem can be resolved if it is considered that the main purpose of this kind of model is to reduce the frequency scale ratio. This is possible by choosing an acoustic medium with low value of the sound velocity. Looking at table (3.VII) Freon 11 and Freon 12 show the lower value of c_o. As it is most desirable that the pressure and the temperature of the gas in the model are as in the room, the Freon 11 has been choosen. From table (5.I) it follows in fact that at room temperature (20-24 °C) the saturation pressure is about 1 bar. In addition this gas is inflammable, not explosive, has a low toxicity and a low chemical incompatibility with plastic materials.

Having choosen the acoustic medium, the thickness ratio can be obtained from the structural condition (XI.1) of table (3.XI):

$$\frac{h_m}{h_p} = \frac{L_m}{L_p} \cdot \frac{c_p}{c_m} \cdot \frac{c_{om}}{c_{op}} \cdot \frac{(1-\nu_m^2)^{\frac{1}{2}}}{(1-\nu_p^2)^{\frac{1}{2}}} \qquad (5.11)$$

From table (5.II) one finds for air c_{op} = 346 m/s and for Freon 11 C_{om} = 140 m/s; from table (3.I) the following value of the sound velocity in aluminium and Perspex are used c_p = 5150 m/s, c_m = 2030 m/s. The Poisson's moduli are respectively ν_p = 0.34 and ν_m = 0.38. With this values equation

(5.11) gives:

$$\frac{h_m}{h_p} = 1 \qquad (5.12)$$

Therefore it is possible to conclude that in the model the thickness of the Perspex plate which closes the cavity will be 1 mm, and the gas will be Freon 11.

Before introducing the discussion of the experimental measurements, some words will be said about the scale ratios, and about the effects produced by the model distortions.

5.2.1. - Discussion of the chosen scale ratios and of the effects produced by the distortions of the model.

From the acoustic condition (XI.2) of table (3.XI), being $L_m/L_p = 1$, it follows that the frequency scale ratio will be given by this value:

$$\frac{\omega_m}{\omega_p} = \frac{c_{om}}{c_{op}} = \frac{1}{2.47} \qquad (5.13)$$

From the general structural condition of table (3.I), one obtains:

$$\frac{\omega_m}{\omega_p} = \frac{1}{2.50} \qquad (5.14)$$

which is practically equal to the value given by equation (5.13).

The ratio between the dimensionless numbers of the coupling condition gives this value:

$$\left| \frac{\rho_o c_o^2 L^3 (1-\nu^2)}{Eh^3} \right|_m \Big/ \left| \quad \right|_p = 11.5 \qquad (5.15)$$

This high value shows that the model will be much more sensitive to the feed-back produced by the inner acoustic field: the effect will be an increase of the apparent stiffness of the flexible panel and therefore an increase of its first resonance frequency.

From relation (3.60) of table (3.I) one can obtain the force scale ratio given by:

$$\frac{(F_n)_m}{(F_n)_p} = \frac{(q_n L^2)_m}{(q_n L^2)_p} = \frac{1}{14.4} \qquad (5.16)$$

The exciting forces must therefore comply with this value. Finally from relation (XI.5) of table (3.XI) it is possible to obatin the pressure scale ratio of the acoustic field inside the cavity; that is:

$$\frac{p_m}{p_p} = \frac{(\rho_o c_o^2)_m}{(\rho_o c_o^2)_p} = \frac{1}{1.25} \qquad (5.17)$$

this means that the difference between the sound pressure levels in the cavity for the model and the prototype will be about 2 dB. Table (5.III) summarises all the previous scale ratios.

5.3. - Experimental measurements.

All the measurements performed on this second model have been carried out at the Institute of Technical Physics of Engineering Faculty - University of Bologna, Italy. They aimed, both for the prototype and the model, at the determination of the sound pressure level inside the cavity when its flexible end wall was excited by a sinusoidal force concentrated at the center of the panel.

Three openings on the opposite rigid end wall allowed

the insertion a 1/2" microphone mounted on a travelling rod to read the sound pressure levels across the cavity at the three radial distances: r = 0, 0.06, 0.13 m. (figure 5.1. and figure 5.2).

5.3.1. - Description of the measurement procedure for the prototype and the model

A block diagram of the instrumentation and the equipment arrangement is shown in figure (5.3). A random generator (B&K 1023) and a power amplifier (B&K 2706) provide the signal to the exciter (B&K 4810). The frequency was measured on a HP frequencymeter. The exciter was connected to the plate through a force transducer (B&K 8200); its signal was amplified and monitored on a voltmeter so as to hold the force constant. The signal from the microphone was amplified and plotted on a graphic leve recorder (B&K 2307) as a function of distance along the axis of the cylinder.

5.3.2. - Measurements on the prototype.

In this case the exciting force was applied to an aluminium plate of 1 mm thickness with a constant value of 14 N. In the cavity there was air. The measuring procedure was as previously described.

5.3.3. - Measurements on the model.

The measurements on the model were performed as on the prototype and carried out after having substituted the air with Freon 11, and the aluminium panel with a Perspex plate.

The applied force was in this case 0.1 N.

The filling and control system of Freon 11 is obtained by holding the gas in a tank immersed in a thermostatic

bath. This permits the gas flow rate to be adjusted inside the test cylinder (Fig. 5.2). In fact, the Freon 11 at the usual room temperature (20-22 °C) has a saturation pressure of about 1 bar. Then in order to evaporate the gas at a convenient rate it is necessary to heat it to a temperature slighthy higher than the room one. During the filling of the cavity the composition of the mixture of air-Freon 11 was checked by the observation of the change in the position of the minimum value of sound pressure level along the axis of the cylinder, while the Freon was replacing the air. When further addition of Freon caused no change in the position of the minimum it was concluded that the gas within the cavity was completly full of Freon. Whit this procedure the sound velocity of Freon 11 was also evaluated.

5.5.3.1. - Measurement of the sound velocity of Freon 11.

From relations (5.7) and (5.8) it is possible to see that the position of the minimum in the acoustical potential function along the axis is given by:

$$k(1 - z_{min}) = \pi/2 \tag{5.18}$$

or

$$c_o = 4\ f(1 - z_{min}) \tag{5.19}$$

For a known value of the frequency excitation (f) and the measured value of z_{min} which yields the minimum sound pressure level in the cavity, equation (5.19) gives the value of the velocity. This can be evaluated with an accuracy of about 2% which is determined by the accuracy with which it is possible to measure the position of the minimum of the sound pressure level. With this method a value of 140 m/s was obtained for the sound velocity of Freon 11 at a temperature of about 24 °C.

5.4. - Comparison of the experimental results.

Figure 5.4) compares the values of sound pressure levels inside the cavity as a function of distance along the axis of the test cylinder.

The solid and dashed lines correspond to the value obtained for prototype and model respectively. The frequency ratio between each pair of curves is given by relation (5.13), while the sound pressure levels were shifted by a quantity of 2 dB derived from condition (5.17).

For a more convenient comparison between these experimental results fig. (5.5) was prepared, where the ratio between the sound pressure levels at $z = 20\ 10^{-2}$ m is given as a function of the dimensionless parameter $\omega D/c_o$ ($D = 0.38$ m the diameter of the cavity). The shift of this ratio from the value 1, gives an index of the lack in the similarity between the two systems.

5.5. Considerations of the experimental results.

Figures (5.4) and (5.5) show a good agreement between prototype and model with the exception of a significant difference at $\omega D/c_o = 3.3$. This value corresponds to the first frequency resonance of the cavity: 280 Hz and 114 Hz when the test cylinder is filled with air and Freon 11 respectively. Near the resonance frequencies in fact the whole system is on a dynamic and acoustic unstable state. Non-linearity phenomena, sound absorption of the acoustic medium, loss factor of the structural modes, are some ot the parameters which can not be modelled and which are very important at the resonances frequencies.

As regards the use of Freon 11 in presence of Perspex a slight chemical incompatibility was observed, expecially

for those parts having an initial state of internal stresses. Care has to be taken to avoid saturation conditions for the gas. For this purpose the room temperature must be carefully controlled and kept just above the saturation temperature corresponding to the room pressure. Under these conditions the gas is certainly superheated and air ingress may be avoided.

5.6. - Conclusions.

This second series of experiments confirmes the conclusion that Freon 11 can be a suitable acoustic medium for substituting air in the case of plastic models. This gas has a very low value of sound velocity. This allows a drastic reduction in the frequency scale ratio to a value less than the inverse of the length scale ratio. However from the structural condition it follows that small values of c_o reduce the thickness scale ratio. For thin structure this is likely to be a major limitation.

Freon 11 is a gas which can be easily handled and can be used at room pressure and temperature. The filling of the model may be achieved by holding the gas in a tank immersed in a thermostatic bath. This control system allows one to adjust the gas flow and avoids air ingress into the model.

Freon 11 shows a slight chemical incompatibility with acrylic material.

Acrylic materials and Freon 11 can not satisfy the structural and the coupling conditions simultaneously if the prototype is built of steel or aluminium and the acoustic medium is air at the room conditions. However, when the coupling interaction is not critical for the prototype, this

combination of materials may be used to model structures which are mechanically and/or acoustically excited.

Finally the present investigation has shown a simple experimental method for the measurement of the sound velocity of a gas at given values of pressure and temperature. The results obtained for Freon 11 showed a good agreement with the theoretical values of the sound velocity.

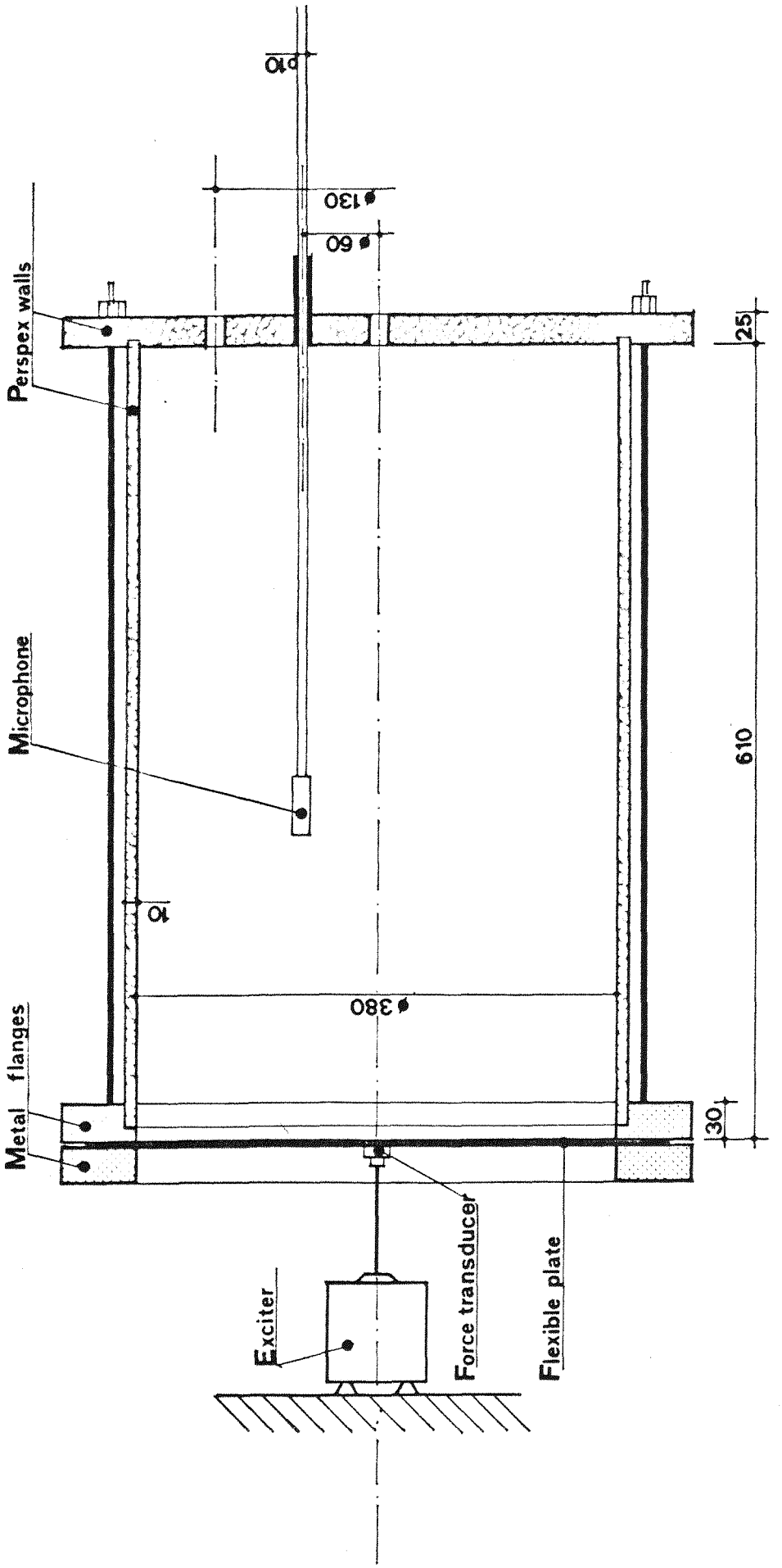

Figure 5.1 Cross-section of the experimental apparatus.

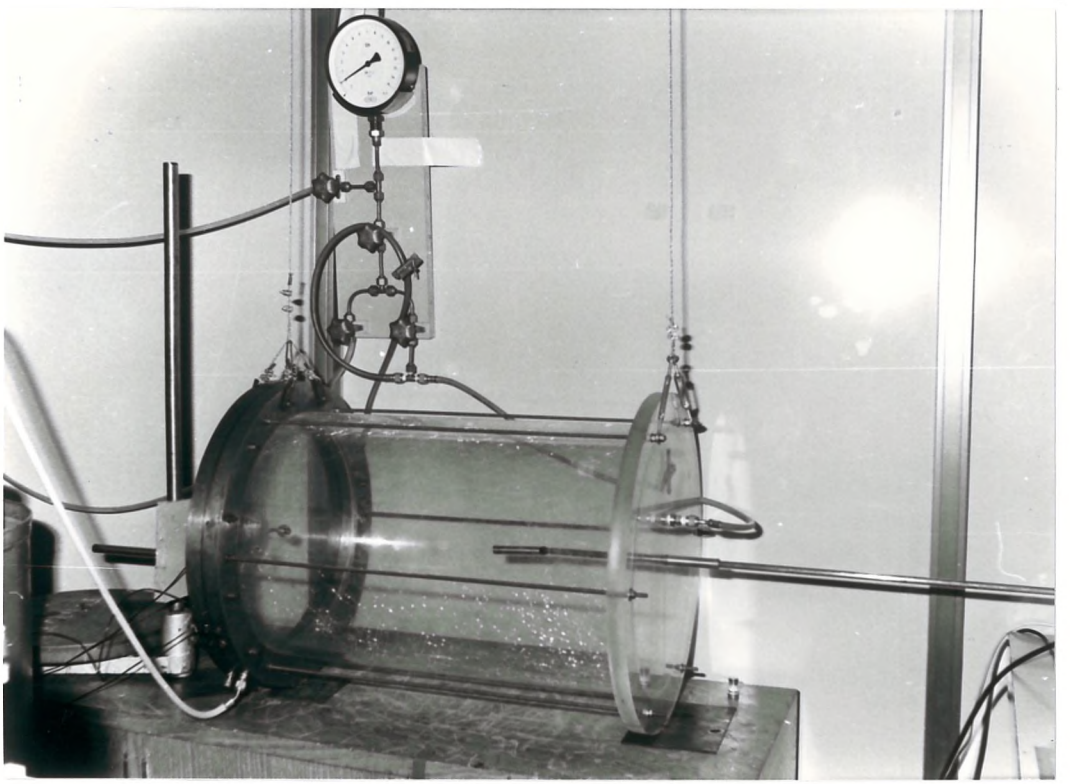

Figure 5.2 Picture of the experimental apparatus.

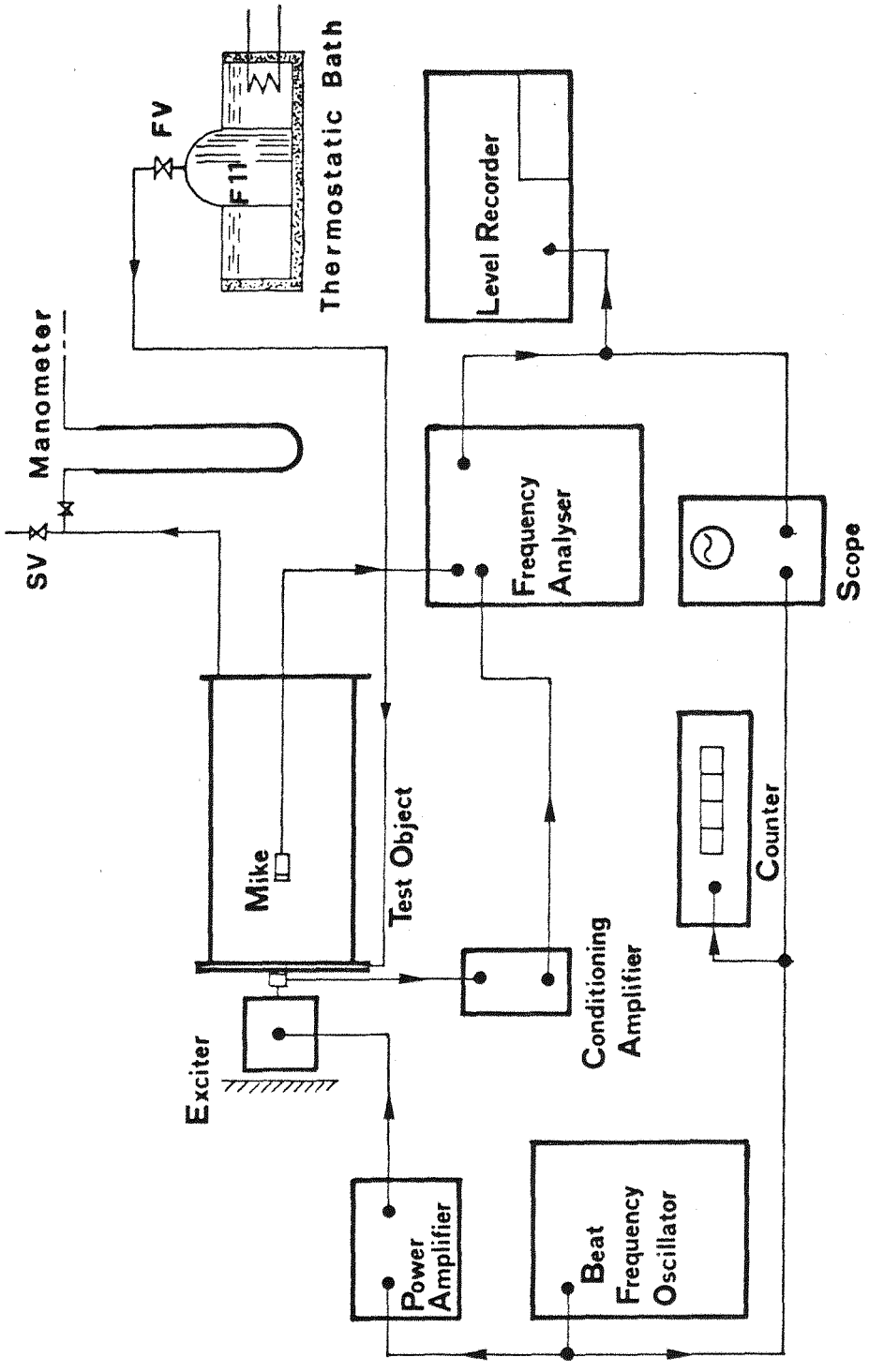

Figure 5.3 Block diagram of the instruments and equipment for the test apparatus.

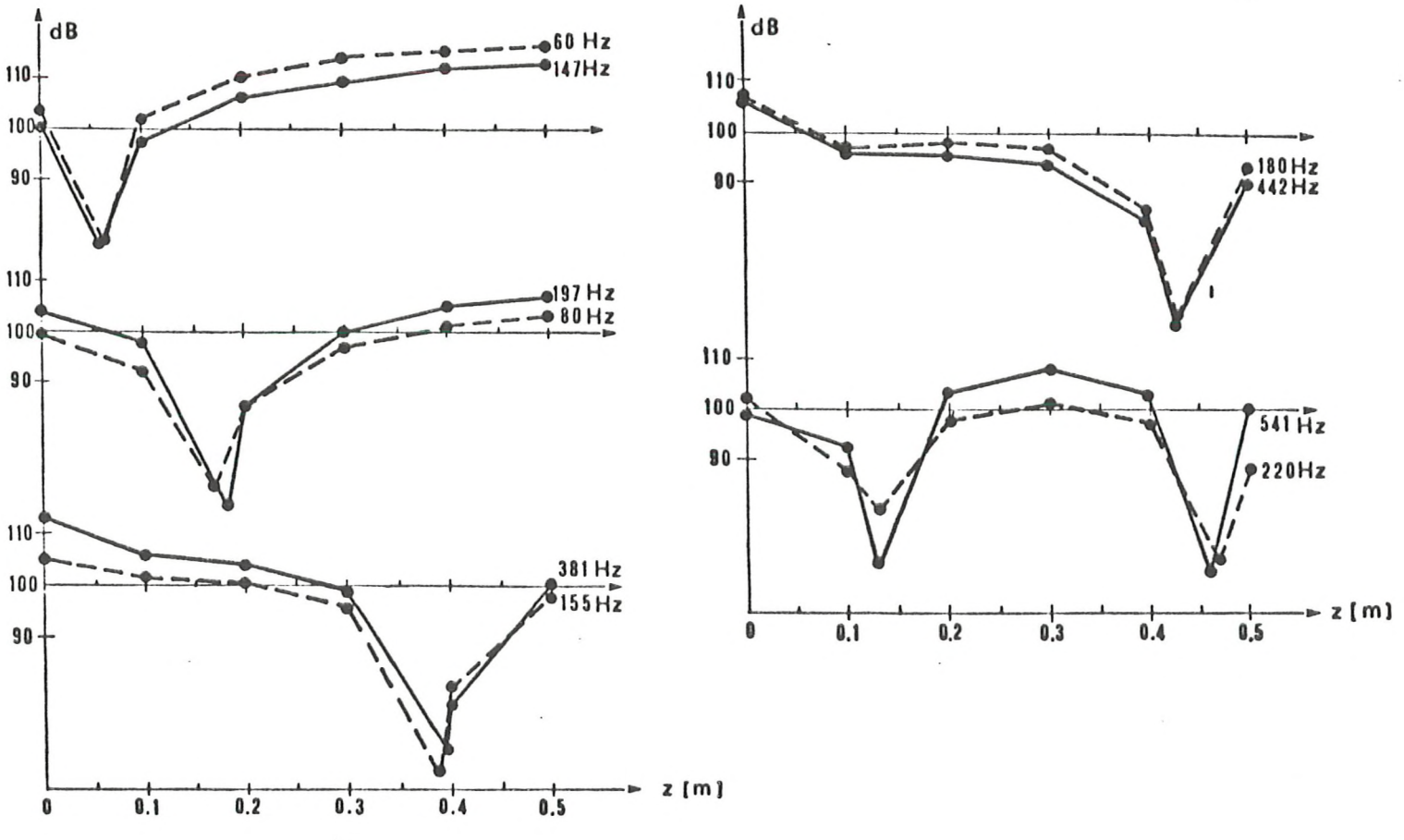

Figure 5.4 Comparison between the sound pressure levels in the cavity at R = 0.
Solid line: Aluminium — Air (F = 1.4 N (RMS)).
Dashed line: Perspex — Freon 11 (F = 0.1 N (RMS)).

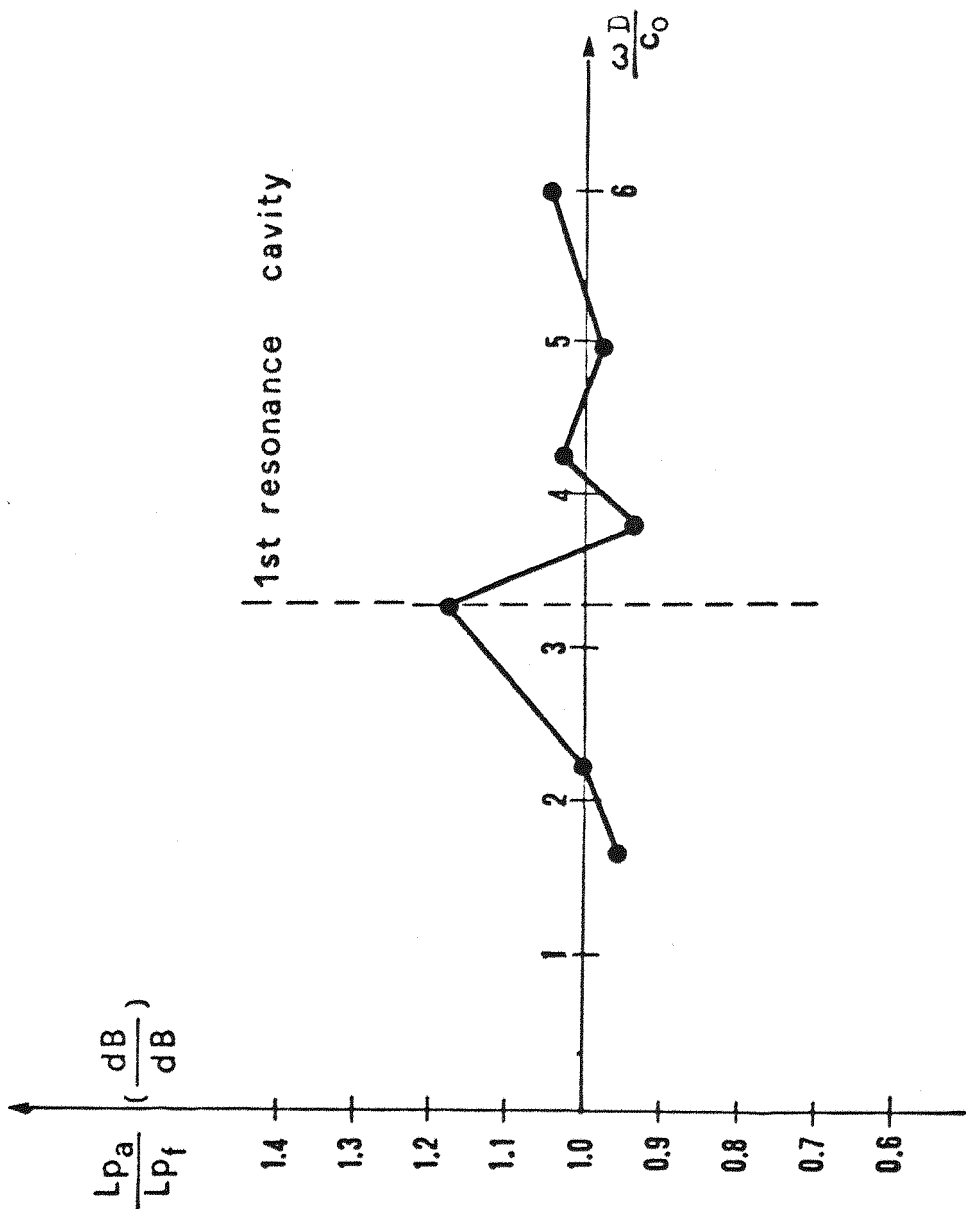

Figure 5.5 Sound pressure levels ratio versus dimensionless parameter $\omega D/c_0$ at $z = 0.2$ m.

Tab. 5.I - Saturation temperature and pressure for Freon 11 at room temperature [69]

[°C]	[bar]	[°C]	[bar]
14	0.71	22	0.95
16	0.76	24	1.02
18	0.82	26	1.09
20	0.88	28	1.17

Tab. 5.II - Physical properties of Freon 11 ($C Cl_3 F$) at $t = 24\,°C$ [69] and air.

GAS	SATURATION PRESSURE	DENSITY	SPEED OF SOUND
	p[bar]	ρ_0[kg/m^3]	c_0[m/s]
FREON 11	1.02	5.80	140 (*)
AIR	1.00	1.119	346

(*) Experimental value (section 5.3.3.1)

Tab. 5.III - Second model: values of dimensionless parameters.

DIMENSIONLESS PARAMETER	RATIO
$\frac{L}{h}$	$\left(\frac{L}{h}\right)_m / \left(\frac{L}{h}\right)_p = 1$ (5.12)
$\frac{\omega \cdot L}{c}$	$\omega_p/\omega_m = 2.47$ (5.13)
$\frac{\omega^2 L^4 \rho(1-\nu^2)}{Eh^2}$	$\omega_p/\omega_m = 2.50$ (5.14)
$\frac{FL(1-\nu^2)}{Eh^3}$	$F_p/F_m = 14.4$ (5.16)
$\frac{\rho_0 c_0^2 L^3(1-\nu^2)}{Eh^3}$	$[\ ]_p/[\ ]_m = 1/11.5$ (5.15)

CHAPTER 6

General conclusions

The present investigation has shown that acoustic - dynamic scale models may have practical application for the "acoustic design" of vehicles. Scale models may provide a convenient method for determining the behaviour of complex mechanical systems at least in comparison with the direct investigation of the real structure. Where prototypes of large physical size are involved, small scale models often are inexpensive to build and test. Measurements on acoustic-dynamic models make it possible to determine whether a cavity resonance is strongly excited or an individual panel contributes to the interior noise. The effect of proposed structural changes may be also evaluated, since the measurements on the model are usually simpler than they would be on the prototype.

The application of this model technique is also valuable when a structural-acoustic finite element program is available for the vehicle. Structural vibrations of the cavity walls may be measured on the model and put into the finit element program as input-data. The greatest potential of the acoustic finite element method is in fact achieved when it is combined with structural analysis measurements. In this way model techniques and finite element analysis become vesatile design tools able to predict vehicle interior noise at the design concept stage. They allow to investigate experimentally and analytically the effects of structural modifications on noise before prototype development.

Basically, four types of models may be used: 1) same struc-

tural material and acoustic medium as in the prototype, 2) different structural materials and same acoustic medium, 3) same structural material and different acoustic media, 4) different structural materials and acoustic media. The choice of the type of model depends on the particular problem which has to be investigated. The prototype's sizes, structural materials and acoustic medium, measurements to be made, frequency range of investigation, exciting forces etc, are the parameters which influence the choice of the model.

Models of the first type satisfy the Newtonian scaling law and show scale ratios which are a function only of the length scale ratio. This obvious type of model is sometimes too restrictive since it is not always convenient to scale the thickness of the structure in proportion with its typical surface dimension. This last condition actually reduces the possibility of obtaining small length scale ratios.

The present investigation has shown that the models of the second and fourth type are the most suitable in the case of vehicles which can be modelled by bars, plates or shells. Acrylic materials are the most suitable to model steel or glass surfaces and aluminium to model steel bars. Acrylic materials have not only the advantage of being easily handled for cutting, cementing and finishing, but they allow one to obtain also more favorable values of the thickness scale ratio being $c_m < c_p$. The force scale ratio is also convenient because the Young's modulus of plastic materials is less than that one of steel or glass.

The use of these plastic materials in the presence of air (models of the second type) is particularly suitable when the length scale ratio is not too small, and the fre-

quency range of investigation is restricted to low values. These conditions are met very often in the case of the acoustic design of vehicles, specifically for cars, vans, tractor and lorry cabs. Low frequency noise in the passenger compartment (in approximately 20-200 Hz frequency range) is of primary interest. The sizes of such vehicles allow one to obtain length scale ratios which are not too small: for example 1/5 is very often a convenient value.

These plastic models can not satisfy the structural and the coupling conditions simultaneously. They can not be used when such interaction gives radiation loading comparable to the inertial and elastic forces of the structure. But this restriction is not usually important in vehicle compartments.

Plastic models can model correctly only plane surfaces: if bars are in the prototype, they must be modeled with a structural material which has to have the same longitudinal sound velocity of the prototype. This condition is particularly important although it is derived from the longitudinal vibrations of the bars. These vibrations are not themselves an important source of sound radiation but they can excite flexural waves in plates and shells that might be attached to them. The experimental work has shown that aluminium can correctly model the bars.

When the prototype sizes are large and/or the frequency range of investigation is high, the models of the fourth type are particularly useful. They reduce, in fact, the frequency scale ratio to a value less than that of the length scale ratio if $(c_o)_m < (c_o)_p$. The present investigation has shown that Freon 11 is the most suitable gas when

plastic materials are used to model the structure. This gas has a sound velocity of about 1/2.5 of the sound velocity in air. It can be used at room pressure and temperature. It is easily handled and has a slight chemical incompatibility with acrylic materials. Freon 11 is inflammable and not toxic.

Acrylic materials and Freon 11 do not allow one to satisfy the structural and the coupling condition simultaneously. In this case the distortion introduced in the model is much more important than in the previous case. When coincidence is not required, the structural condition imposes a thickness scale ratio which is equal to the length scale ratio. Acrylic materials and Freon 11 show a ratio c_o/c which is the same as for steel and air.

The experimental investigation allowed a comparison of the results obtained from a 1/5 scale model of a safety cab of a tractor with those obtained from the prototype itself. The model was made by Perspex and aluminium and was tested in air, the same acoustic medium as for the prototype. Satisfactory agreement was found in the frequency range of investigation (0 - 200 Hz). The experimental results obtained by the model well reproduced the behaviour of the frequency response functions of the prototype, as well as their magnitude and phase.

The measurements on the model were easy to carried out and repeated tests could be made. The influence of different boundary conditions on the resonance frequencies of the cavity was cheked: i.e. wall vibrations and presence of a driver in the cab.

Very useful information was obtained from a finite

element analysis of the cavity. In the case of rigid walls, this theoretical analysis computed the resonance frequencies of the cavity and showed the distribution of the sound pressure at each mode. These theoretical results gave a better understanding of the experimental results: for example it was easy to discriminate acoustic and structural resonances and to indicate whether a cavity resonance was strongly excited. At the same time the components which mainly contribute to the interior noise level were identified.

REFERENCES

[1] GALILEI, G. Two new Sciences (1638).

[2] FROUDE, W. British Assn. Report (1872).

[3] REYNOLDS, O. Phil. Trans. Royal. Soc.London, 174, 935, (1883).

[4] EISNER, F.J. Discussion of theory of similarity and models by Groat. Trans. A S C E, 329-335 (1932).

[5] SHIH, C.C. Investigation of scaling characteristics for defining design environments due to transient ground winds and nearfield. Non linear acoustic fields. NASA-CR 120101 (Sept. 1973).

[6] MURPHY, G.
SHIPPY, D.J.
LUO, H.L. Engineering analogies. Iowa S t a t e Univ. Press (1963).

[7] DORSCH, R.G. Externally blown flap noise research. NASA TM-X-71541 (1974).

[8] FALARSKI, M.D.
AIKEN, T.N.
AOYAGI, K.
KOENIG, D.G. Comparison of the acoustic characteristics of large - scale models of several propulsive lift concepts. J. Aircraft, 12 (7), 600-604 (July 1975).

[9] FALARSKI, M.D.
AOYAGI, K.
KOENIG, D.G. Acoustic characteristics of a large scale wind tunnel model of an upper - surface blown flap transport having two engines. NASA-TM-X-62319 (Sept. 1973).

[10] GOODYKOONTZ, J.
VON GLAHN, U.
DORSCH, R. Forward velocity effects on under - the-wing externally blown flap noise. NASA-TM-X-71656 (1975).

[11] KARCHMER, A.M.
FRIEDMAN, R.
Noise tests on an externally blown flap with the engine in front of the wing. NASA-TM-X-2942 (1973).

[12] VON GLAHN, U.
GROESBECK, D.
RESHOTKO, M.
Geometry considerations for jet noise shielding with CTOL engine-over-the wing concept. NASA-TM-X-71562 (June 1974).

[13] McKINZIE, D.J.
BURNS, R.J.
WAGNER, J.M.
Noise reduction tests of large-scale model externally blown flap using trailing edge blowing and partial flap slot covering. NASA-TM-X-3379, E-8598 (Apr. 1976).

[14] RENSELAER, D.J.
NISHIDA, R.S.
WILKIN, C.A.
Small scale noise and wind tunnel tests of upper surface blowing nozzle flap concepts. Vol. 1: Aerodynamic tests results. NASA-CR-137737 (Dec. 1975).

[15] JUTRAS, R.R.
KAZIN, S.B.
Acoustic and aerodynamic testing of a scale model variable pitch fan. NASA-CR-121232 (Mar 1974).

[16] KAZIN, S.B.
PAAS, J.E.
MINZNER, W.R.
Acoustic testing of a 1.5 pressure ratio low tip speed fan with a serrated rotor (QEP fan B scale model). NASA-CR-120846 (1973).

[17] HARKONEN, D.L.
MARRS, C.C.
O'KEEFE, J.V.
Static performance and noise tests on a thrust reverser for an augmentor wing aircraft. NASA-CR-137561 (July 1974).

[18] CUMMINS, J.F.
Acoustic Characteristics of a gas turbine exhaust model. J. Engr.Power Trans. ASME, 96(3),181-184(July 1974).

[19] HASSAN, H.A.
Scaling of combustion generated noise. J.Fluid Mech.,66(3),445-453(Nov.1974).

[20] JOHNSTON, G.W.
RUFTER, F.
CHAPPELL, M.S.
Model study of a proposed engineering acoustic research facility. DME-ME-243, NRC-15480 (July 1976).

[21] SULE, W.P.
PULCHER, E.T.
Experimental evaluation of NAS Miramar hush house (Project P.114).NAEC-GSED 96-Vol. 1 (Feb. 1976).

[22] POSKITT, T.J.
Dynamic behaviour of box-girder jetties. ASCE J. Waterways Harbors Coastal Engr. Div., 101(ww2),181-200 (May 1975).

[23] MANSOUR, A.
D'OLIVEIRA, J.
Hull bending moment due to ship bottom slamming in regular waves. J. Ship. Res. 19(2), 80-92 (June 1975).

[24] CHAKRABARTI, S.K.
TAM, W.A.
Interaction of waves with large vertical cylinder. J. Ship. Res. 19(1), 23-33 (Mar. 1975).

[25] SENGUPTA, S.
BREEN, J.E.
The effect of diaphragms in prestressed concrete girder and slab bridges. CFHR-3-5-71-158-IF (Oct. 1973).

[26] SNELL, R.F.
Study of an experimental technique for application to structural dynamic problems. Shock Vib. Bull. U.S Naval Res. Lab.,Proc.44,Pt 3,82-100(Aug. 1974).

[27] THORNTON, P.H.
Static and dynamic collapse characteristics of scale model corrugated tabular sections. J. Engr. Matl. Tech.Trans. ASME 97(4), 357-362 (Oct. 1975).

[28] TAKEI, A.
MATSUMMURA, M.
KAWAGUCHI, O.
OKABAYASHI, K.
ANDO, Y.
KONDO, S.
Structural shock tests of prototype FBR MONJU scale models. Nucl. Engr. Des., 38(1), 109-129 (July 1976).

[29] VERSOWSKY, P.E.
HERBICH, J.B.
Wave forces on models of submerged offshore structures. TAMU-SG-74-215, COE-175, NOAA-76030304 (Aug. 1975).

[30] BEAVERS, G.S.
PLUNKETT, R.
Modelling of flow-induced vibrations in heat exchangers and nuclear reactors. J. Fluids Engr. Trans. ASME, 96(4), 358-364 (Dec. 1974).

[31] RIVENAES, U.
Design and acoustic tests of a dynamically scaled nuclear reactor gas circuit structure. University of Southampton, Ph.D. Thesis (1972).

[32] FIRTH, D.
BENTLEY, P.G.
ROWLEY, R.
BEESLEY, M.J.
On acoustic vibration model of a fast reactor. B.N.E.S. Vibration in nuclear plant. Keswick (May 1978).

[33] BANNISTER, R.L.
Structural models for vibration control. Noise Control Engineering,4(2), 84-92, (March-April 1975).

[34] ARNOLD, R.N.
MAUNDER, L.
Gyrodynamics and its engineering applications. Academic Press, New York, (1961).

[35] HARVEY, M.E.
Model analysis ands designer.Machine Design, 120-121 (Jan. 1948).

[36] WRIGHT, D.V.
BANNISTER, R.L.
Plastic models for structural analysis. Part I: Testing Types.Shock and Vibration Digest, 2-10 (Nov. 1970).

[37] BANNISTER, R.L.
Comparison of the dynamic response of complex plastic model with its prototype. J. Acoust. Soc. Am.43(6), 1306-1310 (1968).

[38] BANNISTER, R.L.
Determination of machinery foundation vibration transmission with impedance technique applied to plastic models.J. Acoust.Soc.Am., 51(1), 99(A) (1972).

[39] WRIGHT, D.V. Impedance analysis of distributed mechanical systems. Colloquium on mechanical impedance methods of mechanical vibrations. ASME, 19-42, N.Y. (1958).

[40] MORSE, P.M. FESHBACH, H. Methods of theoretical physics. N.Y. McGraw-Hill Book Co., pp. 949 ff. (1953).

[41] JUNGER, M.C. FEIT, D. Sound, structures, and their interaction. MIT Press Cambridge, Massachusetts (1972).

[42] PRETLOVE, A.J. Free vibration of a rectangular panel backed by a closed rectangular cavity. J. Sound. Vib. 2(3), 197-209 (1965).

[43] PRETLOVE, A.J. CRAGGS, A. A simple approach to coupled panel-cavity vibrations. J. Sound Vib. 11 (2), 207-215 (1970).

[44] PAGLIARINI, G. POMPOLI, R. The sound pressure level within a cylindrical chamber with a sinusoidally driven end wall.Proceedings of "International Conference on Recent Advances in Structural Dynamics. University of Southampton, July (1980).

[45] CRAGGS, A. The transient response of a coupled plate-acoustic system using plate and acoustic finite elements. J. Sound Vib. 15, 509-528 (1971).

[46] CRAGGS, A. The use of simple three-dimensional acoustic finite elements for determining the natural modes and frequencies of complex shaped enclosures. J. Sound. Vib. 23, 331-339 (1972).

[47] CRAGGS, A. An acoustic finite element approach for studying boundary flexibility and sound transmission between irregular enclosures. J. Sound Vib. 30, 343-357, (1973).

[48] LESALVER, R. JENNEQUIN, G. Méthod de calcul pour les bruits basse fréquence dans un habitacle de voiture. Proceedings of the 14th FISITA Conference, London 89 - 100, (1972).

[49] SHUKU, T. ISHIHARA, K. The analysis of the acoustic field in irregularly shaped rooms by the finite element method. J. Sound.Vib. 29, 67-76 (1973).

[50] MAC NEAL, R.H. The NASTRAN theoretical manual. NASA Special Publication, 211(01) (1972).

[51] MC CORMICK, C.W. The NASTRAN users' manual. NASA Special Publication, 222(01) (1973).

[52] WOLF, J.A. NEFSKE, D.J. Nastran modelling and analysis of rigid and flexible walled acoustic cavities. NASA TM-X-3278, 615 - 631 (1975).

[53] WOLF, J.A. NEFSKE, D.J. HOWELL, L.J. Structural-acoustic finite element analysis of the automobile passenger compartment. Transactions of the Society of Automative Engineers, 85, 857-864 (1976).

[54] SUNG, S.H. Automative applications of three-dimensional acoustic finite elements. Society of Automative Engineer,Paper No 810397 (1981).

[55] PETYT, M. LEA, J. A finite element method for determining the acoustic modes of irregularly

KOOPMANN, G.H. shaped cavities. J. Sound Vib. 45, 495-507 (1976).

[56] RICHARDS, T.L. JHA, S.K. A simplified finite element method for studying acoustic characteristics inside a car cavity. J. Sound Vib. 63, 61-72 (1979).

[57] EVERSTINE, G.C. SCHROEDER, E.A. MARCUS, M.S. The dynamic analysis of submerged structures. NASA TM-X-3278, 419-429 (1975).

[58] SAYHI, M.N. OUSSET, Y. Solution of radiation problems by collocation of integral formulations in terms of single and double layer potentials. J. Sound Vib., 74 (2), 187-204 (1981).

[59] BRIDGMAN, P.W. Dimensional analysis.Yale University Press, New Haven, Conn. (1931).

[60] LANGHAAR, H.L. Dimensional analysis and theory of models. John Wiley & Sons, Inc., New York (1951).

[61] WILSON, E.B. An introduction to Scientific Research. McGraw Hill Book Company, Inc., New York (1952).

[62] BUCKINGHAM, E. Model experiments and the form of empirical equations. Trans. Am. Soc. Mech. Engrs.37, 263-296 (1915).

[63] TIMOSHENKO, S. WOINOWSKI, S. Theory of plates and shells. McGraw Hill, Co., 81-83, New York (1959).

[64] REISNER, E. A new derivation of the equations for the deformation of elastic shells. Am. J. Math. 63, 177 - 184 (1941).

[65] LOVE, E.H. On the small free vibrations and deformations of thin elastic shells.

Phil. Trans. Roy. Soc.(London), 17A, 491-546 (1888)

[66] PECCHIOLI, M. The data acquisition and processing system of Italiana Keller Company at Santhià: Experiences and results. UNIKELLER (1981).

[67] BENDAT, J.S. PIERSOL, A.G. Measurement and analysis of random data. N.Y., John Wiley & Sons, (1966).

[68] BERANEK, L.L. Noise and vibration control. McGraw Hill, 308-309, N.Y. (1971).

[69] I.I.F. Thermodynamic tables for refrigerant R11 in S.I. Units, arranged according to saturation temperature and superheat. International Institute of Refrigeration (1972).

The following published paper was included in the bound thesis. This has not been digitised due to copyright restrictions, but a citation is provided.

Pagliarini, G. and Pompoli, R. (1980). The sound pressure level within a cylindrical chamber with a sinusoidally driven end wall. In: Petyt, M., *Recent advances in structural dynamics: papers presented at an international conference on recent advances in structural dynamics, 7-11 July 1980, University of Southampton, England, volume 2.* Southampton: University of Southampton Institute of Sound and Vibration Research, 457-476.